DIAMONDS AND RELATED MINERALS FROM THE DOKOLWAYO KIMBERLITE, KINGDOM OF SWAZILAND

L.R.M. DANIELS

Thesis submitted in fulfilment of the requirements for the degree of Doctor of Philosophy in the Department of Geochemistry of the University of Cape Town

Department of Geochemistry
University of Cape Town
Rondebosch
South Africa

August 1991

DECLARATION

I hereby declare that:

(i) this thesis is my own unaided work, both in concept and execution, and that apart from the normal guidance from my supervisor, I have received no assistance except as stated below:

(ii) except as stated below, neither the substance nor any part of this thesis has been submitted in the past, or is being, or is to be submitted for a degree in the University or any other university.

Signature: Signed by candidate

Signature Removed

DATE: 22 August 1991

'In the romantic hunt for diamonds, for the rich pot-holes and jewel patches in which they sometimes collect, many men have been inclined to lose sight of the strange storehouses from which they have come. That is to say, most men have. On the other hand, some have not.'

Hedley Chilvers in 'The Seven Lost Trails of Africa' (1930)

Dedicated to H.S. Richter who discovered the Klipfontein, Makganyene, Bellsbank and Finsch kimberlites, amongst many others.

CONTENTS

ABSTRACT

CHAPTER 1 - INTRODUCTION

INTRODUCTION 1
Aims of Study 3

CHAPTER 2 - ANALYTICAL TECHNIQUES

1) Mineral Analysis 4
2) Carbon Isotopes 5

CHAPTER 3 - GEOLOGICAL HISTORY

3.1 Introduction 6
3.2 Geology of Swaziland 6
3.3 Pre-Dokolwayo Igneous History of Swaziland 7
3.4 Archaean Tectonics 8
3.5 Summary 9

CHAPTER 4 - DOKOLWAYO DIAMONDS

ABSTRACT 10
INTRODUCTION 10
Group I 11
Group II 11
CLASSIFICATION SCHEME 11
Morphology 11
Colour 12
Size 12
RESULTS 13
I) Size - Mass Relationship 13
II) Size - Morphology Relationship 13
a) +22* Size Range 14
b) +17 Size Range 15
c) +12* Size Range 15
d) +11 Size Range 16
e) +9 Size Range 16
f) +3* Size Range 16
III) Size - Colour Relationship 17
IV) Colour - Morphology Relationship 18
DISCUSSION 20
APPENDIX 4.a

CHAPTER 5 - DIAMOND INCLUSIONS

ABSTRACT 27
5.1 Introduction 27
5.2 Objectives 28
5.3 Diamond Selection 28
5.4 Mineral Abundances 29
5.5 Coexisting Minerals 30

5.6 Mineral Compositions 30
5.6.1 Peridotitic Minerals 31
5.6.1a Olivine 31
5.6.1b Orthopyroxene 31
5.6.1c Clinopyroxene 32
5.6.1d Garnet 32
5.6.1e Spinel 33
5.6.1f Zircon 34
5.6.2 Eclogitic Minerals 34
5.6.2a Clinopyroxene 34
5.6.2b Garnet 35
5.6.2c Coesite 35
5.6.2d Rutile 35
5.6.2e Feldspar 35
5.6.2f Ilmenite 36
5.6.2g Staurolite 36
5.6.2h Diamond 36
5.6.2i Sulphide 36
5.6.3 Websteritic Minerals 37
5.6.4 Miscellaneous Minerals 37
5.6.4a Diamond, Graphite and Sulphide 37
5.6.4b Ilmenite 37
5.6.4c Biotite 37
5.6.4d Zircon 38
5.6.4e Magnetite and Sphene 38
5.6.4f Chlorite and TiKAl-Silicate 38
5.7 Discussion 39
Physical Conditions 39
Exposed and Non-Exposed Diamond Inclusions 40
Compositional Diversity 41
Eclogitic Environments 42
Staurolite in the Mantle 44
APPENDIX 5.a

CHAPTER 6 - DOKOLWAYO DIAMOND CARBON ISOTOPES

ABSTRACT 47
Introduction 47
Previous Work 48
Results 50
Discussion 52
APPENDIX 6.a

CHAPTER 7 - DOKOLWAYO CONCENTRATE GARNETS

ABSTRACT 55
7.1 Introduction 55
7.2 Dokolwayo Garnet Populations 56
7.2.1 Crustal Garnets 57
7.2.2 Eclogitic Garnets 57
7.2.3 Chromium-Poor Garnet Megacrysts 58
7.2.4 Peridotitic Garnets 59
7.2.4a Lherzolitic Garnets 59
7.2.4b Chromium-rich Subcalcic Garnets 60
7.2.4c Deformed Peridotitic Garnets 60
7.2.4d Green Garnet 61

7.3 Discussion 61
7.3.1 Eclogitic Garnets 61
7.3.2 Megacrysts and Deformed Peridotites 62
7.3.3 Alexandritic Garnets 64
7.3.4 TiO_2-Rich Lherzolitic Garnets 65
7.3.5 Chromium-Rich Subcalcic (G10) Garnets 66
APPENDIX 7.a
APPENDIX 7.b
APPENDIX 7.c (MOORE ET AL., 1990)

CHAPTER 8 - DOKOLWAYO CONCENTRATE SPINELS

ABSTRACT 68
8.1 Introduction 68
8.2 Concentrate Spinel Compositions 69
8.2.1 Cr^{3+} vs $Al^{3+} + Fe^{3+} + Ti^{4+}$ 69
8.2.2 $Cr^{3+} - Ti^{4+}$ 70
8.2.3 Al_2O_3 and TiO_2 71
8.2.4 Fe_2O_3 and Cr^{2+} 71
8.2.5 Inverse Spinels 73
8.2.6 Mg^{2+} vs $Fe^{2+}-(2*Ti^{4+})$ 73
8.2.7 Zoning 73
8.2.8 Trace Elements 74
8.3 Discussion 76
APPENDIX 8.a
APPENDIX 8.b
Oxidation States of Chromium in Minerals
Oxidation States of Chromium in Silicate Melts
The Behaviour of Iron and Chromium in Silicate Melts
The Coexistence of Cr^{2+} and Fe^{3+} in Silicate Melts

CHAPTER 9

Cr-SPINEL COMPOSITION-PRESSURE RELATIONSHIPS IN THE MANTLE

ABSTRACT 81
Introduction 81
Spinel-Garnet Peridotite Geothermometry 83
Results and Discussion 84
Cr/(Cr+Al) in Spinels 85
Kimberlite Concentrate Spinels 87
Conclusions 89

CHAPTER 10

OXYGEN FUGACITY CONSTRAINTS ON THE SOUTHERN AFRICAN LITHOSPHERE

ABSTRACT 90
Introduction 90
Samples Studied 93
Results and Discussion 95
Summary and Conclusions 100

CHAPTER 10 - ADDENDUM

OXYGEN FUGACITY CONSTRAINTS ON THE SOUTHERN AFRICAN LITHOSPHERE: ADDENDUM

Introduction	103
Sample Description	104
Results	104
Discussion	105
Summary and Conclusions	108

ACKNOWLEDGEMENTS

REFERENCES

ABSTRACT

Several physical characteristics, the carbon isotopic compositions, inclusion mineralogy, and distribution of the Dokolwayo diamonds were investigated. A representative suite of concentrate garnet megacrysts and macrocrysts were analyzed for their compositions. Concentrate macrocryst spinels and silicate inclusions recovered from these spinels were analyzed.

The physical characteristics of the diamonds investigated were mass, size, morphology and colour. The relationship between mass and size in a population of diamonds recovered from a single hypabyssal intrusion and the general production as a whole, was found to be statistically the same. The most recognizable morphology is the dodecahedron. Octahedra decrease in significance with a decrease in size. Colourless stones predominate. Brown stones are more common than yellow stones, which is uncommon in primary southern Africa diamond populations. Diamonds characterized by "Tanganyika naats" have hitherto not been described from southern Africa. The relationship between the various physical characteristics investigated indicate that the general Dokolwayo diamond population consists of at least four sub-populations.

The primary mineral inclusions recovered from the Dokolwayo diamonds fall predominantly into the peridotitic and eclogitic suites recognized world wide. The peridotitic suite predominates. Several inclusions of unknown paragenesis were recovered. Spinels are the most common peridotitic inclusions and may have less than 60 wt% Cr_2O_3. Spinel inclusions exposed on the surface of diamonds tend to contain more Cr_2O_3 than unexposed spinels recovered from the same diamond. The most common eclogitic inclusion is garnet and at least three different populations are recognised. Clinopyroxene was not found to co-exist with eclogitic garnet. The first occurrence of staurolite as a diamond inclusion is reported and this staurolite is therefore a stable phase in the mantle to at least 45 kilobars pressure. The presence of staurolite in diamond infers a metamorphic origin for that diamond. Calculated equilibrium pressures and temperatures are consistent with a subsolidus origin for the peridotitic diamonds.

The carbon isotopes of 88 diamonds were analyzed using standard methods. The majority of the diamonds range between $\delta^{13}C$ -1 and -10$^{o}/_{oo}$. The peridotitic diamonds are slightly enriched compared to the eclogitic diamonds. No distinct relationship exists between the composition of eclogitic diamond inclusions and the isotopic compositions of the host diamonds. A negative relationship exists between Cr_2O_3 in spinels in peridotitic diamonds and carbon isotopic compositions. The source of the carbon from which the majority of the eclogitic and peridotitic diamonds crystallized is considered to be CH_4. The source of the vapour is suggested to be CH_4 degassing on a continuous basis from the core or lower mantle. Significant zonation of $\delta^{13}C$ values from a single diamond suggests Rayleigh fractionation of a subducted carbonaceous source. Fractionation of carbon isotopes from a cubic and a single crystal diamond with a polycrystalline coat appears to be limited.

Approximately 55% of the Dokolwayo kimberlite concentrate is garnet. A representative suite of concentrate garnets was analyzed and the majority of these garnets are Cr-poor. The presence of granulite facies rocks at depth is suggested by compositions of crustal garnets. Eclogitic garnets were more magnesian and less sodic than eclogitic diamond inclusion garnets, suggesting a shallower, more refractory source for the concentrate garnets. Both megacryst and macrocryst garnets were identified to belong to the Cr-poor megacryst suite which is common in Group I kimberlites. The megacryst garnets have

>0.7 wt% Na_2O suggesting a high pressure source. Prior to this study such garnets had not been reported from Group II kimberlites. Garnets similar in composition to garnets from high-temperature deformed peridotites were also identified. Approximately 5% of the Dokolwayo concentrate consists of subcalcic G10 garnets, which is consistent with the presence of diamonds.

Approximately 45% of the concentrate from the Dokolwayo kimberlite is spinel. More than 80% of the spinels (n=288) have Cr_2O_3 > 60 wt%. Approximately 10% of the spinels are deficient in divalent cations and are stoichiometrically Fe_2O_3-free. These spinels are suggested to have a significant content of divalent chromium, i.e. CrO. Two main populations are recognized. One population has TiO_2 < 0.6 wt% and TiO_2/Al_2O_3 < 0.2 whereas the second population is TiO_2-rich (generally > 0.6 wt%) and has TiO_2/Al_2O_3 > 0.2. The TiO_2-poor population is similar in composition to the diamond inclusion population. The TiO_2-rich population may be an early cumulate phase of komatiite melts.

The behaviour of the Cr\(Cr+Al) ratio of chromium spinels with respect to mantle pressures and temperatures has been investigated utilizing spinels from spinel-garnet peridotites derived from the southern African lithosphere.

Chromium spinels and garnets coexist in the mantle to at least 50 kbars pressure, which is significantly in excess of the CMAS predicted limit of 18 kbar. The Cr/(Cr+Al) ratio of chromium spinels increases with increasing pressure in the mantle. At pressures in excess of 40 kbars the Cr/(Cr+Al) ratio of spinels may be restricted by stoichiometric constraints. A limited study of the concentrate spinels from kimberlites indicate that economically diamondiferous kimberlites are characterized by spinel compositions in which the average Cr/(Cr+Al) > 0.8. Concentrate spinels from kimberlites characterized by a paucity of diamonds have an average Cr/(Cr+Al) < 0.8.

Oxygen fugacities were calculated for olivine-spinel$\pm$orthopyroxene assemblages recovered from diamonds and the concentrate of the Dokolwayo kimberlite. In addition, thermobarometric oxygen fugacities were obtained for chromium spinel-garnet peridotites and diamonds from several other southern African kimberlites. The southern African lithosphere appears to be laterally homogeneous with respect to oxygen fugacity. Vertically the oxygen fugacity of the lithospheric upper mantle decreases with an increase in pressure. Locally, oxygen fugacities calculated for Dokolwayo mineral assemblages are indicative of an upper mantle characterized by diverse redox conditions which may vary by > 4 log units. The reduced nature of the Kaapvaal lithosphere at depth (fO_2 < QFM) suggests that Fe^{2+}/Fe^{3+} equilibria do not provide effective fO_2 buffering. It is suggested that an open-system buffering through pervasive C-H-O degassing prevails.

CHAPTER 1 - INTRODUCTION

INTRODUCTION

The Dokolwayo kimberlite diatreme, K1, was discovered in 1976 and first described by Hawthorne et al. (1979). The kimberlite is located in the northeastern sector of the Hhohho district, Kingdom of Swaziland. It is an "on-craton" kimberlite situated close to the inferred present day northeastern margin of the Kaapvaal Craton. The diatreme, now deeply eroded, intruded the ~3000 My Mliba granodiorite pluton. The kimberlite contains abundant basement xenoliths as well as sandstone, siltstone and coal correlated with the much younger Beaufort Group sediments of the Karoo rocks which were present at the time of emplacement. The isotopic character of the kimberlite indicates that it is a Group II kimberlite (Smith 1983). It has the preferred emplacement age of 200±5 My (Allsopp and Roddick, 1984), making it the oldest Group II kimberlite known in southern Africa. Unlike the majority of kimberlites in southern Africa it predates the Stormsberg volcanism which in the vicinity of Dokolwayo is associated with the Lebombo monocline. The emplacement age of the Stormsberg volcanics is not well established, but the best estimates are 193±5 My (Manton, 1968; Fitch and Miller, 1984).

The diatreme is diamondiferous and present mining operations have to date exposed at least eleven intrusive phases within the diatreme. Their inter-relationships are not clear since the near surface material is highly weathered and difficult to study in detail. Two major components are: hypabyssal porphyritic kimberlite which occupies about 35% of the diatreme and is generally confined to the margins, and a central core of younger tuffisitic kimberlite breccia.

The kimberlite is geographically well separated from other established kimberlite mines and affords the opportunity for investigating pre-Stormsberg mantle processes and

physiochemical conditions of the upper mantle on the northeastern margin of the Kaapvaal Craton.

Upper mantle physiochemical conditions are best evaluated with the use of diamonds, their mineral inclusions and associated concentrate minerals. The detailed study of the compositions of diamond inclusions made a quantum leap in the late 1960's when it became possible to analyze them with electron microprobes. The significance of diamond inclusions is that they provide information on the chemical and physical conditions of the Earth's upper mantle at pressures in excess of 45 kilobars. A study of diamond inclusions from a single locality provides insight into the complexity of the upper mantle on a local basis. Combining information from several localities within a craton provides the opportunity to evaluate the development of the upper mantle within the diamond stability field on a regional cratonic scale.

A diamond inclusion study would be best augmented by a comprehensive study of a mantle derived xenolith suite for a detailed reconstruction of the upper mantle. In the absence of xenoliths a study of the compositions of xenocryst concentrate minerals derived from the disaggregation of xenoliths will suffice, albeit with limitations.

This study reports a number of physical properties, the inclusion compositions and carbon isotopic compositions of the diamond population from the Dokolwayo kimberlite. Due to the high degree of weathering in the kimberlite, no concentrate olivines or orthopyroxenes were recovered in the upper regions of the kimberlite. A very small number of clinopyroxenes were recovered, but these are not sufficient in number to report without statistical bias. An insignificant number of xenoliths were recovered over a period of three and a half years. However, a comprehensive suite of garnet megacrysts and macrocrysts and spinel macrocrysts were collected and analyzed. The lower size limit of macrocrysts analyzed in this study was 500 microns.

Aims of the Study

The results of this study of the physical characteristics of the diamonds, their carbon isotopic compositions, the compositions of their mineral inclusions and the associated concentrate garnets and spinels will be combined to evaluate

- the relationship between mass, size, morphology and colour as well as the unique character of the diamond population;

- the range of the mineral inclusions in the diamonds, their parageneses, abundances and compositional characteristics;

- the range in carbon isotopic compositions and their relationship to diamond inclusion compositions and parageneses;

- the diversity in compositions of garnet megacrysts and macrocrysts and possible source rocks for the garnet xenocrysts;

- the diversity in compositions of the concentrate spinel macrocrysts, their inclusions and possible paragenesis;

- the relationship between mantle pressure and composition of mantle-derived spinels;

- the oxygen fugacity conditions of the lithosphere beneath the Kaapvaal Craton.

CHAPTER 2 - ANALYTICAL TECHNIQUES

1) Mineral Analysis

Major element mineral analyses were obtained on a Cameca Camebax microprobe at the University of Cape Town. The instrumental conditions were as follows:

Beam Current: 40nA

Accelerating Voltage: 15kV

Beam Size: 5 microns

Counting Time: 10 seconds

Counting Time Na, Ni: 10 - 60 seconds

Analyzing Crystals: TLAP for Na, Mg, Si, Al

LIF 200 for Fe, Mn, Ni

PET for Ca, K, Ti, Cr

Standards	**Garnet**	**Pyroxene**	**Olivine**	**Spinel**
Si	K-P	Diop	M-Ol	K-P
Ti	Rut	Rut	Rut	Rut
Al	K-P	K-P	K-P	Chro
Cr	Chro	Chro	Chro	Cr-Oxide
Fe	K-P	K-P	M-Ol	Ilm
Mn	Rhod	Rhod	Rhod	Rhod
Mg	K-P	Diop	M-Ol	K-P
Ca	K-P	Diop	K-P	K-P
Ni		NiSi	NiSi	NiSi
Na	K-H	K-H		
K		K-H		

Reduction of all data was performed on-line. Raw counts were corrected for dead time background, normal concentrations were calculated from standard K-factors. These nominal concentrations were then corrected using ZAF correction factors (modified after Henoc et al., 1973).

2) **Carbon Isotopes**

Diamond fragments were picked from the crush remaining from inclusion recovery as well as fragments recovered from selected stones without inclusions. The diamond fragments were cleaned in HCl overnight and rinsed in distilled H_2O, checked for visible impurities and dried overnight at 100°C. The diamonds were weighed to the nearest .001 mg. The diamond fragments were combusted in purified oxygen following similar procedures as described by Deines and Wickman (1973). Measured yields usually agreed within $\pm$ 2% of the calculated yield. The CO_2 produced was analyzed using a VG Micromass 602E mass spectrometer. Results are reported as $\delta^{13}C$ (relative to PDB) with a maximum 2σ error (95% confidence limits) of 0.3 $^{o}/_{oo}$ as determined from replicate analyses of an in-house graphite standard. This error accounts for mass spectrometer precision as well as possible system errors derived during CO_2 production and sampling handling.

CHAPTER 3 - GEOLOGICAL HISTORY

3.1 INTRODUCTION

A study of mantle-derived material in a kimberlite makes it possible to investigate certain aspects of the upper mantle of the Earth. It is, however, essential to place constraints on the mantle that is being investigated. While it may not be possible to account for processes such as possible mantle melting events that are not represented on surface, a study of the regional geology in the vicinity of a kimberlite may assist in determining important features of the mantle sampled by the kimberlite. The regional geology may, for example, indicate whether subduction could have taken place in the area or may reflect different mantle melting events that pre- or post-dated the emplacement of the kimberlite and hence will have important bearing on the mantle assemblages sampled by the kimberlite. The geology of Swaziland will be argued to have significant relevance to the mantle assemblages sampled by the Dokolwayo kimberlite. It is therefore considered expedient to briefly review a number of salient aspects of the geology of Swaziland.

3.2 GEOLOGY OF SWAZILAND

The western two thirds of the country are characterized by one of the best documented Archaean basement assemblages which record the evolutionary development of the Kaapvaal Province over a period of one billion years. These exposed Archaean rocks consist predominantly of granitic plutons, gneisses, volcano-sedimentary assemblages (Swaziland Supergroup, Pongola Supergroup) and granodiorites (Figure 3.1). It is not the intention of this study to discuss the Archaean development of Swaziland in detail. For a comprehensive summary of the Archaean rocks of Swaziland the reader is referred to Tankard et al. (1982).

The eastern third of Swaziland is covered by Karoo sediments and volcanics which rest unconformably on the Archaean basement rocks. There appears to be no major representation of any geological events between the early Proterozoic and the deposition of the Permo-Carboniferous Karoo glacial sediments in this area.

3.3 Pre-DOKOLWAYO IGNEOUS HISTORY of SWAZILAND

The early geological history of Swaziland is characterized by numerous igneous events. A simplified stratigraphic succession for this period is presented in Table 3.1.

The primordial radiogenic Sr ratios of the siliceous gneisses of the Bimodal Gneiss Suite (Barton et al., 1980) are indicative of a mantle source. Tankard et al. (1982) considered, on structural grounds, the Bimodal Gneiss suite to be the oldest unit of the Ancient Gneiss complex in Swaziland and concluded that no older sialic crust existed in Swaziland prior to the formation of the Bimodal Suite.

The oldest ultramafic rocks in Swaziland are represented by the Onverwacht Group volcanics. The ages of the Onverwacht ultramafics and the siliceous Bimodal Suite gneisses (Table 3.1) indicate an approximate contemporaneity. However, the relationship between these rocks has not been clearly established.

The Onverwacht volcanics have been widely interpreted to represent primordial oceanic basic and ultrabasic rocks (e.g. Herrman et al., 1976; De Wit and Stern, 1980). The total thickness of these volcanics has been subject to debate, and tectonic repetition may have been involved. Although the present stratigraphic thickness of the Onverwacht volcanics is about 15 km, De Wit and Stern (1980) have suggested an original thickness of only 2 km. Nevertheless, when the total volume of these mantle-derived volcanics is considered it is apparent that volumetrically a significant portion of the mantle below Swaziland and surrounding areas would have been affected by the melting events that resulted in the

extrusion of these volcanics. Precambrian basic to ultrabasic volcanics in Swaziland are not confined to the Onverwacht volcanics, such rocks have also been identified in the Nsuze volcanic sequence of the Pongola Supergroup, in the Ushuswana intrusive complex and as early Proterozoic diabase dikes and sills. However, volumetrically the Onverwacht volcanics are the most significant.

Precambrian igneous activity in Swaziland culminated in the early Proterozoic. There is no evidence of any major igneous activity in Swaziland after the Proterozoic until the emplacement of the Dokolwayo kimberlite.

3.4 ARCHAEAN TECTONICS

The Onverwacht volcanics in the Archaean Barberton greenstone belt have been interpreted as part of a thick (~16 km) continuous mafic to ultramafic volcanic sequence (Viljoen and Viljoen, 1969). However, more recent work (De Wit and Tredoux, 1987) has revealed a complex intrusive - extrusive simatic complex overlying a high temperature tectonometamorphic base. The observed sequence of peridotitic tectonite zones, magma chambers and conduits, pillow lavas and sediments has led De Wit and Tredoux (1987) to classify the Onverwacht volcanics as an ophiolite sequence. In contrast to Phanerozoic ophiolites, the Barberton ophiolite sequence is suggested to be relatively thin and obduction may have been the most active tectonic process (De Wit et al., 1990). Continental nuclei in the region of Dokolwayo may thus have formed as a result of rapid regional intracratonic obduction, leading to stacking and subsidence of hydrated simatic thrust piles containing a large (25%) ultramafic component (Figure 3.2; De Wit et al., 1990). The subsiding thrust piles would have the effect of depressing depleted dunitic-harzburgitic residues to increasing depths forming tectospheric keels of metamorphosed peridotites and basalts with possible intercalated metasediments.

3.5 SUMMARY

Both field evidence as well as radiogenic ages (Hawthorne et al., 1979; Allsopp and Roddick, 1984) indicate that the Dokolwayo kimberlites were emplaced prior to the commencement of Karoo volcanism. The apparent small age differential between the emplacement of these kimberlites and the commencement of Karoo volcanism suggests that the kimberlites sampled a mantle reflecting physical and chemical conditions immediately prior to the melting event that resulted in the extrusion of the Karoo volcanics. There is no available evidence that the mantle sampled by these kimberlites had undergone any major melting event for over 1.5 billion years prior to being sampled. Volumetric considerations suggest that the major melting event affecting the mantle prior to the emplacement of the kimberlites is related to the extrusion of the Archaean Onverwacht komatiites and basalts.

Archaean tectonic considerations suggest that oceanic basalts may have been initially obducted and subsequently subsided to form part of the stable metamorphosed continental keel. The presence of eclogitic minerals and xenoliths in the Dokolwayo kimberlite would be consistent with the tectonic model presented for this region by De Wit et al. (1990).

TABLE 3.1

SIMPLIFIED PRE-KAROO STRATIGRAPHIC SUCCESSION OF SWAZILAND

AGE Ma	LITHOLOGY
1800 - 2400	Diabase dykes and sills
2175 ± 50	Mooihoek granitic pluton
2286 ± 304	Mhlosheni Granite
2417 ± 148	Hlatikulu Granite
2244 ± 355	Nhlangano Gneiss
2520 ± 422	Kweta Granite
?	Mahamba Gneiss
?	Mhlatuzane Gneiss
2610	Sicunusa Pluton
2687 ± 6	Mbabane Granite
2734 ± 226	Sphene - Orthogneiss
2802 ± 285	Sinceni Pluton
2802 ± 56	Ngwempisi Pluton
2876 ± 30	Usushwana Complex
2940 ± 45	Mliba Granodiorite
2950	Pongola Supergroup
3028	Lochiel Batholith
?	Mponono Gabbroic Intrusives
3320	Tsawela Gneiss
3350 ± 57	Granodiorite Suite
~3500	Dwalile Metamorphic Suite
3540 ± 30	Onverwacht Group Volcanics
3555 ± 111	Bimodal Gneiss Suite

? Based on field relationships.

Geochronology data sources: Allsopp et al. (1962); Davies (1971); Davies and Allsopp (1976); Hamilton et al. (1979); Anhaeusser (1980); Barton et al. (1980, 1983, 1983b); Carlson et al. (1983); Hegner et al. (1984); Hunter and Wilson (1988); Layer et al., (1989).

CHAPTER 3 - FIGURE CAPTIONS

FIGURE 3.1

A simplified geologic map of Swaziland after Barton et al. (1983). Black areas represent the greenstone succession of the Barberton greenstone belt and the Dwalile Metamorphic Suite. Horizontal stripes indicate the cover of the Karoo Supergroup. The stippled pattern indicates the rocks of the approximately 2 900 Ma old Pongola Supergroup and the Ushushwana Complex. MG = Mahamba Gneiss and MTG = Mhlatuzane Gneiss, both of uncertain age. Sampling localities for age dating are indicated by solid triangles, in most cases those of the labelled fields in which they occur. That associated with an "M" denotes the Mponono Igneous Suite while that associated with an "S" denotes the sphene-bearing orthogneiss. Vertical stripes denote units with Rb-Sr whole rock ages less than about 2 600 Ma.

FIGURE 3.2

Schematic model showing the formation of Archaean oceanic crust and proto-craton (granite-greenstone terrain and depleted ultramafic keel) with subducting basaltic slabs being metamorphosed to eclogite facies (in part after DeWit and Tredoux, 1987).

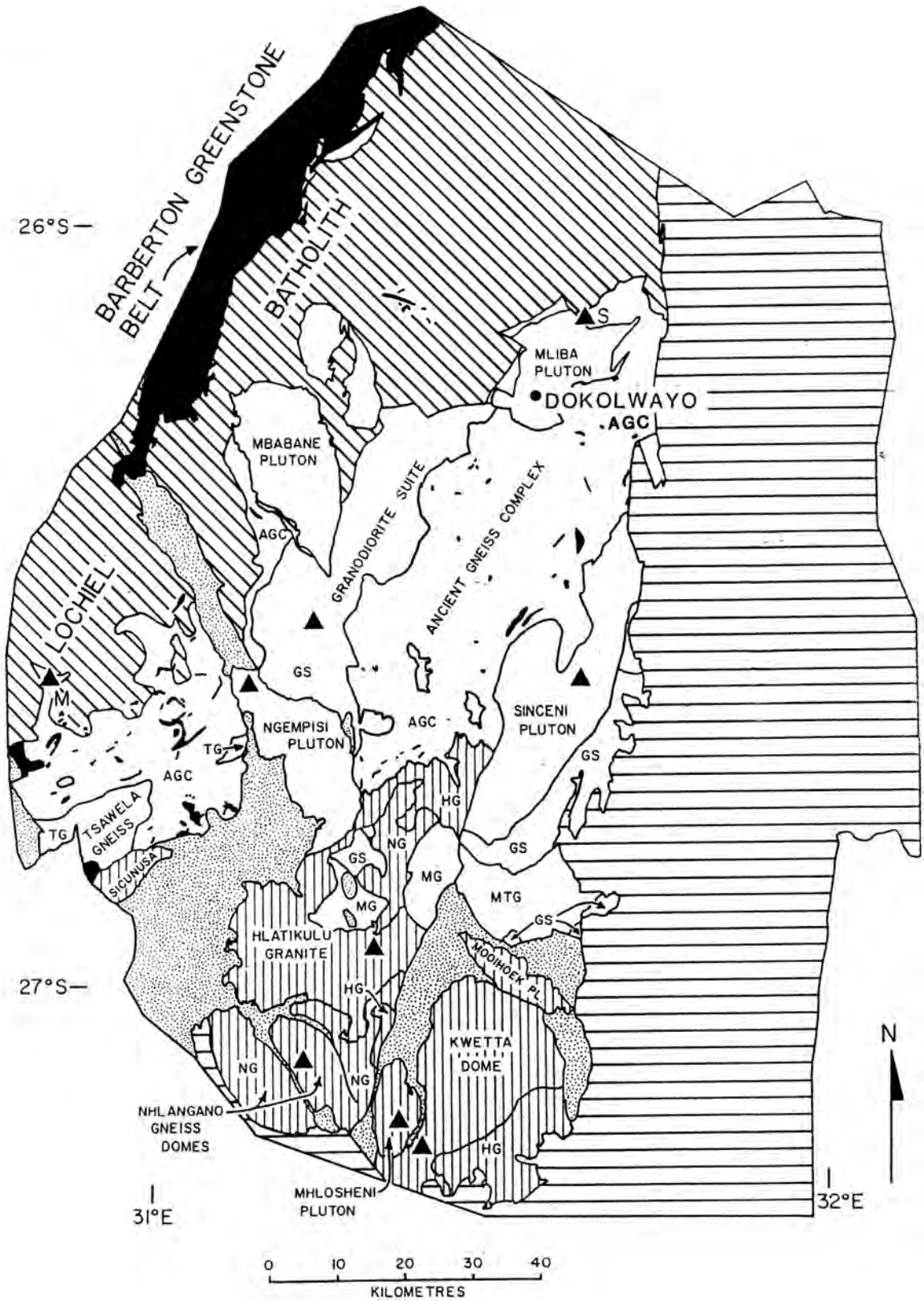
BARBERTON GREENSTONE BELT
BATHOLITH
26°S
27°S
31°E
32°E
N
S
MLIBA PLUTON
DOKOLWAYO
AGC
MBABANE PLUTON
GRANODIORITE SUITE
ANCIENT GNEISS COMPLEX
LOCHIEL
M
GS
NGEMPISI PLUTON
AGC
SINCENI PLUTON
TG
TSAWELA GNEISS
SICUNUSA
HG
NG
MG
MTG
HLATIKULU GRANITE
MODIMOLLE PL.
KWETTA DOME
NHLANGANO GNEISS DOMES
MHLOSHENI PLUTON
0 10 20 30 40
KILOMETRES

Fig 3·1

Fig 3·2

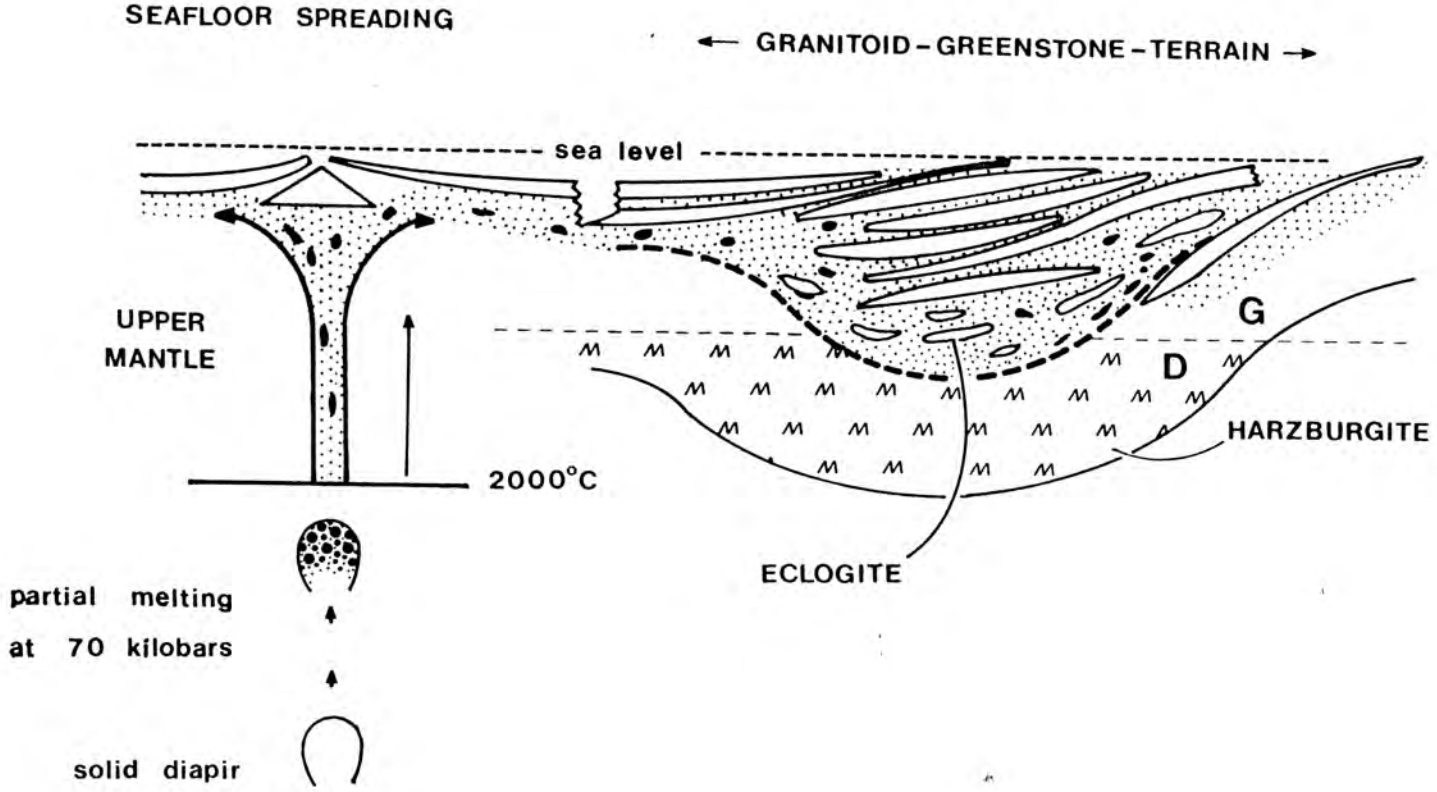
SEAFLOOR SPREADING
← GRANITOID - GREENSTONE - TERRAIN →
sea level
UPPER MANTLE
2000°C
G
D
HARZBURGITE
ECLOGITE
partial melting at 70 kilobars
solid diapir

CHAPTER 4 - DOKOLWAYO DIAMONDS

ABSTRACT

A detailed study of the physical features of the Dokolwayo diamonds has shown that the diamond population as a whole consists of a number of complex sub-populations which have experienced different crystallization and post-crystallization histories. No significant difference was observed in the size-mass relationship between a population of diamonds recovered from a single intrusion in the diatreme and the general production of the kimberlite as a whole. Morphologically, dodecahedra are the most common recognisable form. Colourless diamonds predominate. Large diamonds with "Tanganyika naats" are described from a southern African kimberlite for the first time. The Dokolwayo diamonds are distinguished from other southern African diamond populations (Harris et al., 1975, 1979) in that brown diamonds predominate over yellow diamonds. This feature of the Dokolwayo diamonds, together with the "Tanganyika naats" suggest that this may be a unique population of diamonds.

INTRODUCTION

Detailed studies of the physical features of diamonds from southern African localities have been reported by Whitelock (1973), Harris et al. (1975,1979) and Robinson (1979). Various classification schemes based on morphology, colour, size and surface features have been used by these authors. Harris et al. (1975) found that diamonds from primary kimberlite sources exhibit distinct relationships with respect to crystal form versus diamond size.

In this study several physical features of the Dokolwayo diamond population are described. A combination of classification schemes was used to examine a number of properties of the

Dokolwayo diamonds. Two groups of diamonds were examined. All the diamonds were from the general production of Dokolwayo.

GROUP I

The first group was a sample collected from run of mine production and was used to determine the relationship between diamond size and total mass of production. This sample was in excess of 13 800 carats, and was collected in such a way as to be considered representative of production in general. A sub-population of this sample was recovered from a single intrusive in the northern end of the diatreme referred to as the Green Micaceous kimberlite. This kimberlite is hypabyssal in character. The sub-population from this intrusive had a total mass of 437.43 carats.

GROUP II

A second group of 4880 diamonds was examined in terms of size, colour and shape. These diamonds were also collected from run of mine production.

CLASSIFICATION SCHEME

The first group of diamonds were sieved into several size ranges as described below. Diamonds in the second group were first sieved and then classified using a hybrid version of the classification schemes of Whitelock (1973) and Harris et al. (1975).

Morphology

The diamonds were classified into five basic groups of crystal form. The forms recognized were octahedron, dodecahedron, macle, polycrystalline and irregular. The dodecahedra included flattened dodecahedra tetrahedra and tetrahexahedroida. The criteria used by

Whitelock (1973) for distinction between octahedra and dodecahedra were adopted in this study. Macles were limited to the flattened octahedral twin on {111}. Polycrystalline diamonds were defined as all diamonds excluding macles that consisted of more than one crystal. This included framesites. Irregular stones were generally fragments of stones that exhibited less than 50% of the original shape, but also included ballas stones and hailstone boart. No distinction was made between fragments of crystal shape and stones without crystal form. Cubes are very rare.

Colour

Seven categories of colour were used in the classification. The colours used were colourless, grey, yellow, brown, black, green and orange. The colour of the diamond was determined visually against a white background under fluorescent light commonly used by diamond evaluators. No distinction was made with respect to the intensity of the colour, e.g. light yellow or deep yellow. In the event of a diamond being zoned with respect to colour the dominant body colour was recorded.

Size

In contrast to the sizing method used by Whitelock (1973), Harris et al. (1975, 1979) and Robinson (1979) the diamonds in this study were screened using Pierre Sieve sizes. The approximate aperture sizes in millimeters are presented in Table 4.1.

Eleven size ranges were used. Three have a lower aperture diameter smaller than the size ranges used by Whitelock (1973) and Harris et al. (1975,1979).

It should be noted that throughout this study only the lower aperture within a specific size range is quoted, e.g. +34 should be read as -40 +34.

RESULTS

I) Size - Mass Relationship

The relationship between diamond size and total mass of the Dokolwayo diamond population is graphically illustrated in Figure 4.1a. The most striking feature of this relationship at first glance is the bimodality of the population with respect to the +34 and -34 sieve size populations. However, this bimodality is probably a function of combining all the +40 diamonds together in one size. A more likely situation is that the bar chart will tail off normally if the +40 diamonds were subdivided into several regularly spaced individual sizes. In addition to this pseudo bimodality the -34 diamond population also appears to be characterised by a bimodal population around the +11 size range. The same population characteristics are exhibited by the much smaller sample from the Green Micaceous kimberlite (Figure 4.1b).

The non-parametric Spearman rank correlation coefficient for these two samples has been calculated to test whether there is any significant difference between the two samples. The results strongly suggest that these two populations of diamonds are representative of the same source, and that the observed bimodality within the -40 population itself is not a sampling effect but an inherent characteristic of the diamond population from Dokolwayo. Unfortunately, size - mass relationships of diamond populations from other kimberlites are not freely available and it was impossible to establish if this feature of the Dokolwayo diamond population is unusual.

II) Size - Morphology Relationship

The relationship between size and morphology of the Dokolwayo diamonds has been investigated for the Group II population as a whole as well as for individual size ranges.

Several of the size ranges contained a smaller number of diamonds (n <= 500) than recommended by Harris et al. (1975). However, only three size ranges (+40, +34, +22) consisted of a smaller number of diamonds than the minimum number of diamonds in a sample (n = 100) from individual kimberlite intrusives considered by Whitelock (1973). The results have been tabulated (Appendix 4a) and presented graphically in Figure 4.2.

The sample was characterised by an octahedra/dodecahedra ratio of ~1:8 (i.e. O/D = 0.12). Irregular stones constitute 46% of the total population. Polycrystalline diamonds marginally exceeded the number of octahedral stones (6% and 5% respectively). Macles were found to represent the smallest percentage (<2%) of crystal forms considered, probably due to the rigorous classification criteria used in this study for this particular diamond shape. Cubes are too rare to be considered. Dodecahedra represented the largest fraction (41%) of the identifiable morphologies.

The statistical validity of the observations made for the four largest size ranges (+40, +34, +28, +22) on an individual basis is poor due to the small number of stones in these size ranges. In addition, reporting the detailed analysis of each size range would prove to be cumbersome. For these reasons, several size ranges with particular features have been grouped together and the characteristics of the sub-populations in the diamonds are reported.

a) +22* Size Range

Octahedra constitute 13.3 % of the +22* (+40, +34, +28 and +22 combined) size range (n = 284). Macles comprise 3.6% and polycrystalline diamonds 17.6% of this size range (Figure 4.3). The ratio between octahedra and dodecahedra (O/D ratio) for the +22* diamonds is 0.76 (Figure 4.4). The OMD/IP ratio of these diamonds is 0.51 (Figure 4.5). Within the +22* size range there is a general decrease in polycrystalline diamond content with decrease in size. In contrast, there is a general increase from 12.5% to 51.2% in the

irregular diamond population with a decrease in size. The percentage of macles in this size range peaks to a maximum in the +28 size range (8.4%) and then rapidly decreases to 1.3% for the +22 size diamonds.

b) +17 Size Range

The significant increase in the number of stones in the +17 size range (n = 420; Table 4.2f) and subsequent smaller size ranges over the preceding larger size ranges allows for greater confidence in determining the morphological characteristics of the diamonds in these smaller size ranges. The +17 diamonds are characterised by an O/D = 0.22 and an ODM/IP = 0.74 (Figures 4.4; 4.5). The proportion of macles in this fraction is less than 2%. The percentage of +17 irregular stones (47%) closely approximates the percentage (46%) of irregular stones in Dokolwayo diamonds as a whole. The population of polycrystalline diamonds in the +17 fraction (11%) is significantly in excess of the percentage observed for the respective morphology in the general production sample.

c) $+12^{*}$ Size Range

The most significant feature of the $+12^{*}$ size range (+14 and +12 combined; Table 4.2g, n = 1314) is that it marks a distinct change in the percentage of polycrystalline diamonds present in each individual size range. In all the size ranges larger than $+12^{*}$ the polycrystalline diamond population is in excess of 10%. An additional significant feature is the marked increase of dodecahedra in the $+12^{*}$ diamonds (Figure 4.3). This is clearly reflected in the relationship between the observed number of dodecahedra and octahedra (O/D = 0.14; Figure 4.4). The percentage of macles recorded in this fraction is less than 2% and the ODM/IP = 1.04 (Figure 4.5). There is a slight increase in the O/D ratio and decrease in the OMD/IP ratio with decrease in size within the $+12^{*}$ range.

d) +11 Size Range

A considerably smaller number of diamonds (n = 375; Appendix 4.a) was recovered in the +11 size range when compared to the immediately larger and smaller fractions. This smaller number of stones does not appear to have a major influence on the distribution of the different morphologies present in this size range when compared with the results obtained for the immediately smaller and larger size ranges. The +11 diamonds have an O/D = 0.11 and an ODM/IP = 1.09 which are very similar to the ratios computed for the +14 fraction (Figures 4.4; 4.5). The proportion of polycrystalline diamonds (7%; Figure 4.3) and macles (<2%) in the +11 fraction are also similar to the fractions recorded for these morphologies in the +14 size range.

e) +9 Size Range

The O/D (0.10) and ODM/IP (1.01) of the +9 size range show a slight decrease from the ratios computed for the +11 fraction. There is also a marginal decrease in the proportion of polycrystalline diamonds (n = 679; Figure 4.3) relative to the +11 fraction.

f) +3* Size Range

The largest number of stones (n = 1808; Appendix 4.a) occurred in the +3* size range (+6, +3). Significant deviations in the relationship between size and morphology relative to larger size ranges is exhibited in this size range. Both the O/D and ODM/IP ratios (0.06 and 0.87 respectively; Figures 4.4; 4.5) decrease markedly when compared with the results obtained from the next four larger fractions. There is also a noticeable decrease in the populations of both the polycrystalline and octahedral morphologies (Figure 4.3). There is no significant change in the proportion of the macles (<2%) in this size range relative to the -28 sizes. Within the group there is a decrease in the O/D ratio, but a reversal in the ODM/IP ratio.

III) Size - Colour Relationship

The Group II sample of Dokolwayo diamonds that was used to investigate the relationship between size and morphology was also used to determine the relationship between size and colour for the Dokolwayo diamond production. Both the total sample (n = 4880) as well as individual size ranges were investigated. Seven colours (i.e. colourless, grey, brown, yellow, green, black and orange) were identified. Additional colours, e.g. pink and lilac, have also been observed in the run of mine production, but were absent from the sample used in this study. This suggests that the colours not recorded in this evaluation must be rare. The results of this investigation are presented in Table 4.2 and Figure 4.6.

The majority of the diamonds (68.0%) from this sample of general Dokolwayo production is colourless (Appendix 4.a). The proportions of grey and brown diamonds are very similar (13.8% and 12.9% respectively; Figure 4.6). Yellow diamond content is approximately 4%; black (0.7%) and green (0.3%) diamonds are minor, orange diamonds (<0.1%) are rare.

With the exception of the +11 size range there is a general increase in the proportion of colourless stones with a decrease in size range for all the -40 diamonds (Figure 4.7). The +11 size range has at least 5% fewer colourless stones than the size ranges immediately smaller or larger. Plotting the percentage of colourless stones against size for the -40 size ranges initially defines three distinct trends defined by the +34 to +22, +17, +14 to +12, and -12 size ranges. However, if the $+22^{*}$ size range group is considered, then only two distinct trends are defined (Figure 4.7).

In general, there is a constant decrease in the proportion of grey stones with a decrease in size range. The +11 size range is an exception to this observation in that it contains at

least 6% more grey stones compared to the adjacent size ranges (Figure 4.7). The smallest percentage of grey stones is in the +3 size range.

Considering the +22* size range as a single size range, brown stones comprise between 11.0% and 15.7% of the total number of diamonds in all size ranges. However, within the +22* size range alone, large fluctuations occur. The +3 size range has the smallest proportion of brown diamonds.

There is an nearly constant decrease in the percentage of yellow stones from +34 (14.3%) to +11 (1.9%). The percentage of yellow stones in the -11 size ranges appears to plot as a separate population (Figure 4.7).

Green diamonds were absent from most size ranges, and concentrate a very minor component (0.3%) of the diamond population at Dokolwayo. However, the occurrence of green diamonds in the +34 and +3 size ranges suggest that these diamonds span the entire size range.

No black diamonds were recorded in the +40, +22 and +11 size fractions. Black diamonds are marginally more common than green diamonds, but are also a minor component of the Dokolwayo diamond population as a whole.

In the entire sample of 4880 stones only two orange diamonds (one in +11 and one in +6) were recorded. These two diamonds were recovered from the same area in the diatreme. A regular inspection of Dokolwayo production confirmed that orange is a rare colour.

IV) Colour - Morphology Relationship

The recorded data provided the opportunity to determine the relationship between colour and morphology. Due to the small number or total absence of diamonds in some of the colour groups the study of this relationship has been restricted to the four most dominant colour groups, i.e. colourless, grey, brown and yellow. This has been done for the Group II diamonds. The results are tabulated in Appendix 4.a and are presented graphically in Figures 4.8 and 4.9. Since macles comprise less than 2% of the total population this diamond form will not be commented on although the results are presented graphically.

In all the morphologies colourless diamonds are the most common. Grey diamonds are the second most common colour in dodecahedra, irregular and polycrystalline diamonds. In the octahedral populations brown is the second most common colour. In all morphologies, except octahedra, yellow is the least common of the four colours considered (Figure 4.8).

The majority of the colourless diamonds (45%) are dodecahedra. The second most common morphology amongst the colourless diamonds is the irregular population. Octahedra and polycrystalline diamonds are present in approximately equal amounts (5%). Less than 2% of the grey diamonds are octahedra. The majority (53%) of the grey diamonds are classified as irregular in shape. This particular colour is relatively more abundant in polycrystalline diamonds (12%) than any other colour. Approximately 32% of the grey diamonds are dodecahedra.

Irregular morphologies are slightly more common amongst the brown diamonds (54%) than in the grey diamonds (53%). There are relatively more octahedra and polycrystalline diamonds amongst the brown diamonds than in the colourless population.

Yellow diamonds are characterised by having the biggest proportion of octahedra ($>10\%$) relative to the other colour groups. It was found that yellow diamonds are more commonly polycrystalline than the brown or the colourless diamonds. More than 35% of the yellow diamonds are dodecahedra (Figure 4.9).

Colourless octahedra generally decrease with a decrease in size range (Figure 4.10). Colourless polycrystalline diamonds show a distinct bimodal distribution (Figure 4.11). There is a general decrease in colourless polycrystalline diamonds from +34 to +14 while the -17 size ranges appear to be a separate population.

All the +22* size ranges have <20% grey dodecahedra. In contrast, all the -22 size ranges have >25% grey dodecahedra. There is a more than 5% increase in grey dodecahedra between the +9 size diamonds and the two smaller size ranges (Figure 4.12). Grey polycrystalline diamonds generally decrease in significance from +40 to +11. There is a very marked increase in grey polycrystalline diamond content in the -11 size ranges compared with the +11 size range (Figure 4.13).

The most significant morphological feature amongst the brown diamonds is the a sharp increase in smaller dodecahedra, from < 15% for the +22* diamonds to >20% for the -22 size ranges (Figure 4.14).

Yellow is most characteristic of dodecahedral diamonds, and a distinct increase occurs in the +14, +12 and -11 size ranges (Figure 4.15). The distribution of yellow polycrystalline diamonds is erratic (Figure 4.16).

DISCUSSION

The physical features of diamonds are a record of the physiochemical conditions during and subsequent to crystallization. A study of the relationships amongst size, mass, colour and morphology of the Dokolwayo diamond population suggests that the diamonds may be divided into three distinct sub-populations. These three sub-populations can be correlated to a lesser or greater extent with size, i.e. the +22, -22+12 and -11 size ranges. The +11

size range is anomalous in various significant features and may represent a fourth sub-population.

Octahedra constitute 13% of the $+22^{*}$ population (Figure 4.3). This is in contrast to all the size ranges smaller than +22 in which the octahedral population represents less than 10%. Similarly, the proportion of macles (3.5%) and polycrystalline diamonds (18%; Figure 4.3) in the $+22^{*}$ group is significantly higher than in the smaller sizes (<2% and <9% respectively). The O/D ratio in the $+22^{*}$ range at 0.76 is also significantly higher than observed for the smaller fractions (O/D < 0.25; Figure 4.4). However, the OMD/IP (0.51) of the $+22^{*}$ is markedly lower (Figure 4.5).

A closer inspection of the $+22^{*}$ size ranges shows that only 20% of the $+22^{*}$ macles are found in the +22 size range which constitutes over 55% of the $+22^{*}$ population. The proportion of macles in the +22 size range is similar to the percentage of macles observed in the -22 size ranges. There is a regular marked increase in the irregular diamond populations from the +34 to the +22 size ranges. The irregular diamond population in the size ranges greater than 2mm reaches a peak in the +22 size range (Figure 4.3). There is an almost constant decrease in the percentage of polycrystalline diamonds present in individual size ranges from the +40 to the +11 size range with the largest proportional decrease from the +28 to the +22 size range (22% and 14% respectively; Figure 4.3).

A comparison of the O/D, OMD/IP ratios and proportion of polycrystalline diamonds in the Group II diamond population from Dokolwayo (Figure 4.3, 4.4, 4.5) shows major changes between the $+22^{*}$, $+12^{*}$ and $+3^{*}$ size ranges. It has been demonstrated by Moore and Lang (1974) and Robinson (1979) that rounded dodecahedral diamonds are usually resorbed octahedra. The presence of dodecahedra in the Dokolwayo diamond population is thus indicative of a carbon corrosive environment. Whether the diamonds were resorbed in situ prior to being in contact with the kimberlite (assuming a xenocrystic diamond origin) or by the kimberlite and/or its precursor fluids itself is speculative. What

is of relevance to this discussion is that the proportion of dodecahedra increase with a decrease in size range. In contrast, octahedra decrease in proportion to other morphologies with a decrease in size, but not necessarily with a change in stone colour. This is clearly reflected in the O/D ratio of the different size ranges (Figure 4.4). The observed trend may be due to the smaller stones experiencing a greater degree of resorption than the larger stones as a result of their increased surface area per unit mass.

On site observations of a larger population of diamonds than reported on in this study have indicated that the +40 diamonds are characterised by a sub-population of poor quality, highly fractured stones. Fragments of these diamonds are predominantly present in the $+22^{*}$ size ranges. They are generally colourless or grey (predominant) in colour. They are also characterised by "Tanganyika naats", a combination of plastic deformation planes giving rise to a ribbed and tartan pattern of lamination lines on the diamond. The diamonds are irregular in shape, but commonly are flat, and their surface textures suggest intense resorption. These "Tanganyika diamonds" have not been described from other southern African diamond populations. The high proportion of irregular gray stones in the $+22^{*}$ group (34.6%) may be largely attributed to such diamonds. It is tentatively suggested that this sub-population of diamonds consists predominantly of large diamonds and that their representation in the -40 sizes is mainly due to disaggregation of these diamonds during pressure release while being transported from the mantle or at the time of eruptive emplacement of the kimberlite. Unfortunately, due to their size, these diamonds were not available for carbon isotopic or mineral inclusion studies to characterize them with respect to a chemical environment, e.g. eclogitic or peridotitic, or carbon source. Nevertheless, based on their physical appearance, they do contribute to defining the $+22^{*}$ diamonds. It should be noted that they do not contribute to the number of octahedra in the $+22^{*}$ size range. This implies that if these "Tanganyika diamonds" were not present in the $+22^{*}$ range then the proportion of octahedra present would be even more enhanced with respect to the octahedra in the -22 size ranges and the resultant O/D and OMD/IP ratios would also be enhanced.

It is concluded that the +22* diamonds owe their character to a combination of at least two populations of diamonds. The one population ("Tanganyika diamonds") has a hitherto undetermined primary environmental history, but has experienced a post-crystallization history of intense deformation and resorption. The second population, characterised by a large proportion of octahedra, has experienced very little apparent deformation and resorption. This population may be part of a larger population which is primarily represented in the smaller size ranges.

A number of significant differences in diamond colour occur in the different size ranges. The proportion of colourless stones is generally less than 50% in the size ranges above +22. The +22* size range have a colourless diamond content of 48.9%. This size range is also characterised by higher grey diamond content (Figure 4.7) and a lower content of yellow diamonds (Figure 4.7) than found in the -22 size ranges.

In the -22 sizes the proportions of colourless diamonds generally increase from 58% in the +17 range to 78% for the +3 range. However, a major decrease in colourless stones occurs in the +11 range. This decrease is concomitant with a significant increase in grey and brown stones and a sharp decrease in yellow diamonds. In all the size ranges above +9 there are more grey stones than brown stones, whereas in the -11 size ranges the reverse is true (Figure 4.7). The -11 diamonds have higher proportions of colourless and decreasing proportions of grey and brown stones with decreasing size, whereas yellow stones remain uniformly low.

It appears that the diamond population of the Dokolwayo kimberlite may be divided into four distinct groups based on the relationship between colour and size. These groups may be broadly defined as the +22*, the -22 to +12, the +11, and the -11 size range groups. The +11 size range appears to have anomalous diamond colour distributions with respect to the size ranges immediately above and below it.

Several interesting trends were observed in the relationship between colour and morphology in the different size ranges. Polycrystalline diamonds commonly predominate over dodecahedral diamonds in all four colours in the four largest size ranges. The relationship between colour and morphology for the $+22^{*}$ range indicates that polycrystalline diamonds are more common than dodecahedra amongst the grey and brown diamonds (Figures 4.8 and 4.9). In none of the size ranges that comprise the $+22^{*}$ range do the number of dodecahedra exceed 30% in any of the four diamond colours.

The largest size range in which dodecahedra exceed 30% of the total population in any of the four colours is the +17 range. In the size ranges smaller than +17 the general pattern is for dodecahedra to be in excess of 30% in all colours. The two exceptions are yellow in +11 and grey in +9. Amongst the dominant colourless diamonds, there is a tendency for octahedra to decrease relative to the other morphologies with decreasing size. In the -17 size ranges the percentage of brown octahedra and polycrystalline diamonds also tends to decrease with decreasing size range.

Harris et al. (1975) have discussed the role of nitrogen aggregation in the determination of colour in diamonds. Nitrogen-free diamonds (Type IIa, Bruton, 1970) or diamonds with small impurities of platelet nitrogen (Type Ia) are essentially colourless. Small aggregates of nitrogen associated with platelet nitrogen may result in pale yellow or brown colours occur in Type Ia diamonds, but if nitrogen substitutes for for carbon in the diamond lattice of a Type Ia diamond, canary-yellow or amber diamonds result (the so-called Type Ib diamonds; Kaiser and Bond, 1959; Clark, 1965; Harris et al., 1975). The brown colour of diamonds may also be due to small concentrations of amorphous or graphitic carbon in the diamond lattice (Clark et al., 1956), commonly associated with deformation lamellae. Harris et al. (1975, 1979) have observed a predominance of yellow diamonds over brown diamonds in several southern African kimberlites. However, the relationship between these two colour groups at Dokolwayo tends to be the reverse and brown diamonds are

predominant. Unfortunately, it is not possible at present to distinguish between Dokolwayo brown diamonds that owe their colour to nitrogen aggregation or amorphous carbon and this relationship cannot be fully evaluated. There is a tendency for the combined yellow and brown diamond total to be in excess of 20% in all the +17 size ranges while being <20% in the -17 sizes. The smallest size range (+3) has the smallest percentage of brown and yellow diamonds. This may be due to a dominant Type I growth environment for the larger diamonds and an increasing importance of Type II growth environment for the smaller diamonds. However, a more detailed evaluation of these trends will only be possible once the ratio of Type I and Type II diamonds in the colourless diamond population has been established. Such a study is envisaged.

The percentage of the total mass of the Dokolwayo diamonds represented by the +11 size range is distinctly less than the adjacent size ranges (Figure 4.1). The +11 size range is also characterised by an anomalously high percentage of yellow polycrystalline and a small percentage of grey polycrystalline diamonds (Figures 4.13 and 4.16). It would therefore seem that the diamonds in the +11 size range represent a population of diamonds not predominant in either the smaller or the larger sizes and serves as a marker between all the +12 and the -11 diamonds. The +12 and -11 diamonds are also distinguished from each other by lower O/D ratios, proportionally fewer yellow diamonds and more colourless diamonds in the -11 ranges than in the larger size ranges. The physical features of the -11 diamonds suggest that they have been resorbed to a greater degree than the larger diamonds. In addition, the decreased proportion of yellow diamonds in this smaller size range suggests that they may have experienced a very different thermal history and hence would have a different rate of nitrogen aggregation than the larger diamonds. Alternatively, the primary crystallization environment of these -11 diamonds was depleted in nitrogen relative to the larger sized diamonds. It should be noted that the majority of the diamonds selected for diamond inclusion and carbon isotope studies were selected from the -12 range of diamonds. At least two distinct parageneses (eclogitic and peridotitic) were recognized amongst these diamonds. The peridotitic paragenesis predominates (Chapter 5).

It is possible that the -11 population and the +12 population may be related to different parageneses. However, inclusion and carbon isotope data on the +12 population will have to be obtained to establish the validity of this suggestion.

The differences in the physical properties of the $+22^{*}$ and -11 diamonds suggest that these two groups of diamonds are, in the main, unrelated. Their distinct differences in size and hence volume of carbon required may indicate a major diversity in elemental carbon supply at the point of crystallization in the mantle or early versus late nucleation in a crystallization continuum.

In conclusion, a detailed study of the physical features of the Dokolwayo diamonds has shown that the diamond population as a whole consists of a number of complex sub-populations which have experienced different crystallization histories in possibly different chemical environments (e.g. different concentrations of nitrogen, elemental carbon supply) and which experienced different post crystallization histories (e.g. deformation and resorption). In a southern African context, the Dokolwayo diamonds are distinguished from other southern African diamond populations (Harris et al., 1975, 1979; Robinson, 1979) by having a predominance of brown diamonds versus yellow stones. This colour characteristic, together with the "Tanganyika diamonds" suggest that the Dokolwayo diamonds may be a unique population.

TABLE 4.1

PIERRE SIEVE SIZES

MESH	MILLIMETRES
40	8.55
34	7.35
28	6.10
22	4.90
17	4.00
16	3.75
15	3.50
14	3.30
13	3.10
12	2.85
11	2.65
9	2.25
6	1.60
3	1.25

Table 4.1 Pierre sieve sizes in millimetres.

CHAPTER 4 - FIGURE CAPTIONS

FIGURE 4.1

Histogram showing the relationship between diamond mass and Pierre Sieve size in (a) general production from the Dokolwayo kimberlite and (b) production from a single hypabyssal phase, the green micaceous kimberlite, within the diatreme.

FIGURE 4.2

Pie diagram of the distribution of major morphologies for the general Dokolwayo diamond production.

FIGURE 4.3

Plot illustrating the relationship between Pierre Sieve size and diamond morphology of the Dokolwayo production.

FIGURE 4.4

Plot illustrating the variation in the ratio between octahedra and dodecahedra (the O/D ratio) in the different Pierre Sieve size ranges for the Dokolwayo diamond production.

FIGURE 4.5

Plot showing the relationship between the Pierre Sieve size and the [Octahedra + Dodecahedra + Macle]/[Irregulars + Polycrystallines] i.e. (OMD/IP) for the Dokolwayo diamonds.

FIGURE 4.6

Pie diagram of the distribution of major colours for the general Dokolwayo diamond production.

FIGURE 4.7

Plot showing the relationship between Pierre Sieve size and the percentage of colourless, grey, brown and yellow stones of the Dokolwayo diamond production.

FIGURE 4.8

Plot showing the distribution of diamond colours for the major morphologies of the Dokolwayo diamonds.

FIGURE 4.9

Plot showing the distribution of diamond morphologies for the major colours of the Dokolwayo diamonds.

FIGURE 4.10

Plot illustrating the variation in percentage colourless octahedra in the different size ranges of the Dokolwayo diamonds.

FIGURE 4.11

Plot illustrating the variation in percentage colourless polcrystalline diamonds in the different size ranges of the Dokolwayo production.

FIGURE 4.12

Plot illustrating the variation in percentage grey dodecahedra in the different size ranges of the Dokolwayo diamonds.

FIGURE 4.13

Plot illustrating the variation in percentage grey polycrystalline diamonds in the different size ranges of the Dokolwayo production.

FIGURE 4.14

Plot illustrating the variation in percentage brown dodecahedra in the different size ranges of the Dokolwayo diamonds.

FIGURE 4.15

Plot illustrating the variation in percentage yellow dodecahedra in the different size ranges of the Dokolwayo diamonds.

FIGURE 4.16

Plot illustrating the variation in percentage yellow polycrystalline diamonds in the different size ranges of the Dokolwayo production.

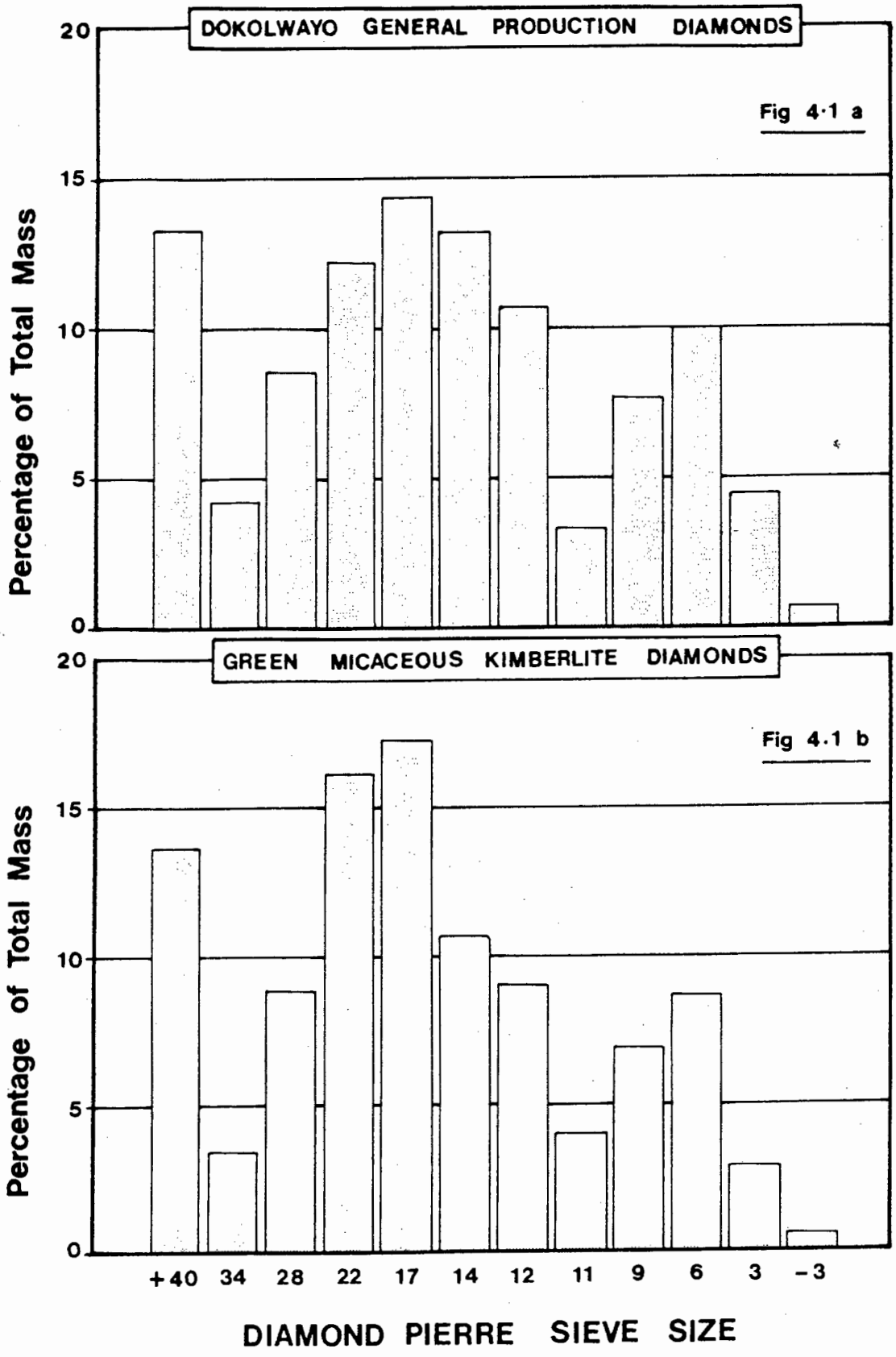
DOKOLWAYO GENERAL PRODUCTION DIAMONDS
Fig 4·1 a
Percentage of Total Mass
20
15
10
5
0
GREEN MICACEOUS KIMBERLITE DIAMONDS
Fig 4.1 b
Percentage of Total Mass
20
15
10
5
0
+40 34 28 22 17 14 12 11 9 6 3 -3
DIAMOND PIERRE SIEVE SIZE

DOKOLWAYO DIAMONDS
TOTAL POPULATION MORPHOLOGY

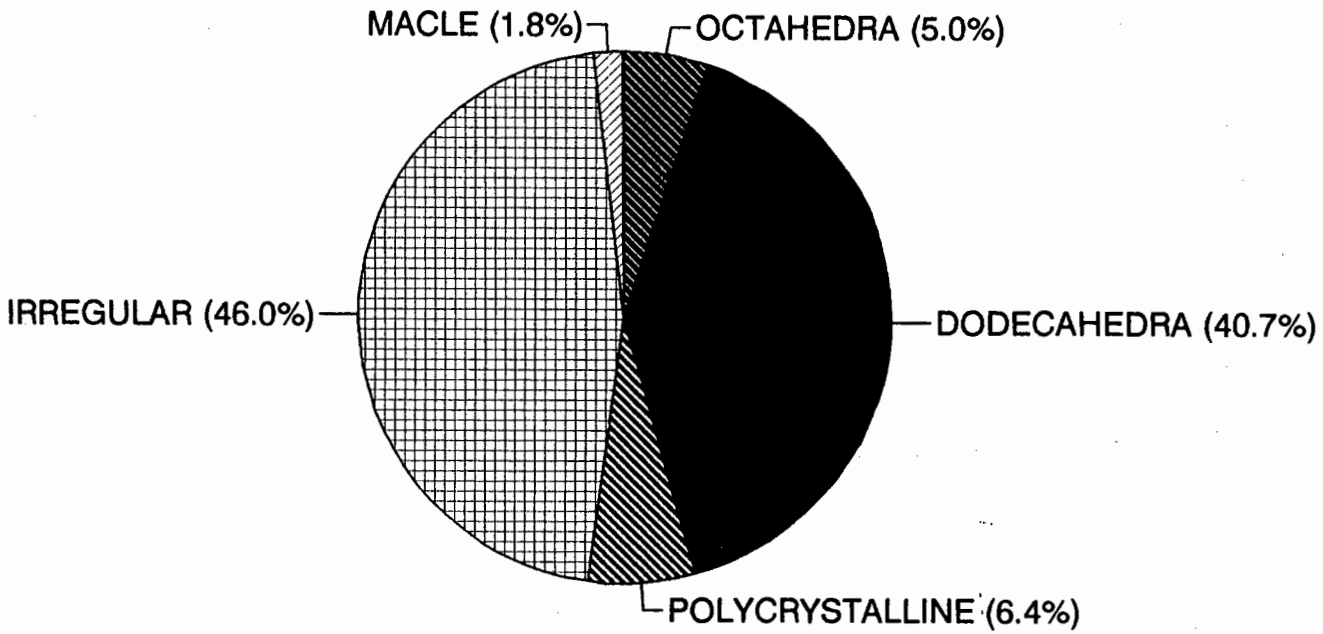

FIGURE 4.2

DOKOLWAYO DIAMONDS
MORPHOLOGY vs SIZE RELATIONSHIP

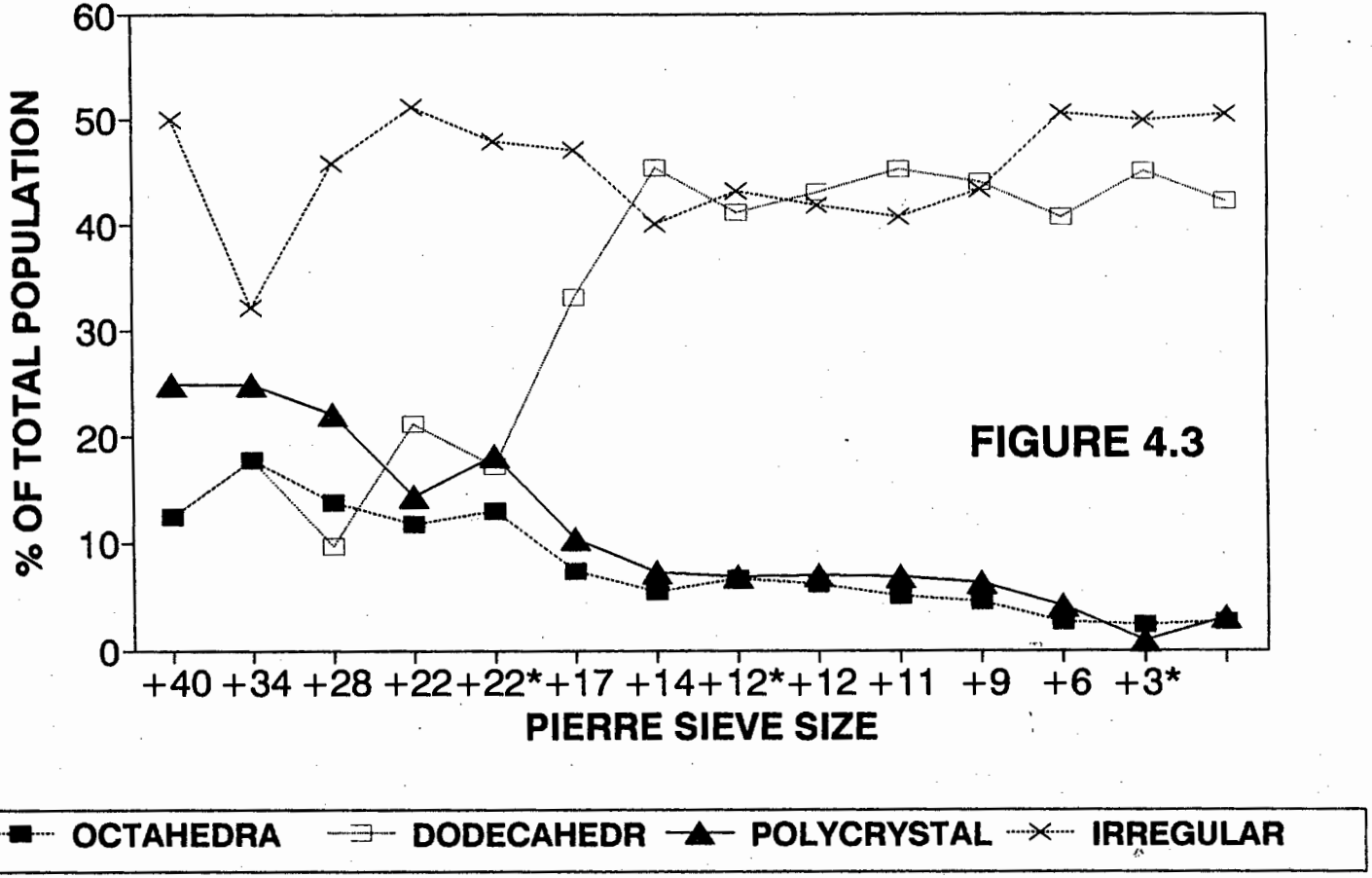

FIGURE 4.3

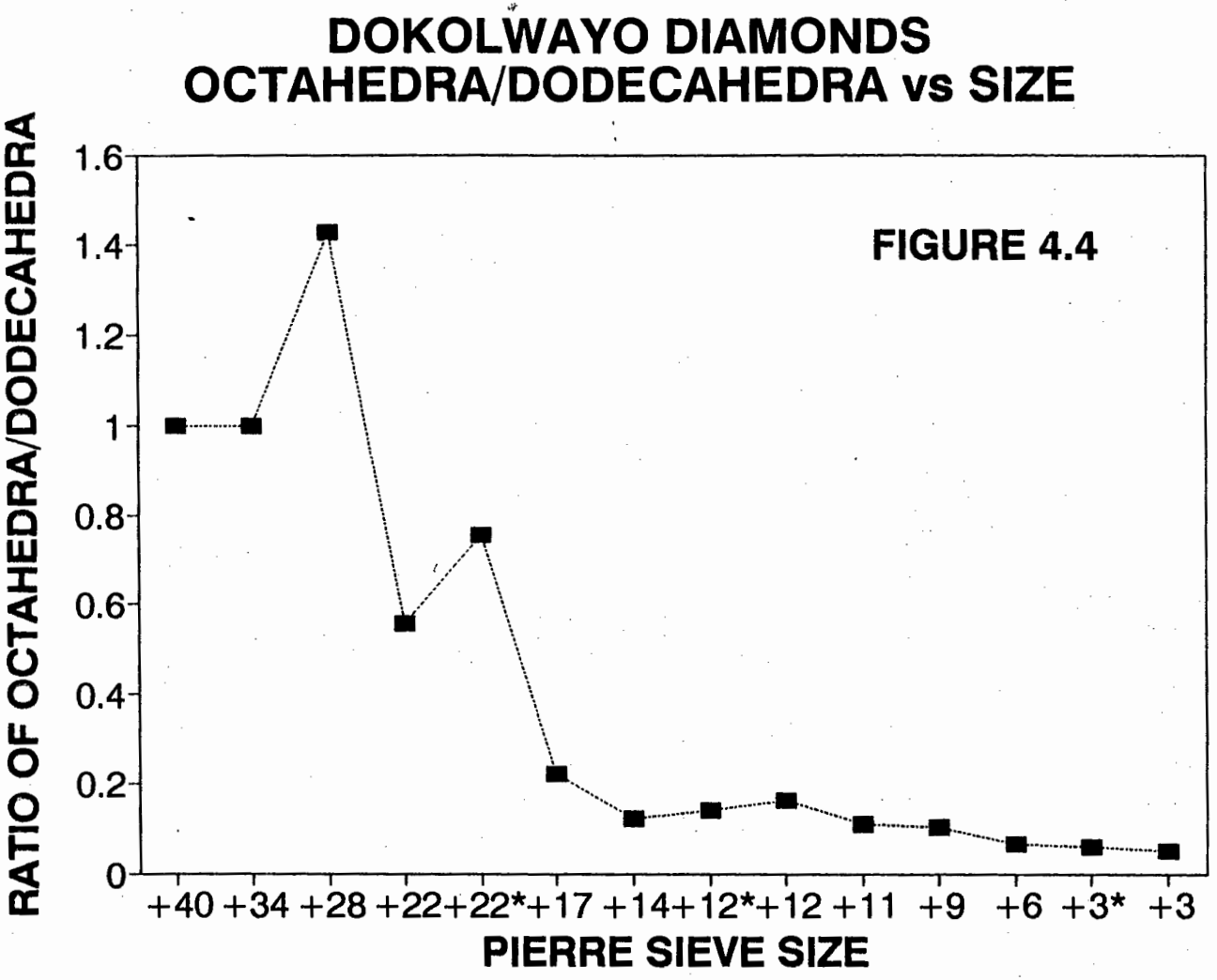
DOKOLWAYO DIAMONDS
OCTAHEDRA/DODECAHEDRA vs SIZE
FIGURE 4.4
RATIO OF OCTAHEDRA/DODECAHEDRA
1.6
1.4
1.2
1
0.8
0.6
0.4
0.2
0
+40 +34 +28 +22 +22* +17 +14 +12* +12 +11 +9 +6 +3* +3
PIERRE SIEVE SIZE

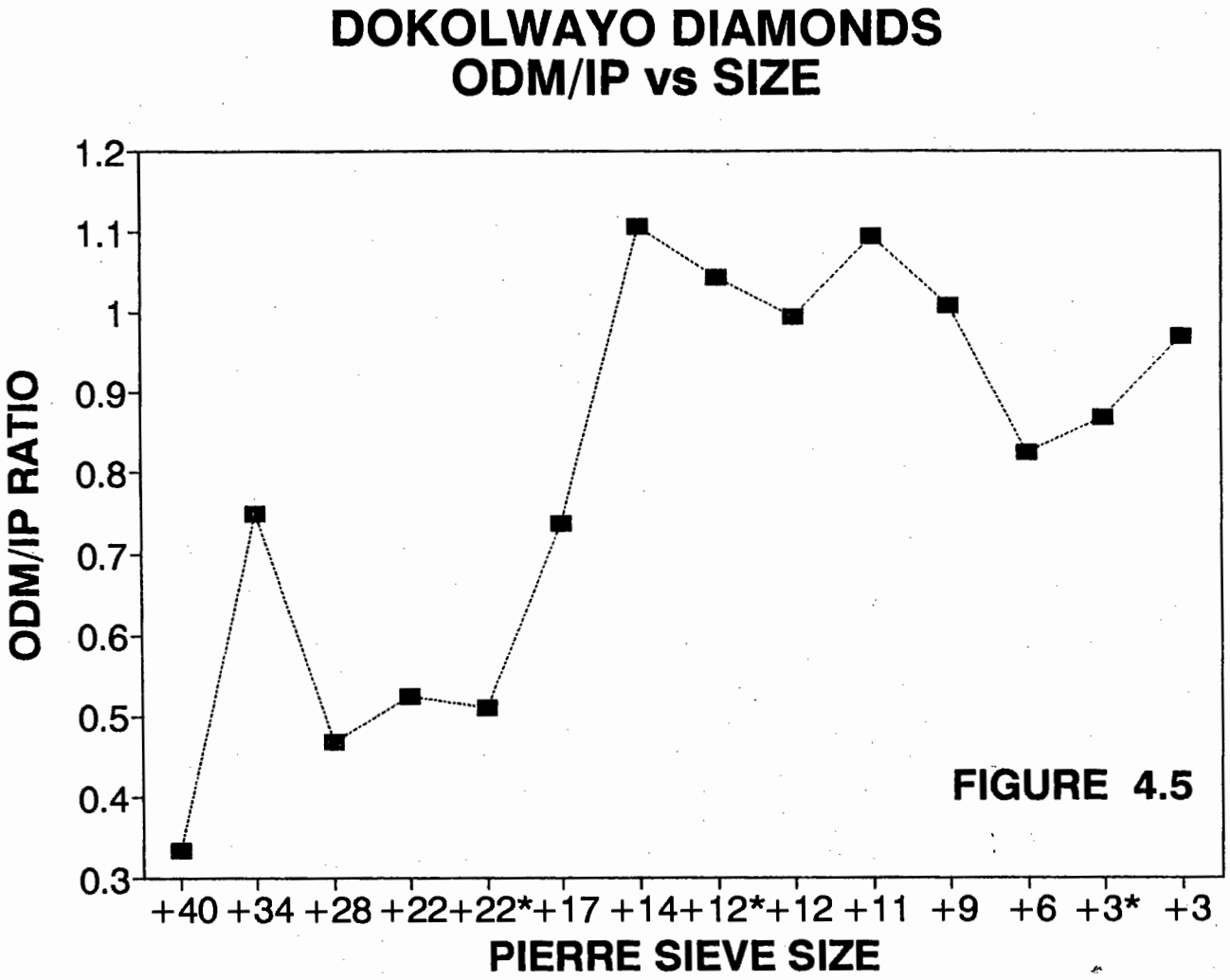
DOKOLWAYO DIAMONDS
ODM/IP vs SIZE
ODM/IP RATIO
1.2
1.1
1
0.9
0.8
0.7
0.6
0.5
0.4
0.3
+40 +34 +28 +22 +22* +17 +14 +12* +12 +11 +9 +6 +3* +3
PIERRE SIEVE SIZE

FIGURE 4.5

DOKOLWAYO DIAMONDS
TOTAL POPULATION COLOUR DISTRIBUTION

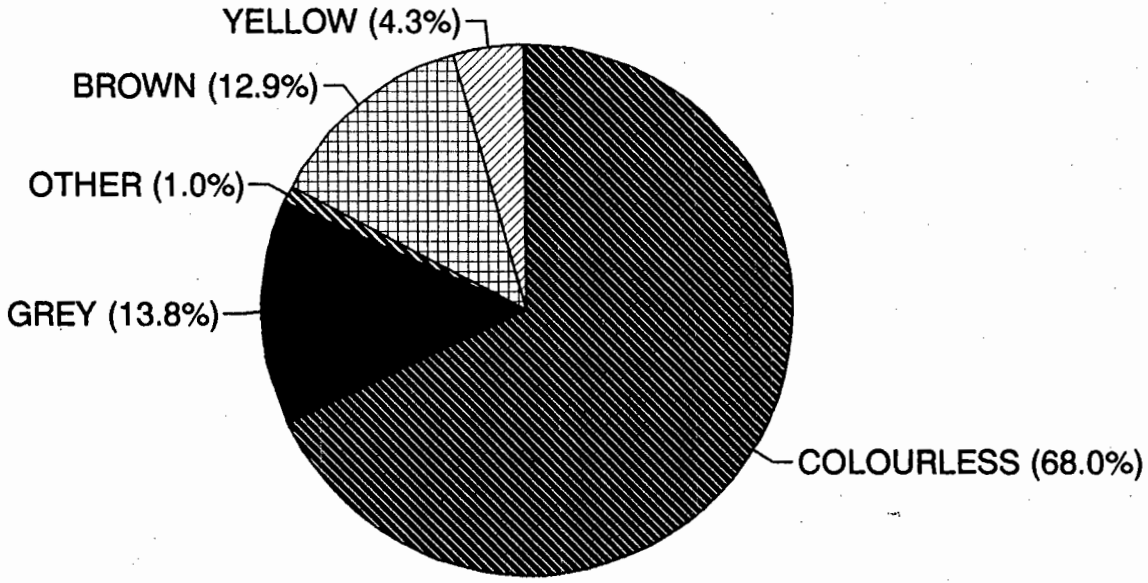

FIGURE 4.6

DOKOLWAYO DIAMONDS
COLOUR vs SIZE RELATIONSHIP

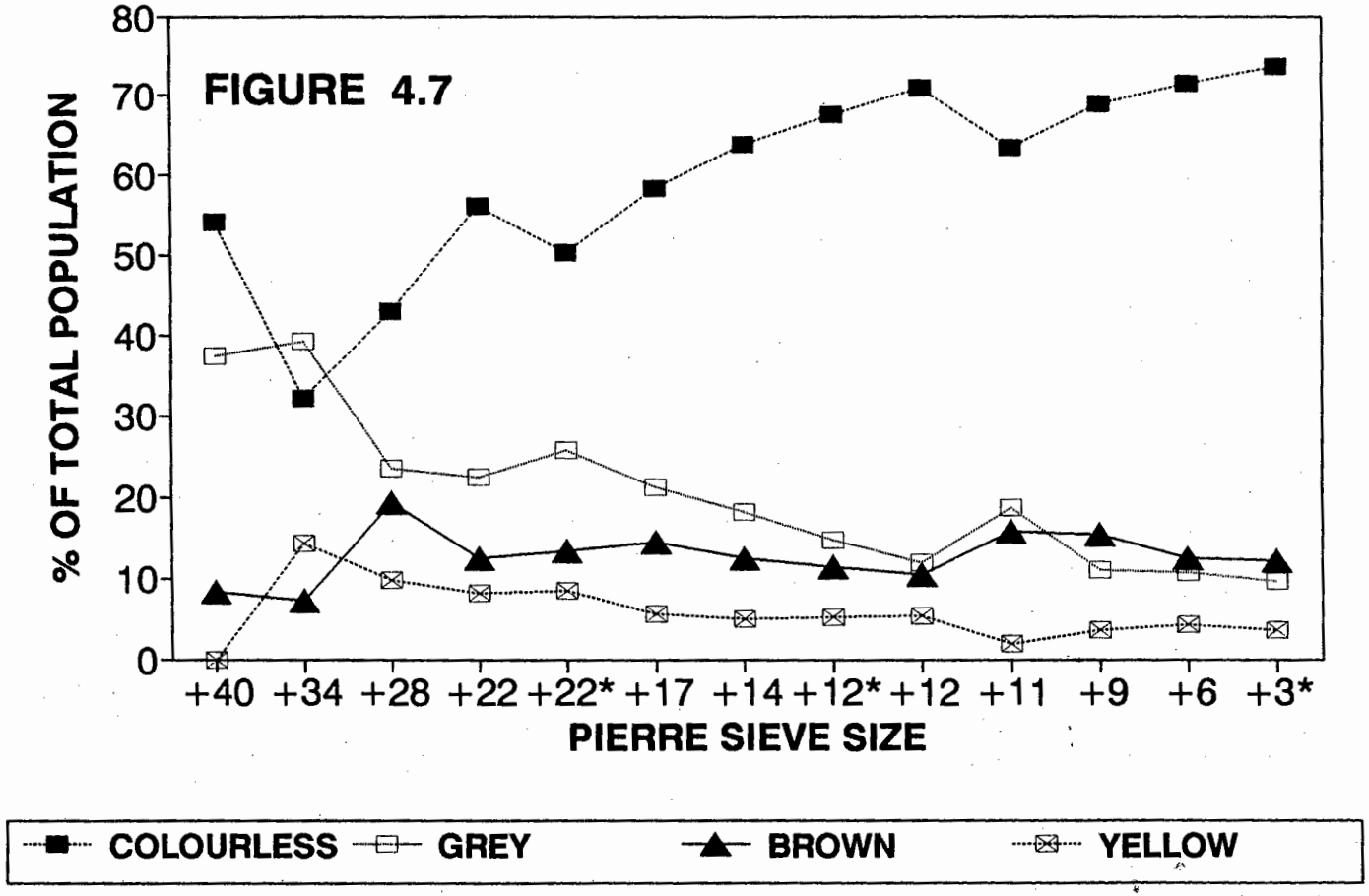

DOKOLWAYO DIAMONDS
MORPHOLOGY VS COLOUR

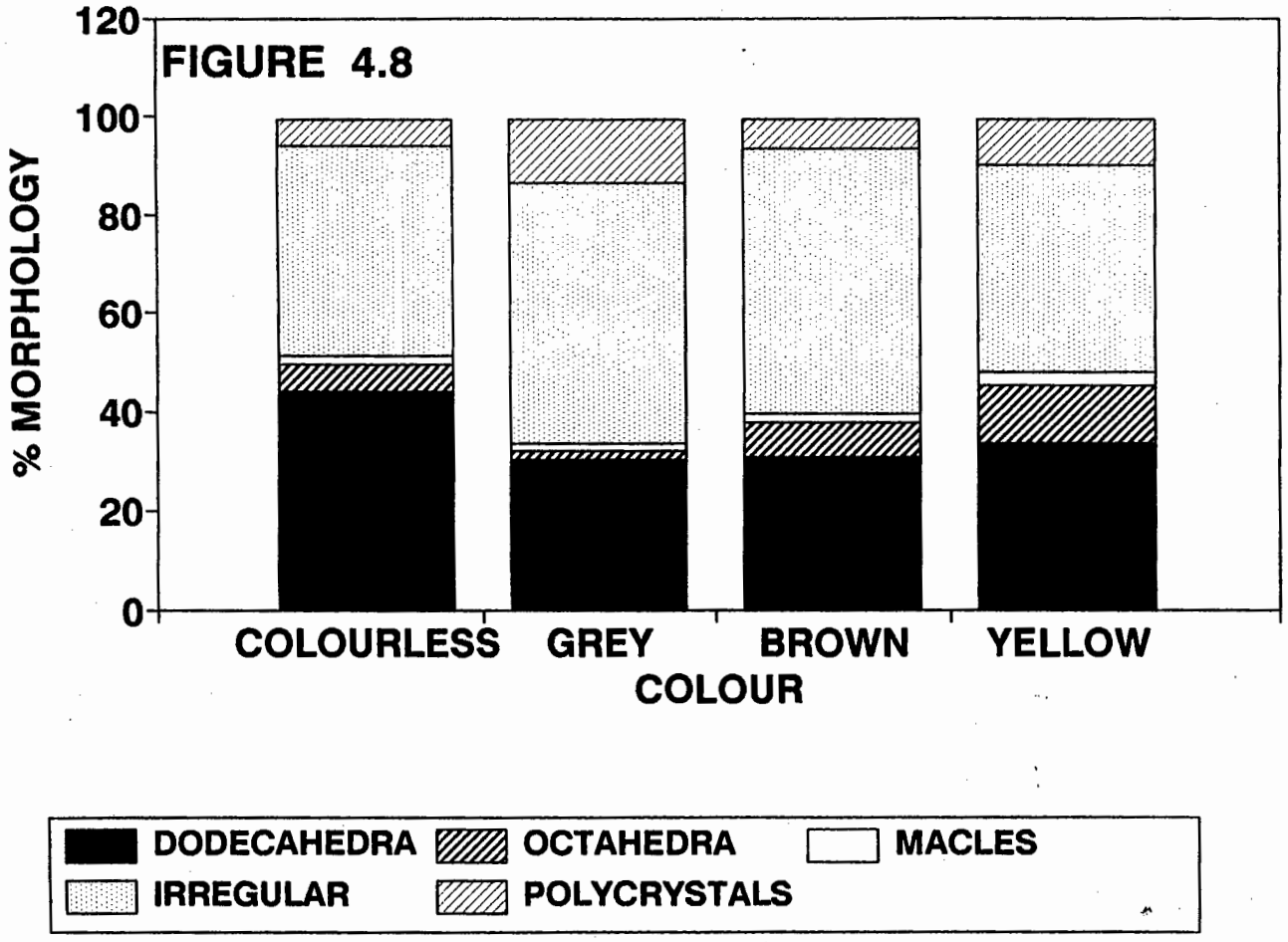

DOKOLWAYO DIAMONDS
COLOUR DISTRIBUTION vs MORPHOLOGY

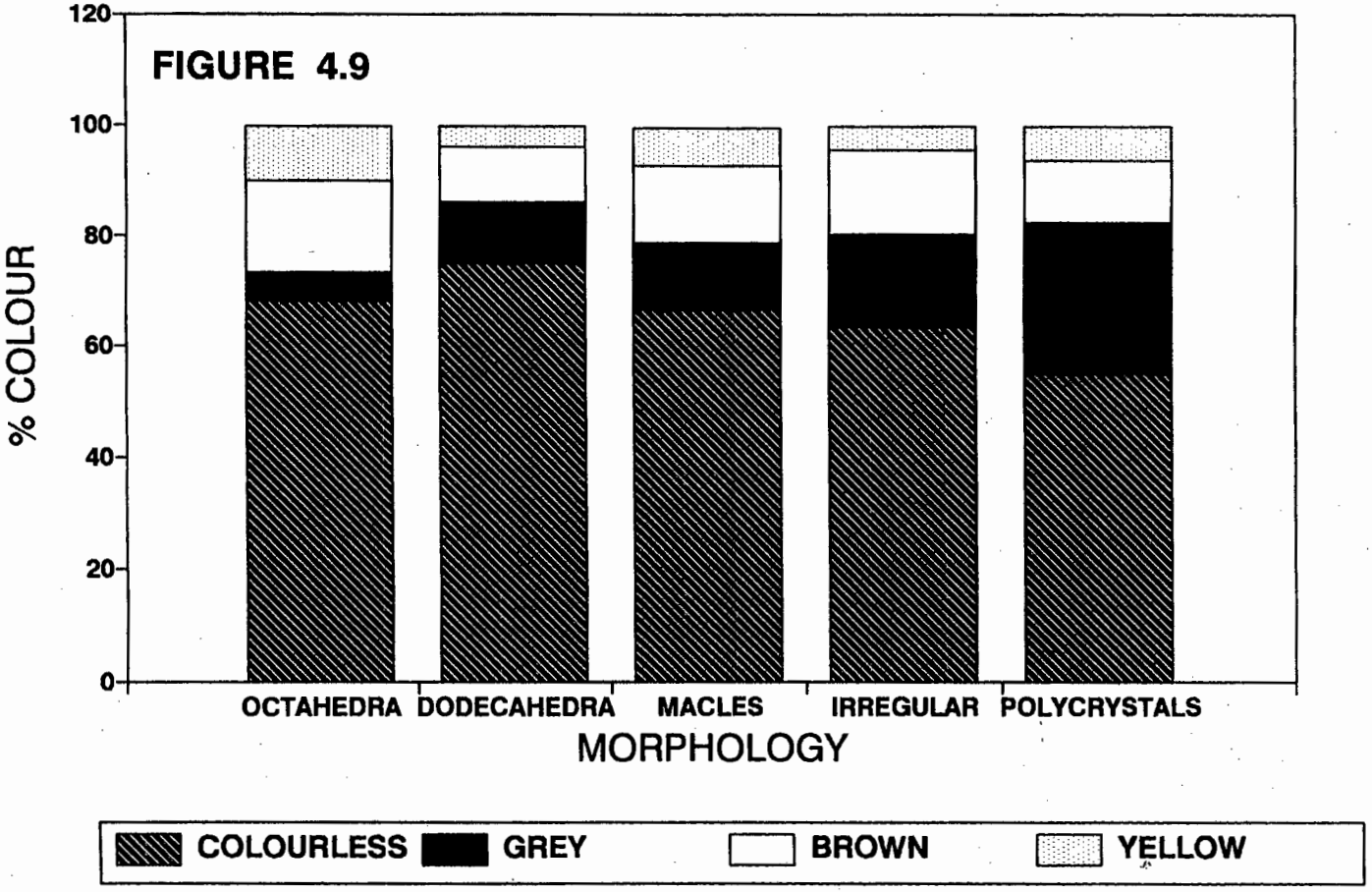

DOKOLWAYO DIAMONDS
COLOURLESS OCTAHEDRA vs SIZE

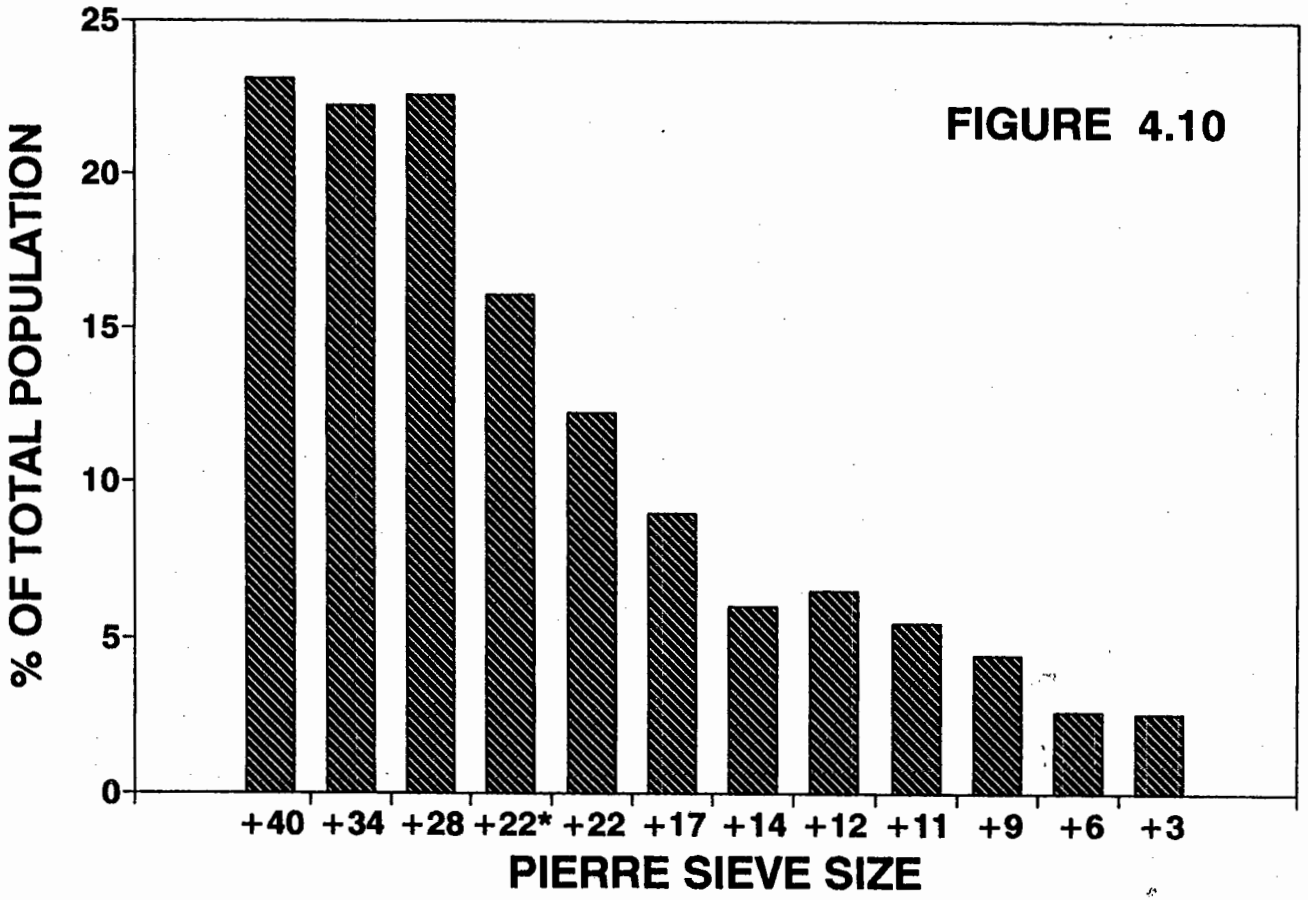

FIGURE 4.10

DOKOLWAYO DIAMONDS
COLOURLESS POLYCRYSTALS vs SIZE

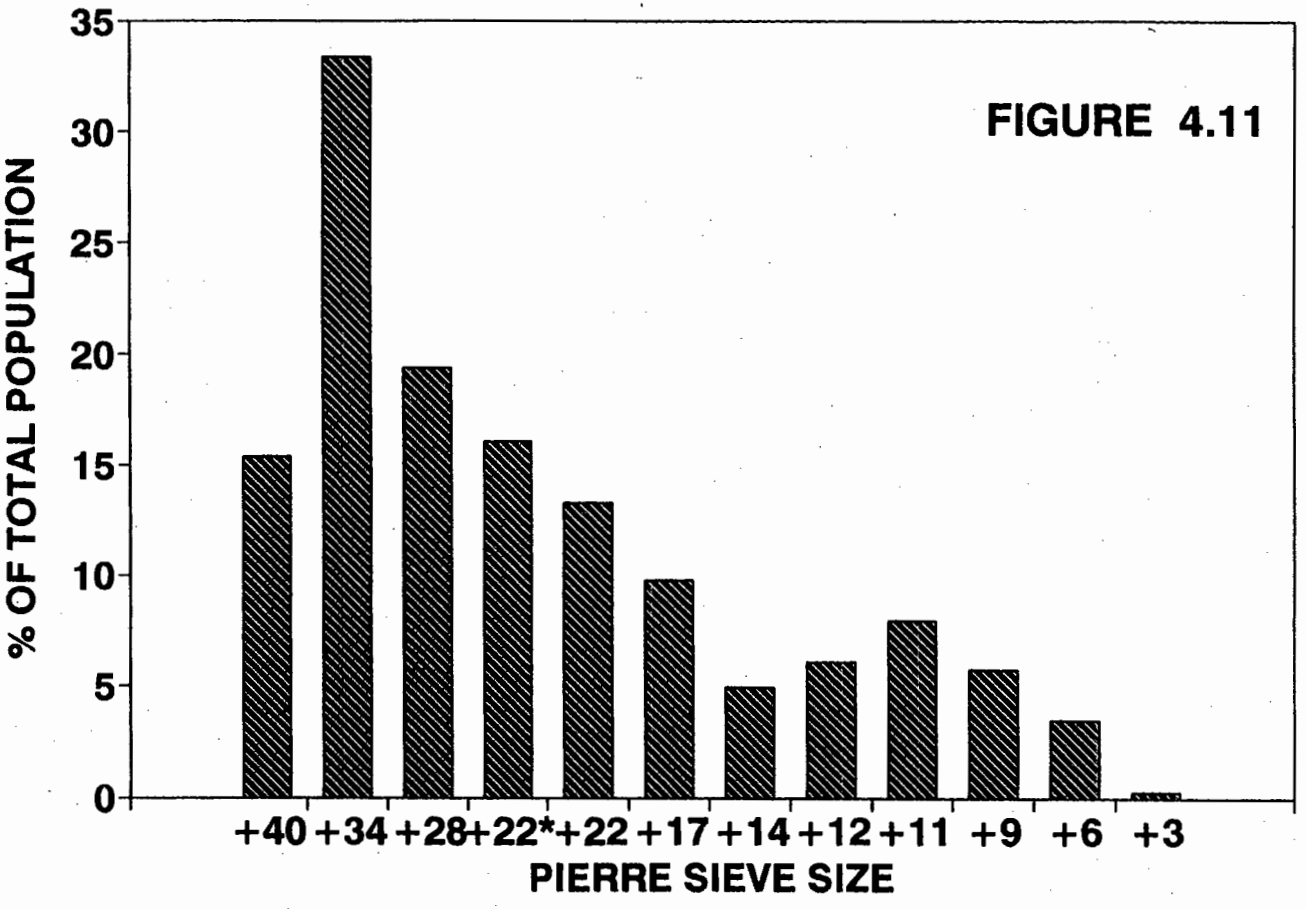

FIGURE 4.11

DOKOLWAYO DIAMONDS
GREY DODECAHEDRA vs SIZE

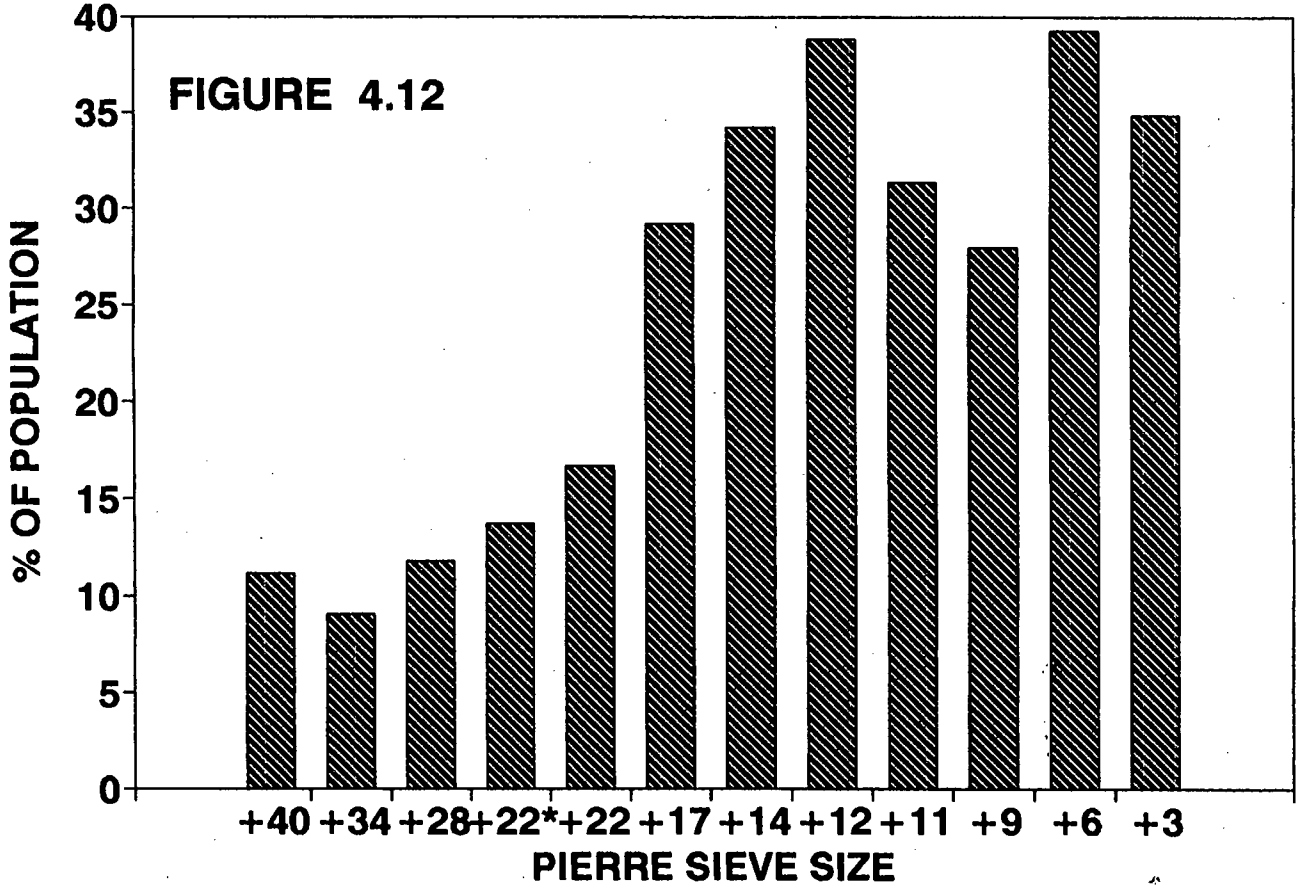

DOKOLWAYO DIAMONDS
GREY POLYCRYSTALS vs SIZE

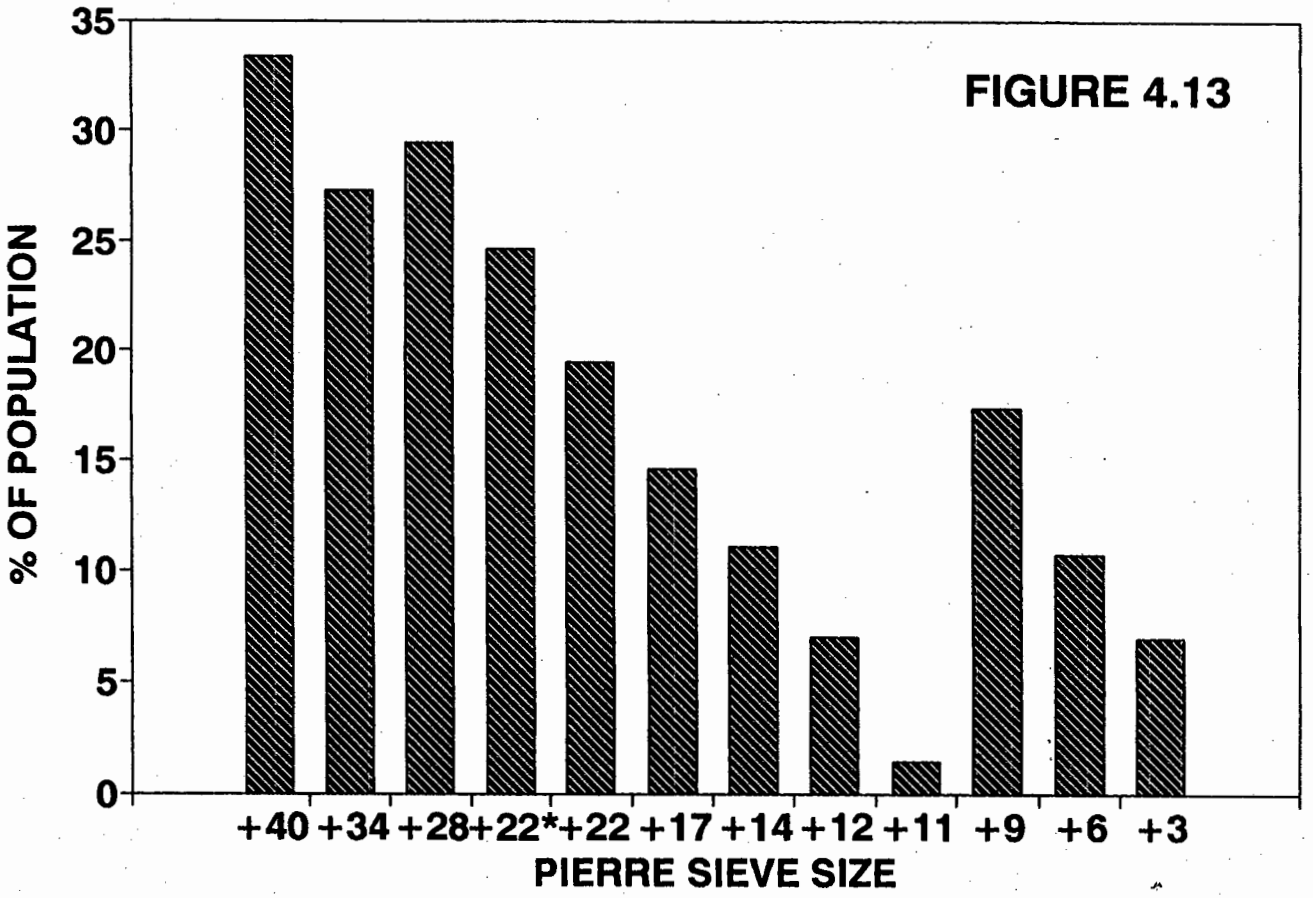

DOKOLWAYO DIAMONDS
BROWN DODECAHEDRA vs SIZE

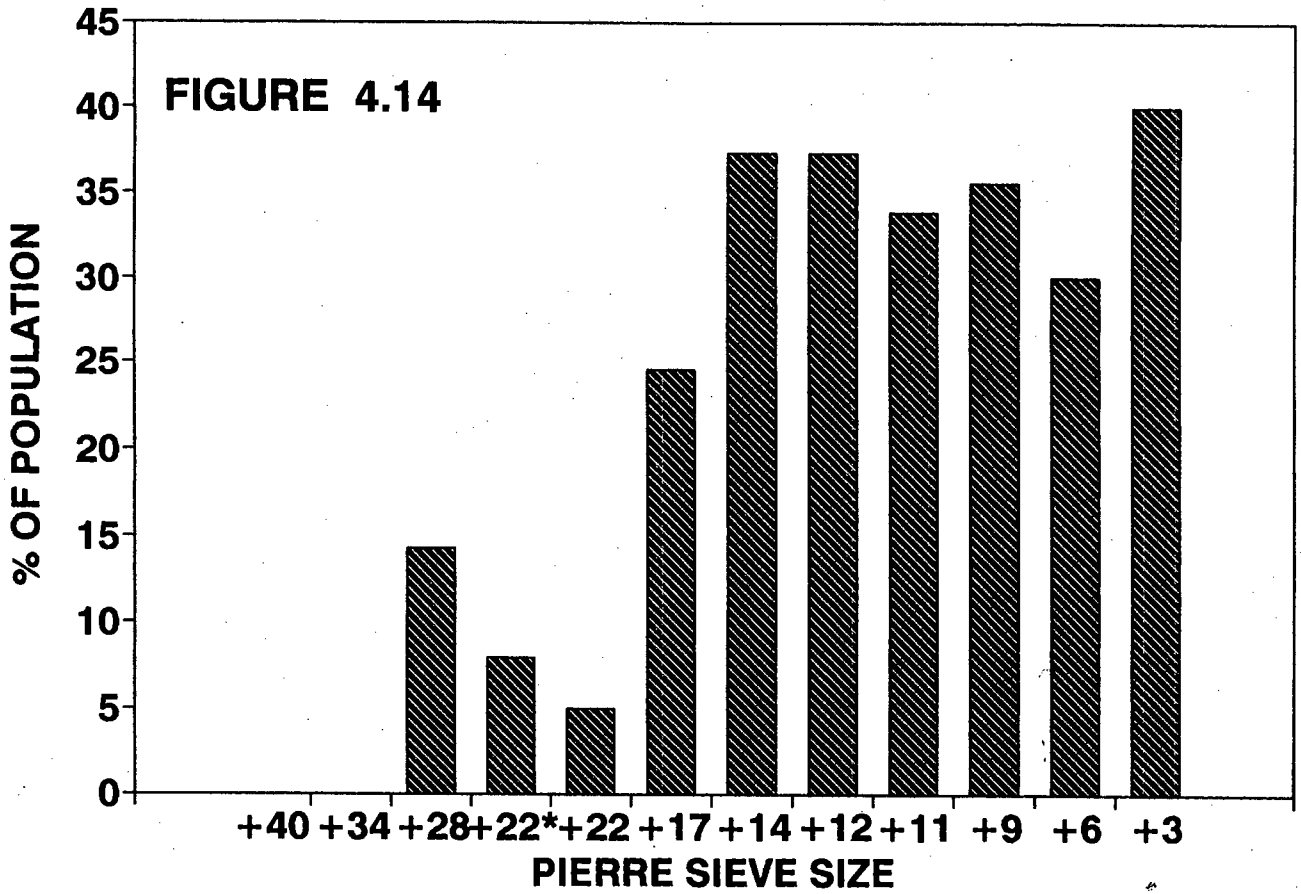

DOKOLWAYO DIAMONDS
YELLOW DODECAHEDRA vs SIZE

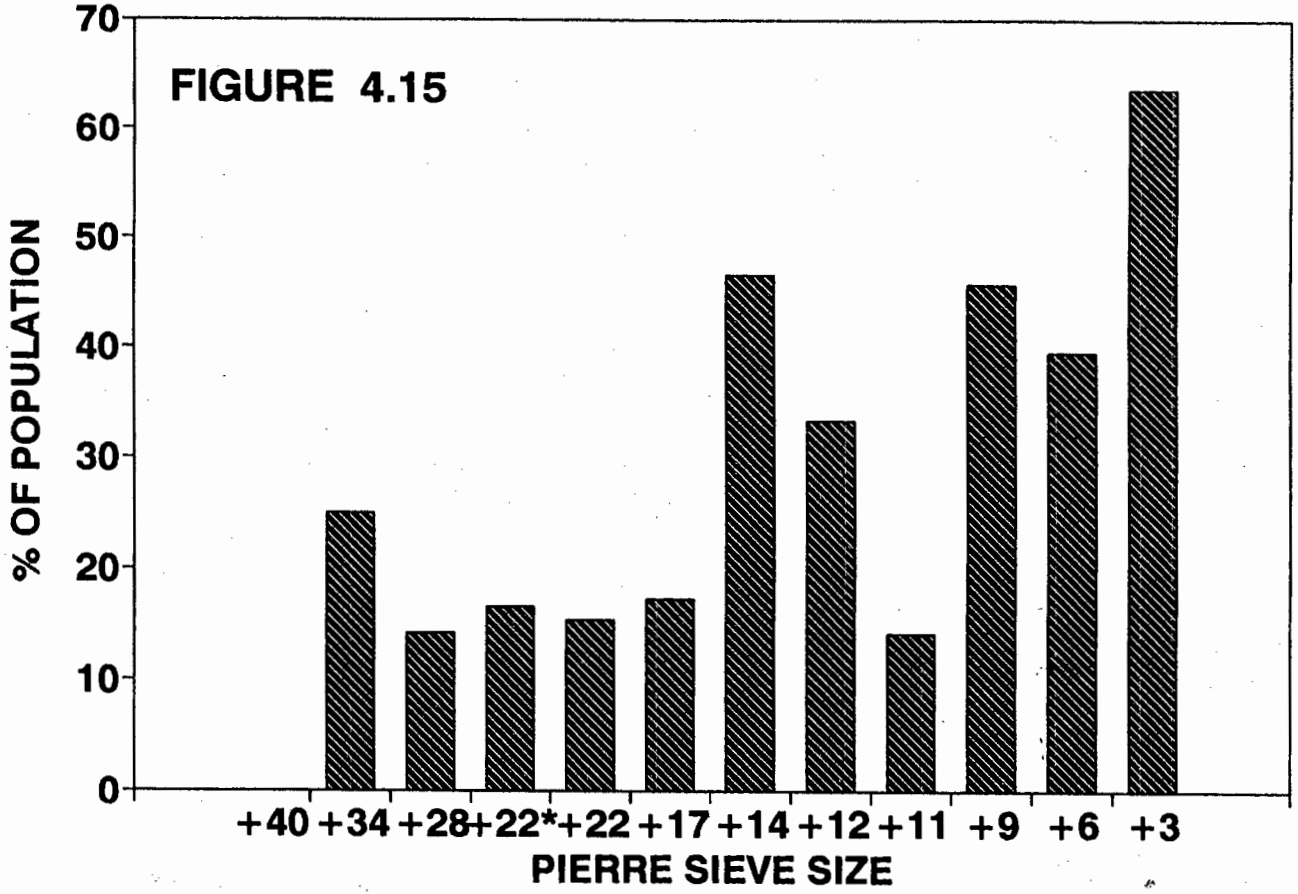

DOKOLWAYO DIAMONDS
YELLOW POLYCRYSTALS vs SIZE

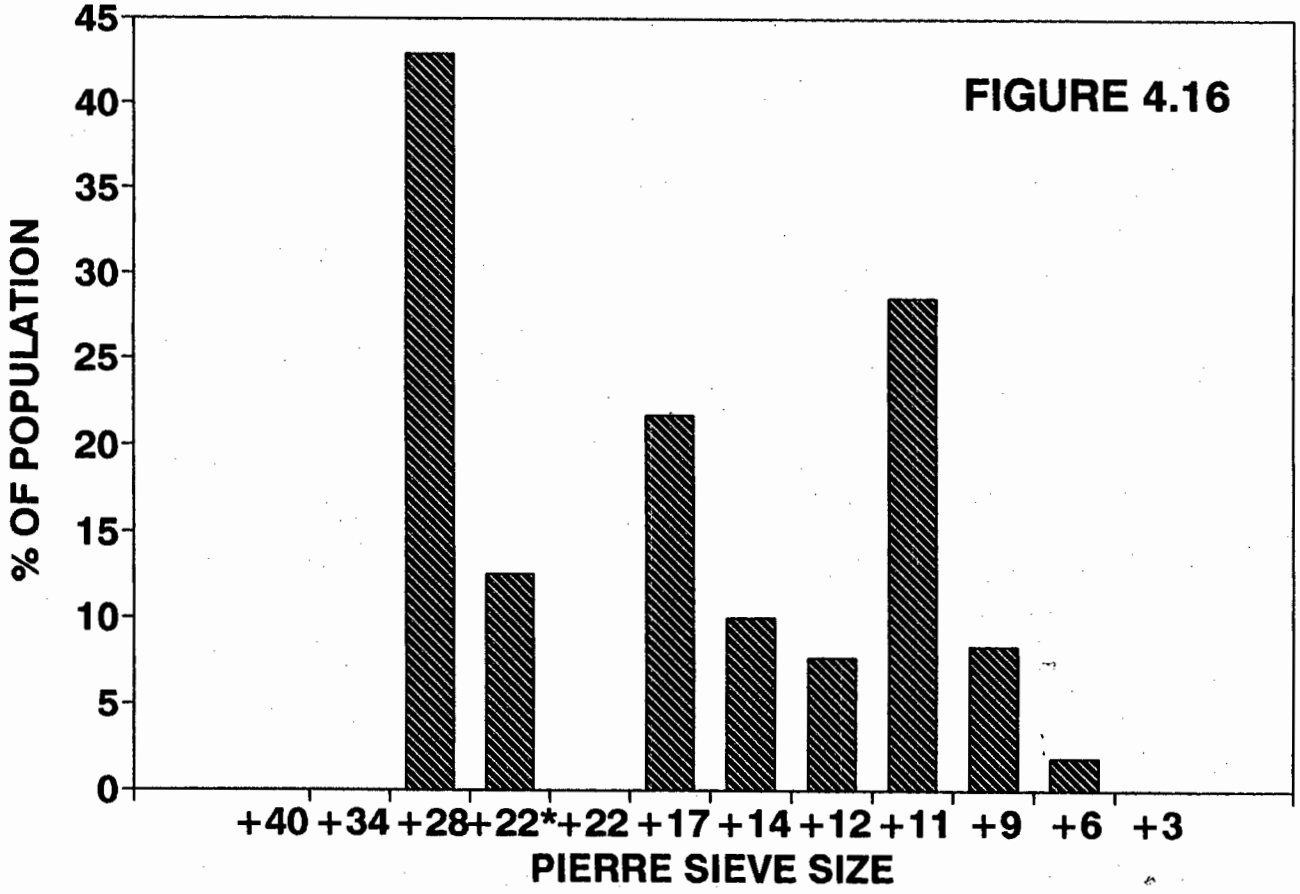

APPENDIX 4.a

DIAMOND COLOUR	PIERRE SIEVE SIZE	OCTA	DODEC	MACLE	IRREG	POLY	TOTAL
COLORLESS	+3	12	219	7	223	1	462
GREY	+3	0	15	1	24	3	43
BROWN	+3	2	26	1	35	1	65
YELLOW	+3	0	7	1	3	0	11
GREEN	+3	0	0	0	3	0	3
BLACK	+3	0	0	0	7	0	7
ORANGE	+3	0	0	0	0	0	0
TOTAL	+3	14	267	10	295	5	591
COLORLESS	+6	23	379	15	423	30	870
GREY	+6	1	51	2	62	14	130
BROWN	+6	8	46	2	92	5	153
YELLOW	+6	1	21	1	29	1	53
GREEN	+6	0	0	0	5	0	5
BLACK	+6	0	0	0	5	0	5
ORANGE	+6	0	0	0	1	0	1
TOTAL	+6	33	497	20	617	50	1217
COLORLESS	+9	21	228	7	185	27	468
GREY	+9	2	21	1	38	13	75
BROWN	+9	6	37	2	58	1	104
YELLOW	+9	2	11	1	8	2	24
GREEN	+9	0	2	0	3	0	5
BLACK	+9	0	0	0	3	0	3
ORANGE	+9	0	0	0	0	0	0
TOTAL	+9	31	299	11	295	43	679
COLORLESS	+11	13	127	4	75	19	238
GREY	+11	1	22	1	45	1	70
BROWN	+11	4	20	2	29	4	59
YELLOW	+11	1	1	0	3	2	7
GREEN	+11	0	0	0	0	0	0
BLACK	+11	0	0	0	0	0	0
ORANGE	+11	0	0	0	1	0	1
TOTAL	+11	19	170	7	153	26	375
COLORLESS	+12	33	221	8	215	31	508
GREY	+12	3	33	2	41	6	85
BROWN	+12	6	28	2	31	8	75
YELLOW	+12	6	13	2	15	3	39
GREEN	+12	0	0	0	0	0	0
BLACK	+12	0	0	0	8	1	9
ORANGE	+12	0	0	0	0	0	0
TOTAL	+12	48	295	14	310	49	716

APPENDIX 4.a

DIAMOND COLOUR	PIERRE SIEVE SIZE	OCTA	DODEC	MACLE	IRREG	POLY	TOTAL
COLORLESS	+14	23	193	7	140	19	382
GREY	+14	1	37	2	56	12	108
BROWN	+14	7	28	0	30	10	75
YELLOW	+14	2	14	0	11	3	30
GREEN	+14	0	0	0	0	0	0
BLACK	+14	0	0	0	3	0	3
ORANGE	+14	0	0	0	0	0	0
TOTAL	+14	33	272	9	240	44	598
COLORLESS	+17	22	94	6	99	24	245
GREY	+17	3	26	1	46	13	89
BROWN	+17	2	15	1	41	2	61
YELLOW	+17	4	4	0	10	5	23
GREEN	+17	0	0	0	0	0	0
BLACK	+17	0	0	0	1	0	1
ORANGE	+17	0	0	0	0	0	0
TOTAL	+17	31	139	8	197	44	419
COLORLESS	+22	11	25	2	40	12	90
GREY	+22	0	6	0	23	7	36
BROWN	+22	3	1	0	12	4	20
YELLOW	+22	5	2	0	6	0	13
GREEN	+22	0	0	0	1	0	1
BLACK	+22	0	0	0	0	0	0
ORANGE	+22	0	0	0	0	0	0
TOTAL	+22	19	34	2	82	23	160
COLORLESS	+28	7	2	3	13	6	31
GREY	+28	1	2	1	8	5	17
BROWN	+28	2	2	1	9	0	14
YELLOW	+28	0	1	1	2	3	7
GREEN	+28	0	0	0	0	0	0
BLACK	+28	0	0	0	1	2	3
ORANGE	+28	0	0	0	0	0	0
TOTAL	+28	10	7	6	33	16	72
COLORLESS	+34	2	2	1	1	3	9
GREY	+34	1	1	0	6	3	11
BROWN	+34	1	0	1	0	0	2
YELLOW	+34	1	1	0	2	0	4
GREEN	+34	0	1	0	0	0	1
BLACK	+34	0	0	0	0	1	1
ORANGE	+34	0	0	0	0	0	0
TOTAL	+34	5	5	2	9	7	28

APPENDIX 4.a

DIAMOND COLOUR	PIERRE SIEVE SIZE	OCTA	DODEC	MACLE	IRREG	POLY	TOTAL
COLORLESS	+40	3	2	0	6	2	13
GREY	+40	0	1	0	5	3	9
BROWN	+40	0	0	0	1	1	2
YELLOW	+40	0	0	0	0	0	0
GREEN	+40	0	0	0	0	0	0
BLACK	+40	0	0	0	0	0	0
ORANGE	+40	0	0	0	0	0	0
TOTAL	+40	3	3	0	12	6	24
COLORLESS	+22*	23	31	6	60	23	143
GREY	+22*	2	10	1	42	18	73
BROWN	+22*	6	3	2	22	5	38
YELLOW	+22*	6	4	1	10	3	24
GREEN	+22*	0	1	0	1	0	2
BLACK	+22*	0	0	0	1	3	4
ORANGE	+22*	0	0	0	0	0	0
TOTAL	+22*	37	49	10	136	52	284

CHAPTER 5 - DIAMOND INCLUSIONS

ABSTRACT

A wide range of oxides, silicates and sulphides were recovered from the diamonds of the Jurassic Dokolwayo kimberlite. The peridotitic paragenesis predominates at this locality. The discovery of staurolite as an inclusion in a diamond has significant petrological implications for the stability of staurolite and implies that some diamonds crystallize in a metamorphic environment. The identification of black films in diamonds as silicates enriched in Ti, K and Al suggests that visually identified sulphides may be misleading. Calculated temperatures and pressures from suitable silicate and oxide inclusions are consistent with physical conditions reported from other southern African localities. Distinct compositional differences between inclusions within a single diamond as well as inclusions assigned to a common paragenesis, but from different diamonds, suggest that the mantle is characterized by geochemical inhomogeneities on a macro and a micro scale. Spinel inclusions exposed on the surface of diamonds tend to be more chrome-rich than spinels totally encapsulated by the diamond. Eclogitic garnets do not exhibit major zonation patterns. Three distinct populations of southern African eclogitic garnets are recognized.

5.1 INTRODUCTION

Studies of diamond inclusions from southern African kimberlites over the past decade have concentrated on characterizing the diamond inclusion populations from single localities (Gurney et al., 1979, 1984a, 1984b, 1985; Hill, 1989; Moore and Gurney, 1989; Rickard et al., 1989; Gurney, unpbl. data). The armouring effect of diamonds shields syngenetic inclusions against alteration through diffusive processes. Diamond inclusions may therefore be unique sources of information pertaining to the roots of Archaean cratonic

areas (Richardson et al., 1984; Moore and Gurney, 1985; Daniels and Gurney, 1991). Diamond inclusions from Dokolwayo are of particular interest in that the kimberlite is of pre-Stormsberg age and therefore sampled a mantle unaffected by the extraction of Karoo volcanic melts. With the exception of the Precambrian Premier Mine and Jwaneng in Botswana, all other southern African diamond inclusion populations investigated were obtained from kimberlites younger than the Karoo volcanics. The Dokolwayo kimberlite is geographically well separated from other established diamond mines (Figure 5.1) and therefore provides a unique opportunity to study the root zones of the north-eastern margin of the Kaapvaal Craton.

5.2 OBJECTIVES

The aim of this study was to identify the suite of minerals occurring as inclusions in diamonds from Dokolwayo and to establish the range of chemical compositions for individual mineral species. It was also considered a priority to establish, where possible, the physiochemical conditions under which these minerals crystallized and hence to obtain information regarding the crystallization processes of natural diamonds. This latter aspect emphasized the importance of diamonds with more than one inclusion. Diamonds encapsulating more than one mineral species were particularly important to this latter aspect of the study. In addition to these aims, it was considered important to establish the compositional differences between inclusions exposed on the surface of a diamond and inclusions totally encapsulated by the diamond.

5.3 DIAMOND SELECTION

Diamonds in the sieve range -11+5 (Table 4.1) were selected from thousands of carats of general production. They were cleaned in concentrated HF for 48 hours. Most of these diamonds are <3mm in largest dimension and average ~0.10 c st^{-1}. As far as possible stones with no apparent cracks on inspection under binocular microscope were selected. A

number of stones were characterized by having inclusions exposed on the surface of the diamond as well as totally encapsulated inclusions. No evidence for major element alteration by HF was observed. The inclusions exposed on the surface of diamonds were completely removed from the diamond before totally encapsulated inclusions were extracted. The encapsulated inclusions were extracted from the diamonds by mechanical crushing in an enclosed steel cracker. The inclusions were mounted in epoxy resin on glass and polished. All minerals were analyzed with the use of a Cameca Camebax electron microprobe, using standards of similar compositions to the unknowns and on-line correction procedures.

5.4 MINERAL ABUNDANCES

Inclusion abundances presented in Table 5.1 must not be regarded as representative of the diamond population as a whole. It should be noted that spinels, in particular, are far more abundant than presented here. During the search for diamonds with inclusions from the general production at Dokolwayo it was found that spinels are more common as inclusions than all silicate phases combined. In an attempt to obtain a sample of all the possible phases present, greater emphasis was placed on selecting diamonds encapsulating silicate phases. Inclusions were successfully recovered from a total of 106 diamonds.

The majority of the inclusions were assigned to the eclogitic and peridotitic parageneses which have been reported from diamonds both regionally and world-wide (e.g. Hawthorne et al., 1979; Meyer, 1985). The results of this study (Table 5.1) have shown that the peridotitic suite of diamonds predominates over the eclogitic suite, particularly when it is taken into consideration that spinel-bearing diamonds are under represented. One diamond was assigned to the websteritic paragenesis, which has previously been reported from Orapa (Gurney et al., 1984a) and Monastery (Moore and Gurney, 1989). Inclusions that have not been assigned to specific parageneses are diamond, graphite, sulphides, zircon, ilmenite, biotite, magnetite, sphene, chlorite, and TiKAl-silicates. It should be noted that

diamond, graphite, sulphide and ilmenite were found to coexist individually with eclogitic minerals and zircon was found to coexist with peridotitic minerals. However, in the absence of coexisting diagnostic phases encapsulated minerals were assigned to the miscellaneous category (Table 5.1). The common occurrence of spinels as inclusions in diamonds at Dokolwayo is a most unusual feature of diamond inclusion populations in southern Africa and had previously been observed only in the Star diamond population (Hill, 1989). The unique discovery of a staurolite as an inclusion in one of the Dokolwayo diamonds is perhaps one of the most exciting finds of this study.

5.5 COEXISTING MINERALS

Thirty nine of the Dokolwayo diamonds from which inclusions were extracted were characterized by multiple inclusions. In 18 of these stones different minerals coexisted with each other (Table 5.1). The other 21 diamonds contained multiple monomineralic inclusions: lherzolitic garnet (1); olivine (1); peridotitic clinopyroxene (1); spinel (12); eclogitic garnet (5) and coesite (1). Single inclusions were recovered from 67 stones. It is of interest to note that although eclogitic garnets were recovered from seventeen diamonds and eclogitic clinopyroxenes were present in five diamonds, these two minerals were not found together in any diamond at Dokolwayo. This feature of the Dokolwayo diamonds contrasts with the eclogitic diamond populations from other southern African kimberlites where it is common to find eclogitic garnets and clinopyroxenes coexisting in the same diamond (e.g. Orapa and Premier Mine; Gurney et al., 1984a, 1985).

5.6 MINERAL COMPOSITIONS

The mineral compositions of all the diamond inclusions analyzed in the course of this study are presented in Appendix 5.a.

5.6.1 PERIDOTITIC MINERALS

5.6.1a Olivine

Thirteen olivines were recovered from eight diamonds. The olivines from five of these diamonds have a very restricted forsterite range (Fo 92.0 - 92.8) with Cr_2O_3 ranging from below the detection limit to 0.04 wt% and NiO 0.34 - 0.42 wt%. One of these olivines was recovered from a diamond (DI 310) that also contained two spinels. A single olivine crystal was also found coexisting in a diamond (DI 362) with orthopyroxene and three spinel grains. This olivine is slightly more forsteritic (Fo 93.3) than the olivine found coexisting with spinels in DI 310. Five olivine inclusions were recovered from a single diamond (DDI 54) which also contained subcalcic garnets. These olivines are characterized by ranges of forsterite contents (Fo94.1 - 94.6), Cr_2O_3 (0.02 - 0.06 wt%) and NiO (0.28 - 0.35 wt%) suggesting minor disequilibrium within the diamond. The remaining two olivines were recovered from the same diamond (DI 342) and are characterized by Fo 93.6 - 93.8, Cr_2O_3 below the detection limit and NiO 0.35 wt%.

5.6.1b Orthopyroxene

Three peridotitic orthopyroxenes were recovered from three Dokolwayo diamonds. These orthopyroxenes are characterized by a narrow range in enstatite component (En 93.9 - 94.9), Cr_2O_3 0.49 - 0.68 wt%, Al_2O_3 0.83 - 0.93 wt% and CaO 0.17 - 0.38 wt%. The orthopyroxene recovered from diamond DI 362 coexisted with olivine and spinel. The other two orthopyroxenes were extracted from diamonds DK 24 and DI 307, and coexisted with subcalcic garnets.

5.6.1c Clinopyroxene

The assignment of clinopyroxenes to either the peridotitic or eclogitic suite is problematic. All except one of the clinopyroxenes recorded from diamonds in southern Africa which have been designated as "eclogitic" have Cr_2O_3 < 0.4 wt%. The policy adopted in this study was to assign all Dokolwayo diamond inclusion clinopyroxenes with Cr_2O_3 > 1.00 wt% to the peridotitic suite (Figure 5.2). Four clinopyroxenes are assigned to the peridotitic suite. These peridotitic clinopyroxenes have a wide range in Cr_2O_3 (1.10 - 7.58 wt%), Na_2O (0.57 - 5.91 wt%), K_2O (0.06 - 0.53 wt%) and TiO_2 (< 0.20 wt%).

5.6.1d Garnet

Four different groups of peridotitic garnets were recovered from Dokolwayo diamonds. These four groups are characterized by distinctive compositions as well as the colour of the garnets.

Lilac subcalcic garnets were extracted from six diamonds. The garnets from four of these diamonds (DK 24, DK 42, DDI 45, DI 307) have exceptionally high Cr_2O_3 contents (9.84 - 13.1 wt%) and low CaO (0.43 - 2.50 wt%; Figure 5.3). Two of these diamonds (DK 24 and DI 307) also contained orthopyroxene. The subcalcic garnets from diamond DDI 54 (Cr_2O_3 7.54 - 7.85 wt%; CaO 1.31 - 1.34 wt%) which coexisted with olivines have significantly less Cr_2O_3 than the subcalcic garnets recovered from the aforementioned four diamonds above. Distinct compositional differences with respect to Al_2O_3, Cr_2O_3, FeO and MgO concentration levels exist amongst the three garnets from diamond DDI 54. These compositional differences are consistent with possible disequilibrium within the diamond as observed in the olivine compositions. The subcalcic garnet (CaO 1.52 wt%) with the lowest level of Cr_2O_3 (5.45 wt%) was recovered from diamond DI 350.

Two purple garnets were recovered from one diamond (DK 06). One of these garnets was exposed to a crack in the diamond. The garnet that was not exposed to a crack has Cr_2O_3 5.96 wt%, MgO 20.5 wt% and CaO 5.96 wt%. This composition is similar to that of garnets derived from calcium saturated lherzolites. The exposed garnet was slightly altered.

Two diamonds (DI 353 and DI 375) yielded single green garnets. These garnets are characterized by high calcium and chromium contents (CaO 24.0 - 24.3 wt%; Cr_2O_3 13.1 - 13.3 wt%). Garnets of similar composition have not previously been reported as diamond inclusions, but have been found in concentrates from the Newlands, Bellsbank and Dokolwayo concentrates (Lawless, 1974; LRD Unpbl data).

A blue garnet, similar in colour to kyanite, was recovered from diamond DI 304. This garnet is characterized by Cr_2O_3 13.0 wt% and CaO 7.94 wt%. Both the colour and the composition of this garnet are unusual and have not previously been reported for garnet inclusions in diamonds from Southern Africa.

5.6.1e Spinel

Chromium-rich spinels are the single most common mineral inclusion in Dokolwayo diamonds. A total of fifty five spinels were recovered from twenty eight diamonds. The majority of these spinels are characterized by $Cr_2O_3 > 60$ wt%. However, four spinels (three coexisting with olivine and orthopyroxene) contain $Cr_2O_3 < 60$ wt%. The Cr/(Cr+Al) ratio of the spinels is restricted between 0.900 and 0.738. A significant feature of these diamond inclusion spinels is their low TiO_2 contents which range from below detection limit to 0.62 wt% (Figure 5.4). Most of the spinels have Mg/(Mg+Fe) > 0.5. The exceptions to this compositional feature are two spinels coexist with a zircon (DI 324). These two spinels have Mg/(Mg+Fe) < 0.5. Compositional inhomogeneity amongst spinels from the same diamond (e.g. DI 328, DI 331) is common. In cases where

spinels were exposed on the surface of a diamond (DI 302, DI 319) the exposed spinel contains significantly more Cr_2O_3 than unexposed spinels. In one diamond (DI 319) relative sizes of unexposed spinels were recorded, but no significant difference in composition amongst the inclusions was observed.

Twenty nine of the diamond inclusion spinels were analyzed by J.J. Gurney for trace concentrations of Ni (584 -1160 ppm), Zn (335 - 526 ppm) and Ga (not detected to 31.6 ppm). These trace element results are discussed in Chapter 8.

5.6.1f Zircon

Zircon was found to coexist with two spinels in Dokolwayo diamond DI 324. This mineral assemblage has been assigned to the peridotitic suite due to the common association of spinels with peridotitic minerals in diamonds from southern Africa. However, the carbon isotopic composition of this diamond (Chapter 6) places a question mark over the paragenesis of these inclusions.

5.6.2 ECLOGITIC MINERALS

5.6.2a Clinopyroxenes

Five clinopyroxenes considered to be eclogitic are characterized by high TiO_2 (0.34 - 0.66 wt%), a wide range in Al_2O_3 (2.58 - 14.0 wt%), MgO (7.26 - 20.3 wt%), Na_2O (1.53 - 7.14 wt%), and K_2O (0.03 - 0.51 wt%) and low Cr_2O_3 (< 0.30 wt%, Figure 5.2). One of the diopsides (DD 32/01) has an excess of Al over Na with a slight deficiency in Si representing a small proportion of Ca-Tschermack molecule.

5.6.2b Garnets

Eclogitic garnets are the second most abundant mineral recovered from Dokolwayo diamonds. A total of thirty six eclogitic garnets was recovered from twenty one diamonds. These garnets were found to coexist with coesite, sulphide, diamond and ilmenite respectively. All of these garnets have trace levels of sodium (Na_2O 0.06 - 0.54 wt%) which is positively correlated with TiO_2 (0.11 - 0.66 wt%; Figure 5.5). The range of compositions for this group of garnets reported previously (Daniels and Gurney, 1989) has been extended. These garnets show a wide range in FeO (8.41 - 21.6 wt%), MgO (7.44 - 20.7 wt%) and CaO (4.21 - 15.5 wt%). The Cr_2O_3 content of the eclogitic garnets is generally <0.20 wt%.

5.6.2c Coesite

Eight high SiO_2 (93.8 - 97.8 wt%) inclusions are assumed to be eclogitic coesite rather than quartz in that the inclusions were recovered from diamonds without cracks. These coesites coexist with eclogitic garnet and diamond inclusions respectively.

5.6.2d Rutile

Rutile (TiO_2 98.4 wt%) was recovered from a framesite crystal and is considered to be of eclogitic paragenesis, which is in agreement with the results of similar inclusions described by Gurney and Boyd (1982).

5.6.2e Feldspar

A single feldspar was recovered from Dokolwayo diamond DI 344. This feldspar is similar in composition to an albite that was recovered from the Roberts Victor kimberlite (Gurney et al., 1984b) which was assigned to the eclogitic paragenesis.

5.6.2f Ilmenite

Ilmenite was found coexisting with two eclogitic garnets in Dokolwayo diamond DI 351. The absence of Cr_2O_3 and the high MgO (9.05 wt%) contents of the ilmenite are similar to compositional trends observed in ilmenites from Orapa eclogites (Tollo, 1986).

5.6.2g Staurolite

A staurolite coexisting with graphite was recovered from diamond DI 3a11. Staurolite has not previously been reported from a diamond. The staurolite is characterized by FeO 13.6 wt%, MgO 2.13 wt% and ZnO 1.09 wt%. This composition is similar to the compositions of staurolites from eclogite-facies metapelites from the Champtoceaux Nappe in Brittany, France (Ballevre et al., 1989) and the Dokolwayo staurolite is therefore placed in the eclogitic paragenesis.

5.6.2h Diamond

Diamond inclusions within diamond were found in association with eclogitic garnet as well as coesite.

5.2.6i Sulphide

Sulphide inclusions were found as single inclusions in diamonds and also in association with eclogitic garnet inclusions. The sulphides were not analyzed in detail.

5.6.3 WEBSTERITIC MINERALS

An orthopyroxene (DI 363) was found coexisting with clinopyroxene and coesite which have compositional characteristics similar to eclogitic minerals. Hence this orthopyroxene is similar to orthopyroxenes reported from Orapa (Gurney et al., 1984a) and Monastery (Moore and Gurney, 1989). The orthopyroxenes from these localities have been interpreted to represent a websteritic paragenesis and the Dokolwayo sample is therefore also considered to be of websteritic origin.

5.6.4 MINERALS OF QUESTIONABLE AFFINITY

5.6.4a Diamond, Graphite and Sulphide

Diamonds, graphite and sulphide were recovered as inclusions in diamond in addition to those found in association with eclogitic minerals. Graphite has been recorded as diamond inclusions at Star (Hill, 1989). Sulphides are far less common than previously estimated (Daniels and Gurney, 1989).

5.6.4b Ilmenite

One ilmenite was recovered from Dokolwayo diamond DI 366. The ilmenite has Cr_2O_3 1.05 wt% and MgO 12.4 wt%. Similar ilmenites have been reported as diamond inclusions from Finsch (Meyer and Tsai, 1976) and Monastery (Moore and Gurney, 1989). The paragenetic affinity of these latter ilmenites are also unknown.

5.6.4c Biotite

Biotite (TiO_2 5.34 wt%; FeO 17.55 wt%; MgO 13.15 wt%) was recovered from a diamond that had no visible cracks and is therefore considered to be primary. Biotite has

previously been recorded from diamonds by Williams (1932) and Giardini et al. (1974). However, the paragenetic affinity of biotite is unknown.

5.6.4d Zircon

A single zircon was recovered from diamond DI 381. The diamond from which this zircon was recovered has a distinctly different carbon isotopic signature to the diamond from which the zircon described in **5.6.1f** above was recovered. The paragenetic assignment of this zircon is therefore uncertain, but it may be eclogitic. The carbon isotopes are described in Chapter 6.

5.6.4e Magnetite and Sphene

Two magnetite crystals were extracted from diamond DI 340. Both magnetite crystals were about 500 microns in diameter. One magnetite contains TiO_2 1.37 wt% and MgO 2.47 wt% while these oxides were not detected in the second magnetite. The magnetite containing TiO_2 and MgO was further characterized by two small sphene inclusions. In the absence of diagnostic minerals the paragenesis of this assemblage is uncertain. However, sphene and magnetite have been found in diamondiferous eclogites in the Soviet Union (Tugovik et al., 1987). It is therefore possible that this assemblage is related to the eclogitic paragenesis.

5.6.4f Chlorite and TiKAl-Silicate

An Fe-rich chlorite with 46.4 wt% FeO (total iron) 0.74 wt% Cr_2O_3, 0.14 wt% Na_2O, 1.28 wt% K_2O and 0.32 wt% F was recovered from diamond DI 380. This chlorite coexisted with sulphide and diamond inclusions. In addition to these inclusions, black films of unknown material were observed. These black films were previously assumed to be sulphide rosettes. However, a qualitative analysis with a scanning electron microscope

has shown that these films consist predominantly of Si and Al with minor Ti, Fe, Mg, Ca, Na, K and Cl (Figure 5.6a). Similar black films were recorded on the interface between a diamond inclusion and its host diamond (DI 383). The SEM analytical result obtained for these black films is virtually identical to the results from DI 380 (Figure 5.6b).

5.7 DISCUSSION

The peridotitic and eclogitic mineral inclusions in the Dokolwayo diamonds have many compositional similarities with diamond inclusions reported from both the Precambrian Premier Mine (Gurney et al., 1985) and the post-Stormsberg volcanism kimberlites in southern Africa (Gurney et al., 1979, 1984a, 1984b; Hill, 1989; Rickard et al., 1989; Moore and Gurney, 1989). It is therefore unlikely that the conditions of crystallization of the Dokolwayo diamonds would in principle be significantly different to the processes of diamond formation in southern Africa as a whole.

Physical Conditions

Unfortunately, none of the diamonds containing mineral inclusions of eclogitic paragenesis allowed for the calculation of equilibrium pressures or temperatures. An evaluation of the physiochemical conditions of Dokolwayo diamond crystallization is therefore restricted to the peridotitic suite.

Two diamonds contained garnet-orthopyroxene pairs and allowed for pressure calculations (Nickel and Green, 1985). Both of these diamonds (DI 307 and DK-24) contained multiple garnet inclusions. The pressure range between 1000°C and 1200°C for DI 307 was 43.6 and 54.4 kbar. Assuming a minimum pressure of 45 kbar for diamond stability suggests a minimum temperature of 1040°C for this diamond. Similarly, a pressure range of 45.4 to 56.8 kbar between 1000°C and 1200°C was calculated for DK-24.

Only one diamond (DDI 54) contained a garnet-olivine pair that could be used for temperature determinations (O'Neill and Wood, 1979 (*1*)). Three garnets and five olivines from this diamond were analyzed. The temperatures for this diamond was calculated at an assumed pressure of 50 kbar. Three diamonds contained peridotitic clinopyroxenes. Temperatures were calculated for these three diamonds using the Lindsley and Dixon (1976, (*2*)) diopside solvus (20 kbar). Two diamonds (DI 310 and DI 362) contained both olivine and spinel inclusions. Temperatures were calculated for these diamonds at a pressure of 50 kbars using the O'Neill and Wall (1987, (*3*)) olivine-spinel geothermometer. The temperatures are presented in Table 5.2.

Temperatures calculated for the Dokolwayo peridotitic diamonds are similar to the temperatures obtained from the Premier diamonds (Gurney et al., 1985), but lower than the temperatures characteristic of the Roberts Victor diamonds (Gurney et al., 1984b). Despite the Jurassic age of the Dokolwayo kimberlite, the peridotitic diamond temperatures from this locality do not deviate significantly from the peridotitic trend established for other kimberlites in southern Africa (Gurney et al., 1979; 1984a; 1984b; 1985; Rickard et al., 1989; Hill, 1989).

Exposed and Non-exposed Diamond Inclusions

The diamonds with exposed spinels on the surface were significantly resorbed diamonds. It is reasonable to argue that the exposed spinels were closer to the exterior of the diamonds prior to resorption than were the unexposed spinels. In two cases investigated, the exposed spinels were more chromium-rich than the unexposed spinels. In the event that these exposed spinels were altered in a secondary environment, it would be necessary to find a process that enriches the spinel in chromium. An appropriate environment would be a kimberlite or proto-kimberlite melt. However, the immobility of chromium in secondary environments and the refractory nature of chromium spinels suggest that chromium enrichment of diamond inclusion spinels is an unlikely process to occur and it is concluded

that little, if any alteration of the exposed spinels occurred. This implies that spinels within a single diamond may increase in chromium from centre to edge. A similar zoning pattern is observed in Dokolwayo concentrate spinels (Chapter 8) with compositional characteristics similar to those of the diamond inclusion spinels. Daniels (1991) suggested that diamond inclusion-type spinels, together with subcalcic G10 garnets, crystallize as exsolution phases from residual orthopyroxenes in the mantle after komatiite extraction. The exsolution of the garnets from the residual orthopyroxenes will progressively deplete Al in the residual pyroxene while Cr-enrichment occurs. Spinel exsolving from the pyroxene will therefore become increasingly Cr-rich. This may result in zonation patterns within the spinels exhibiting increasing Cr_2O_3 contents from centre to edge (Daniels, 1991).

Two eclogitic garnets, the larger exposed and the smaller totally encapsulated were recovered from diamond DI 336. The larger, exposed garnet was marginally poorer in FeO and richer in MgO than the smaller, unexposed garnet. The exposed garnet was analyzed for centre and edge compositional variations. No significant variations were observed.

Compositional Diversity

A significant feature of the Dokolwayo diamond inclusions is that they perhaps illustrate a far more diverse assemblage of chemical environments than previously reported from other southern African localities. On a macro scale the Dokolwayo diamond inclusions can predominantly be divided into the peridotitic and eclogitic parageneses. Significant differences between these two parageneses are illustrated by the clinopyroxenes. The eclogitic pyroxenes are characterized by distinctly lower Cr_2O_3 and higher TiO_2 contents than observed in the peridotitic clinopyroxenes. This indicates a fundamental distinction between the eclogitic and the calcium saturated lherzolitic/wehrlitic regions of these environments.

Within a single macro chemical environment (peridotitic or eclogitic) there is significant diversity. This is clearly illustrated by the diverse characteristics of the peridotitic garnets, where, based on the relationship between CaO and Cr_2O_3, there are at least four different groups of garnets. Furthermore, it is possible to illustrate chemical diversity on an even smaller scale. Within the subcalcic environment there is a broad range in the degree of calcium depletion (0.43 - 2.50 wt% CaO) which is not linearly correlated with relative chromium enrichment (5.45 - 13.1 wt% Cr_2O_3; Figure 5.3). Therefore, within a micro environment (e.g. subcalcic) there is distinct inhomogeneity. This inhomogeneity is even more dramatically illustrated by the gross variation in the compositions of spinels recovered from single diamonds (DI 328, DI 331) and by the observed inhomogeneity in olivine and garnet compositions in diamond DDI 54. All three of these diamonds are less than 2 mm in diameter. It is of interest to note that Gurney et al. (1984b) and Hill (1989) have recorded similar major inhomogeneities in spinel compositions from a Roberts Victor diamond and Star diamond respectively.

The chemical diversity and inhomogeneity of the upper mantle as indicated by mantle-derived xenoliths have received considerable attention in the past (e.g. Gurney and Harte, 1980; Dawson, 1980). Assuming a minimum pressure of formation of 45 - 50 kbars for the crystallization of the Dokolwayo diamonds, the diamond inclusions from Dokolwayo point to a very inhomogeneous and chemically diverse upper mantle at pressures greater than 45 kbars in the vicinity of Dokolwayo. In turn, this observed diversity and inhomogeneity suggests a complex history of upper mantle development within the diamond stability field.

Eclogitic Environments

A peculiar feature of the Dokolwayo eclogitic diamond inclusions is that garnet and clinopyroxene were not found to co-exist in any of the diamonds in this study, although

both minerals were recovered as inclusions. Due to their bulk chemical compositions, mantle-derived eclogites are commonly suggested to be subducted basalts. The fundamental mechanism for the transition from basalt to eclogite is associated with the breakdown of the plagioclase end-members albite and anorthite to form jadeite ($NaAlSi_2O_6$)- and grossular ($Ca_3Al_2Si_3O_{12}$)-bearing phases. In the case of Dokolwayo a subducted basalt origin for eclogitic material would be consistent with the early Archaean tectonic models proposed for the area by De Wit and co-workers (1987; 1990). Eclogitic garnet inclusions in diamonds from southern African kimberlites define three distinct compositional fields with a few outliers within an FeO-CaO plane (Figure 5.7). All but four inclusions defining Field I are from Premier. The four exceptions are one garnet from Orapa and three from Dokolwayo. Field II is defined by inclusions from Finsch, Koffiefontein, Jwaneng, Roberts Victor, Orapa, Premier and Dokolwayo. Field III represents diamond inclusions from Koffiefontein, Jwaneng, Orapa, Finsch, Premier and Dokolwayo. Two garnets from Star are the most calcic eclogitic garnets recovered from diamonds in southern Africa. Assuming that eclogites are subducted oceanic basalts and that the garnet compositions from eclogitic-suite diamonds are determined by the original basalt composition then there are at least three major geochemically distinct basalts that have been subducted into the diamond stability field. Alternatively, the inclusions may represent three different environments of metamorphism of subducted basalts. Only three kimberlites, Premier (Precambrian), Dokolwayo (Jurassic) and Orapa (Cretaceous) are represented in all three fields identified above. The wide geographical distribution and diverse age of the kimberlites within southern Africa from which these three distinct groups of eclogitic diamonds are recognized, suggest that:

a) Kimberlites sampled similar eclogitic material from the deeper parts of the Kaapvaal Craton over a long period of time.

b) Subduction of oceanic basalts, probably during the formation of the stable Kaapvaal Craton, took place over a wide geographical area.

Staurolite in the Mantle

The unique discovery of staurolite in a diamond from Dokolwayo has several paragenetic and petrological implications. The staurolite was totally enclosed within the diamond from which it was recovered and there were no cracks leading to the inclusion. Due to slight frosting on the surface of the diamond it was impossible to observe any morphological control of the diamond on the staurolite crystal morphology. However, the staurolite was present as a discrete crystal within the diamond and is considered to be of primary origin. In addition to staurolite, graphite was recovered from the same diamond (DI3a11). The composition of this staurolite (Appendix 5.a) is similar to the composition of staurolites from metapelites (Kasch, 1987) but has slightly higher concentrations of both FeO and MgO than staurolites from eclogite-facies metapelites from the Champtoceaux Nappe in France (Ballevre et al., 1989).

The primary nature of this staurolite inclusion in the diamond suggests that staurolite is a stable mineral phase in the mantle to a minimum depth of diamond crystallization. Diamond is considered to be a stable mantle phase at pressures in excess of 45 kbars (Kennedy and Kennedy, 1976). Schreyer (1988) has experimentally shown that Mg-staurolite can be stable at temperatures in excess of 700°C and pressures from 13 kbar to beyond 50 kbar within the experimental MgO-Al_2O_3-SiO_2-H_2O system. However, there is no experimental work available to predict the stability of Fe-staurolite at high pressures. Staurolites have higher Mg/(Mg+Fe) ratios (X_{Mg}) than coexisting garnets in low- to medium-pressure metapelites, but the reverse is true in high-pressure metapelites (Ballevre et al., 1989). When $X_{Mg}^{St} \geq X_{Mg}^{Gt}$ and Fe-Mg partitioning between staurolite and garnet is normal, the degenerate reaction

Staurolite (St) = Garnet (Gt) + Kyanite (Ky)

will be coincident with

Fe-St = Alm + Ky

which is a terminal staurolite-out reaction. However, where $X_{Mg}^{St} < X_{Mg}^{Gt}$ and a reversal of Fe-Mg partitioning between garnet and staurolite occurs, the staurolite stability field is extended towards higher pressures and temperatures than in the case of a normal partitioning (Ballevre et al., 1989).

The X_{Mg} of the Dokolwayo diamond inclusion staurolite is <0.25. The diamond inclusion eclogitic garnets from Dokolwayo all have $X_{Mg} > 0.35$. Assuming that these two mineral inclusions are derived from the same environment, then $X_{Mg}^{St} < X_{Mg}^{Gt}$ which is consistent with an extension of the staurolite stability field into higher pressures.

The association of staurolite and elemental carbon (diamond and/or graphite) is not unique to Dokolwayo. The Fe-staurolite in the eclogitic facies matapelites in the Champtoceaux Nappe, France, also coexists with graphite (Ballevre et al., 1989). Tugovik et al. (1987) described diamonds from sphene-rutile eclogite bodies lacking omphacite pyroxene. These eclogitic bodies occur within local ring structures in an area of Archaean granulites. Amongst the accessory minerals in these diamondiferous eclogites Tugovik et al. (1987) recorded staurolite.

The similarity between the compositions of staurolites from metapelites (Kasch, 1987) and the Dokolwayo staurolite, the presence of staurolite and graphite in eclogite facies metapelites (Ballevre et al., 1989), and the presence of diamonds and staurolite in eclogites (Tugovik et al., 1987) strongly suggests that the Dokolwayo staurolite - diamond association is indicative of pelitic sediments having been subducted to pressures in excess of 45 kilobars and metamorphosed under eclogite facies conditions.

The presence of subducted metapelites in the mantle below Dokolwayo is consistent with the model of De Wit et al. (1990) for the formation of early cratonic nuclei which suggests that, in addition to ocean floor basalts, small amounts of overlying sediments may have been subducted during the Archaean. Mazzone and Haggerty (1989) have suggested that

peraluminous xenoliths in the Jagersfontein kimberlite may be derived from an integrated multi-stage melting-metamorphic process which was preceded by the subduction of Archaean sediments.

There is to date no evidence that staurolite crystallizes from a melt. Staurolite is commonly accepted as a metamorphic mineral. The encapsulation of a metamorphic mineral in a diamond as a primary inclusion raises questions about diamond crystallization within an eclogitic environment.

A study of the internal structures of several Russian diamonds led Sunagawa (1984a,b) to conclude that diamonds crystallize from a solution and cannot be products of crystallization under metamorphic conditions. The paragenesis, i.e. eclogitic or peridotitic, of the diamonds Sunagawa studied was not known. Yefimova and Sobolev (1977) indicate that the Siberian diamonds from Yakutia are predominantly (98%) represented by the peridotitic suite. It would thus seem likely that Sunagawa studied peridotitic diamonds rather than eclogitic diamonds to reach his conclusions on diamond crystallization. The encapsulation of a staurolite, which is commonly regarded as a metamorphic mineral, in a Dokolwayo diamond as a primary mineral inclusion suggests that this diamond crystallized under metamorphic conditions and not from a melt as proposed by Sunagawa (1984). Further evidence supporting the crystallization of diamonds under metamorphic conditions is the discovery of accessory diamonds included in garnets and zircons from garnet-biotite gneisses and schists in northern Kazakhstan, USSR (Sobolev and Shatsky, 1987). With increasing metamorphic grade and decreasing H/C ratios, graphite is the final product of the maturation of organic carbon (Kirkley and Gurney, 1989). At pressures within the diamond stability field this process of thermal maturation, recrystallization and metamorphism will result in the conversion of graphite to diamond. It therefore seems reasonable that diamonds grew during metamorphism of Archaean subducted basalts and associated sediments which were sampled from the mantle by the Dokolwayo kimberlite.

TABLE 5.1

DOKOLWAYO DIAMOND INCLUSION ABUNDANCES

PERIDOTITIC MINERAL(S)	DIAMONDS (N)
Olivine (Olv)	4
Clinopyroxene (Cpx)	2
Orthopyroxene (Opx)	1
Garnet (Gar)	5
Spinel (Spn)	13
Olv - Olv	1
Olv - Gar	1
Olv - Spn	1
Cpx - Cpx	1
Opx - Gar	2
Gar - Gar	1
Spn - Spn	12
Spn - Zircon	1
Olv - Opx - Spn	1

ECLOGITIC MINERAL(S)	DIAMONDS (N)
Clinopyroxene (Cpx)	5
Garnet (Gar)	12
Coesite (Coes)	2
Staurolite - Graphite	1
Gar - Gar	5
Gar - Coes	2
Gar - Ilmenite	1
Gar - Diamond	1
Coes - Coes	1
Rutile	1
Feldspar	1
Magnetite - Sphene	1
Zircon	1
Ilmenite	1

WEBSTERITIC MINERAL(S)	DIAMONDS (N)
Opx - Cpx - Coesite	1

SUMMARY STATISTICS	(N)	%
PERIDOTITIC	46	42.2
ECLOGITIC	35	32.1
WEBSTERITIC	1	0.9
MISCELLANEOUS	27	24.8
TOTAL NUMBER OF DIAMONDS	109	100.0
MINIMUM PERIDOTITIC : ECLOGITIC RATIO	57 : 43	

TABLE 5.1 Dokolwayo diamond inclusion abundances.

Table 5.2 Calculated Dokolwayo Diamond Inclusion Temperatures

Diamond No		°C	Thermometer	Minerals
DDI 54	Minimum	1007	(1)	Gt - Ol
DDI 54	Maximum	1170	(1)	Gt - Ol
DDI 54	Average	1103	(1)	Gt - Ol
DDI 54	Standard Deviation	47.5°C		
DI 45		1230	(2)	Cpx
DI 39A		1150	(2)	Cpx
DI 364A		1194	(2)	Cpx
DI 364B		1208	(2)	Cpx
DI 310		1081	(3)	Ol - Sp
DI 362		1266	(3)	Ol - Sp

Table 5.2: Equilibrium temperatures calculated from Dokolwayo diamond inclusions using the thermometers of (1) O'Neill and Wood (1979), (2) Lindsley and Dixon (1976) and (3) O'Neill and Wall (1987).

CHAPTER 5 - FIGURE CAPTIONS

FIGURE 5.1

Locality map of selected kimberlites in southern Africa. The approximate boundary of the present day Kaapvaal Craton is indicated.

FIGURE 5.2

Plot of Cr_2O_3 vs TiO_2 (wt%) for diamond inclusion clinopyroxenes from Dokolwayo. Two of the peridotitic clinopyroxenes plot as a simgle point.

FIGURE 5.3

Plot of CaO vs Cr_2O_3 (wt%) for peridotitic diamond inclusion garnets from Dokolwayo. The 85% line is after Gurney (1984).

FIGURE 5.4

Histogram of the TiO_2 (wt%) contents of the diamond inclusion spinels from Dokolwayo.

FIGURE 5.5

Plot of Na_2O vs TiO_2 (wt%) for eclogitic diamond inclusion garnets from Dokolwayo.

FIGURE 5.6

Electron microprobe scan spectra of black films in Dokolwayo diamonds (a) DI 380 and (b) DI 383.

FIGURE 5.7

Plot of CaO vs FeO (wt%) for all southern African eclogitic diamond inclusion garnets defining at least three distinct compositional fields.

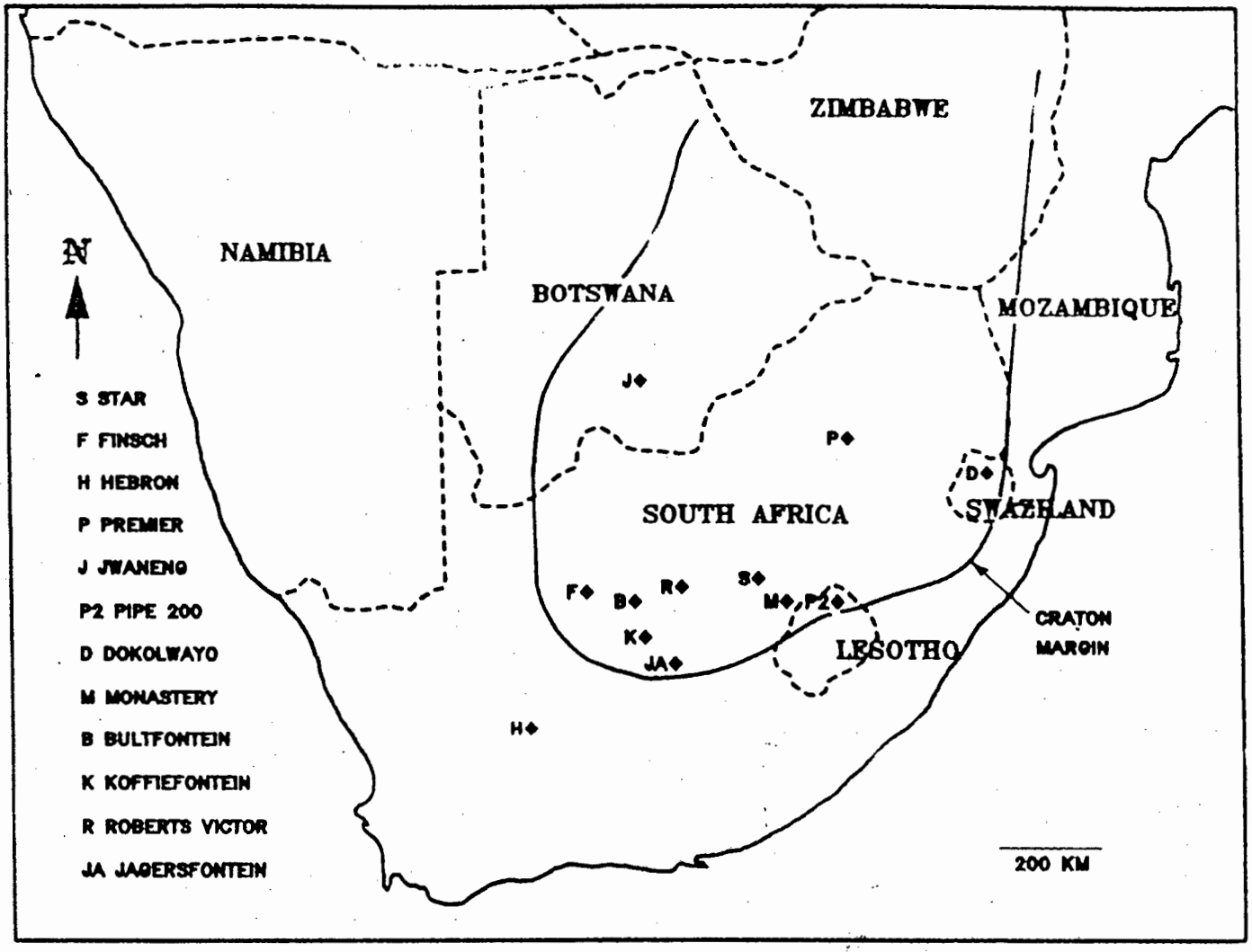
ZIMBABWE
NAMIBIA
BOTSWANA
MOZAMBIQUE
SOUTH AFRICA
SWAZILAND
LESOTHO
CRATON MARGIN
200 KM
S STAR
F FINSCH
H HEBRON
P PREMIER
J JWANENG
P2 PIPE 200
D DOKOLWAYO
M MONASTERY
B BULTFONTEIN
K KOFFIEFONTEIN
R ROBERTS VICTOR
JA JAGERSFONTEIN

Fig 5.1

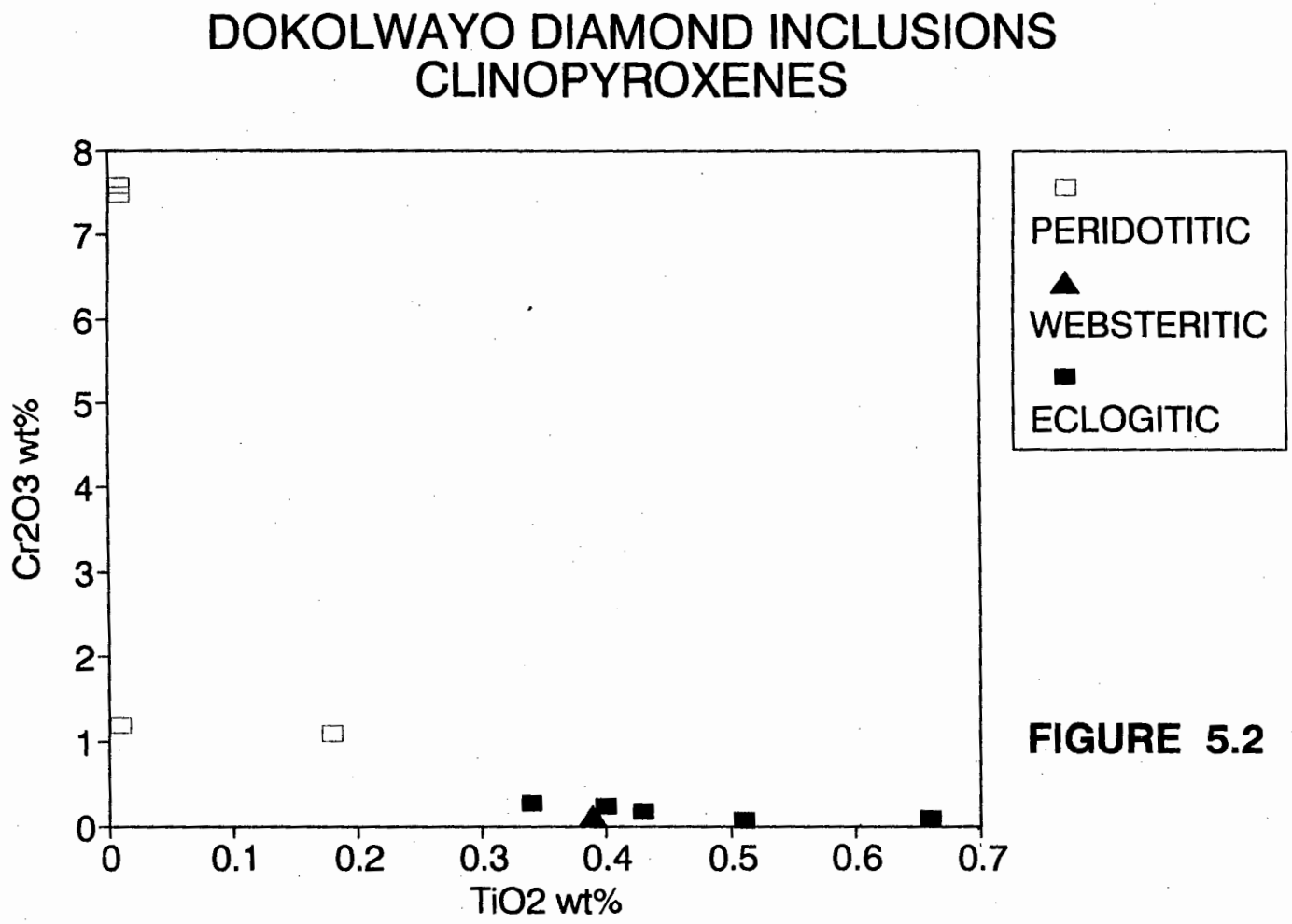
DOKOLWAYO DIAMOND INCLUSIONS
CLINOPYROXENES
Cr2O3 wt%
TiO2 wt%
0
1
2
3
4
5
6
7
8
0
0.1
0.2
0.3
0.4
0.5
0.6
0.7
PERIDOTITIC
WEBSTERITIC
ECLOGITIC

FIGURE 5.2

DOKOLWAYO DIAMOND INCLUSIONS
PERIDOTITIC GARNETS

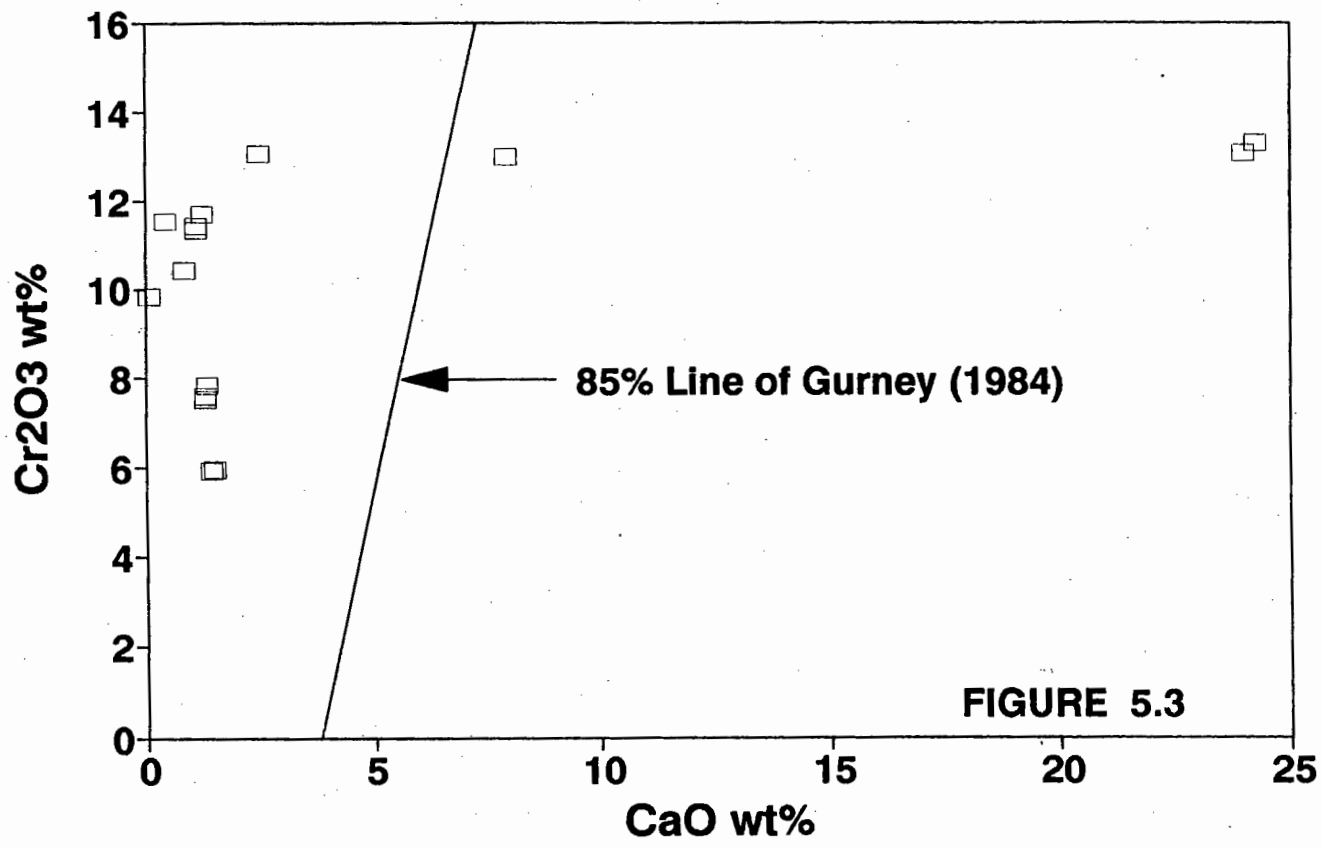

FIGURE 5.3

DOKOLWAYO DIAMOND INCLUSIONS
SPINELS

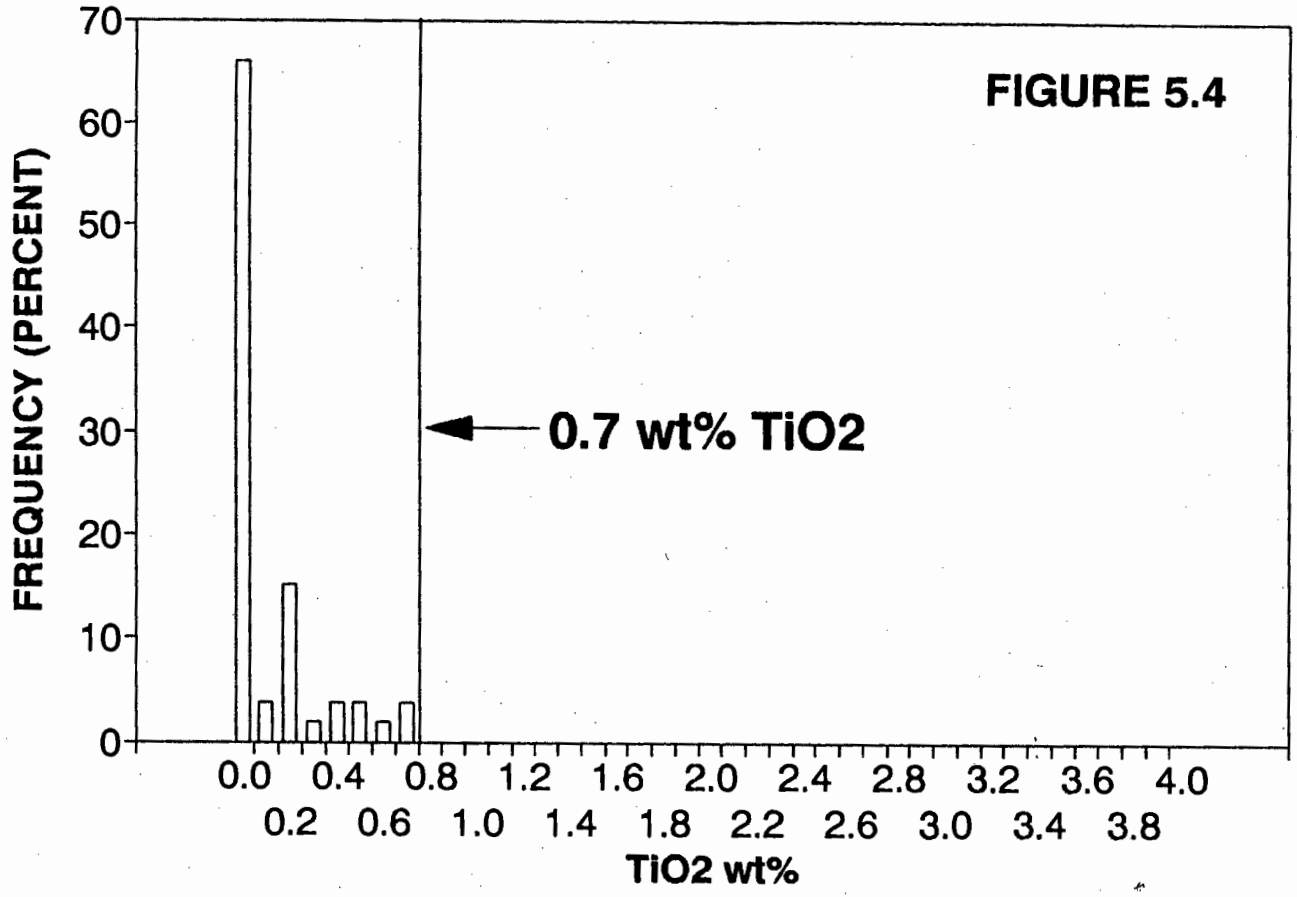

DOKOLWAYO DIAMOND INCLUSIONS
ECLOGITIC GARNETS

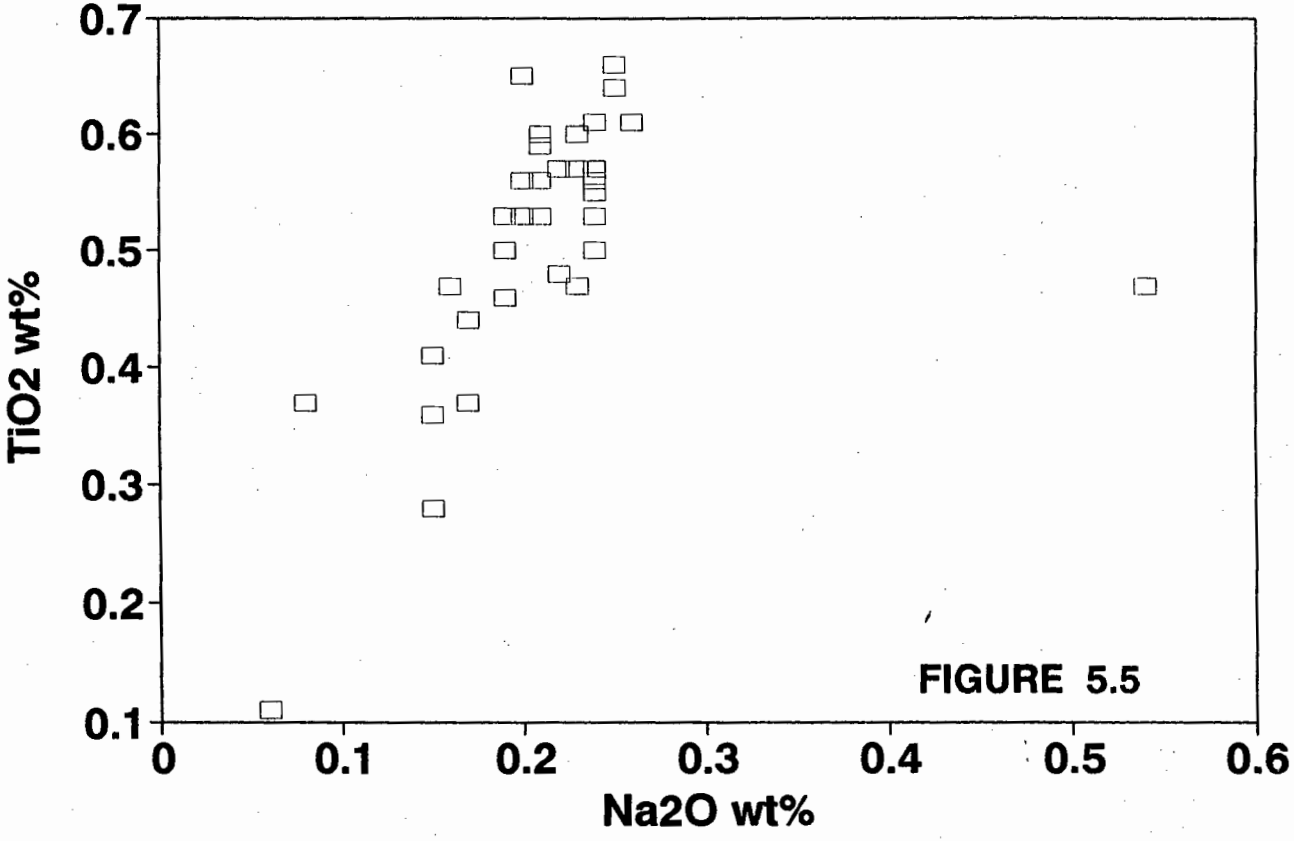

FIGURE 5.5

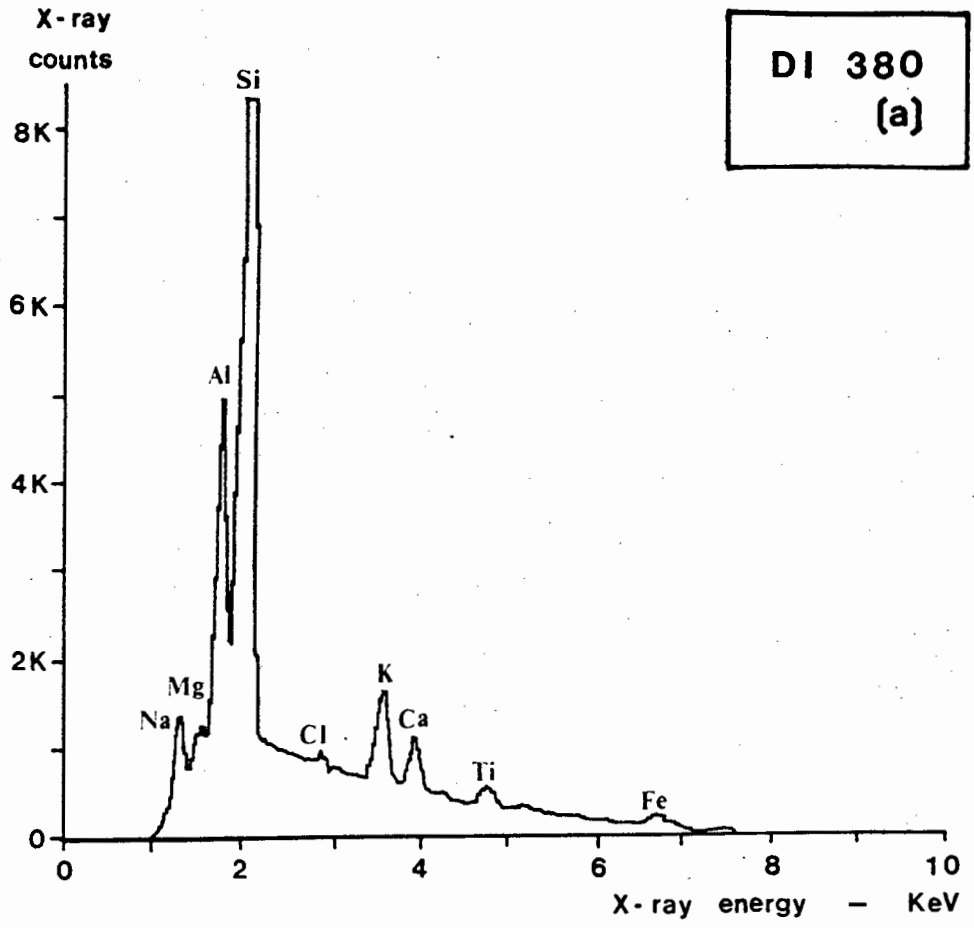
DI 380
(a)
X-ray
counts
8K
6K
4K
2K
0
Si
Al
Mg
Na
Cl
K
Ca
Ti
Fe
0
2
4
6
8
10
X-ray energy — KeV

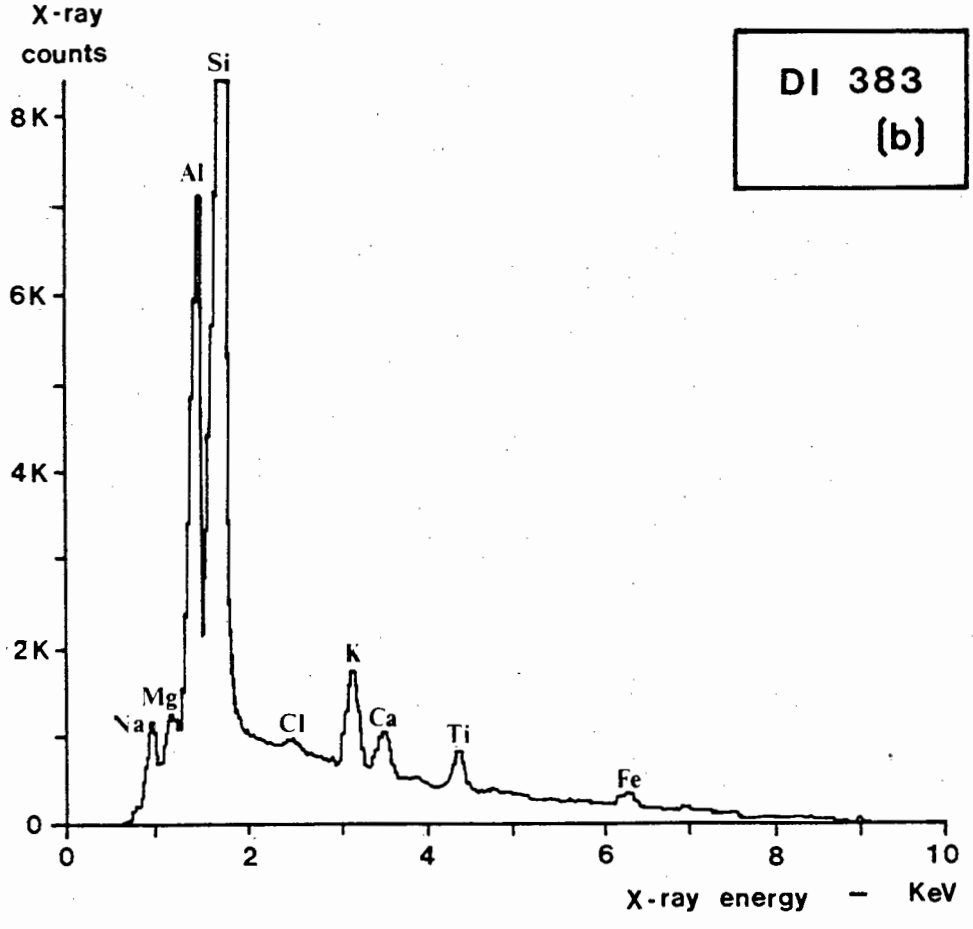
DI 383
(b)
X-ray
counts
8K
6K
4K
2K
0
Si
Al
Mg
Na
Cl
K
Ca
Ti
Fe
0
2
4
6
8
10
X-ray energy — KeV

Fig 5·6

SOUTHERN AFRICAN DIAMONDS

ECLOGITIC GARNET INCLUSIONS

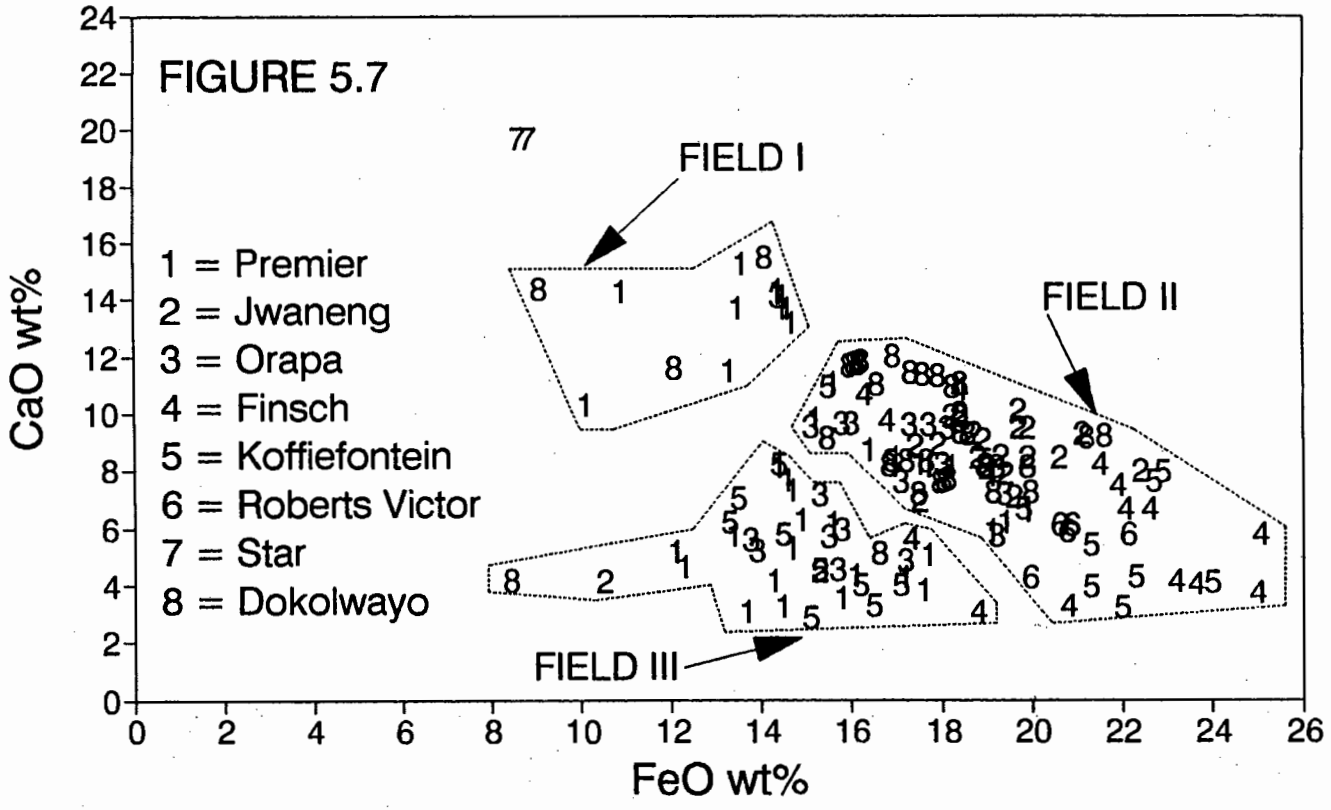

DOKOLWAYO DIAMOND INCLUSIONS APPENDIX 5.a

SAMPLE NUMBER	PARAGENESIS	MINERAL	OXIDE WT% SiO2	TiO2	Al2O3	Cr2O3	Fe2O3	FeO	MnO	MgO	CaO	NiO	Na2O	K2O	TOTAL
DDI44B	PERIDOTITIC	CLINOPYROXENE	55.92	0.18	6.86	1.10		3.73	0.09	14.21	13.37		3.81	0.53	99.80
DDI39A	PERIDOTITIC	CLINOPYROXENE	54.73	0.01	0.85	1.19		2.95	0.10	19.13	19.92		0.57	0.10	99.55
DI364A	WEHRLITIC	CLINOPYROXENE	55.34	ND	4.15	7.48		1.53	ND	13.00	12.83		5.55	0.07	99.95
DI364B	WEHRLITIC	CLINOPYROXENE	54.98	ND	4.09	7.58		1.61	ND	13.28	12.87		5.91	0.06	100.38
DDI04A	ECLOGITIC	CLINOPYROXENE	55.12	0.34	7.24	0.27		6.47	0.09	13.75	12.39		4.02	0.20	99.89
DDI32-1	ECLOGITIC	CLINOPYROXENE	55.76	0.51	12.08	0.08		3.77	0.02	8.79	12.96		5.51	0.51	99.99
DDI33A	ECLOGITIC	CLINOPYROXENE	55.41	0.43	7.09	0.18		6.17	0.12	13.36	12.51		4.31	0.34	99.92
DDI62A	ECLOGITIC	CLINOPYROXENE	54.61	0.40	2.58	0.24		5.46	0.13	20.25	14.58		1.53	0.03	99.81
DI353	ECLOGITIC	CLINOPYROXENE	55.90	0.66	13.98	0.09		3.84	ND	7.26	10.17		7.14	0.48	99.53
DI363	WEBSTERITIC	CLINOPYROXENE	52.28	0.39	1.49	0.13		8.36	0.19	18.82	19.26		0.21	ND	99.13
DI336G	ECLOGITIC	COESITE	95.09	ND	ND	ND		ND	ND	ND	ND		ND	ND	95.09
DI336H	ECLOGITIC	COESITE	95.32	ND	ND	ND		ND	ND	ND	ND		ND	ND	95.32
DI338A	ECLOGITIC	COESITE	94.19	ND	0.03	ND		ND	ND	ND	NO	ND	ND	ND	94.22
DI338B	ECLOGITIC	COESITE	94.85	ND	ND	ND		ND	ND	ND	ND		ND	ND	94.85
DI348B	ECLOGITIC	COESITE	95.24	ND	ND	ND		ND	ND	ND	ND		ND	ND	95.24
DI363B	ECLOGITIC	COESITE	95.57	ND	ND	ND		ND	ND	ND	ND		ND	ND	95.57
DI382A	ECLOGITIC	COESITE	93.95	ND	0.05	ND		ND	ND	ND	ND		ND	ND	94.00
DI388A	ECLOGITIC	COESITE	94.44	ND	ND	ND		ND	ND	ND	NO		ND	ND	94.44
DDI20A	PERIDOTITIC	OLIVINE	40.98	ND	ND	ND		7.11	0.08	50.71	0.05	0.42			99.35
DDI30A	PERIDOTITIC	OLIVINE	40.28	ND	0.13	0.04		7.91	0.14	51.24	0.12	0.34			100.20
DDI32A	PERIDOTITIC	OLIVINE	41.68	ND	ND	ND		7.03	ND	50.71	ND	0.37			99.79
DDI54Q	PERIDOTITIC	OLIVINE	40.80	ND	ND	ND		5.68	0.09	52.26	ND	0.29			99.12
DDI54R	PERIDOTITIC	OLIVINE	41.66	ND	ND	0.06		5.69	0.10	51.41	ND	0.35			99.27
DDI54S	PERIDOTITIC	OLIVINE	41.54	ND	ND	0.04		5.62	0.09	50.49	ND	0.32			98.10
DDI54T	PERIDOTITIC	OLIVINE	43.09	ND	ND	ND		5.33	0.06	50.51	ND	0.28			99.27
DDI54U	PERIDOTITIC	OLIVINE	42.43	ND	0.05	ND		5.29	0.07	51.88	0.04	0.32			100.08
DDI54V	PERIDOTITIC	OLIVINE	41.27	ND	0.14	ND		7.29	0.12	50.27	0.06	0.38			99.53
DI309A	PERIDOTITIC	OLIVINE	40.92	ND	ND	ND		6.52	0.11	50.58	0.09	0.08			98.30
DI310D	PERIDOTITIC	OLIVINE	40.27	ND	ND	ND		7.45	ND	50.61	ND	0.38			98.71
DI342C	PERIDOTITIC	OLIVINE	41.23	ND	ND	ND		6.40	ND	52.10	ND	0.35			100.08
DI362E	PERIDOTITIC	OLIVINE	40.87	ND	ND	ND		6.24	0.11	52.84	ND	0.35			100.41
DK-24C	PERIDOTITIC	ORTHOPYROXENE	57.90	ND	0.83	0.49		3.48	0.09	36.42	0.17		ND	ND	99.38
DI307C	PERIDOTITIC	ORTHOPYROXENE	57.41	ND	0.88	0.68		4.16	0.12	36.13	0.28	0.10	0.06	ND	99.82
DI362D	PERIDOTITIC	ORTHOPYROXENE	57.50	ND	0.93	0.49		3.85	ND	36.85	0.38	0.08	ND	ND	100.08
DI363A	WEBSTERITIC	ORTHOPYROXENE	56.16	0.26	0.98	NO		9.35	0.19	31.44	1.17	0.06	0.20	ND	99.82
DDI03B	ECLOGITIC	GARNET	39.79	0.36	21.88	0.06		18.15	0.31	11.45	7.75		0.15		99.90
DDI03C-1	ECLOGITIC	GARNET	39.92	0.41	22.42	0.06		17.96	0.29	11.29	7.64		0.15		100.14
DDI18A	ECLOGITIC	GARNET	39.22	0.59	22.25	0.08		19.92	0.30	9.76	8.18		0.21		100.51
DDI36-1	ECLOGITIC	GARNET	38.99	0.47	22.10	0.07		18.40	0.27	8.90	10.05		0.54		99.79
DDI43A	ECLOGITIC	GARNET	40.41	0.37	22.79	0.06		12.06	0.22	12.84	11.60		0.17		100.52
DDI03C-2	ECLOGITIC	GARNET	39.94	0.44	22.15	0.07		18.06	0.31	11.46	7.67		0.17		100.27
DI334A	ECLOGITIC	GARNET	40.33	0.11	23.75	0.11		9.07	0.19	12.42	14.38		0.06		100.42
DI335B	ECLOGITIC	GARNET	38.83	0.56	22.60	ND		17.59	0.29	8.35	11.44		0.20		99.86
DI335C	ECLOGITIC	GARNET	39.11	0.57	22.71	0.06		17.31	0.26	8.60	11.45		0.22		100.29
DI335D	ECLOGITIC	GARNET	38.78	0.56	21.62	ND		17.91	0.31	8.68	11.36		0.21		99.43
DI336C	ECLOGITIC	GARNET	39.39	0.56	22.49	0.07		19.20	0.27	9.59	8.17		0.24		99.98
DI336D-C	ECLOGITIC	GARNET	38.33	0.57	22.49	0.05		18.98	0.30	10.26	8.23		0.24		99.45

Sample Number	Paragenesis	Mineral	SiO_2	TiO_2	Al_2O_3	Cr_2O_3	Fe_2O_3	FeO	MnO	MgO	CaO	NiO	Na_2O	K_2O	Total	
DI336D-E	ECLOGITIC	GARNET	39.26	0.59	22.72	0.08		18.93	0.33	10.22	8.18		0.25		100.54	
DI339A	ECLOGITIC	GARNET	39.42	0.46	22.53	0.08		18.58	0.33	9.46	9.32		0.19		100.35	
DI339B	ECLOGITIC	GARNET	39.76	0.44	22.52	0.08		18.40	0.31	9.27	9.38		0.19		100.35	
DI341A	ECLOGITIC	GARNET	38.16	0.60	21.80	0.06		21.19	0.42	7.44	9.23		0.21		99.11	
DI341B	ECLOGITIC	GARNET	38.03	0.65	22.09	ND		21.60	0.36	7.70	9.28		0.20		99.91	
DI347A	ECLOGITIC	GARNET	39.28	0.53	22.99	0.06		16.54	0.26	9.40	11.03		0.19		100.28	
DI351B	ECLOGITIC	GARNET	40.39	0.64	23.08	ND		16.89	0.30	11.05	8.39		0.25		100.99	
DI351C	ECLOGITIC	GARNET	39.14	0.66	22.35	ND		17.21	0.31	10.92	8.37		0.25		99.21	
DI354A	ECLOGITIC	GARNET	39.86	0.53	22.78	0.12		17.47	0.29	11.58	7.22		0.21		100.08	
DI356A	ECLOGITIC	GARNET	39.84	0.50	22.29	0.08		17.66	0.36	11.06	8.38		0.19		100.36	
DI356B	ECLOGITIC	GARNET	40.22	0.56	22.36	0.07		16.81	0.29	11.10	8.21		0.20		99.82	
DI360A	ECLOGITIC	GARNET	39.84	0.55	22.27	ND		16.22	0.32	9.10	11.87		0.24		100.21	
DI360B	ECLOGITIC	GARNET	39.49	0.57	22.25	0.05		16.14	0.35	9.17	11.77		0.23		100.02	
DI360C	ECLOGITIC	GARNET	39.86	0.53	22.12	0.05		16.05	0.32	9.12	11.74		0.24		100.03	
DI360D	ECLOGITIC	GARNET	39.82	0.57	22.17	0.05		15.96	0.34	9.11	11.72		0.24		99.98	
DI367A	ECLOGITIC	GARNET	41.93	0.37	23.53	0.20		8.41	0.31	20.72	4.20		0.08		99.75	
DI370A	ECLOGITIC	GARNET	40.48	0.28	23.13	ND		16.61	0.36	14.27	5.15		0.15		100.41	
DI388B	ECLOGITIC	GARNET	39.17	0.60	22.52	ND		18.40	0.32	8.29	11.08		0.23		100.61	
DI388D	ECLOGITIC	GARNET	39.37	0.61	22.55	ND		18.23	0.31	8.34	11.00		0.24		100.65	
DK12-2	ECLOGITIC	GARNET	39.45	0.61	22.34	ND		14.10	0.21	7.64	15.48		0.26		100.09	
DK27-2	ECLOGITIC	GARNET	39.26	0.47	22.35	0.06		19.98	0.29	10.44	7.30		0.23		100.38	
DK29-1	ECLOGITIC	GARNET	39.44	0.48	22.67	0.04		19.15	0.31	10.93	7.29		0.22		100.53	
DK31-1	ECLOGITIC	GARNET	39.48	0.47	22.66	0.06		15.45	0.27	11.92	9.18		0.16		99.65	
DK44-1	ECLOGITIC	GARNET	39.08	0.50	22.51	ND		16.91	0.31	8.01	12.02		0.24		99.58	
DI324C	UNKNOWN	ZIRCON	32.84	ND	ND	ND		ND	ND	ND	ND				99.22	ZrO2 66.38
DI381A	ECLOGITIC ?	ZIRCON	32.98	ND	ND	ND		ND	ND	ND	ND				99.02	ZrO2 66.04
DI380A	UNKNOWN	CHLORITE	22.39	0.74	23.69	0.74		46.40	ND	0.29	0.32		0.14	1.28	95.99	F 0.32
DI3A11B	ECLOGITIC	STAUROLITE	27.63	0.53	53.59	ND		13.63	0.34	2.08	ND		ND	ND	99.43	ZnO 1.63
DI366	ECLOGITIC ?	ILMENITE	ND	54.46	0.34	1.06		31.02	0.27	12.37	ND	0.12			99.63	
DI351A	ECLOGITIC	ILMENITE?	ND	45.70	0.61	ND		34.07	0.17	9.05	ND	0.07	ND	ND	89.67	Nb2O5 ND
DI392	UNKNOWN	GRAPHITE	ND	ND	ND	ND		ND	ND	ND	ND	ND	ND	ND	0.00	
DI340A	ECLOGITIC ?	MAGNETITE	ND	1.37	0.79	ND	67.09	27.73	0.38	2.47	ND	0.09			99.92	
DI340B	ECLOGITIC ?	MAGNETITE	ND	ND	ND	ND	69.23	29.11	ND	ND	ND	ND			98.34	
DI340AI1	ECLOGITIC ?	SPHENE	29.70	36.41	2.68	ND		2.01	0.11	ND	28.27		0.09	0.15	99.42	
DI340AI2	ECLOGITIC ?	SPHENE	30.33	36.36	2.37	ND		1.83	0.12	ND	28.08		0.07	ND	99.16	
DI344A	ECLOGITIC	SANIDINE	68.29	ND	22.60	ND		ND	ND	ND	2.20	ND	7.96	0.21	101.26	
DI353A	PERIDOTITIC	GARNET	38.43	0.33	11.32	13.05		5.27	0.26	6.64	24.00		0.04		99.34	
DI350A-C	PERIDOTITIC	GARNET	42.64	0.10	19.95	5.98		5.45	0.31	24.08	1.52		0.03		100.06	
DI350A-E	PERIDOTITIC	GARNET	42.37	0.09	19.74	5.95		5.51	0.28	24.05	1.46		0.03		99.48	
DI375A	PERIDOTITIC	GARNET	38.54	0.32	10.89	13.28		4.79	0.25	6.81	24.26		0.02		99.16	
DI307A	PERIDOTITIC	GARNET	41.74	ND	15.88	11.41		5.68	0.28	23.78	1.14		ND		99.91	
DI307B	PERIDOTITIC	GARNET	41.72	ND	15.53	11.68		5.88	0.24	23.53	1.25		0.02		99.85	
DI307C	PERIDOTITIC	GARNET	41.78	ND	15.62	11.32		6.00	0.32	23.63	1.12		ND		99.79	
DK42A	PERIDOTITIC	GARNET	40.45	0.06	13.93	13.07		6.25	0.34	21.92	2.50		ND		98.52	
DK24-01	PERIDOTITIC	GARNET	42.27	ND	16.81	10.42		5.63	0.21	23.75	0.88		0.02		99.99	
DK24-02	PERIDOTITIC	GARNET	41.52	ND	16.95	9.84		5.15	0.20	25.04	0.09		0.03		98.82	
DDI45A	PERIDOTITIC	GARNET	42.25	0.02	15.17	11.53		5.81	0.32	23.95	0.43		0.02		99.50	
DDI54A	PERIDOTITIC	GARNET	42.14	ND	18.28	7.85		5.55	0.30	23.93	1.34		ND		99.39	
DDI54C	PERIDOTITIC	GARNET	42.54	ND	18.51	7.59		5.67	0.24	24.39	1.31		ND		100.25	
DDI54E	PERIDOTITIC	GARNET	42.60	ND	18.80	7.54		5.70	0.26	23.20	1.33		0.08		99.51	
DI304A	PERIDOTITIC	GARNET	40.53	ND	14.26	12.98		5.89	0.34	18.14	7.94		ND		100.08	
DDI14A	PERIDOTITIC	SPINEL	0.00	0.00	7.71	64.47	1.80	11.17	0.17	13.93	0.00	0.00			99.25	
DDI42A	PERIDOTITIC	SPINEL	0.00	0.00	7.71	64.91	1.43	11.43	0.25	13.79	0.00	0.00			99.52	
DDI51	PERIDOTITIC	SPINEL	0.00	0.31	4.96	66.61	0.00	11.46	0.21	13.88	0.00	0.14			97.57	

Sample Number	Paragenesis	Mineral	SiO_2	TiO_2	Al_2O_3	Cr_2O_3	Fe_2O_3	FeO	MnO	MgO	CaO	NiO	Na_2O	K_2O	Total	
DDI52A	PERIDOTITIC	SPINEL	0.00	0.00	6.90	64.82	1.64	12.27	0.30	13.23	0.00	0.00			99.16	
DI202B	PERIDOTITIC	SPINEL	0.00	0.00	7.96	63.28	2.35	11.35	0.24	13.79	0.00	0.13			99.10	
DI302A	PERIDOTITIC	SPINEL	0.00	0.00	8.21	64.77	0.47	12.67	0.19	12.79	0.00	0.00			99.10	
DI302C	PERIDOTITIC	SPINEL	0.00	0.00	7.82	63.25	2.66	11.23	0.25	13.72	0.00	0.08			99.01	
DI302D	PERIDOTITIC	SPINEL	0.00	0.00	7.90	63.42	2.49	11.54	0.21	13.82	0.00	0.08			99.46	
DI302E	PERIDOTITIC	SPINEL	0.00	0.00	7.94	63.76	2.68	11.34	0.22	13.92	0.00	0.09			99.95	
DI303A	PERIDOTITIC	SPINEL	0.00	0.35	7.02	64.19	2.41	10.35	0.24	14.62	0.00	0.08			98.26	
DI305A	PERIDOTITIC	SPINEL	0.00	0.00	8.86	63.11	2.80	9.54	0.19	15.25	0.00	0.08			99.83	
DI305B	PERIDOTITIC	SPINEL	0.00	0.00	8.84	62.53	4.07	8.43	0.00	15.23	0.00	0.00			99.10	
DI305C	PERIDOTITIC	SPINEL	0.00	0.00	8.55	63.58	2.50	10.19	0.21	14.73	0.00	0.12			99.88	
DI306A	PERIDOTITIC	SPINEL	0.00	0.00	7.65	63.99	2.41	11.07	0.24	13.90	0.00	0.08			99.34	
DI306C	PERIDOTITIC	SPINEL	0.00	0.00	7.82	64.79	1.16	12.28	0.23	13.47	0.00	0.07			99.82	
DI310A	PERIDOTITIC	SPINEL	0.00	0.00	7.49	65.13	2.44	10.26	0.23	14.61	0.00	0.00			100.16	
DI310B	PERIDOTITIC	SPINEL	0.00	0.00	7.03	65.17	2.03	10.71	0.20	14.39	0.00	0.14			99.67	
DI311A	PERIDOTITIC	SPINEL	0.00	0.00	7.67	64.33	2.42	10.59	0.16	14.37	0.00	0.08			99.62	
DI311C	PERIDOTITIC	SPINEL	0.00	0.12	7.67	63.68	3.77	9.56	0.00	14.58	0.00	0.09			99.47	
DI311D	PERIDOTITIC	SPINEL	0.00	0.14	7.51	64.12	2.08	10.72	0.19	14.26	0.00	0.08			99.10	
DI315A	PERIDOTITIC	SPINEL	0.00	0.14	5.03	67.61	2.01	10.35	0.26	14.35	0.00	0.08			99.85	
DI317AA	PERIDOTITIC	SPINEL	0.00	0.08	8.62	63.67	2.15	9.76	0.27	15.09	0.00	0.07			99.71	
DI317B	PERIDOTITIC	SPINEL	0.00	0.00	8.88	63.83	2.06	9.10	0.18	15.20	0.00	0.08			99.33	
DI319A	PERIDOTITIC	SPINEL	0.00	0.13	7.40	67.00	0.00	10.98	0.27	13.19	0.00	0.11			99.08	
DI319B	PERIDOTITIC	SPINEL	0.00	0.14	7.76	64.42	1.83	9.69	0.18	15.11	0.00	0.07			99.20	
DI319C	PERIDOTITIC	SPINEL	0.00	0.14	7.83	64.02	2.09	9.65	0.16	15.06	0.00	0.09			99.04	
DI319D	PERIDOTITIC	SPINEL	0.00	0.18	7.71	64.40	2.29	9.70	0.24	15.16	0.00	0.11			99.79	
DI320A	PERIDOTITIC	SPINEL	0.00	0.00	8.11	63.38	2.47	10.76	0.20	14.28	0.00	0.14			99.34	
DI320B	PERIDOTITIC	SPINEL	0.00	0.00	7.98	63.51	2.91	10.97	0.20	14.22	0.00	0.13			99.92	
DI320C	PERIDOTITIC	SPINEL	0.00	0.00	8.01	63.49	3.05	10.26	0.23	14.66	0.00	0.09			99.79	
DI323B	PERIDOTITIC	SPINEL	0.00	0.26	5.72	66.27	1.92	11.03	0.27	14.01	0.00	0.14			99.62	
DI324A	UNKNOWN	SPINEL	0.00	0.00	5.00	65.75	3.21	13.18	0.36	12.14	0.00	0.00			99.64	
DI324B	UNKNOWN	SPINEL	0.00	0.00	5.02	65.04	3.72	12.86	0.40	12.24	0.00	0.00			99.28	
DI326A	PERIDOTITIC	SPINEL	0.00	0.62	13.90	58.21	1.65	8.05	0.14	17.20	0.00	0.15			99.92	
DI328B	PERIDOTITIC	SPINEL	0.00	0.47	10.55	61.45	1.30	9.48	0.21	15.68	0.00	0.11			99.25	
DI328C	PERIDOTITIC	SPINEL	0.00	0.49	10.61	62.11	0.00	11.04	0.17	14.60	0.00	0.17			99.19	
DI330A	PERIDOTITIC	SPINEL	0.00	0.18	6.07	64.83	3.01	11.57	0.16	13.81	0.00	0.07			99.70	
DI331A	PERIDOTITIC	SPINEL	0.00	0.00	6.50	67.88	0.72	9.01	0.16	15.23	0.00	0.00			99.50	
DI331B	PERIDOTITIC	SPINEL	0.00	0.00	6.42	67.76	1.01	8.92	0.20	15.45	0.00	0.07			99.83	
DI331D	PERIDOTITIC	SPINEL	0.00	0.00	6.87	66.04	2.00	8.18	0.23	15.75	0.00	0.07			98.14	
DI331E	PERIDOTITIC	SPINEL	0.00	0.00	5.67	68.47	1.03	8.40	0.27	15.31	0.00	0.05			99.20	
DI332A	PERIDOTITIC	SPINEL	0.00	0.59	8.00	63.10	2.72	9.98	0.28	15.32	0.00	0.09			100.06	
DI332B	PERIDOTITIC	SPINEL	0.00	0.61	7.76	63.58	2.03	10.55	0.25	14.85	0.00	0.10			99.73	
DI333A	PERIDOTITIC	SPINEL	0.00	0.08	7.54	64.56	2.08	10.83	0.22	14.38	0.00	0.09			99.78	
DI337A	PERIDOTITIC	SPINEL	0.00	0.00	8.35	63.63	2.42	10.36	0.16	14.52	0.00	0.13			99.57	
DI337B	PERIDOTITIC	SPINEL	0.00	0.00	8.25	63.64	2.44	10.39	0.23	14.51	0.00	0.12			99.58	
DI362F	PERIDOTITIC	SPINEL	0.00	0.00	12.98	59.55	1.57	11.06	0.23	14.74	0.00	0.12			100.25	
DI362I	PERIDOTITIC	SPINEL	0.00	0.00	13.00	59.23	2.08	10.53	0.19	15.22	0.00	0.09			100.34	
DI362J	PERIDOTITIC	SPINEL	0.00	0.00	12.68	59.21	2.38	10.24	0.00	14.58	0.00	0.09			99.18	
DI374B	PERIDOTITIC	SPINEL	0.00	0.00	8.51	63.31	2.41	10.62	0.20	14.60	0.00	0.09			99.74	
DI391A	PERIDOTITIC	SPINEL	0.00	0.00	8.14	63.96	2.81	9.63	0.18	15.00	0.00	0.09			99.81	
DK038A	PERIDOTITIC	SPINEL	0.00	0.00	8.38	64.16	1.34	10.74	0.18	14.50	0.00	0.10			99.40	
DK038B	PERIDOTITIC	SPINEL	0.00	0.00	8.13	64.78	1.74	10.03	0.24	14.76	0.00	0.00			99.68	
DI3A11B	ECLOGITIC	STAUROLITE	27.63	0.53	53.59	ND		13.63	0.34	2.08	ND		ND	ND	99.43	ZnO 1.63
Average Metapelitic Staurolite Analyses (Kasck, 1967)																
K23Arim	METAPELITE	STAUROLITE	27.87	0.66	53.74			14.02	0.27	1.78					99.20	ZnO 0.88
K23Acore	METAPELITE	STAUROLITE	28.23	0.68	53.29			14	0.25	1.96					99.29	ZnO 0.89
K320Crim	METAPELITE	STAUROLITE	27.69	0.78	54.26			12.79	0.27	1.44					98.96	ZnO 1.72
K320Core	METAPELITE	STAUROLITE	27.55	0.78	54.17			12.99	0.25	1.48					98.85	ZnO 1.63
K516Brim	METAPELITE	STAUROLITE	27.56	0.72	54.48			13.1	0.3	1.5					99.11	ZnO 1.45
K516Core	METAPELITE	STAUROLITE	27.69	0.73	54.43			13.4	0.33	1.54					99.61	ZnO 1.49

CHAPTER 6 - DOKOLWAYO DIAMOND CARBON ISOTOPES

ABSTRACT

The carbon isotopic compositions of 88 diamonds from the Dokolwayo kimberlite were analyzed using standard methods (Chapter 2). The majority of the diamonds range between $\delta^{13}C$

-1 and -10‰. The peridotitic diamonds are slightly enriched compared to the eclogitic diamonds. No distinct relationship exists between the compositions of eclogitic diamond inclusions and the isotopic compositions of the host diamonds. A correlation exists between Cr_2O_3 in the spinels and carbon isotopic compositions. The vapour source of the carbon from which the majority of the eclogitic and peridotitic diamonds crystallized is considered to be CH_4. The source of the vapour is suggested to be CH_4 degassing from the lower mantle or core and subsequent CH_4 permeation of the upper mantle on a continuous basis. Significant zonation of $\delta^{13}C$ values from a single diamond suggests Rayleigh fractionation of a subducted carbonaceous source. Fractionation of carbon isotopes from a cubic diamond and a diamond with a polycrystalline coat appears to be limited.

INTRODUCTION

Carbon isotope compositions of diamonds have in the recent past attracted considerable amount of interest. The main feature of interest is the wide range in $\delta^{13}C$ values (~35‰ vs PDB) obtained from diamonds world wide (Galimov, 1984; Deines et al., 1984, 1986, 1987, 1989; Hill, 1989; Otter, 1990; Kirkley et al., 1991). The majority of diamonds have $\delta^{13}C$ values between -2 and -9‰ with an average of approximately -6‰. This average value is considered by most workers to be representative of primordial carbon in the mantle. A significant proportion of diamonds, commonly diamonds of eclogitic

paragenesis, have $\delta^{13}C$ values which cover the range between organic carbon ($\delta^{13}C$ ~-30$^{o}/_{oo}$) and inorganic carbon ($\delta^{13}C$ ~0$^{o}/_{oo}$). This range in carbon isotope values has precipitated debate whether the carbon source of the diamonds are crustal and recycled or mantle in origin.

In previous studies of southern African diamonds the tendency has been to investigate any possible relationship between the carbon isotopic composition of the diamond host and the chemical composition of the minerals included in the diamond (Deines et al., 1984; 1987, 1989; Hill, 1989; McCandless et al., 1989; Kirkley et al., 1991). A similar approach has been adopted in this study of Dokolwayo diamonds. The carbon isotopic composition for the majority of the diamonds from which minerals were recovered have been determined. For most of the sub-populations of diamond inclusions recognized at Dokolwayo the data are too limited to test for correlations between the $\delta^{13}C$ values and the chemical composition of the inclusions. However, it has been possible to investigate this relationship between $\delta^{13}C$ and the composition between (1) peridotitic spinel and (2) eclogitic garnet inclusions. These two suites of inclusions are assumed to represent mantle and subducted material respectively and thus provides an opportunity to evaluate carbon isotopes of diamonds from "primordial" and "subducted or recycled" sources.

In addition to the inclusion diamonds, the carbon isotopic compositions of a cubic diamond and a polycrystalline diamond with a single crystal core were determined. A total of 88 diamonds were analyzed for their isotopic compositions. Results are presented in Appendix 6.a.

PREVIOUS WORK

Comprehensive data are at present only available from four southern African localities (Deines et al., 1984, 1987, 1989; Hill, 1989). Three of these localities are Cretaceous Group II kimberlites (Finsch, Star, Roberts Victor) while the other (Premier) is a

Precambrian Group I kimberlite (Smith, 1983). Dokolwayo is a Jurassic Group II kimberlite (Smith, 1983; Allsopp and Roddick, 1984). Deines et al. (1984) found that diamonds containing peridotitic clinopyroxenes and garnets tend to have higher $\delta^{13}C$ values than diamonds encapsulating olivine or orthopyroxene. It was also found that there was a broad correlation between the Mg/(Mg+Fe) ratio of the olivines, orthopyroxenes and garnets and the $\delta^{13}C$ values of the host diamonds. The diamonds with the more ^{13}C depleted content were invariably characterized by minerals with lower Mg/(Mg+Fe) ratios.

The Premier diamonds containing eclogitic mineral inclusions exhibit a significant positive correlation between $\delta^{13}C$ and CaO and negative correlations between $\delta^{13}C$ and MgO, Al_2O_3 and the Mg/(Mg+Fe) ratios of the garnets. It was also found that eclogitic diamonds with $\delta^{13}C$ values larger than $-4^{o}/_{oo}$ contain garnets with higher Ca/(Ca+Mg) ratios than those with $\delta^{13}C$ values smaller than $-4^{o}/_{oo}$.

The carbon isotopes from Finsch peridotitic diamonds follow the same trends with respect to the compositions of the inclusions as observed for the Premier diamonds. In contrast, compositions and the $\delta^{13}C$ values for eclogitic diamonds from Finsch that encapsulate garnets are significantly different compared to the Premier E-type diamonds (Deines et al., 1984).

Deines et al. (1987) found no correlation between $\delta^{13}C$ values and peridotitic silicate inclusions at Roberts Victor. It was found that spinel inclusions may be separated on the basis of their FeO/MgO and Cr_2O_3/Al_2O_3 ratios into two populations whose hosts show a significant difference in their carbon isotopic composition.

Two groups of eclogitic diamonds based on mineral compositions were identified at Roberts Victor. These two groups of E-type diamonds could also be distinguished on the basis of their carbon isotopic compositions. The one mode of eclogitic diamonds lies at -15 to $-16^{o}/_{oo}$ whereas the other coincides with that of P-type diamonds around -5 to $-6^{o}/_{oo}$.

Eclogitic garnets were recovered from the depleted diamonds only. Clinopyroxenes were recovered from both groups of eclogitic diamonds. The clinopyroxenes recovered from the depleted diamonds are relatively enriched in Al_2O_3, FeO and MnO and depleted in SiO_2, MgO and CaO compared to those from the second group of eclogitic diamonds (Deines et al., 1987).

The carbon isotopes of the Premier and Finsch peridotitic diamonds have been suggested to be related to depth of crystallization (Deines et al., 1984), but no such correlation could be found for the Roberts Victor diamonds. It was suggested that peridotitic diamonds with higher $\delta^{13}C$ values crystallized from a magma from an undepleted mantle at depths below the lithosphere. Diamonds with less depleted $\delta^{13}C$ values were suggested to have crystallized, together with highly depleted minerals, from melts at the base of the lithosphere (Deines et al., 1984). The carbon source for the peridotitic diamonds was suggested to be mantle-derived and therefore presumably "primordial" in origin.

The compositions of the eclogitic inclusions in diamonds from Premier, Roberts Victor and Finsch together with the $\delta^{13}C$ values of the associated diamonds suggest that these diamonds are not related to a continuous magmatic differentiation process, but indicates a source with compositional differences (Deines et al., 1984).

RESULTS

The Dokolwayo diamonds predominantly have $\delta^{13}C$ values between -1 and $-10^{o}/_{oo}$ (Figure 6.1). Only five diamonds were characterized by $\delta^{13}C$ values more depleted than $-10^{o}/_{oo}$. Two of these depleted diamonds had coesite inclusions. The most depleted diamond ($\delta^{13}C = -22.3^{o}/_{oo}$) contained an albite inclusion. The diamond exhibiting the largest range in $\delta^{13}C$ values (DI 339; $-15.2^{o}/_{oo}$ to $-20.8^{o}/_{oo}$) had eclogitic garnet and sulphide as inclusions. Four of the five diamonds more depleted than $-10^{o}/_{oo}$ are of eclogitic paragenesis. The only other highly depleted diamond (DI 324) was characterized

by zoning in colour as well as $\delta^{13}C$ values. The diamond had a colourless core and was progressively zoned to yellow on the external surface. Three pieces of diamond were selected for carbon isotope analysis. The colourless core was the most depleted ($\delta^{13}C$ = -19.7$^{o}/_{oo}$). A yellow fragment without any external surfaces had a $\delta^{13}C$ of -17.3$^{o}/_{oo}$ and a yellow fragment with external surfaces was the heaviest with $\delta^{13}C$ = -16.4$^{o}/_{oo}$. The diamond contained two chromium-rich spinels and a zircon as inclusions. The spinels recovered from this diamond were the only inclusion spinels recovered from diamonds during the course of this study with Mg/(Mg+Fe) < 0.50.

The cubic diamond was split in half. Fragments were recovered from the centre, middle and edge of this diamond. The $\delta^{13}C$ values of this cubic diamond show a consistent depletion signature from -3.6$^{o}/_{oo}$ at the centre to -3.9$^{o}/_{oo}$ at the edge. However, the range obtained is within 2σ of experimental error. Similarly, the $\delta^{13}C$ values determined between the core of the single crystal diamond (-3.88$^{o}/_{oo}$) with a polycrystalline coat (-4.05$^{o}/_{oo}$) are statistically insignificant.

Six peridotitic diamonds were investigated for $\delta^{13}C$ variations. All four diamonds containing spinels and with $\delta^{13}C$ < -10$^{o}/_{oo}$ were characterized by variations marginally in excess of experimental error. The one diamond containing olivine had a variation in $\delta^{13}C$ values of -1.2$^{o}/_{oo}$. The largest range in $\delta^{13}C$ values observed in a peridotitic diamond was observed in the zoned diamond described above.

Two fragments were analyzed from each of three eclogitic diamonds. No significant variation was observed in diamond DI 341, but diamond DI 367 containing an eclogitic garnet and a diamond as inclusions had a $\delta^{13}C$ range of -1.8$^{o}/_{oo}$ from -3.4$^{o}/_{oo}$ to -5.2$^{o}/_{oo}$. Diamond DI 354 contained a garnet only and had a $\delta^{13}C$ range from -6.4$^{o}/_{oo}$ to -7.1$^{o}/_{oo}$.

The peridotitic diamonds have an average $\delta^{13}C$ value of -4.1‰. The carbon isotopes of the main population of peridotitic diamonds appear to have a bimodal distribution (Figure 6.2). This may be a function of sampling statistics. In contrast to the observations of Deines et al. (1984) there is no significant relationship between $\delta^{13}C$ and FeO of the spinels (Figure 6.3). However, there does appear to be a correlation between the carbon isotopic composition of the host diamonds and the Cr_2O_3 contents of the inclusion spinels (Figure 6.4).

The average $\delta^{13}C$ value for eclogitic diamonds is -7.1‰. No compositional relationship between host diamond isotopic composition and garnet inclusion composition was observed.

DISCUSSION

Deines (1980) determined that under expected constraints on mantle physiochemical conditions CO_2 and CH_4 are the only plausible vapour sources from which diamond could precipitate. Deines (1980) invoked Rayleigh fractionation to model the distribution and range of diamond $\delta^{13}C$ that would result during carbon precipitation from CO_2 vapour upon decreasing fO_2 and CH_4 vapour upon increasing fO_2 in the diamond stability field. The initial conditions assumed were 1020°C at 45 kilobars and an initial isotopic composition and variability of the carbon source vapour of -5.0±0.3‰ (1σ). Diamond precipitating from a CO_2 vapour would be depleted in ^{13}C relative to the CO_2 vapour by approximately 4‰ (Bottinga, 1969a). Therefore, the first diamond to precipitate from the CO_2 reservoir would have a $\delta^{13}C$ value of -9‰. Removal of this relatively ^{13}C-depleted diamond from the reservoir will result in a vapour becoming increasingly enriched in ^{13}C during diamond crystallization. The distribution of $\delta^{13}C$ values in diamonds resulting from this process will be skewed toward $\delta^{13}C$ values greater than the initial diamond $\delta^{13}C$ value (Figure 6.5a). In contrast, diamond is enriched in ^{13}C relative to

CH_4 vapour by approximately $1^{o}/_{oo}$ (Bottinga, 1969a) and hence diamond precipitation from CH_4 will give rise to a less marked negatively skewed distribution (Figure 6.5b).

The main Dokolwayo eclogitic diamond population has a $\delta^{13}C$ distribution similar to the model distribution of Deines (1980) for the crystallization of diamonds from the oxidation of CH_4 (Figure 6.6). This distribution suggests that the predominant carbon source of the eclogitic diamonds is CH_4. It is unlikely that these Dokolwayo diamonds have a recycled source of carbon since their $\delta^{13}C$ values are consistent with a "primordial" carbon isotope range and not a "subducted, recycled" range of carbon isotopic compositions (Kirkley et al., 1991). There is a possibility that the carbon from which these eclogitic diamonds have crystallized was subducted and that very little fractionation from the primordial carbon in the subducted slab has occurred. However, the preferred alternative is the introduction of primordial CH_4 into an oxidized eclogite. Elemental carbon will precipitate according to the reaction:

$$CH_4 + O_2 = C + 2H_2O$$

The introduction of the CH_4 into the oxidized eclogite may be as a product of core or mantle degassing. It should be noted that the carbon isotopic fractionation between graphite and diamond is small ($<0.5^{o}/_{oo}$ at 700°C; Bottinga, 1969b) and the isotopic composition of graphite is unlikely to change significantly through recrystallization to diamond. The CH_4 reduction in eclogite is therefore not necessarily confined to within the stability field of diamond.

The $\delta^{13}C$ distribution of the peridotitic diamonds is characteristic of a "primordial" signature. The distribution curve does not conform exactly with the model distributions developed by Deines (1980) for the precipitation of carbon from either CO_2 or CH_4. Nevertheless, the average $\delta^{13}C$ value of the peridotitic diamonds is not consistent with CO_2 being the carbon source of these diamonds. It is suggested that the main source of

carbon for the peridotitic diamonds is, similar to the main group of eclogitic diamonds, primordial CH_4 degassing from the core or lower mantle.

Swart et al. (1983) suggested that the trend from isotopically light cores to heavier rims on coated diamonds could be the result of Rayleigh fractionation of CO_2. The maximum δ13C value attained during metamorphism of organic carbon is approximately $-10^{o}/_{oo}$. Crustal carbonaceous material range in $\delta^{13}C$ values from $-35^{o}/_{oo}$ to $-20^{o}/_{oo}$ (Kirkley et al., 1991). The zonation pattern and values of carbon isotopes of diamond DI 324 suggest that the diamond is the product of Rayleigh fractionation of carbonaceous material. The refractory nature of the inclusions in this diamond suggests that it did not crystallize within an eclogitic environment. It is suggested that this diamond crystallized in a refractory spinel peridotite subducted in an Archaean tectonic environment as described by De Wit and Tredoux (1987).

Cubes and polycrystalline diamonds have been suggested to be products of rapid crystallization from a saturated carbon source. The insignificant variation in carbon isotopes analyzed from a cubic diamond and from a diamond with a single crystal core and a polycrystalline coat suggests that these diamonds crystallized in an environment that was not conducive to large scale fractionations. In the event that these diamonds crystallized from a CO_2 vapour one would expect major depletion signatures during the early stages of crystallization and a gradual enrichment. The carbon isotopic values of these diamonds indicate that they are enriched in 13C. CO_2 therefore appears to be an unlikely vapour source for the crystallization of these diamonds.

CHAPTER 6 - FIGURE CAPTIONS

FIGURE 6.1

Distribution of $\delta^{13}C$ values of all Dokolwayo diamonds analysed in this study.

FIGURE 6.2

Distribution of $\delta^{13}C$ values of peridotitic Dokolwayo diamonds. These diamonds encompass all types of peridotitic assemblages, i.e. harzburgitic, lherzolitic, wehrlitic and dunitic.

FIGURE 6.3

Plot of $\delta^{13}C$ values of spinel bearing diamonds from Dokolwayo versus the FeO (wt%) contents of the inclusion spinels.

FIGURE 6.4

Plot of $\delta^{13}C$ values of spinel bearing diamonds from Dokolwayo versus the Cr_2O_3 (wt%) contents of the inclusion spinels.

FIGURE 6.5

$\delta^{13}C$ sampling frequency distributions of diamonds resulting from (a) $CO_2 <-> C + O_2$ and (b) $CH_4 <-> C + 2H_2$ at T = 1020°C, P=45 kbar, the carbon isotopic composition of the total vapour is initially -5.0 $\pm$ 0.3 $^{o}/_{oo}$ (one standard deviation). After Deines (1980).

FIGURE 6.6

Distribution of $\delta^{13}C$ values of eclogitic Dokolwayo diamonds. These diamonds include all types of eclogitic assemblages, e.g. garnet, clinopyroxene, coesite, ilmenite, staurolite, graphite, feldspar, and diamond.

DOKOLWAYO DIAMONDS
CARBON ISOTOPE DISTRIBUTION

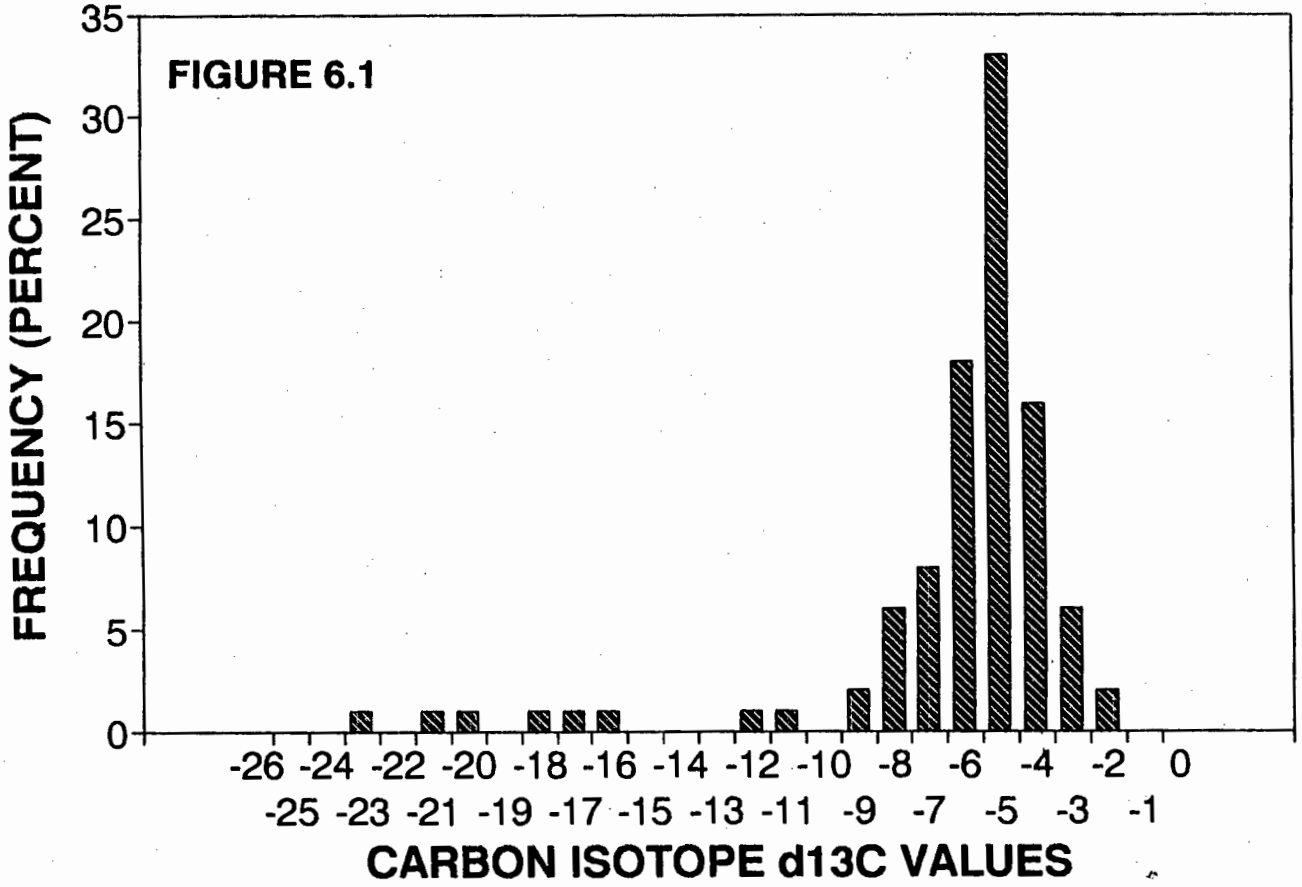

DOKOLWAYO PERIDOTITIC DIAMONDS
CARBON ISOTOPE DISTRIBUTION

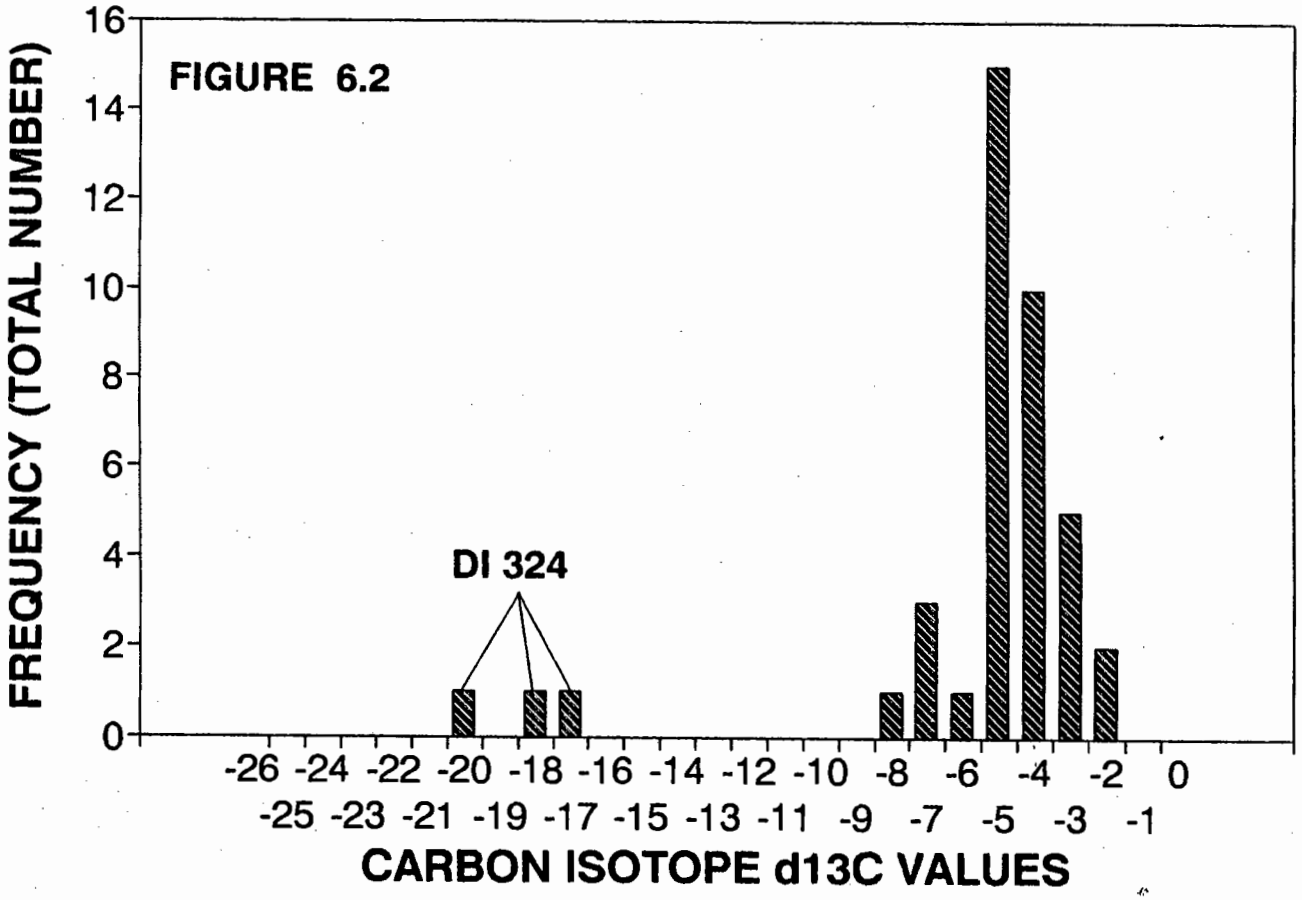

DOKOLWAYO DIAMOND INCLUSIONS
CARBON ISOTOPES VERSUS FeO IN SPINELS

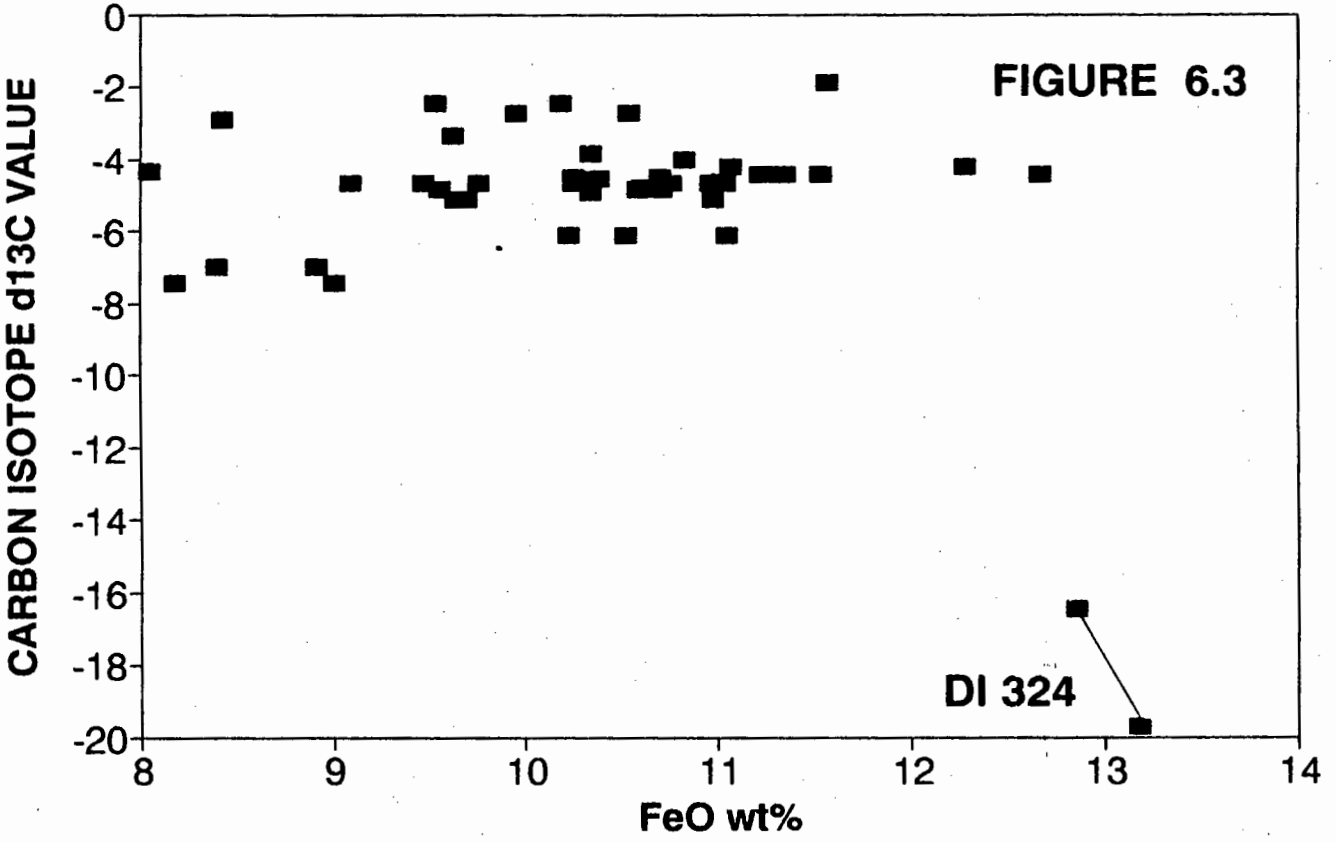

DOKOLWAYO DIAMOND INCLUSIONS
CARBON ISOTOPES VERSUS Cr2O3 IN SPINELS

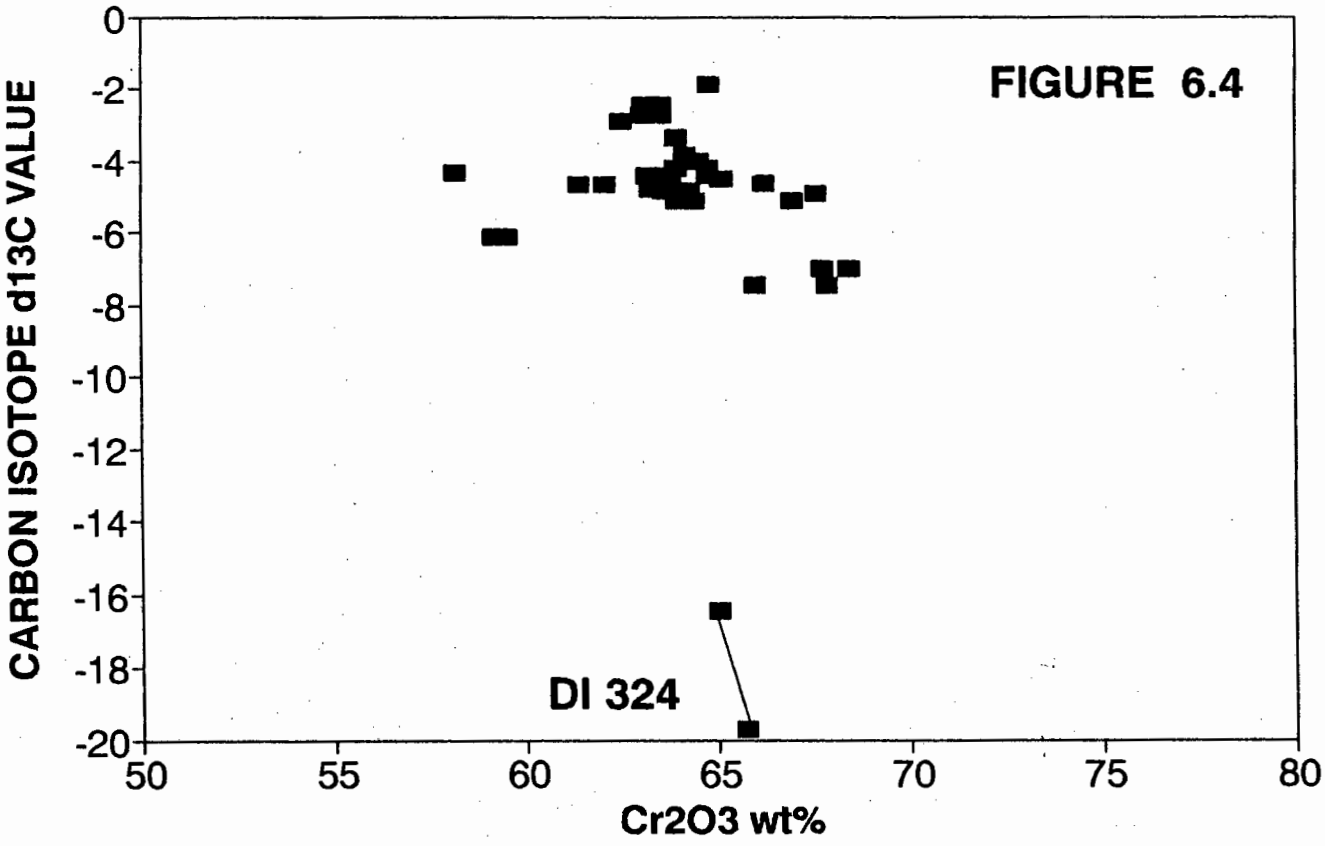

(a) $CO_2 \longrightarrow C + O_2$

(fO_2 decreases)

$\Delta_{vap-dmd} \sim 4\%$

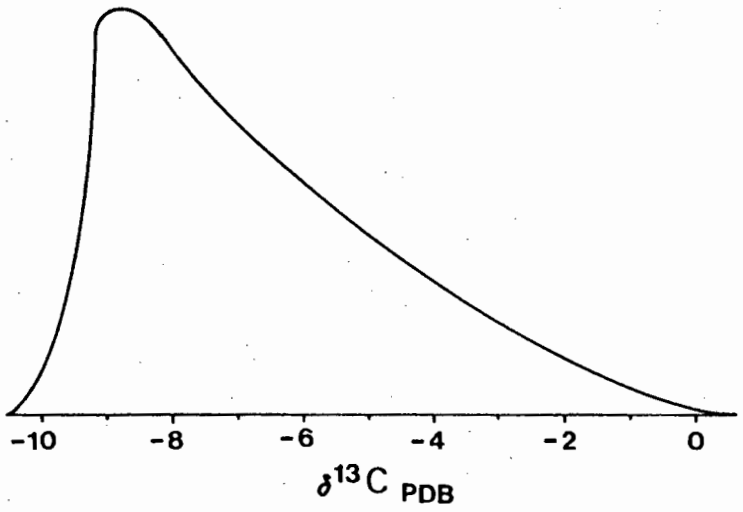

(b) $CH_4 \longrightarrow C + 2H_2$

(fO_2 increases)

$\Delta_{vap-dmd} \sim -1\%$

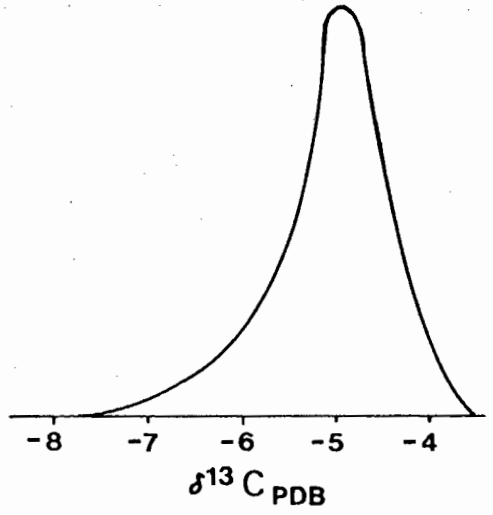

Fig 6·5

DOKOLWAYO ECLOGITIC DIAMONDS
CARBON ISOTOPE DISTRIBUTION

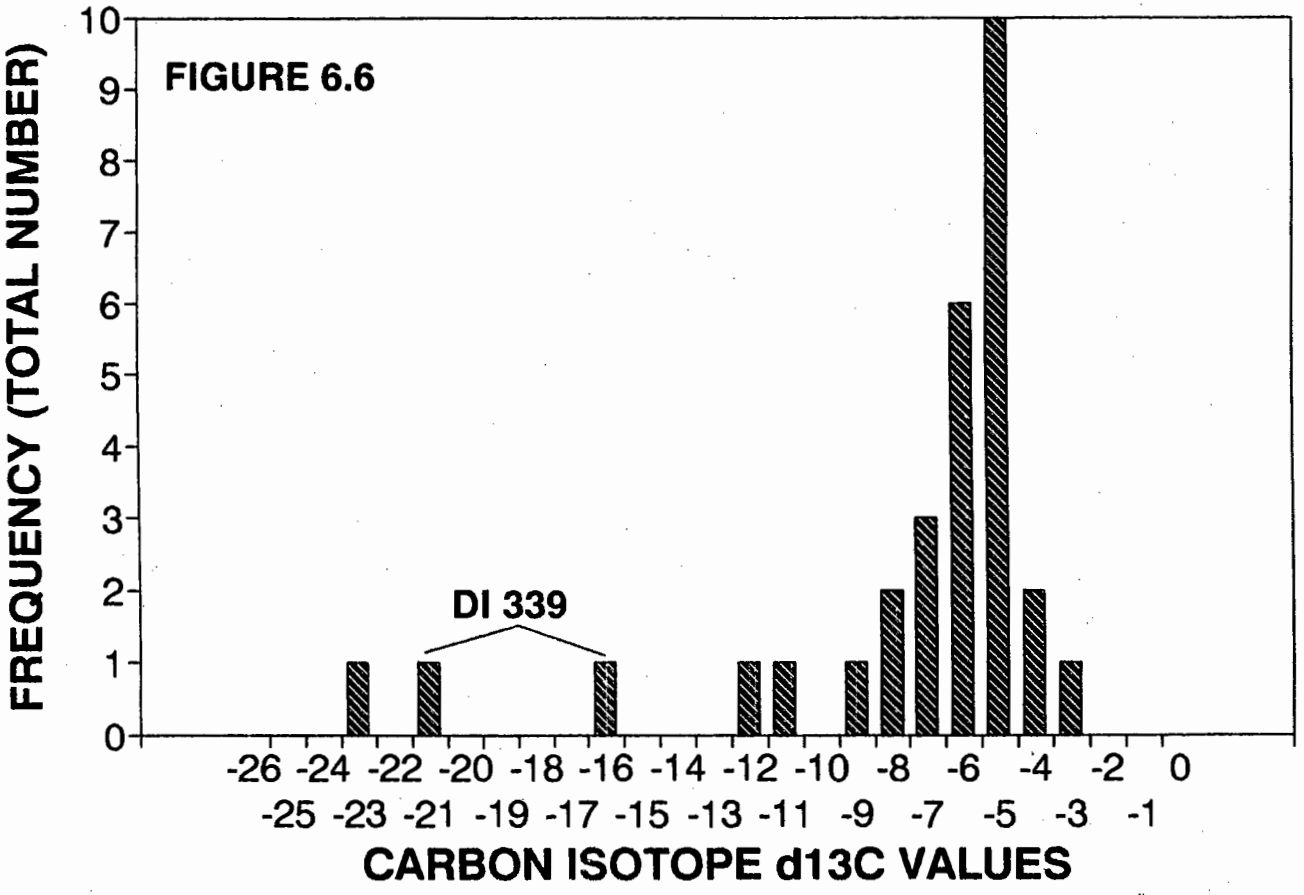

APPENDIX 6a

DOKOLWAYO DIAMOND CARBON ISOTOPES

SAMPLE NUMBER	δ13C	PARAGENESIS	INCLUSIONS
DI 351	-5.5	ECLOGITIC	GARNET, ILMENITE
DI 360	-5.7	ECLOGITIC	GARNET
DI 334	-4.2	ECLOGITIC	GARNET
DI 356	-4.3	ECLOGITIC	GARNET
DK 44	-5.8	ECLOGITIC	GARNET
DI 355	-7.1	ECLOGITIC	CLINOPYROXENE
DK 24	-5.8	ECLOGITIC	GARNET
DK 29	-8.7	ECLOGITIC	GARNET
DI 354	-7.7	ECLOGITIC	GARNET
DI 388	-6.0	ECLOGITIC	GARNET, COESITE
DI 349	-6.9	ECLOGITIC	COESITE
DI 382	-11.5	ECLOGITIC	COESITE
DI 348	-4.7	ECLOGITIC	COESITE, DIAMOND
DI A311	-5.1	ECLOGITIC	STAUROLITE, GRAPHITE
DI 347	-6.2	ECLOGITIC	GARNET
DI 367	-5.2	ECLOGITIC	GARNET, DIAMOND
DI 344	-22.3	ECLOGITIC	FELDSPAR
DI 366	-7.1	ECLOGITIC	ILMENITE
DI 341	-4.3	ECLOGITIC	GARNET
DI 341	-4.4	ECLOGITIC	GARNET
DK 14	-5.5	ECLOGITIC	GARNET
DK 16	-4.9	ECLOGITIC	COESITE
DI 339	-20.8	ECLOGITIC	GARNET, SULPHIDE
DI 339	-15.2	ECLOGITIC	GARNET, SULPHIDE
DI 376	-5.2	ECLOGITIC	CLINOPYROXENE
DI 367	-3.4	ECLOGITIC	GARNET, DIAMOND
DI 338	-10.8	ECLOGITIC	COESITE
DK 31	-4.1	ECLOGITIC	GARNET
DI 336	-4.9	ECLOGITIC	GARNET, COESITE
DI 370	-3.9	ECLOGITIC	GARNET
DK 36	-5.0	ECLOGITIC	GARNET
DI 335	-5.7	ECLOGITIC	GARNET
DI 353	-3.1	PERIDOTITIC	GARNET
DI 353	-3.8	PERIDOTITIC	GARNET
DI 306	-4.2	PERIDOTITIC	SPINEL
DI 323	-4.7	PERIDOTITIC	SPINEL
DI 332	-2.7	PERIDOTITIC	SPINEL
DI 320	-4.7	PERIDOTITIC	SPINEL
DI 331	-7.0	PERIDOTITIC	SPINEL
DI 331	-7.4	PERIDOTITIC	SPINEL
DI 307	-6.5	PERIDOTITIC	GARNET, ORTHOPYROXENE
DI 330	-2.1	PERIDOTITIC	SPINEL
DI 330	-1.6	PERIDOTITIC	SPINEL
DI 317	-4.7	PERIDOTITIC	SPINEL
DI 342	-2.9	PERIDOTITIC	OLIVINE
DI 308	-3.3	PERIDOTITIC	SPINEL
DI 304	-3.3	PERIDOTITIC	GARNET

APPENDIX 6a

DOKOLWAYO DIAMOND CARBON ISOTOPES

SAMPLE NUMBER	δ13C	PARAGENESIS	INCLUSIONS
DI 305	-2.9	PERIDOTITIC	SPINEL
DI 305	-2.5	PERIDOTITIC	SPINEL
DI 391	-3.4	PERIDOTITIC	SPINEL
DI 350	-1.9	PERIDOTITIC	GARNET
DI 364	-4.0	PERIDOTITIC	CLINOPYROXENE
DI 302	-4.4	PERIDOTITIC	SPINEL
DI 389	-4.9	PERIDOTITIC	OLIVINE
DI 310	-4.5	PERIDOTITIC	SPINEL, OLIVINE
DI 316	-3.0	PERIDOTITIC	ORTHOPYROXENE
DI 319	-5.1	PERIDOTITIC	SPINEL
DI 315	-4.9	PERIDOTITIC	SPINEL
DI 329	-3.1	PERIDOTITIC	SPINEL
DI 309	-4.6	PERIDOTITIC	SPINEL
DI 309	-3.7	PERIDOTITIC	SPINEL
DI 328	-4.3	PERIDOTITIC	SPINEL
DI 328	-4.7	PERIDOTITIC	SPINEL
DK 6	-2.5	PERIDOTITIC	SPINEL
DI 333	-4.0	PERIDOTITIC	SPINEL
DI 337	-4.6	PERIDOTITIC	SPINEL
DI 374	-4.8	PERIDOTITIC	SPINEL
DI 375	-3.4	PERIDOTITIC	GARNET
DI 362	-6.1	PERIDOTITIC	SP, OL, CPX, OPX
DI 303	-3.8	PERIDOTITIC	SPINEL
DI 311	-4.8	PERIDOTITIC	SPINEL
DI 324a	-19.7	PERIDOTITIC	SPINEL, ZIRCON
DI 324b	-17.3	PERIDOTITIC	SPINEL, ZIRCON
DI 324c	-16.4	PERIDOTITIC	SPINEL, ZIRCON
DI 312	-5.2	SULPHIDE	SULPHIDE
DI 368	-3.4	SULPHIDE	SULPHIDE
DI 361	-4.2	SULPHIDE	SULPHIDE
DI 346	-5.2	SULPHIDE	SULPHIDE
DI 380	-7.7	SULPHIDE	SULPHIDE
DI 313	-6.9	SULPHIDE	SULPHIDE
DI 357	-6.2	SULPHIDE	SULPHIDE
DI 363	-8.0	WEBSTERITIC	CPX, OPX, COESITE
DI 381	-8.9	ZIRCON	ZIRCON
DI 401	-4.6	UNKNOWN	UNKNOWN
DI 301	-5.3	UNKNOWN	DIAMOND
DI 390	-4.2	UNKNOWN	UNKNOWN
DI 394	-4.3	UNKNOWN	DIAMOND
DI 396	-5.7	UNKNOWN	DIAMOND
DI 378	-4.3	UNKNOWN	GRAPHITE
DI 405	-4.2	UNKNOWN	UNKNOWN
DI 340	-4.2	UNKNOWN	MAGNETITE, SPHENE

APPENDIX 6a

DOKOLWAYO DIAMOND CARBON ISOTOPES

SAMPLE NUMBER	δ13C	PARAGENESIS	INCLUSIONS
DI 365	-5.0	UNKNOWN	DIAMOND
DI 392	-3.8	UNKNOWN	GRAPHITE
DI 383	-4.3	UNKNOWN	DIAMOND, TiKAl-SILICATE
DI 386	-5.6	UNKNOWN	UNKNOWN
DI 395	-5.1	UNKNOWN	DIAMOND
DI 380	-7.7	UNKNOWN	CHLORITE, TiKAl-SILICATE
DI S01C	-3.9	SINGLE CORE	
DI S01P	-4.1	POLYCRYSTALLINE	
DI SO2C	-3.6	CUBE - CENTRE	
DI SO2M	-3.6	CUBE - MIDDLE	
DI SO2E	-3.9	CUBE - EDGE	

CHAPTER 7 - DOKOLWAYO CONCENTRATE GARNETS

ABSTRACT

Approximately 55% of the Dokolwayo kimberlite concentrate consists of garnet. A representative suite of concentrate garnets was analyzed. Crustal garnets suggest the presence of granulite facies rocks at depth. The majority of the garnets are Cr-poor. Eclogitic garnets were more magnesian and less sodic than eclogitic diamond inclusion garnets, suggesting a shallower, more refractory source for the concentrate garnets. There is a positive relationship between TiO_2 and Na_2O in the eclogitic garnets. Both megacryst and xenocryst garnets were identified to belong to the Cr-poor megacryst suite common in Group I kimberlites. The megacrystic garnets have > 0.07 wt% Na_2O suggesting a high pressure source. Prior to this study these garnets had not been reported from Group II kimberlites. Garnets similar in composition to garnets from high-temperature deformed peridotites were also identified. Approximately 5% of the Dokolwayo kimberlite concentrate consists of subcalcic G10 garnets, which is consistent with the presence of diamonds.

7.1 INTRODUCTION

Garnet is one of the most common accessory minerals in kimberlite and, due to its resistance to chemical weathering and distinctive chemistry, is an important diagnostic mineral in kimberlite exploration. Garnets are readily obtained from heavy mineral concentrates recovered during diamond extraction processes. Concentrate garnet xenocrysts in a kimberlite are considered to have been derived from the disaggregation of mantle xenoliths and crustal rocks which were sampled by the kimberlite during emplacement.

The mineral compositions of mantle derived garnets are commonly distinctive with respect to source rock. It is thus possible to infer the presence of a garnet-bearing mantle assemblage on the basis of the composition of a specific garnet (e.g. garnet lherzolite, Cr-poor garnet megacryst suite). In the absence of an extensive population of xenoliths from a kimberlite, as in the case of Dokolwayo, a comprehensive study of the concentrate garnet xenocrysts can provide a valuable insight into the broad petrological nature of the upper mantle, even though a study of this nature does suffer certain limitations. It can only be qualitative and not quantitative with respect to the volumetric distribution of garnet-bearing assemblages in the upper mantle, i.e. it is only possible to establish the presence of an assemblage, but it is impossible to relate its abundance to other assemblages. Furthermore, a study based on garnets cannot shed light on the nature, presence or absence of garnet-free assemblages (e.g. MARID-suite rocks, pyroxenites, dunites) which may be petrologically and volumetrically important in mantle reconstructions.

Irrespective of these constraints, a concentrate garnet study can yield useful information regarding the mantle composition, heterogeneity, mantle processes and paragenetic constraints on associated minerals and the kimberlite itself.

7.2 DOKOLWAYO GARNET POPULATIONS

A suite of more than 3500 xenocrystic garnets in the size range +0.5 mm to -2 mm has been examined in terms of colour. The majority of the garnets (~70%) are varying shades of orange, whereas the remaining ~30% are red, mauve and lilac coloured. Pale pink and green garnets form a very minor part (<1%) of the xenocryst suite. Grains from all colour groups were analyzed. In a previous study of the Dokolwayo garnet population (Hawthorne et al., 1979) no subcalcic chromium-rich garnets were reported. These garnets have a distinctive lilac colour and have been shown to be present in the concentrates of diamondiferous kimberlites (Gurney and Switzer, 1973; Sobolev et al., 1973; Boyd and Gurney, 1982; Gurney, 1984). Since the Dokolwayo kimberlite is (a) diamondiferous and

(b) these garnets occur as inclusions in Dokolwayo diamonds, a disproportionate number of lilac coloured garnets were selected for analysis in an effort to establish the presence of these subcalcic garnets in the concentrate. All concentrate analyses are presented in APPENDIX 7.a.

7.2.1 CRUSTAL GARNETS

A number of pale pink garnets (n=23) from the Dokolwayo concentrate were analyzed. These garnets probably have a crustal origin. Two distinctive suites have been recognized.

A very minor suite (<<1%) is represented by a garnet (DG-287) which is characterized by its high MnO (14.8 wt%) and FeO (27.1 wt%) contents and depleted MgO (0.76 wt%) and CaO (0.75 wt%).

The majority of the pink garnets are almandine - pyrope solid solutions with a minor grossular component and characterized by FeO 24.1 - 33.9 wt%, MgO 4.58 - 11.7 wt% and CaO 0.74 - 6.27 wt%. These garnets commonly contain quartz inclusions, which is a major factor in assigning a crustal origin. Quartz does not occur in deep mantle rocks, but may be pseudomorphous after coesite.

Almandine - pyrope garnets are typical phases of granulite facies metamorphic rocks (Deer et al., 1966; Winkler, 1974). The presence of these garnets in the Dokolwayo concentrate suggests that granulite facies rocks are present in the crust below Dokolwayo.

7.2.2 ECLOGITIC GARNETS

The majority of the Dokolwayo garnets (70%) are chromium-poor (<2.5 wt% Cr_2O_3) and, excluding the most calcic garnets analyzed, are restricted to a narrow range of

MgO/(MgO+FeO) ratios [MgO/(MgO+FeO): 0.60 - 0.90; Figure 7.1]. Approximately 55% of these chromium-poor garnets have been assigned to an eclogitic paragenesis. These eclogitic garnets are characterized by a wide range in compositions. MgO is within the range of 12.1 - 22.6 wt%, FeO 5.80 - 19.9 wt% and CaO 2.74 - 9.08 wt%. Two garnets of more calcic compositions which extend this range were reported in an earlier study of Dokolwayo garnets (Hawthorne et al., 1979). The Na_2O content (not detected - 0.15 wt%) of these garnets is positively correlated with TiO_2 (not detected - 0.52 wt%; Figure 7.2).

With the exception of three xenocrysts, all the eclogitic concentrate garnets are depleted in FeO and CaO and enriched in MgO compared with the majority of the eclogitic garnets extracted from Dokolwayo diamonds (Figures 7.3, 7.4).

7.2.3 CHROMIUM-POOR GARNET MEGACRYSTS

Both xenocrystic and megacrystic (>1cm) garnets at Dokolwayo have similar compositional ranges to those established for the Monastery (Jakob, 1977; Moore, 1986), Orapa (Shee, 1978) and Lekkerfontein (Robey, 1981) Cr-poor megacryst suites. The Dokolwayo garnet megacryst suite is characterized by Cr_2O_3 0.04 - 1.55 wt% TiO_2 0.48 - 1.28 wt% and Na_2O 0.09 - 0.22 wt%. The compositions of these garnets show that there is a strong positive correlation between Na_2O and FeO (Figure 7.5a) whereas there is a tendency for TiO_2 to decrease with increasing FeO (Figure 7.5b). Elsewhere this is due to ilmenite crystallization, but ilmenite is not present as xenocrysts or megacrysts at Dokolwayo. In respect to rarity of ilmenite in the megacryst suite, Dokolwayo resembles Jagersfontein.

Fifteen samples spanning the upper range of Mg-numbers (atomic Mg/(Mg+Fe)) displayed by the Dokolwayo megacryst suite was selected for trace element analysis by R.O. Moore using the proton microprobe housed in the HAIF laboratory at the CSIRO in Sydney,

Australia (Moore et al., 1990). The results have been presented by Moore et al. (1990; Appendix 7.c).

7.2.4 PERIDOTITIC GARNETS

7.2.4a Lherzolitic Garnets

The majority of peridotitic garnets analyzed in this study is confined to the lherzolite trend (Figure 7.6) of Sobolev et al. (1973). The compositions of these lherzolitic garnets are characterized by TiO_2 not detected - 0.58 wt%, Cr_2O_3 1.45 - 9.61 wt%, MgO 18.9 - 21.7 wt% and CaO 3.85 - 6.13 wt%. They are further characterized by $Na_2O \leq 0.11$ wt%. Three subgroups of these lherzolitic garnets require more detailed consideration.

i) Alexandritic garnets are identified by their distinctive dichroic behaviour. These garnets generally have a deep purple appearance, but have a greenish-blue tinge at thin edges. Four alexandritic garnets were analyzed from the Dokolwayo concentrate. These garnets have TiO_2 not detected - 0.15 wt%, Al_2O_3 16.8 - 18.2 wt%, Cr_2O_3 8.10 - 9.61 wt% and CaO 5.68 -6.74 wt%. The low Al_2O_3 contents reflect the Cr^{3+} in octahedral coordination. Concomitantly, MgO is replaced by CaO, suggesting a significant uvarovite component in these garnets.

Generally, the lherzolitic garnets at Dokolwayo have $TiO_2 < 0.50$ wt%. However, a number of the garnets on the lherzolite trend have $TiO_2 > 0.50$ wt%. These garnets plot into two distinctive groups in a field defined by the TiO_2 and Cr_2O_3 contents of the lherzolitic garnets (Figure 7.7).

ii) The chromium and TiO_2-rich population has Cr_2O_3 in the range 3.96 - 7.42 wt%, TiO_2 0.52 - 0.58 wt%, MgO 19.3 - 21.2 wt%, CaO 4.73 - 5.78 wt% and Na_2O 0.07 -

0.09 wt%. Similar garnet compositions have been reported from the Finsch garnet concentrate (Gurney and Switzer, 1973).

iii) The second TiO_2-rich lherzolite population is characterized by low Cr_2O_3 (1.57 - 2.15 wt%). They are also characterized by TiO_2 0.55 - 0.68 wt%, MgO 20.3 - 21.1 wt%, CaO 4.02 - 4.82 wt% and Na_2O 0.07 - 0.10 wt%. These garnets are the "Lo-chrome metasome" garnets in Figure 7.7.

7.2.4b Chromium-rich Subcalcic Garnets

The results of this study indicate that approximately 5% of the Dokolwayo garnet concentrate may be classified as chromium-rich subcalcic garnets. These garnets have TiO_2 not detected to 0.17 wt%, Cr_2O_3 2.24 - 8.75 wt%, MgO 20.7 - 25.1 wt% and CaO 0.29 - 3.84 wt%. These garnets are similar in composition (Figure 7.6) to the subcalcic garnets reported from the Finsch concentrate (Gurney and Switzer, 1973) and plot within the subcalcic field as defined by the 85% line of Gurney (1984). Although the TiO_2 contents of these Dokolwayo garnets may appear to be high for this type of garnet, the maximum observed concentration of TiO_2 (0.17 wt%) in the Dokolwayo subcalcic garnets is within analytical error of the TiO_2 concentrations reported by Gurney and Switzer (1973) for the Finsch concentrate subcalcic garnets (i.e. 0.15 wt% TiO_2).

7.2.4c Deformed Peridotite Garnets

Chromium-poor and titanium-rich garnets, similar in composition to garnets reported from deformed peridotites (Nixon and Boyd, 1973), were analyzed from the Dokolwayo concentrate. These garnets have TiO_2 0.88 - 1.08 wt%, Cr_2O_3 1.45 - 2.63 wt%, FeO 7.93 - 9.10 wt%, CaO 4.19 - 4.62 wt% and Na_2O 0.11 - 0.14 wt%. They are more titaniferous than the lherzolitic garnets described above (Figure 7.7) and have higher Cr_2O_3 concentrations than the chromium-poor megacrysts (Figure 7.7). Their sodium

contents are similar to the Na_2O concentrations of the chromium-poor megacrysts, but are generally higher than the Na_2O levels of the lherzolitic garnets (Figure 7.8).

7.2.4d Green Garnet

One green garnet was analyzed from the concentrate. This garnet (DG-001) has Cr_2O_3 13.6 wt%, MgO 15.5 wt% and CaO 11 wt%.

7.3 DISCUSSION

7.3.1 Eclogitic Garnets

The general disparity between the compositions of the concentrate and diamond inclusion eclogitic garnets (Figures 7.2, 7.3, 7.4) is a phenomenon that has been recorded at other kimberlites in Southern Africa (Gurney et al., 1984b, Deines et al., 1987). In the past the tendency has been to attribute the differences in composition between concentrate and diamond inclusion garnets to post diamond formation equilibration processes (Gurney et al., 1984b); of rationale for this argument is that diamonds are geochemically impermeable and protect inclusions from open system re-equilibration processes. While it would be convenient to argue that similar reasoning accounts for the observed differences in concentrate and diamond inclusion eclogitic garnets at Dokolwayo, alternatives should be investigated.

Archaean tectonic models suggest that continental nuclei in the region of Dokolwayo may have formed as a result of rapid regional intracratonic obduction of oceanic basalts and sediments, leading to stacking and subsidence of hydrated simatic thrust piles containing a large (25%) ultramafic component (Figure 3.2; De Wit et al., 1990). The subsiding thrust piles would have the effect of depressing depleted dunitic-harzburgitic residues to

increasing depths forming tectospheric keels of metamorphosed peridotites and basalts with possible intercalated metasediments.

It is unlikely that all the basalt being metamorphosed to eclogitic facies will be subducted to within the diamond stability field. The more probable situation is that the majority of eclogites will equilibrate in the graphite stability field. It is assumed that there is not an undue bias in the method of sampling eclogites in the mantle by the rising kimberlite. The kimberlite will therefore be expected to sample a lesser volume of eclogites in the diamond stability field than the volume sampled at lower pressures. This sampling effect should be apparent in the concentrate.

The MgO/(MgO+FeO+CaO) ratio of the eclogitic concentrate and diamond inclusion garnets suggest that the eclogite from which the diamonds were derived was less depleted than the eclogites from which the majority of the concentrate garnets were derived.

The observation presented above suggests that there may be a negative relationship between depth of subduction, and hence pressure, and the degree of depletion as reflected in the compositions of the eclogitic garnets. It has been suggested that Na is increasingly substituted in garnets with an increase in pressure (Sobolev and Lavrent'ev, 1971; Bishop et al., 1976, 1978). It may therefore be expected that (1) the sodium contents of the concentrate garnets are lower than those in diamond inclusion eclogitic garnets and (2) that the relationship MgO/(MgO+FeO+CaO) vs Na_2O (Figure 7.9) be characterized by a negative slope. The observed trends in Figures 7.2 and 7.9 are consistent with the above observation.

7.3.2 Megacrysts and Deformed Peridotite Garnets

The suite of megacryst garnets analyzed for trace elements by Moore et al. (1990) do not cover the entire spectrum of atomic Mg/(Mg+Fe) ratios [$Mg^{\#}$] exhibited by these garnets

at Dokolwayo. The Dokolwayo garnets (Figure 7.5b) extend to the lower $Mg^{\#}$ observed in the Monastery megacrysts (Gurney et al., 1979b). However the parabolic relationship between the $Mg^{\#}$ and TiO_2 observed at Monastery is absent from Dokolwayo. This is consistent with the apparent absence of ilmenite megacrysts from Dokolwayo. Moore et al. (1990) have observed that the negative trends between Ti, Zr and Y with FeO enrichment are opposite to trends expected from normal igneous fractionation processes.

The deviation from normal igneous fractionation trends may be due to an unusual megacryst assemblage at Dokolwayo. A small number of rutile megacrysts have been recovered from the Dokolwayo concentrate. These rutiles contain <0.50 wt% FeO (Appendix 7.b). It is unlikely that these rutile megacrysts are related to the eclogitic paragenesis as no exsolved rutile needles have been observed in eclogitic garnet xenocrysts. In the event that these rutiles co-precipitated with the megacryst garnets, the partitioning of TiO_2 into rutile would have a negative effect on the concentration of TiO_2 in the garnets. A study of phase relations on the system CaO-FeO-TiO_2 under strongly reducing conditions by Kimura and Muan (1971) has shown that it is unlikely that ilmenite and rutile will coexist at mantle pressures and temperatures. The crystallization of rutile from the system will result in an overall increase in FeO in the liquidus phases and hence an increase in FeO in the coexisting garnets. The observed compositional trends are thus consistent with the presence of coexisting garnet and rutile and the absence of ilmenite from the megacryst suite.

The positive relationship between TiO_2 and Zr in these garnets suggest that Zr is depleted simultaneously with TiO_2 from the garnets. However, analyses of the rutile megacrysts indicated that Zr was below detection limits. It is possible that rare zircon crystallized from the same melt as the megacryst garnets and rutiles, but has as yet not been recovered from the concentrates at Dokolwayo.

It is of interest to note that ilmenite is a common groundmass phase in Group I kimberlites as well as a common megacryst phase in Group I kimberlites. In contrast, ilmenite has been suggested to be absent from Group II kimberlites (Skinner, 1986), although it has been reported as a rare phase both in the concentrate and groundmass of the Group II Newlands kimberlite (Daniels and Gurney, 1990). It would therefore appear that the presence, absence, or rarity of ilmenite as a megacryst phase in a kimberlite is commonly reflected by its abundance in the groundmass of that kimberlite. It is therefore of particular interest to note that the groundmass of the Dokolwayo kimberlite is characterized by the presence of a TiO_2-rich (>90 wt% TiO_2) phase while rutile is present as a megacryst phase. Due to low pressure of crystallization in the near surface kimberlite, the groundmass phase is probably anatase. Due to the small size and the skeletal nature of the probable anatase no attempt has been made to seperate the mineral for verification by X-ray diffraction.

7.3.3 Alexandritic Garnets

Four alexandritic garnets were analyzed from the Dokolwayo concentrate. These garnets have Mg/(Mg+Fe+Ca) 0.707 - 0.733 which is significantly lower than the Mg/(Mg+Fe+Ca) ratios of the subcalcic garnets (0.881 - 0.770). The compositions of these alexandritic garnets suggest that their formation is favoured by the stabilization of uvarovite at the expense of pyrope. Garnets with comparable compositions have been recorded from the Kao and Newlands kimberlites (Hornung and Nixon, 1973; Lawless, 1974). Hornung and Nixon suggested that these Cr_2O_3 and CaO enriched garnets are the residual fraction of an ultra-depleted melt. However, the alexandritic garnets from Dokolwayo appear to be an extension of the lherzolite trend (Figure 7.6) which suggests a bulk compositional trend and not a depletion trend. The Mg/(Mg+Fe+Ca) ratios of these garnets are also not consistent with a depletion trend. Daniels et al. (1991) have argued that the bulk composition of the upper mantle increases in Cr_2O_3 content with increasing

depth. It is possible that these alexandritic garnets are derived from greater depths than the less Cr_2O_3-rich G9 (Dawson and Stephens, 1975) garnets.

7.3.4 TiO_2-Rich Lherzolitic Garnets

High titanium contents are unusual for lherzolitic garnets derived from coarse peridotites and are more consistent with high temperature deformed peridotites or metasomatised rocks. The small number of analyzed samples that are representative of these TiO_2-rich (>0.5 wt% TiO_2) lherzolitic garnet populations, and the absence of xenoliths do not allow for definitive correlation with known garnet bearing xenoliths. However, Hops (1989) recorded deformed and metasomatised garnet peridotites from Jagersfontein with garnets similar in composition to the TiO_2- and Cr_2O_3-rich garnets recorded in the Dokolwayo concentrate. These deformed and metasomatised Jagersfontein peridotites were suggested to be a consequential product of the megacryst suite present at this locality.

Hatton (1978) recorded a garnet peridotite from Roberts Victor (HRV 310) with garnet compositions similar to those of the TiO_2-rich and Cr_2O_3-poor lherzolitic garnets at Dokolwayo. Hatton and Gurney (1987) suggested that these titaniferous Cr_2O_3-poor lherzolites are either in contact with eclogites or are derived from a metasomatised aureole around eclogites and will be metasomatised to a lesser or greater extent.

It is suggested that the Cr-rich and Cr-poor sub-populations of TiO_2-rich Dokolwayo garnets are derived from peridotites similar to those described by Hops (1989) and Hatton (1978). This observation is consistent with the presence of eclogites and megacrysts at Dokolwayo.

7.3.5 Chromium-Rich Subcalcic (G10) Garnets

Subcalcic G10 garnets have a very distinctive lilac colour that is similar in appearance to the colour of methylated spirits when sunlight shines through it. No subcalcic G10 garnets were reported from Dokolwayo in an earlier extensive study of the Dokolwayo garnet compositions (Hawthorne et al., 1979). It has previously been shown that there is a close association between the presence of concentrate G10 garnets and the presence of diamonds in a kimberlite (Gurney and Switzer, 1973; Sobolev et al., 1973; Boyd and Gurney, 1982; Gurney, 1984). The presence of diamonds in the Dokolwayo kimberlite would therefore suggest that subcalcic G10 garnets should be present in the concentrate. In order to investigate the apparent dichotomy between the observations of Hawthorne et al.(1979) and those made elsewhere with respect to the expected presence of G10 garnets at Dokolwayo, emphasis was placed on analyzing lilac coloured concentrate garnets from Dokolwayo.

The results of this study indicate that approximately 5% of the concentrate garnets from Dokolwayo are G10's. This is consistent with the presence of G10 garnets as inclusions in diamonds at this locality (Chapter 5).

Unfortunately, there are insufficient numbers of G10 diamond inclusions from Dokolwayo to make detailed comparisons with the concentrate garnets. However, there are a number of general features that warrant comment. Gurney et al. (1979) found that the diamond inclusion G10's at Finsch were, in general, more depleted in CaO and relatively enriched in Cr_2O_3 when compared with the concentrate G10's from that locality. The difference in composition between the concentrate and diamond inclusion garnets were attributed to the post-crystallization protection of the inclusion garnets from sub-solidus re-equilibration by the chemically inert diamond hosts (Gurney et al., 1979). At Dokolwayo the diamond inclusion garnets plot both within and outside of the field defined by the concentrate population. The affect of armouring the inclusions against post crystallization

compositional changes by the diamonds appears to be less significant at Dokolwayo than at Finsch.

In a study of the diamond inclusions of Dokolwayo (Chapter 5) it was found that within a greater geochemical environment characterized by certain compositional characteristics (e.g CaO depletion and Cr_2O_3 enrichment) there may be distinct inhomogeneity on a small scale. At least two different groups of G10 garnets can be recognized within the Dokolwayo concentrate population, which is consistent with the observations made for the diamond inclusion population. It is therefore concluded that the concentrate is not derived from a horizon that has experienced a single depletion event. In contrast it is suggested that the G10 garnets, both from the concentrate and the diamonds, are derived from a complex environment that has experienced various degrees of depletion of basaltic and/or komatiitic components.

CHAPTER 7 - FIGURE CAPTIONS

FIGURE 7.1

Plot of MgO/(MgO+FeO) versus Cr_2O_3 (wt%) for all the Dokolwayo concentrate garnets.

FIGURE 7.2

Plot showing Na_2O versus TiO_2 (wt%) for eclogitic concentrate and diamond inclusion garnets from Dokolwayo.

FIGURE 7.3

Plot of MgO versus FeO (wt%) for eclogitic concentrate and diamond inclusion garnets from Dokolwayo.

FIGURE 7.4

Plot of MgO versus CaO (wt%) for eclogitic concentrate and diamond inclusion garnets from Dokolwayo.

FIGURE 7.5a

Plot of Na_2O versus FeO (wt%) for Cr-poor megacrystic garnets from the Dokolwayo heavy mineral concentrate.

FIGURE 7.5b

Plot of TiO_2 versus FeO (wt%) for Cr-poor megacrystic garnets from the Dokolwayo heavy mineral concentrate.

FIGURE 7.6

Plot of CaO versus Cr_2O_3 (wt%) for peridotitic garnets from the Dokolwayo heavy mineral concentrate. The 85% line was defined by Gurney (1984).

FIGURE 7.7

Plot of TiO_2 versus Cr_2O_3 (wt%) for peridotitic garnets from the Dokolwayo heavy mineral concentrate.

FIGURE 7.8

Plot of Na_2O versus TiO_2 (wt%) for lherzolitic, megacrystic and deformed peridotitic concentrate garnets from Dokolwayo.

FIGURE 7.9

Plot of MgO/(MgO+FeO+CaO) versus Na_2O (wt%) for eclogitic concentrate and diamond inclusion garnets from Dokolwayo.

DOKOLWAYO - SWAZILAND
CONCENTRATE GARNETS

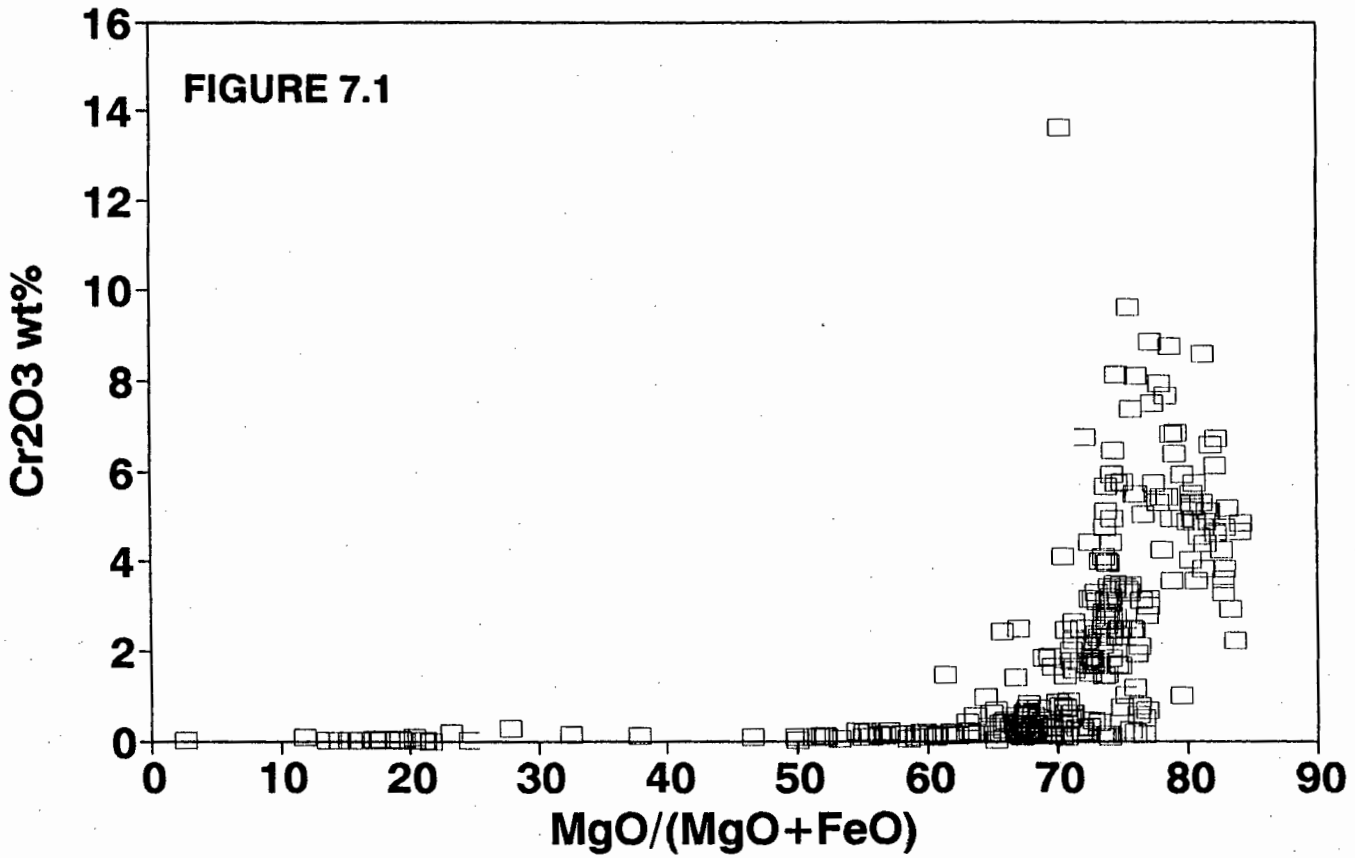

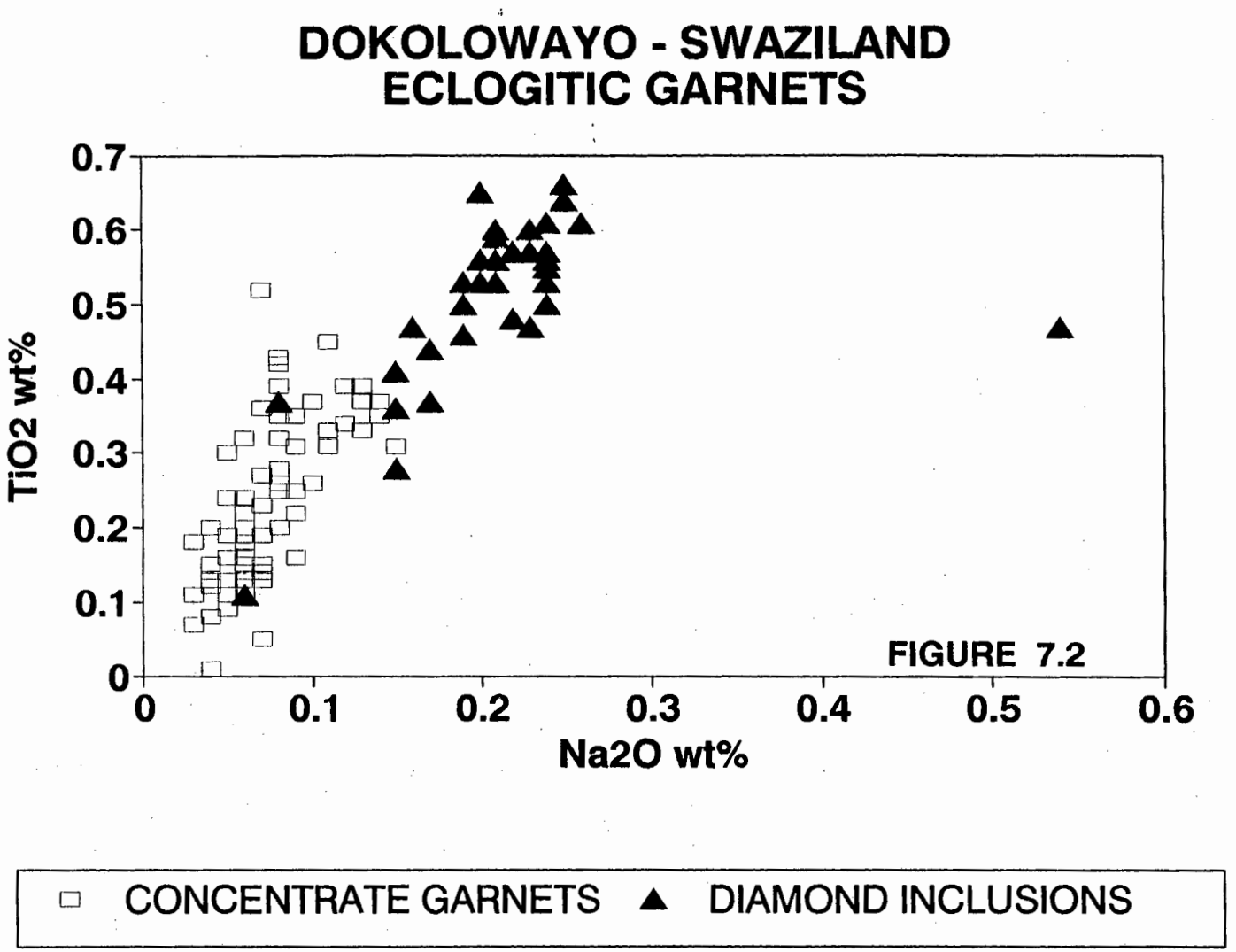
DOKOLOWAYO - SWAZILAND
ECLOGITIC GARNETS
TiO2 wt%
0.7
0.6
0.5
0.4
0.3
0.2
0.1
0
0
0.1
0.2
0.3
0.4
0.5
0.6
Na2O wt%
FIGURE 7.2
CONCENTRATE GARNETS
DIAMOND INCLUSIONS

DOKOLWAYO - SWAZILAND
ECLOGITIC GARNETS

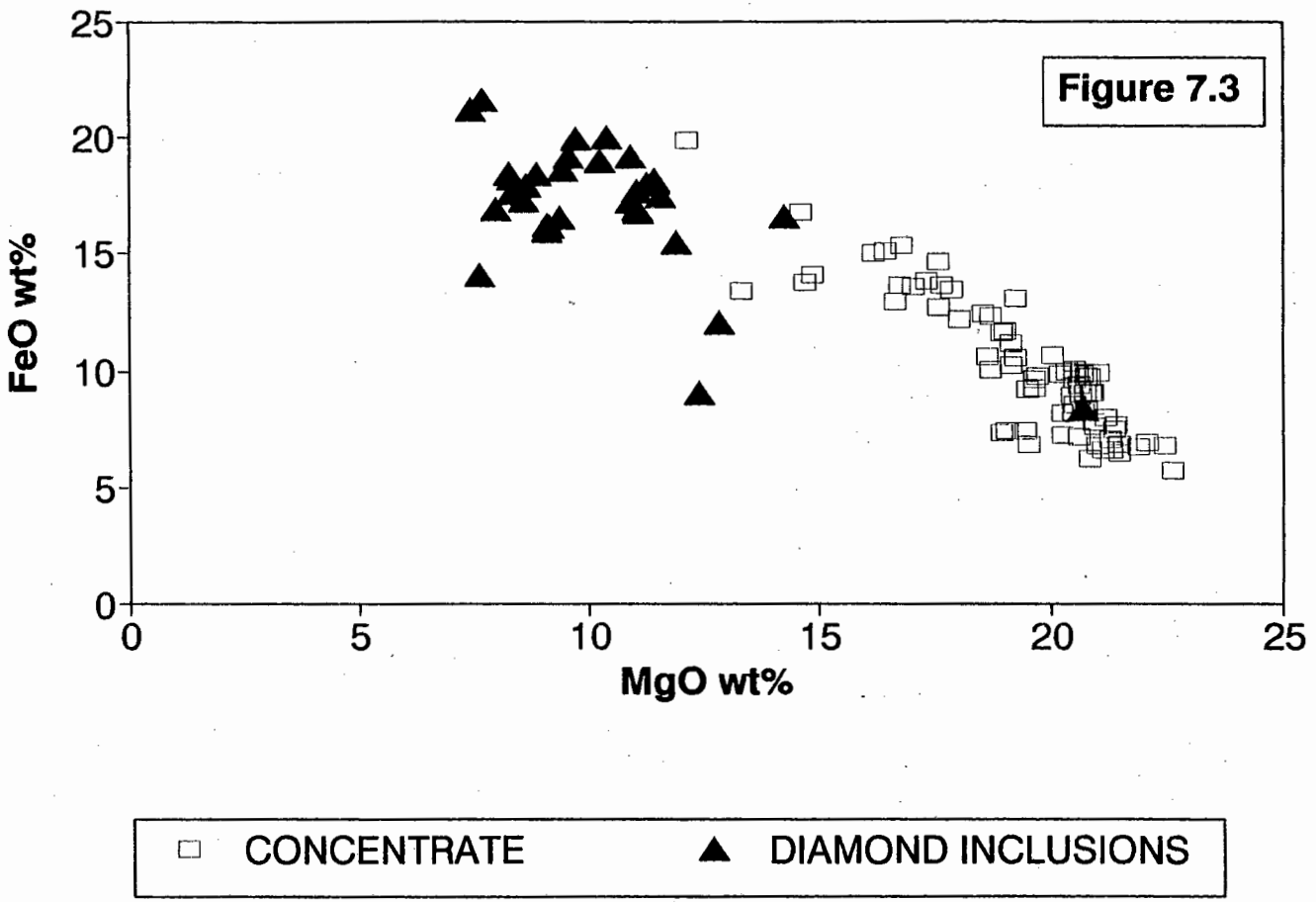

DOKOLWAYO - SWAZILAND
ECLOGITIC GARNETS

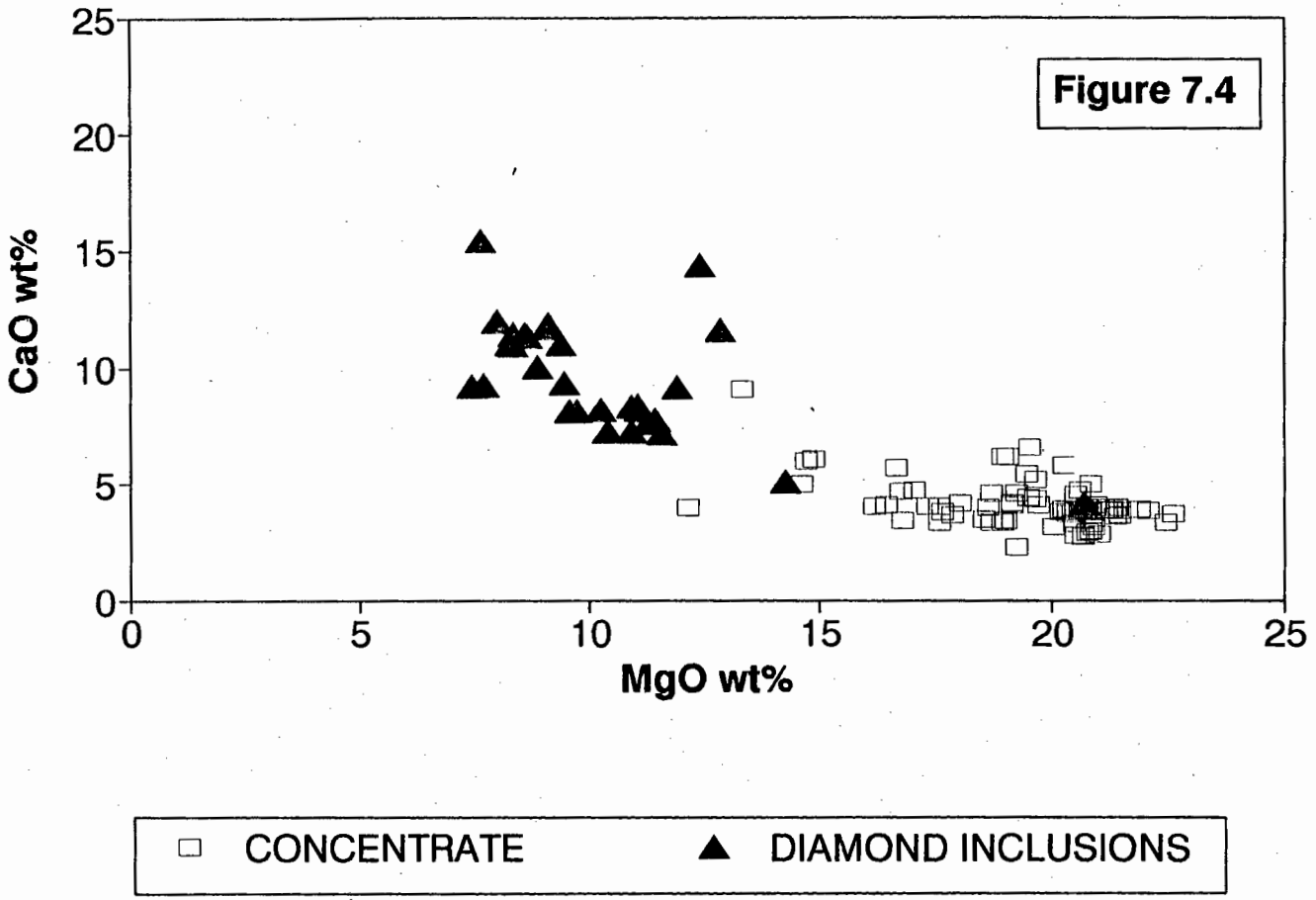

FIGURE 7.5a

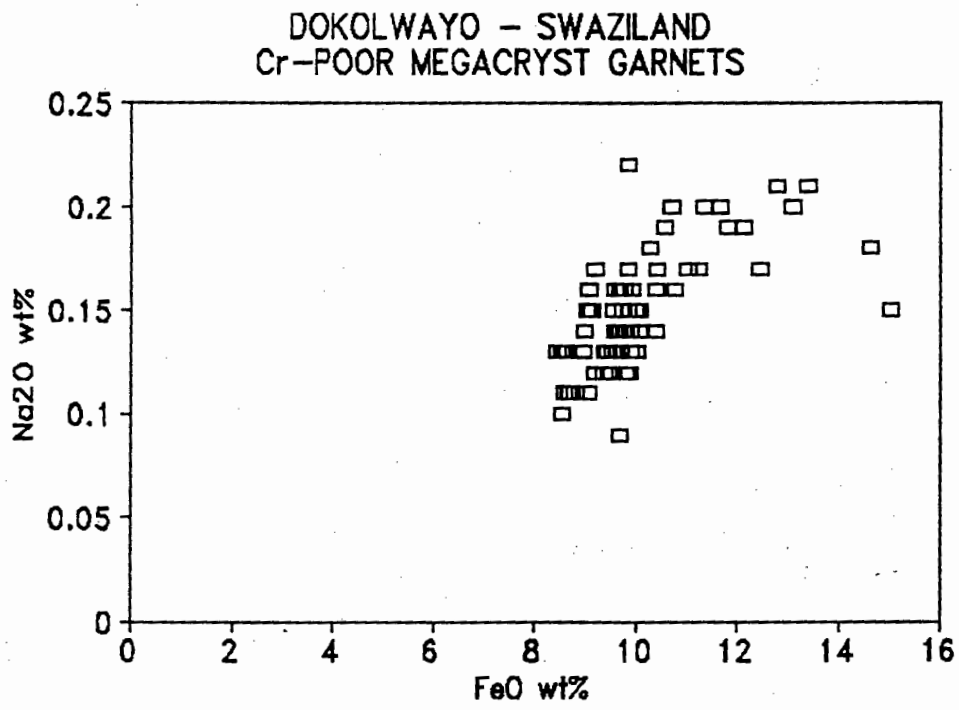

FIGURE 7.5b

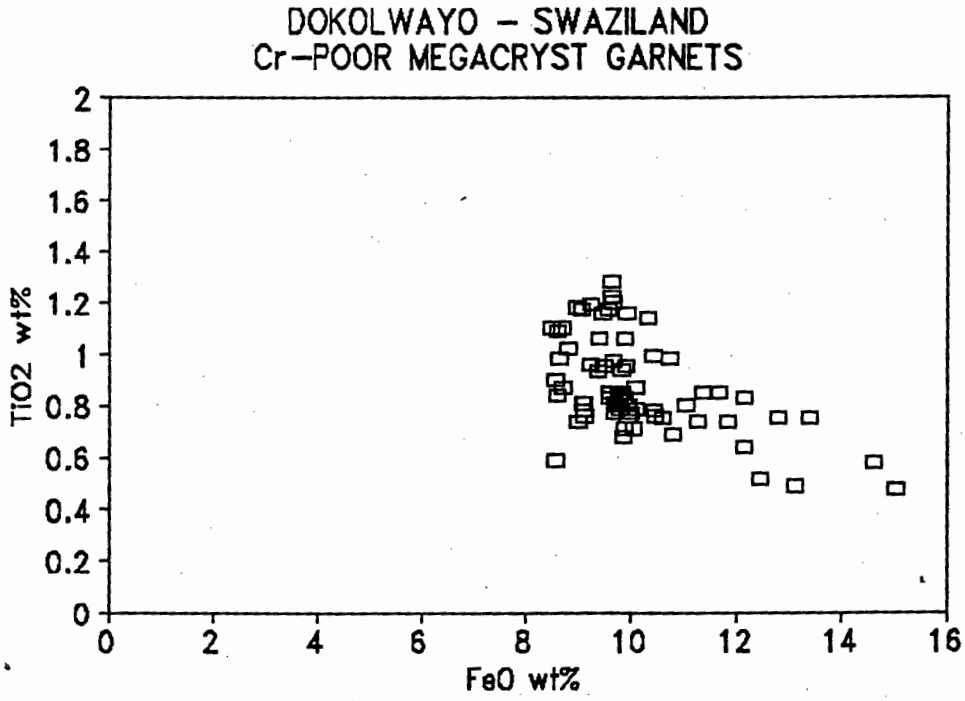

DOKOLWAYO - SWAZILAND
PERIDOTITIC GARNETS

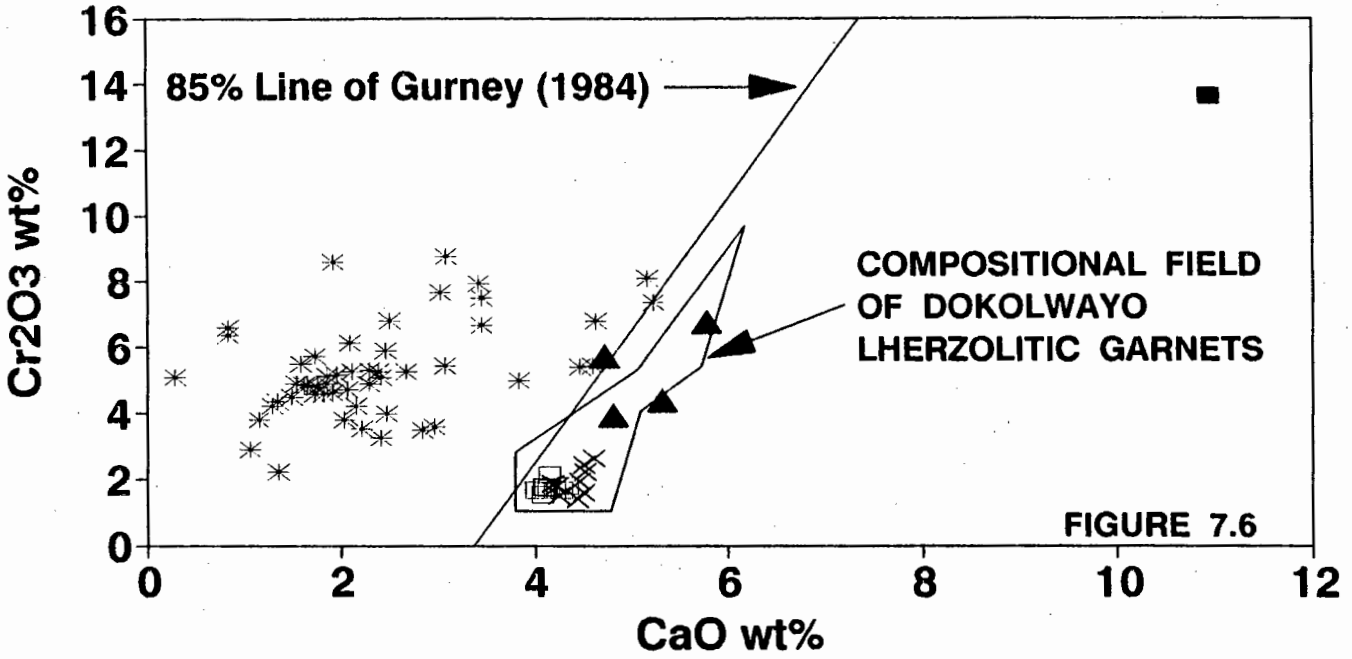

FIGURE 7.6

■ GREEN GARNET ✳ SUBCALCIC × HI-T DEFORMED

□ LO-Cr METASOME ▲ HI-Cr METASOME

DOKOLWAYO - SWAZILAND
PERIDOTITIC GARNETS

FIGURE 7.7

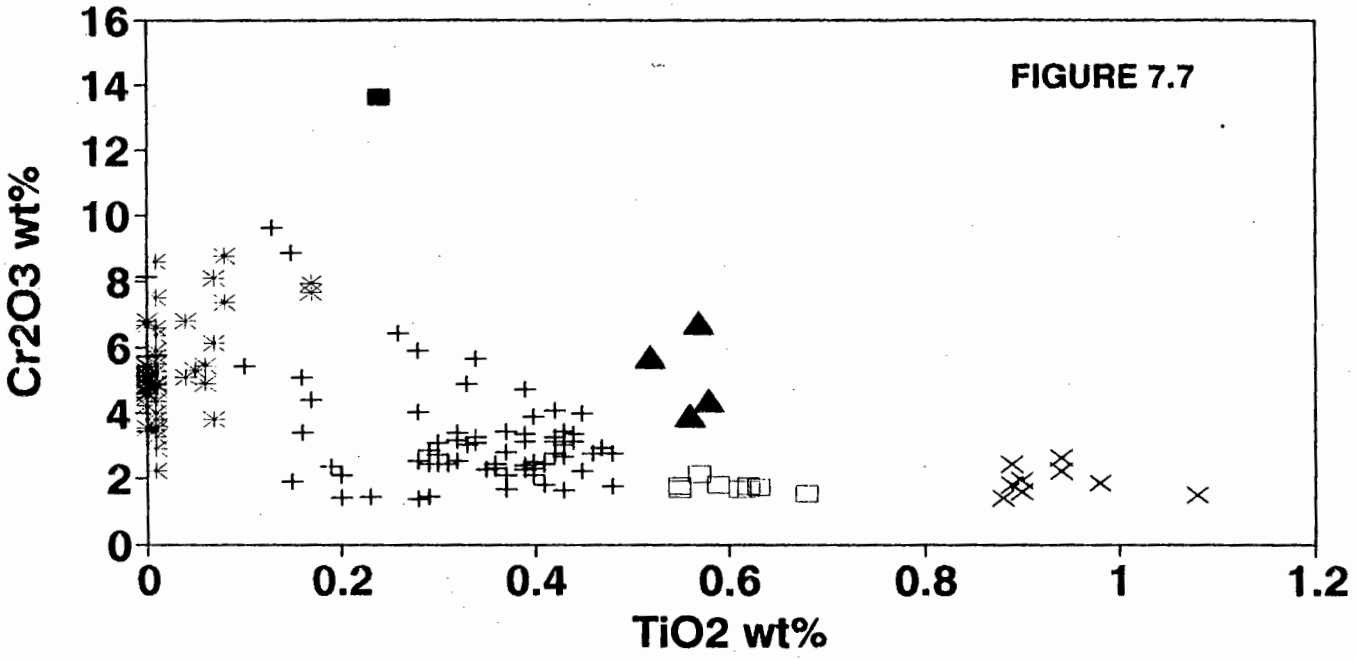

■ GREEN GARNET	+ LHERZOLITIC	✳ SUBCALCIC G10
× HI-T DEFORMED	□ Lo-Cr METASOME	▲ HI-Cr METASOME

DOKOLWAYO - SWAZILAND
CONCENTRATE GARNETS

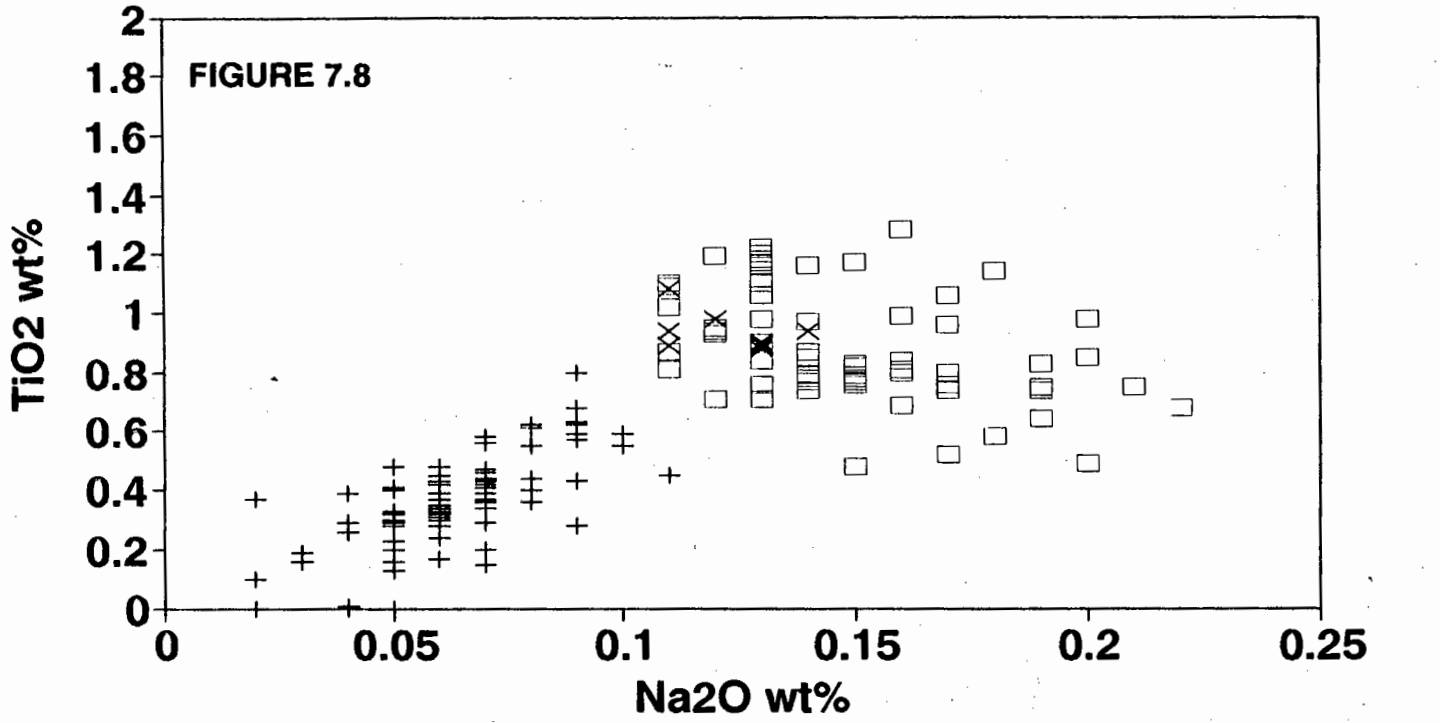

× HI-T DEFORMED □ CR-POOR MEGACR + LHERZOLITIC

DOKOLWAYO - SWAZILAND
ECLOGITIC GARNETS

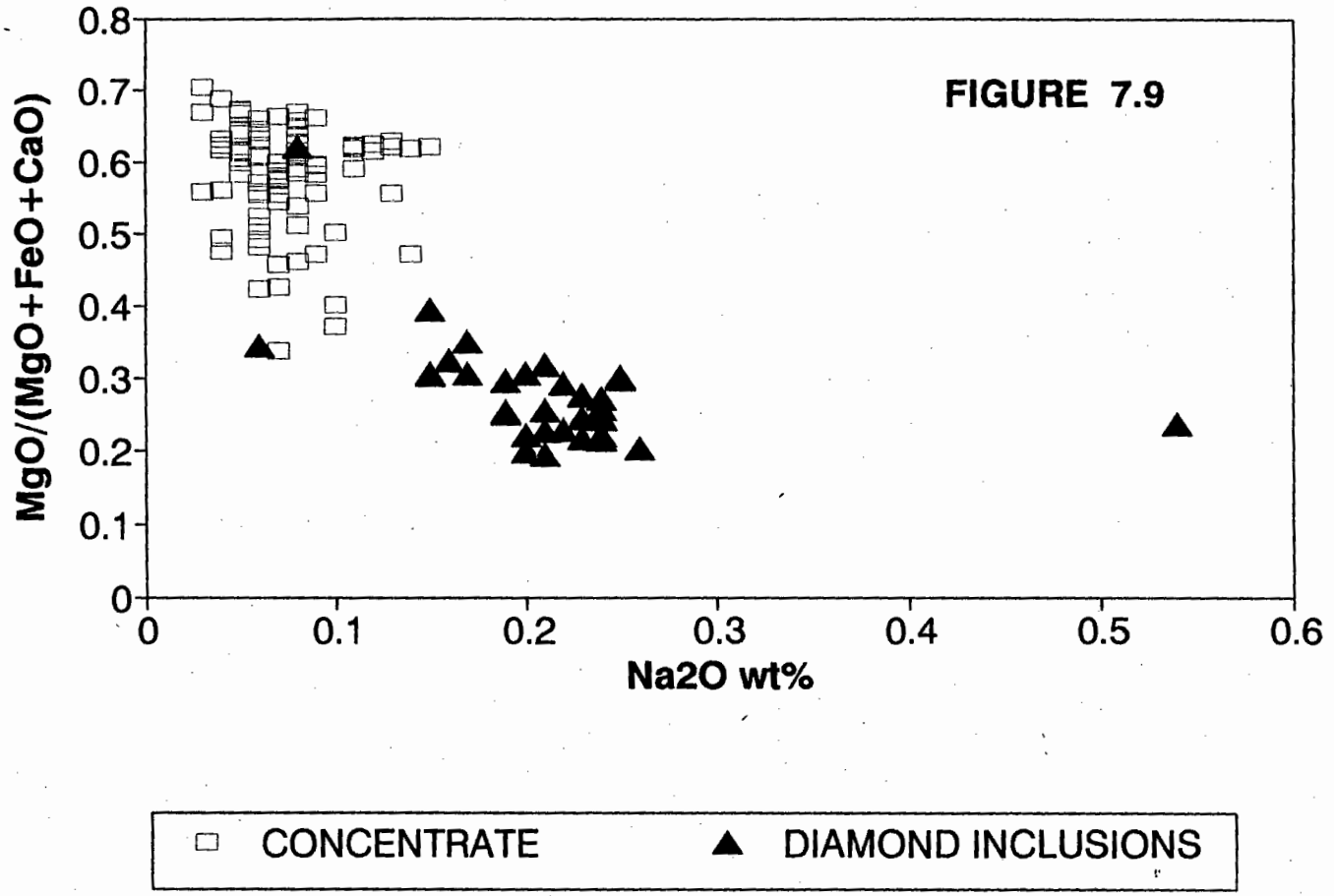

APPENDIX 7.a - DOKOLWAYO CONCENTRATE GARNETS

	OXIDES (wt%)										
SAMPLE NUMBER	SiO2	TiO2	Al2O3	Cr2O3	FeO	MnO	MgO	CaO	Na2O	K2O	TOTAL
DG-001	39.15	0.24	12.75	13.61	6.50	0.41	15.45	10.95	0.06	0.00	99.12
DG-207	41.68	1.08	22.04	1.50	7.93	0.21	20.96	4.25	0.11	0.00	99.76
DG-186	41.43	0.98	21.41	1.88	8.98	0.28	20.42	4.19	0.12	0.00	99.69
DG-015	41.24	0.94	20.88	2.63	8.16	0.31	20.25	4.62	0.11	0.00	99.14
DG-051	41.50	0.94	20.53	2.24	8.29	0.29	20.62	4.53	0.14	0.00	99.08
DG-048	41.89	0.90	21.05	1.98	8.35	0.28	20.49	4.46	0.13	0.00	99.53
DG-054	41.11	0.90	22.24	1.63	8.95	0.25	20.61	4.52	0.13	0.00	100.34
DG-053	42.03	0.89	20.62	2.45	8.51	0.34	20.54	4.52	0.11	0.00	100.01
DG-176	41.72	0.89	21.93	1.83	9.10	0.21	20.29	4.23	0.13	0.00	100.33
DG-023	41.57	0.88	21.84	1.45	8.42	0.28	20.28	4.45	0.13	0.00	99.30
DG-087	40.73	0.57	18.28	6.76	7.42	0.33	19.28	5.78	0.09	0.00	99.24
DG-066	41.19	0.58	20.41	4.41	7.20	0.33	20.75	5.33	0.07	0.00	100.27
DG-204	41.43	0.56	20.76	3.96	7.33	0.35	20.27	4.82	0.07	0.00	99.55
DG-183	41.94	0.57	21.53	2.15	7.85	0.26	21.20	4.16	0.09	0.00	99.75
DG-165	42.26	0.59	22.26	1.83	7.91	0.28	21.07	4.34	0.09	0.00	100.63
DG-174	42.35	0.62	21.91	1.78	8.02	0.24	20.48	4.10	0.09	0.00	99.59
DG-208	42.52	0.55	22.01	1.78	8.30	0.24	20.56	4.12	0.08	0.00	100.16
DG-129	42.01	0.63	21.58	1.76	7.92	0.22	20.73	4.14	0.09	0.00	99.08
DG-200	42.51	0.62	22.04	1.72	7.73	0.31	21.08	4.11	0.08	0.00	100.20
DG-203	42.46	0.55	22.66	1.70	7.80	0.29	20.87	4.29	0.08	0.00	100.70
DG-117	42.70	0.55	22.03	1.70	8.07	0.25	21.07	4.21	0.08	0.00	100.66
DG-199	42.21	0.55	23.06	1.69	7.14	0.33	21.01	4.01	0.10	0.00	100.10
DG-175	42.19	0.61	21.98	1.68	7.74	0.29	20.94	4.02	0.08	0.00	99.53
DG-120	42.29	0.68	21.92	1.57	8.31	0.24	20.69	4.08	0.09	0.00	99.87
DG-272	41.32	0.13	16.77	9.61	6.10	0.38	18.89	6.13	0.05	0.00	99.38
DG-276	41.87	0.15	17.19	8.86	5.68	0.34	19.33	5.95	0.07	0.00	99.44
DG-002	40.29	0.00	18.22	8.14	6.74	0.30	19.88	5.92	0.05	0.00	99.54
DG-084	41.14	0.26	18.76	6.46	6.84	0.37	19.86	5.48	0.04	0.00	99.21
DG-085	41.17	0.28	19.15	5.91	6.93	0.32	19.99	5.30	0.05	0.00	99.10
DG-277	42.05	0.01	19.78	5.77	6.51	0.37	19.60	5.55	0.04	0.00	99.68
DG-008	41.99	0.00	20.16	5.72	6.76	0.36	19.91	5.61	0.04	0.00	100.55
DG-086	41.09	0.34	19.54	5.67	7.04	0.35	19.88	5.26	0.07	0.00	99.24
DG-032	41.68	0.10	19.02	5.48	6.42	0.36	20.33	5.51	0.02	0.00	98.92
DG-028	41.14	0.16	19.92	5.09	7.10	0.35	20.09	5.44	0.05	0.00	99.34
DG-105	41.27	0.33	20.04	4.93	7.02	0.36	20.27	5.26	0.06	0.00	99.54
DG-270	41.70	0.29	22.70	1.48	11.02	0.42	17.56	4.63	0.04	0.00	99.84
DG-181	40.64	0.39	21.75	2.41	9.97	0.28	19.14	4.58	0.06	0.00	99.22
DG-170	41.49	0.29	22.40	2.49	9.68	0.38	19.69	4.32	0.07	0.00	100.81
DG-196	42.17	0.28	23.16	1.40	9.59	0.32	19.35	3.88	0.06	0.00	100.21
DG-206	41.29	0.48	21.98	2.79	7.35	0.26	21.17	4.51	0.05	0.00	99.88
DG-197	41.64	0.46	21.76	2.78	7.29	0.30	20.53	4.57	0.07	0.00	99.40
DG-178	41.81	0.45	20.56	3.99	7.28	0.29	20.52	4.70	0.06	0.00	99.66
DG-082	41.52	0.45	22.55	2.23	7.97	0.31	20.75	4.37	0.11	0.00	100.26
DG-016	41.58	0.44	20.95	3.15	7.55	0.38	20.27	4.78	0.08	0.00	99.18
DG-108	41.64	0.44	21.35	3.36	7.16	0.31	20.81	4.57	0.07	0.00	99.71
DG-171	41.10	0.43	21.42	3.47	7.28	0.29	21.33	4.44	0.09	0.00	99.85
DG-172	40.98	0.43	21.74	3.05	7.36	0.26	21.07	4.39	0.06	0.00	99.34
DG-173	41.13	0.43	21.81	2.69	7.38	0.31	20.82	4.39	0.07	0.00	99.03
DG-297	42.34	0.43	22.39	1.66	7.65	0.42	20.28	4.33	0.09	0.00	99.59
DG-062	41.48	0.42	21.66	3.27	6.73	0.25	20.79	4.75	0.06	0.00	99.41
DG-205	41.61	0.42	21.00	4.08	7.31	0.35	20.41	4.74	0.07	0.00	99.99
DG-180	40.26	0.42	21.87	3.16	7.80	0.25	20.61	4.58	0.07	0.00	99.02
DG-308	41.90	0.41	22.52	1.83	7.19	0.32	20.65	4.48	0.05	0.00	99.35
DG-182	42.24	0.41	22.10	2.49	8.05	0.30	20.55	4.35	0.07	0.00	100.56
DG-068	41.20	0.40	22.16	2.32	6.91	0.32	21.16	4.64	0.08	0.00	99.19
DG-070	41.53	0.40	22.24	2.50	6.94	0.32	21.16	4.55	0.08	0.00	99.72
DG-210	41.55	0.40	21.27	3.94	7.42	0.32	21.03	4.49	0.08	0.00	100.50
DG-167	42.25	0.40	22.43	2.12	7.67	0.24	21.23	4.19	0.05	0.00	100.58
DG-107	41.04	0.39	20.30	4.75	7.11	0.36	20.02	4.99	0.07	0.00	99.03
DG-050	42.01	0.39	20.46	3.36	6.82	0.31	20.98	4.73	0.04	0.00	99.10

Sample Number	SiO_2	TiO_2	Al_2O_3	Cr_2O_3	FeO	MnO	MgO	CaO	Na_2O	K_2O	Total
DG-052	42.11	0.39	20.93	3.14	6.37	0.29	21.42	4.72	0.07	0.00	99.44
DG-049	41.88	0.37	20.57	3.46	7.02	0.38	21.03	4.76	0.02	0.00	99.49
DG-189	42.66	0.37	21.81	2.84	7.03	0.26	20.00	4.27	0.06	0.00	99.30
DG-209	42.60	0.37	22.26	2.11	7.85	0.24	20.53	4.19	0.06	0.00	100.21
DG-169	42.20	0.37	22.84	1.68	7.30	0.27	21.70	4.10	0.07	0.00	100.53
DG-027	41.91	0.36	21.85	2.47	7.04	0.32	20.91	4.61	0.08	0.00	99.55
DG-194	42.45	0.36	22.50	2.32	7.01	0.32	20.62	4.25	0.07	0.00	99.90
DG-198	41.89	0.35	22.18	2.30	7.21	0.27	20.68	4.26	0.06	0.00	99.20
DG-179	41.73	0.34	21.51	3.28	7.62	0.33	20.70	4.51	0.06	0.00	100.08
DG-202	42.07	0.34	21.70	3.11	7.27	0.31	20.53	4.14	0.06	0.00	99.53
DG-192	40.50	0.33	21.88	3.07	7.57	0.38	20.64	4.62	0.05	0.00	99.04
DG-026	41.88	0.32	20.75	3.40	6.85	0.25	20.99	4.69	0.05	0.00	99.18
DG-055	41.71	0.32	20.58	3.19	7.34	0.34	21.13	4.55	0.06	0.00	99.22
DG-177	42.56	0.32	21.49	2.55	7.20	0.32	20.35	4.25	0.05	0.00	99.09
DG-201	42.30	0.31	22.26	2.45	6.63	0.28	20.91	4.39	0.06	0.00	99.59
DG-168	41.72	0.30	21.43	3.12	6.60	0.23	21.41	4.34	0.05	0.00	99.20
DG-317	42.20	0.30	21.72	2.73	7.05	0.38	20.61	4.31	0.06	0.00	99.36
DG-166	42.38	0.30	22.35	2.48	6.86	0.26	21.43	4.14	0.05	0.00	100.25
DG-193	42.78	0.29	21.53	2.86	7.36	0.25	20.58	4.36	0.05	0.00	100.06
DG-190	41.84	0.29	22.44	2.45	7.03	0.28	20.96	4.31	0.05	0.00	99.65
DG-184	41.43	0.28	21.06	4.06	8.30	0.39	19.80	4.84	0.05	0.00	100.21
DG-067	41.86	0.28	22.27	2.55	7.41	0.33	20.62	4.52	0.09	0.00	99.93
DG-195	42.09	0.23	23.62	1.47	7.32	0.23	20.72	4.18	0.05	0.00	99.91
DG-069	41.90	0.20	22.78	2.10	6.68	0.34	21.60	4.54	0.05	0.00	100.19
DG-063	41.97	0.20	22.14	1.45	7.60	0.33	21.22	4.29	0.07	0.00	99.27
DG-024	41.98	0.19	21.95	2.36	7.61	0.37	20.58	4.53	0.03	0.00	99.60
DG-106	41.02	0.17	20.66	4.40	7.51	0.43	19.87	4.93	0.06	0.00	99.05
DG-025	41.68	0.16	21.13	3.42	7.21	0.40	20.62	4.83	0.03	0.00	99.48
DG-307	41.70	0.15	23.46	1.93	6.49	0.32	20.70	4.37	0.07	0.00	99.19
DG-018	42.24	0.00	21.90	3.45	6.76	0.32	21.05	4.54	0.02	0.00	100.28
DG-187	42.15	0.48	22.68	1.81	7.80	0.31	20.96	4.27	0.06	0.00	100.52
DG-191	42.46	0.47	21.36	2.99	6.34	0.27	21.37	4.28	0.07	0.00	99.61
DG-185	42.16	0.39	22.13	2.29	7.59	0.30	20.80	3.85	0.06	0.00	99.57
DG-188	43.01	0.42	21.16	2.80	6.44	0.23	21.56	3.93	0.07	0.00	99.62
DG-072	41.63	0.84	22.85	0.89	8.60	0.30	20.92	4.40	0.13	0.00	100.56
DG-071	41.96	0.87	22.79	0.79	8.70	0.27	20.59	4.45	0.11	0.00	100.53
DG-079	40.80	0.80	23.34	0.16	9.69	0.34	20.25	4.37	0.09	0.00	99.84
DG-282	42.28	1.10	21.76	0.74	8.47	0.17	20.42	4.36	0.13	0.00	99.43
DG-135	42.04	0.90	22.72	0.47	8.55	0.18	20.89	3.79	0.13	0.00	99.67
DG-124	41.30	1.09	22.23	0.86	8.60	0.20	20.90	4.05	0.11	0.00	99.34
DG-137	41.89	0.98	22.15	0.70	8.65	0.22	20.84	3.90	0.13	0.00	99.46
DG-119	42.55	1.10	22.15	0.62	8.68	0.21	21.00	4.18	0.11	0.00	100.60
DG-057	42.07	1.02	21.71	0.37	8.81	0.31	20.99	4.15	0.11	0.00	99.54
DG-130	41.22	1.18	21.91	0.85	8.98	0.23	21.05	4.06	0.13	0.00	99.61
DG-073	42.05	0.80	23.19	0.31	9.94	0.23	20.70	3.52	0.16	0.00	100.90
DG-151	42.54	0.83	22.51	0.35	9.58	0.23	20.66	3.29	0.15	0.00	100.14
DG-077	41.34	0.77	22.78	0.35	9.69	0.23	20.65	3.51	0.14	0.00	99.46
DG-158	42.65	0.95	21.66	0.35	9.88	0.26	20.58	4.02	0.12	0.00	100.47
DG-100	41.92	0.85	22.82	0.34	9.81	0.28	20.49	3.40	0.14	0.00	100.05
DG-131	42.44	0.77	22.83	0.35	10.00	0.20	20.47	3.29	0.15	0.00	100.50
DG-078	41.07	0.87	22.94	0.28	10.07	0.22	20.42	3.54	0.14	0.00	99.55
DG-098	41.54	0.71	22.72	0.35	10.03	0.28	20.40	3.34	0.13	0.00	99.50
DG-097	41.40	0.71	22.89	0.33	9.86	0.28	20.38	3.33	0.12	0.00	99.30
DG-099	41.95	0.76	23.12	0.33	9.92	0.21	20.37	3.36	0.13	0.00	100.15
DG-121	42.16	0.95	22.45	0.22	9.48	0.22	20.33	3.65	0.12	0.00	99.58
DG-132	41.14	0.81	22.50	0.28	9.68	0.22	20.31	3.35	0.16	0.00	98.45
DG-127	41.35	1.28	21.64	0.61	9.61	0.25	20.30	3.97	0.16	0.00	99.17
DG-154	42.56	0.75	23.10	0.16	10.59	0.24	20.29	3.01	0.19	0.00	100.89
DG-136	42.08	0.79	22.47	0.36	9.78	0.18	20.29	3.28	0.14	0.00	99.37
DG-133	41.98	0.84	22.61	0.28	9.77	0.22	20.29	3.30	0.16	0.00	99.45
DG-139	41.76	0.85	22.10	0.81	9.60	0.18	20.28	3.58	0.14	0.00	99.30
DG-279	42.41	0.76	22.60	0.46	9.13	0.20	20.27	3.62	0.15	0.00	99.60
DG-116	42.36	0.93	22.07	0.20	9.38	0.25	20.26	3.80	0.12	0.00	99.37
DG-056	42.03	0.68	22.16	0.31	9.85	0.20	20.23	3.56	0.22	0.00	99.24
DG-278	42.16	0.81	22.76	0.44	9.09	0.19	20.20	3.54	0.16	0.00	99.35
DG-076	40.82	0.78	23.23	0.25	10.43	0.22	20.19	3.39	0.14	0.00	99.45
DG-093	41.76	0.82	22.75	0.33	9.76	0.22	20.18	3.47	0.15	0.00	99.44
DG-114	42.02	0.79	22.62	0.37	10.07	0.22	20.15	3.30	0.15	0.00	99.69

Sample Number	SiO_2	TiO_2	Al_2O_3	Cr_2O_3	FeO	MnO	MgO	CaO	Na_2O	K_2O	Total
DG-125	41.89	1.06	22.36	0.20	9.40	0.23	20.10	3.68	0.13	0.00	99.05
DG-122	41.61	1.22	22.10	0.64	9.62	0.22	20.08	4.14	0.13	0.00	99.76
DG-123	41.72	1.20	21.98	0.62	9.64	0.26	20.06	4.14	0.13	0.00	99.75
DG-118	41.20	1.16	22.00	0.59	9.48	0.24	20.03	4.21	0.13	0.00	99.02
DG-112	41.70	0.97	21.96	0.32	9.65	0.24	20.00	4.08	0.14	0.00	99.06
DG-285	42.06	0.96	22.47	0.29	9.22	0.25	19.99	3.78	0.17	0.00	99.19
DG-136	41.56	1.14	22.10	0.42	10.30	0.27	19.93	3.72	0.18	0.00	99.62
DG-128	42.08	0.94	22.16	0.55	9.81	0.25	19.89	3.79	0.12	0.00	99.59
DG-140	41.48	0.83	22.58	0.37	9.86	0.20	19.88	3.77	0.15	0.00	99.12
DG-141	41.93	0.83	23.12	0.12	12.15	0.22	18.77	3.17	0.19	0.00	100.50
DG-061	41.44	0.74	22.00	0.11	11.84	0.23	19.61	3.26	0.19	0.00	99.42
DG-074	41.66	0.74	23.37	0.21	11.25	0.26	19.36	3.26	0.17	0.00	100.28
DG-280	42.00	0.80	22.76	0.15	11.04	0.23	19.24	3.34	0.17	0.00	99.73
DG-150	41.52	0.69	22.89	0.14	10.78	0.22	19.77	3.27	0.16	0.00	99.44
DG-113	41.84	0.98	22.47	0.32	10.71	0.23	19.73	3.32	0.20	0.00	99.80
DG-115	42.04	0.76	22.23	0.68	10.44	0.20	19.72	3.64	0.17	0.00	99.88
DG-134	41.92	0.99	22.50	0.15	10.41	0.20	19.77	3.33	0.16	0.00	99.43
DG-268	41.55	1.16	22.75	0.38	9.91	0.28	19.01	4.26	0.14	0.00	99.44
DG-269	41.65	1.08	22.82	0.46	9.86	0.23	19.17	3.75	0.17	0.00	99.17
DG-266	41.51	1.17	22.97	0.33	9.55	0.27	19.13	4.16	0.13	0.00	99.22
DG-257	41.89	1.19	22.72	0.71	9.22	0.27	19.37	4.36	0.12	0.00	99.85
DG-263	42.45	0.78	22.81	0.53	9.11	0.18	19.60	3.52	0.15	0.00	99.13
DG-259	42.43	0.81	22.66	0.37	9.07	0.24	19.67	3.71	0.11	0.00	99.07
DG-262	42.09	1.17	21.90	0.72	9.05	0.28	19.76	4.24	0.15	0.00	99.36
DG-075	41.63	0.59	23.73	0.07	8.55	0.18	20.65	4.14	0.10	0.00	99.64
DG-094	40.93	0.75	23.24	0.04	12.80	0.30	18.08	3.46	0.21	0.00	99.81
DG-261	41.60	0.85	22.84	0.16	11.36	0.31	18.07	3.64	0.20	0.00	99.03
DG-258	42.06	0.85	22.89	0.08	11.67	0.30	17.99	3.81	0.20	0.00	99.85
DG-267	41.94	0.64	22.89	0.09	12.16	0.28	17.63	3.50	0.19	0.00	99.32
DG-142	40.30	0.58	23.07	0.05	14.63	0.34	16.69	3.21	0.18	0.00	99.05
DG-260	41.30	0.75	22.74	0.19	13.40	0.30	16.55	3.82	0.21	0.00	99.26
DG-152	41.56	0.52	23.40	0.14	12.46	0.27	18.13	4.18	0.17	0.00	100.83
DG-058	41.63	0.49	22.65	0.13	13.10	0.28	17.14	5.16	0.20	0.00	100.78
DG-126	40.48	0.48	23.10	0.01	15.04	0.29	15.04	5.24	0.15	0.00	99.83
DG-148	36.64	0.04	21.72	0.08	33.86	1.12	4.58	2.39	0.01	0.00	100.44
DG-293	38.03	0.01	22.11	0.01	33.33	0.41	6.10	1.05	0.03	0.00	101.08
DG-294	38.06	0.06	22.06	0.01	32.71	0.24	6.22	1.24	0.03	0.00	100.63
DG-301	37.98	0.01	22.03	0.01	32.60	1.15	5.13	1.83	0.04	0.00	100.78
DG-295	37.74	0.22	22.18	0.01	32.29	0.88	5.48	2.17	0.01	0.00	100.98
DG-147	37.76	0.04	22.14	0.05	31.93	0.26	7.49	0.98	0.01	0.00	100.66
DG-145	36.61	0.07	21.99	0.06	31.76	0.26	7.60	0.74	0.01	0.00	99.10
DG-299	37.74	0.01	22.45	0.01	31.75	1.52	6.09	1.39	0.05	0.00	101.01
DG-146	36.67	0.04	21.61	0.06	31.72	0.79	6.61	2.18	0.01	0.00	99.69
DG-286	37.86	0.05	22.15	0.01	31.43	0.22	6.60	1.41	0.03	0.00	99.76
DG-289	38.51	0.01	22.12	0.01	30.91	0.64	7.24	1.12	0.01	0.00	100.57
DG-302	38.15	0.01	22.55	0.01	30.65	0.21	7.70	1.54	0.05	0.00	100.87
DG-143	38.23	0.05	22.06	0.08	30.46	0.56	7.78	1.33	0.01	0.00	100.56
DG-288	38.54	0.01	22.13	0.01	30.06	0.19	8.08	1.10	0.10	0.00	100.22
DG-291	38.37	0.04	22.06	0.01	30.02	0.19	8.05	1.07	0.08	0.00	99.89
DG-298	38.75	0.01	22.43	0.01	29.90	0.42	7.66	1.54	0.01	0.00	100.73
DG-290	38.70	0.01	22.17	0.01	29.88	0.21	7.99	1.86	0.04	0.00	100.87
DG-064	38.45	0.00	21.78	0.00	29.08	0.49	8.04	2.88	0.03	0.00	100.75
DG-296	39.23	0.01	22.38	0.01	28.09	0.35	9.21	1.50	0.04	0.00	100.82
DG-287	36.61	0.08	21.07	0.01	27.05	14.81	0.76	0.75	0.04	0.00	101.18
DG-292	39.22	0.01	22.25	0.28	25.88	0.42	9.98	2.34	0.04	0.00	100.42
DG-283	38.98	0.23	21.40	0.19	25.56	0.40	7.76	6.27	0.03	0.00	100.82
DG-144	39.16	0.05	22.96	0.14	24.13	0.33	11.66	1.80	0.01	0.00	100.24
DG-310	42.10	0.36	22.43	1.18	6.66	0.35	21.12	4.00	0.07	0.00	98.27
DG-065	42.22	0.11	24.28	1.02	5.79	0.21	22.62	3.74	0.03	0.00	100.02
DG-284	42.39	0.25	23.45	1.00	6.85	0.26	20.99	3.86	0.09	0.00	99.14
DG-080	40.94	0.18	23.30	0.96	10.57	0.32	19.24	4.62	0.03	0.00	100.16
DG-305	41.65	0.08	23.24	0.55	10.61	0.27	18.64	4.02	0.04	0.00	99.10
DG-313	42.26	0.39	23.66	0.69	6.25	0.18	20.83	4.98	0.08	0.00	99.32
DG-081	42.33	0.19	24.37	0.77	6.79	0.29	21.90	3.91	0.05	0.00	100.60
DG-314	42.50	0.18	23.64	0.73	7.08	0.27	21.29	3.87	0.06	0.00	99.62
DG-281	42.48	0.26	23.40	0.62	8.31	0.30	20.49	3.30	0.08	0.00	99.24
DG-153	41.96	0.26	23.30	0.62	8.42	0.31	20.77	3.97	0.08	0.00	99.69
DG-304	41.50	0.17	23.14	0.61	10.07	0.29	18.71	4.63	0.06	0.00	99.18

Sample Number	SiO_2	TiO_2	Al_2O_3	Cr_2O_3	FeO	MnO	MgO	CaO	Na_2O	K_2O	Total
DG-316	42.49	0.16	23.72	0.57	6.65	0.27	21.32	3.93	0.05	0.00	99.16
DG-216	42.82	0.20	23.61	0.50	8.24	0.32	20.25	3.93	0.04	0.00	99.91
DG-309	42.70	0.24	23.66	0.50	6.51	0.29	21.47	3.89	0.05	0.00	99.31
DG-160	42.20	0.30	23.26	0.43	7.83	0.27	20.94	3.79	0.05	0.00	99.07
DG-083	41.28	0.15	23.90	0.42	11.18	0.37	19.14	4.10	0.07	0.00	100.61
DG-212	42.79	0.24	23.97	0.42	7.62	0.28	20.95	4.12	0.06	0.00	100.45
DG-265	40.07	0.19	22.73	0.13	19.87	0.45	12.14	4.03	0.07	0.00	99.68
DG-255	40.04	0.26	23.25	0.08	16.77	0.29	14.62	4.98	0.10	0.00	100.39
DG-252	41.15	0.22	23.03	0.08	15.31	0.27	16.77	3.43	0.09	0.00	100.35
DG-102	40.94	0.20	23.58	0.13	15.06	0.30	16.42	4.10	0.08	0.00	100.81
DG-101	40.82	0.23	23.33	0.12	15.02	0.33	16.17	4.07	0.07	0.00	100.16
DG-043	41.00	0.13	23.02	0.20	14.61	0.31	17.57	3.37	0.04	0.00	100.25
DG-219	40.95	0.14	22.64	0.08	14.10	0.25	14.86	6.10	0.06	0.00	99.18
DG-095	40.90	0.20	23.43	0.22	13.81	0.34	17.31	4.04	0.06	0.00	100.31
DG-211	41.65	0.14	23.59	0.09	13.75	0.23	14.70	6.02	0.07	0.00	100.24
DG-221	41.22	0.12	23.59	0.09	13.66	0.23	16.74	4.66	0.04	0.00	100.35
DG-157	40.82	0.37	23.43	0.11	13.63	0.30	17.65	3.78	0.10	0.00	100.19
DG-224	39.79	0.13	23.61	0.09	13.54	0.27	17.04	4.77	0.06	0.00	99.30
DG-222	40.99	0.22	23.21	0.22	13.44	0.33	17.86	3.68	0.06	0.00	100.01
DG-159	39.96	0.26	22.87	0.08	13.39	0.20	13.34	9.08	0.10	0.00	99.28
DG-164	40.58	0.37	23.15	0.17	13.06	0.20	19.25	2.28	0.13	0.00	99.19
DG-045	41.24	0.37	22.61	0.14	12.97	0.21	16.65	5.68	0.14	0.00	100.01
DG-161	41.03	0.20	23.61	0.14	12.66	0.27	17.58	4.07	0.08	0.00	99.64
DG-096	41.16	0.32	23.50	0.18	12.43	0.33	18.54	3.47	0.08	0.00	100.01
DG-256	42.11	0.23	23.24	0.15	12.29	0.27	18.68	3.35	0.07	0.00	100.39
DG-214	41.24	0.16	23.81	0.09	12.19	0.21	18.01	4.16	0.06	0.00	99.93
DG-215	42.06	0.13	23.65	0.17	11.71	0.19	19.00	3.46	0.06	0.00	100.43
DG-103	41.39	0.25	23.61	0.14	11.63	0.29	18.96	3.38	0.09	0.00	99.74
DG-089	41.99	0.31	23.75	0.25	9.84	0.22	20.66	2.78	0.15	0.00	99.95
DG-047	42.04	0.35	22.94	0.14	9.82	0.23	20.78	2.94	0.14	0.00	99.38
DG-248	42.21	0.39	23.92	0.13	9.10	0.20	20.91	3.21	0.13	0.00	100.20
DG-250	42.21	0.39	23.92	0.13	9.10	0.20	20.91	3.21	0.13	0.00	100.20
DG-059	42.51	0.33	23.09	0.26	9.92	0.24	21.01	2.87	0.13	0.00	100.36
DG-254	42.12	0.34	23.73	0.24	10.02	0.16	20.50	2.78	0.12	0.00	100.01
DG-249	41.06	0.39	24.13	0.15	9.11	-0.23	20.85	3.33	0.12	0.00	99.37
DG-155	41.74	0.45	23.62	0.01	10.65	0.28	20.04	3.17	0.11	0.00	100.07
DG-088	41.65	0.33	23.93	0.24	9.64	0.23	20.50	2.78	0.11	0.00	99.41
DG-090	41.86	0.31	23.80	0.13	9.91	0.24	20.66	2.74	0.11	0.00	99.76
DG-060	42.18	0.31	22.70	0.21	9.74	0.21	20.83	2.96	0.11	0.00	99.25
DG-240	40.98	0.31	23.91	0.08	9.83	0.31	20.18	3.84	0.09	0.00	99.53
DG-239	42.27	0.35	24.13	0.10	9.95	0.34	20.34	3.77	0.09	0.00	101.34
DG-156	42.53	0.42	23.74	0.16	6.91	0.18	19.53	6.58	0.08	0.00	100.13
DG-220	41.52	0.25	23.66	0.22	9.80	0.29	19.71	4.15	0.08	0.00	99.68
DG-042	42.26	0.35	23.13	0.12	9.42	0.32	20.61	3.81	0.08	0.00	100.10
DG-162	42.53	0.28	24.03	0.15	7.53	0.21	21.39	3.59	0.08	0.00	99.79
DG-039	42.17	0.43	23.08	0.19	6.98	0.30	22.09	3.87	0.08	0.00	99.19
DG-046	41.64	0.52	22.46	0.11	9.29	0.36	19.64	5.17	0.07	0.00	99.26
DG-044	41.96	0.27	23.01	0.13	9.83	0.29	20.52	3.83	0.07	0.00	99.91
DG-041	42.13	0.32	23.13	0.15	7.71	0.39	21.41	4.02	0.06	0.00	99.32
DG-040	41.98	0.16	22.98	0.32	9.66	0.19	19.66	4.35	0.09	0.00	99.39
DG-110	41.81	0.15	23.84	0.15	8.99	0.37	20.46	3.72	0.04	0.00	99.53
DG-217	42.54	0.15	23.66	0.27	8.26	0.26	20.72	3.78	0.06	0.00	99.70
DG-038	42.35	0.14	23.29	0.10	8.62	0.19	20.53	4.58	0.06	0.00	99.86
DG-306	41.75	0.13	23.68	0.25	9.22	0.21	19.50	4.43	0.07	0.00	99.24
DG-111	41.66	0.13	23.95	0.30	9.05	0.34	20.64	3.94	0.05	0.00	100.06
DG-223	41.59	0.13	23.68	0.28	9.04	0.30	20.73	3.89	0.05	0.00	99.69
DG-163	41.54	0.11	23.48	0.16	10.21	0.27	19.14	4.17	0.06	0.00	99.14
DG-315	42.25	0.11	23.94	0.15	7.48	0.15	19.45	5.47	0.05	0.00	99.05
DG-303	41.79	0.11	23.67	0.16	7.26	0.14	20.26	5.84	0.06	0.00	99.29
DG-213	41.41	0.11	24.60	0.32	8.03	0.29	21.18	3.91	0.05	0.00	99.90
DG-312	41.89	0.09	24.01	0.28	7.44	0.12	19.06	6.21	0.05	0.00	99.15
DG-225	42.68	0.08	24.36	0.09	7.21	0.15	20.62	4.77	0.04	0.00	100.00
DG-318	42.47	0.07	24.23	0.25	6.91	0.15	21.48	3.70	0.03	0.00	99.29
DG-311	42.87	0.05	23.70	0.23	7.38	0.14	18.94	6.22	0.07	0.00	99.60
DG-149	41.59	0.01	25.06	0.15	6.81	0.15	22.46	3.36	0.04	0.00	99.63
DS-242	42.49	0.01	23.29	2.24	4.88	0.20	25.08	1.36	0.02	0.00	99.57
DG-231	42.96	0.01	22.66	2.93	4.99	0.25	25.00	1.06	0.03	0.00	99.89
DG-218	43.43	0.01	22.21	3.27	4.95	0.20	23.83	2.42	0.06	0.00	100.38

Sample Number	SiO_2	TiO_2	Al_2O_3	Cr_2O_3	FeO	MnO	MgO	CaO	Na_2O	K_2O	Total
DG-248	42.07	0.01	21.67	3.53	5.55	0.28	23.22	2.85	0.03	0.00	99.21
DG-035	42.47	0.00	21.55	3.56	6.18	0.33	23.08	2.21	0.02	0.00	99.40
DG-237	42.26	0.01	22.24	3.59	4.92	0.24	23.72	2.96	0.03	0.00	99.97
DG-243	41.56	0.01	22.04	3.82	5.17	0.24	25.14	1.15	0.03	0.00	99.16
DG-233	42.49	0.07	21.85	3.82	5.50	0.26	23.99	2.03	0.06	0.00	100.07
DG-227	42.17	0.01	21.43	4.02	5.72	0.24	23.22	2.48	0.06	0.00	99.35
DG-009	42.49	0.00	21.55	4.23	6.45	0.29	22.97	2.16	0.03	0.00	100.17
DG-014	42.56	0.00	21.82	4.24	5.14	0.26	24.61	1.30	0.00	0.00	99.93
DG-234	42.40	0.01	21.17	4.36	5.50	0.23	24.05	1.34	0.05	0.00	99.11
DG-010	42.27	0.00	21.24	4.53	5.62	0.30	23.93	1.49	0.02	0.00	99.40
DG-004	42.17	0.00	21.30	4.59	5.18	0.27	24.06	1.82	0.05	0.00	99.44
DG-013	42.61	0.00	21.09	4.62	4.64	0.28	24.43	1.72	0.03	0.00	99.42
DG-006	42.32	0.00	21.12	4.64	5.09	0.26	23.66	1.91	0.03	0.00	99.03
DG-236	42.89	0.01	21.20	4.72	4.98	0.20	24.23	2.06	0.03	0.00	100.32
DG-012	42.25	0.00	21.18	4.83	4.57	0.20	24.41	1.75	0.02	0.00	99.21
DG-226	42.02	0.01	20.90	4.86	5.89	0.23	23.82	1.61	0.03	0.00	99.37
DG-007	42.36	0.00	21.29	4.87	5.53	0.25	24.18	1.65	0.02	0.00	100.15
DG-232	42.69	0.01	20.87	4.90	5.75	0.23	23.89	1.54	0.03	0.00	99.91
DG-244	42.45	0.01	20.47	4.92	6.04	0.24	23.80	1.85	0.03	0.00	99.81
DG-033	42.36	0.06	20.43	4.92	6.20	0.31	23.18	2.29	0.03	0.00	99.78
DG-021	42.33	0.04	20.93	5.09	5.25	0.24	23.65	2.41	0.05	0.00	99.99
DG-005	42.50	0.00	20.97	5.10	5.63	0.31	25.00	0.29	0.00	0.00	99.80
DG-011	42.14	0.00	20.88	5.16	4.85	0.24	23.91	1.85	0.05	0.00	99.08
DG-020	42.12	0.00	20.87	5.19	5.72	0.22	23.59	1.95	0.04	0.00	99.70
DG-228	41.85	0.01	20.90	5.27	5.70	0.26	23.63	2.10	0.04	0.00	99.76
DG-022	42.52	0.00	20.80	5.29	5.43	0.24	23.48	2.39	0.07	0.00	100.22
DG-230	41.71	0.01	20.54	5.30	6.39	0.31	22.46	2.68	0.03	0.00	99.43
DG-017	42.11	0.05	20.42	5.31	5.66	0.30	23.14	2.29	0.02	0.00	99.30
DG-034	41.83	0.00	20.04	5.44	6.07	0.38	22.31	3.08	0.03	0.00	99.18
DG-238	42.45	0.01	20.73	5.49	5.21	0.26	21.40	1.58	0.03	0.00	97.16
DG-235	42.68	0.01	20.30	5.74	5.69	0.28	23.70	1.72	0.06	0.00	100.18
DG-271	42.53	0.01	20.16	5.92	5.64	0.29	22.21	2.46	0.04	0.00	99.26
DG-030	42.54	0.07	19.88	6.12	5.12	0.23	23.66	2.09	0.05	0.00	99.76
DG-229	42.64	0.01	20.23	6.39	5.45	0.27	20.69	0.84	0.01	0.00	96.53
DG-245	41.99	0.01	19.53	6.58	5.43	0.33	24.58	0.83	0.04	0.00	99.32
DG-019	41.66	0.00	19.37	6.70	4.90	0.25	22.96	3.45	0.02	0.00	99.31
DG-029	41.89	0.04	19.10	6.83	5.90	0.27	22.58	2.50	0.00	0.00	99.11
DG-274	42.02	0.01	18.61	7.52	6.19	0.32	21.16	3.46	0.01	0.00	99.30
DG-092	41.53	0.17	18.57	7.68	6.12	0.27	22.27	3.02	0.04	0.00	99.67
DG-109	41.28	0.17	18.77	7.94	6.07	0.27	21.52	3.42	0.03	0.00	99.47
DG-241	41.48	0.01	17.97	8.61	5.46	0.23	23.85	1.92	0.00	0.00	99.53
DG-275	42.36	0.08	17.75	8.75	5.78	0.33	21.53	3.09	0.07	0.00	99.74
DG-273	42.34	0.07	17.86	8.10	6.16	0.31	19.65	5.17	0.05	0.00	99.71
DG-031	41.52	0.08	18.48	7.36	6.49	0.36	20.37	5.23	0.05	0.00	99.94
DG-036	41.56	0.00	19.07	6.80	5.72	0.30	21.35	4.63	0.04	0.00	99.47
DG-037	41.96	0.00	20.29	5.03	6.54	0.35	21.50	3.84	0.03	0.00	99.54
DG-104	41.46	0.52	19.34	5.73	6.12	0.35	21.17	4.73	0.08	0.00	99.50
DG-091	41.16	0.06	20.21	5.48	6.47	0.37	20.62	4.60	0.04	0.00	99.01
DG-003	41.14	0.00	20.24	5.43	6.02	0.29	21.43	4.47	0.06	0.00	99.08

APPENDIX 7.b

OXIDE	RUT - 1	RUT - 2	RUT - 3
SiO_2	N.D.	N.D.	N.D.
TiO_2	98.33	99.37	99.10
Al_2O_3	N.D.	N.D.	N.D.
Cr_2O_3	N.D.	N.D.	N.D.
FeO	0.55	0.48	0.47
MnO	N.D.	N.D.	N.D.
MgO	N.D.	N.D.	N.D.
CaO	N.D.	N.D.	N.D.
Na_2O	N.D.	N.D.	N.D.
K_2O	N.D.	N.D.	N.D.
NiO	-	N.D.	N.D.
BaO	0.54	-	0.39
ZrO_2	N.D.	-	N.D.
SrO	N.D.	-	N.D.
TOTAL	99.42	99.85	99.96

GARNET MEGACRYSTS IN THE GROUP II DOKOLWAYO KIMBERLITE, SWAZILAND.

R.O. Moore, L.R.M. Daniels & J.J. Gurney.
Department of Geochemistry, U.C.T., Rondebosch, 7700, RSA.

In a study of the heavy mineral concentrate from the Group II (Smith, 1983) Dokolwayo kimberlite in Swaziland, Daniels & Gurney (1989) identified a suite of garnets which they interpreted to be representative of the Cr-poor suite of megacrysts. This represented a significant find, since it was previously believed that the occurrence of Cr-poor megacrysts was confined to Group I kimberlites. Directed investigations have since recognised the presence of garnet megacrysts in a large number of Group II kimberlites in South Africa, and work on characterising these suites is currently in progress. None of the other common constituent phases of the Cr-poor megacryst suite such as olivine, cpx, opx and ilmenite have been found at any of these localities to date.

This contribution reports on the compositional characteristics of the Dokolwayo garnet megacrysts. A representative suite of thirty samples was selected for study from a large collection of garnet megacrysts sampled from the coarse tailings dumps at the mine. Since this material has been processed through the primary crusher, all samples were less than 2 cm in longest dimension. The garnets are deep red in colour, highly fractured and have thin kelyphitic rinds developed on grain margins.

Major element compositions were determined on a Cameca Camebax microprobe, using routine analytical procedures. Core-rim analyses on a number of test samples revealed no compositional zoning and consequently analyses were undertaken on grain mounts of chips taken from the megacrysts. Fifteen samples spanning the range of Mg-numbers (atomic Mg/Mg+Fe, henceforth abbreviated to M#) displayed by the suite were selected for trace element analysis. These were undertaken on the proton microprobe housed in the HIAF (Heavy Ion Analytical Facility) laboratory at the CSIRO in Sydney, Australia. Details of this instrument and its application to the analysis of geological materials have been described by Sie (1985), Sie & Ryan (1986) and Griffin *et al.*, (1988). The precision of the data is indicated by the uncertainties quoted for the representative analyses presented in Table 1. The accuracy of the method at similar levels has been established by analysis of standard materials (Griffin *et al.*, 1988).

In assessing the compositional characteristics of the Dokolwayo garnets, they are compared with Cr-poor garnet megacrysts from the Monastery kimberlite. This suite was chosen because it has been well documented and is considered to be broadly representative of garnet megacrysts in Group I kimberlites.

Appendix 7.c

Figure 1: A selection of plots illustrating the compositions of garnet megacrysts from Dokolwayo. Compositional fields for Monastery garnets are included for comparison. Monastery data from Gurney *et al.* (1979) and Moore (unpublished).

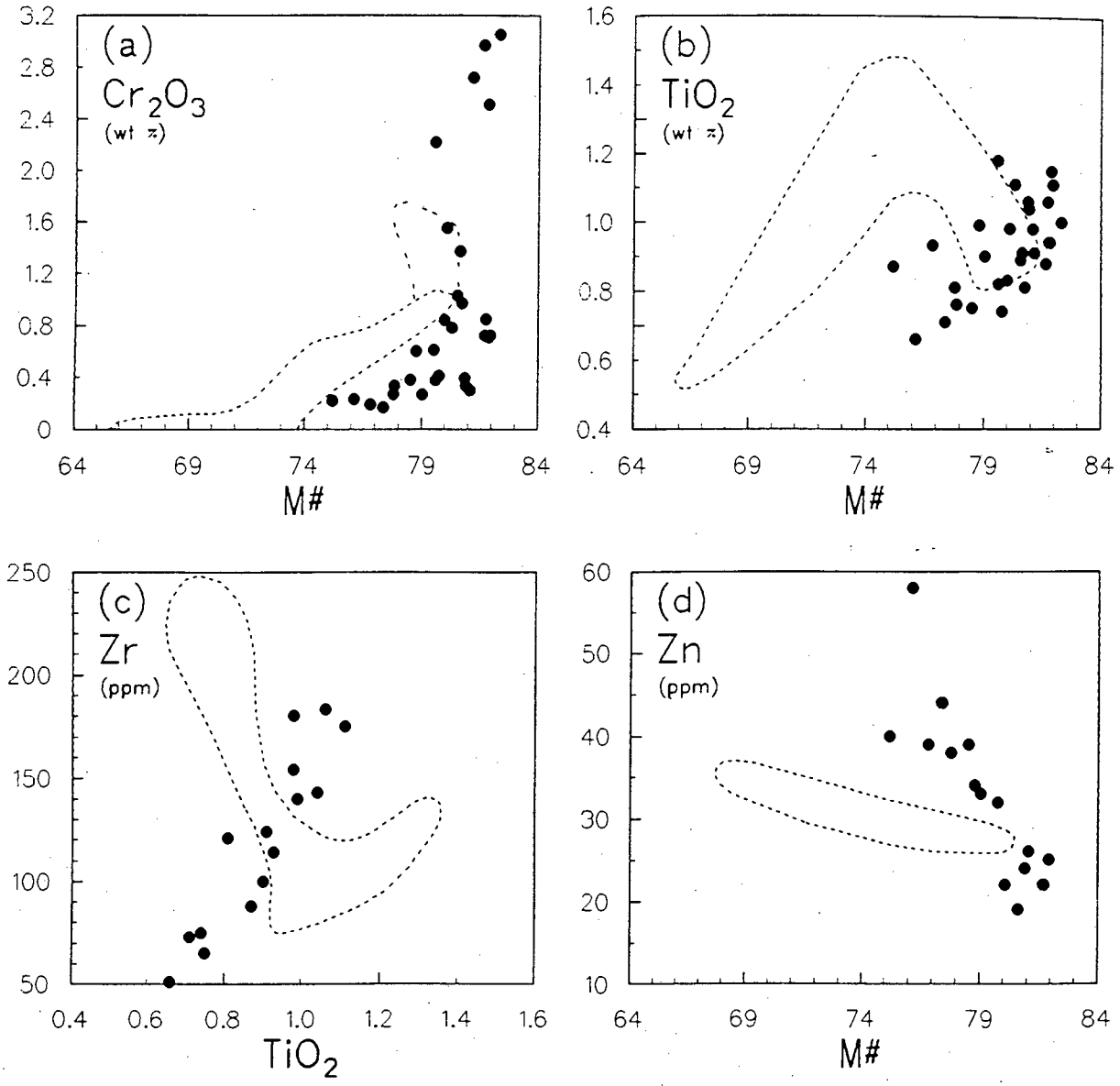

The Dokolwayo garnets show a restricted range in M# (75.2-82.3) which is on average more magnesian (but overlaps with) that observed for Monastery garnets (66.2-81.5) (Gurney *et al.*, 1979; Moore, unpublished data). The plot of Cr_2O_3 vs M# (Fig. 1a) illustrates this and shows that the Dokolwayo garnets range to significantly higher values of chromium (.17-3.05 wt% Cr_2O_3) than those seen at Monastery. Another notable feature is the rapid decrease in chrome over a very small range in M# displayed by the most magnesian Dokolwayo garnets. Titanium contents are high (0.66-1.18 wt% TiO_2), but in contrast with the good correlation observed between Cr_2O_3 and M#, only a very diffuse trend of decreasing TiO_2 with Fe-enrichment is observed (Fig. 1b). This trend is opposite

to what would be expected from a normal igneous fractionation process, and where it occurs in garnet megacrysts from Group I kimberlites, the titanium depletion is correlated with the coprecipitation of ilmenite (e.g. Gurney *et al.*, 1979). The absence of ilmenite megacrysts at Dokolwayo effectively rules out this explanation in this case.

Table 1: Representative Analyses of Dokolwayo Garnet Megacrysts

	GT-27	GT-29	GT-23	GT-18	GT-15	GT-05	GT-16	GT-12
SiO_2	41.84	41.74	42.86	41.76	41.70	42.09	42.00	41.99
TiO_2	.87	.93	.81	.75	.90	.74	.91	1.11
Al_2O_3	22.89	22.84	22.95	22.91	22.83	22.74	22.04	22.07
Cr_2O_3	.22	.19	.27	.38	.27	.41	1.37	.72
FeO	11.59	10.78	9.96	9.99	9.61	9.51	8.68	8.27
MnO	.23	.24	.24	.24	.27	.25	.31	.26
MgO	19.71	20.05	19.57	20.47	20.32	21.01	20.26	21.04
CaO	3.37	3.40	4.02	3.46	3.62	3.51	4.40	4.28
Na_2O	.19	.16	.21	.15	.14	.14	.12	.11
Total	100.91	100.33	100.89	100.11	99.66	100.40	100.09	99.85
Zr	88±3	114±3	121±4	65±2	100±5	75±4	124±6	175±6
Y	28±1	24±2	21±2	26±1	23±1	24±2	22±2	31±3
Ni	79±5	101±4	53±6	156±5	111±4	141±5	58±9	164±5
Zn	40±2	39±2	38±3	39±2	33±1	32±1	19±4	25±2
Ga	17±1	16±1	18±1	17±1	15±1	14±1	18±3	20±3
M#	75.19	76.82	77.78	78.50	79.03	79.74	80.62	81.93

All sample numbers have the prefix LDD-301; major element concentrations in wt%; trace elements in ppm. Uncertainties on trace element values quoted to 1 sigma. A wide range of trace elements was analysed for, but only those present at significant levels are reported in this table.

The Dokolwayo garnets show a limited range in CaO (3.3-4.7 wt%) which is slightly larger than the even more restricted range commonly observed for garnet megacrysts in Group I kimberlites. They also show elevated trace levels of Na_2O (0.10 to 0.21 wt%) which increases with Fe-enrichment. Trace enrichments of Na_2O have been correlated with high formation pressures (>45 Kb) in eclogitic systems (e.g. McCandless & Gurney, 1989), and we believe this to be applicable here as well.

Zr (51-183 ppm) and Y (19-31 ppm) both show a good positive correlation with M# and as such, mimic the behaviour of TiO_2. This is well demonstrated by the good positive correlation observed between Zr and TiO_2 in Fig. 1(c). Ni concentrations range from 53 to 164 ppm and show a general decrease with Fe-enrichment. Zn ranges from 19 to 58 ppm and shows a good negative correlation with M# (Fig. 1d), while Ga (14-23 ppm) shows a general decrease with Fe-enrichment but the trend is poorly defined.

An important feature which has emerged from this preliminary study is that while the Dokolwayo garnets show similar basic compositional features to Cr-poor garnet megacrysts occurring in Group I kimberlites (such as restricted CaO and elevated TiO_2 and Na_2O), the

compositional trends they define are significantly different. This is clearly evident in Fig. 1. The fact that most elements show systematic variations with M#, may indicate that the garnets have formed in an igneous fractionation process, but the nature of the parent magma and coprecipitating phases is not clear at this stage. Assuming that they did have an igneous origin, the differences in trends noted between the Dokolwayo and Monastery suites could be readily explained in terms of differences in the nature and relative proportion of coprecipitating phases.

The observed trends of decreasing Ti, Zr and Y with Fe-enrichment, are opposite to what would normally be expected from an igneous fractionation process. The most likely explanation for this is that these elements are being depleted by the coprecipitation of a phase (s) in which they are highly compatible. Ilmenite and zircon would be the most suitable candidates, but both of these phases are extremely rare (or even absent) in Group II kimberlites (Skinner, 1989). A small number of rutile megacrysts have been found at Dokolwayo and it is possible that the coprecipitation of this phase may account for some of the observed trends.

References

Daniels, L.R.M. & Gurney, J.J. (1989). The chemistry of the garnets, chromites and diamond inclusions from the Dokolwayo kimberlite, Kingdom of Swaziland. *In: Kimberlites and Related Rocks, Vol.2: Their Mantle/Crust Setting, Diamonds and Diamond Exploration,* Blackwell Scientific Publications, 1012-1021.

Griffin, W.L., Jaques, A.L., Sie, S.H., Ryan, C.G., Cousens, D.R. & Suter, G.F. (1988). Conditions of diamond growth: a proton microprobe study of inclusions in West Australian diamonds. *Contrib. Mineral. Petrol.*, **99**, 143-158.

Gurney, J.J., Jakob, W.R.O. & Dawson, J.B. (1979). Megacrysts from the Monastery kimberlite pipe, South Africa. *In: Boyd, F.R., Meyer, H.O.A. (eds) The Mantle Sample: Inclusions in Kimberlites and Other Volcanics.* Am. Geophys. Union Washington, D.C., 227-243.

McCandless, T.E. & Gurney, J.J. (1989). Sodium in garnet and potassium in clinopyroxene: criteria for classifying mantle eclogites. *In: Kimberlites and Related Rocks, Vol.2: Their Mantle/Crust Setting, Diamonds and Diamond Exploration,* Blackwell Scientific Publications, 827-832.

Sie, S.H. (1985). An accelerator facility within a mineral research establishment. *Nucl. Instr. Meth. Phys. Res.*, **B10/11**, 664-670.

Sie, S.H. & Ryan, C.G. (1986). An electrostatic "Russian" quadruplet microprobe lens. *Nucl. Instr. Meth. Phys. Res.*, **B15**, 664-668.

Skinner, E.M.W. (1989). Contrasting Group I and Group II kimberlite petrology: towards a genetic model for kimberlites. *In: Kimberlites and Related Rocks, Vol. 1, Their Composition, Occurrence, Origin and Emplacement,* Geol. Soc. Aust. Spec. Pub. No.14., Blackwell Scientific Publications, 528-544.

Smith, C.B. (1983). Pb, Sr and Nd isotopic evidence for sources of southern African kimberlites. *Nature,* **304**, 51-54.

CHAPTER 8 - DOKOLWAYO CONCENTRATE SPINELS

ABSTRACT

Approximately 45% of the concentrate from the Dokolwayo kimberlite consists of spinel. More than 80% of the spinels (n=288) have Cr_2O_3 > 60 wt%. Approximately 10% of the spinels are deficient in divalent cations and are stoichiometrically Fe_2O_3-free. These spinels are suggested to have a significant content of divalent chromium, i.e. CrO. Two main populations are recognised. The one population has TiO_2 < 0.6 wt% and has TiO_2/Al_2O_3 < 0.2. The second population is TiO_2-rich (generally > 0.6 wt%) and has TiO_2/Al_2O_3 > 0.2. The TiO_2-poor population is similar in composition to the diamond inclusion population. A model is presented for the crystallization of the TiO_2-rich population as an early cumulate phase of komatiite melts.

8.1 INTRODUCTION

Spinels are commonly found in the heavy mineral concentrates of kimberlites, particularly in Type II kimberlites. Although concentrate spinel chemistry has been suggested to be potentially important in the field of kimberlite exploration (Mal'kov and Popova, 1972; Dong and Zhou, 1980; Gurney, 1984) spinel compositions from kimberlite concentrates have received remarkably little attention in the literature. The compositions of concentrate spinels are often reported in very general terms (e.g. Skinner and Scott, 1979), but intensive studies are uncommon.

Lawless (1974), in what is probably the most extensive general investigation of South African kimberlite concentrate compositions available at present, documented the spinel compositions from several southern African kimberlites. It was noted that there is a similarity between the compositions of spinels occurring as inclusions in diamonds and

some of the spinels derived from kimberlite concentrates. Apart from concluding that the chromian concentrate spinels, particularly euhedral spinels, are unlikely to have been derived from spinel-lherzolites, Lawless also concluded that both the high chromium (>60 wt% Cr_2O_3) concentrate spinels and spinel inclusions in diamonds suggested a paragenesis in a chrome-rich environment.

Approximately 45% of the heavy mineral concentrate from the Dokolwayo kimberlite DK1 consists of xenocryst (0.5 - 2mm) chromian-spinels. This abundance has afforded the opportunity to study the compositions of these spinels in detail. The objectives of this study were to identify the possible existence of sub-populations of spinel in the concentrate as well as investigating paragenetic models.

8.2 CONCENTRATE SPINEL COMPOSITIONS

The most outstanding feature of the Dokolwayo concentrate spinels is the consistently high chromium content. More than 80% (n=288) contain >60 wt% Cr_2O_3. The highest determined concentration is 73.9 wt% Cr_2O_3. A similar Cr_2O_3 content in a spinel from Premier has been reported by Hunt (1987). Approximately 20% of the spinels have Cr_2O_3 values in excess of the ideal stoichiometric limit of 67.9 wt%. Compositional ranges are presented in Table 8.1. The Fe_2O_3 contents of the spinels not exceeding the ideal stoichiometric Cr_2O_3 limit were calculated based on stoichiometric requirements. Full analyses are presented in APPENDIX 8.a.

8.2.1 Cr^{3+} vs ($Al^{3+}+Fe^{3+}+Ti^{4+}$)

The Dokolwayo concentrate spinels exhibit a negative correlation between the Cr^{3+} and Al^{3+} (Figure 8.1). The correlation is non-linear at the chrome-rich end of the field and there is a marked deviation from the octahedral-site control line. This deviation from the control line is indicative of either one, or a combination of (a) the presence of cations other

than Cr^{3+} and Al^{3+} in octahedral coordination [e.g. $(Mg,Fe)^{2+}$, Fe^{3+}, Ti^{4+}] and (b) non-stoichiometry (Haggerty, 1976, 1979).

The presence of Fe in both divalent and trivalent oxidation states in octahedral coordination [i.e. $Fe^{2+}+Fe^{3+}O_4$ and $Fe^{2+}(Fe^{2+}Ti^{4+})O_4$] induces non-stoichiometry in spinels (Haggerty, 1979). There is thus a positive correlation between the degree of non-stoichiometry and the concentration of TiO_2 and Fe_2O_3 in the spinels. In addition to contributing to the non-stoichiometry of the spinels, Fe^{3+} and $(Fe^{2+}Ti^{4+})$ successfully compete with Al^{3+} for octahedrally coordinated sites within the spinel structure relative to Cr^{3+}, which further contributes to the observed deviation from the octahedral-site control line in Figure 8.1. The influence of Fe^{3+} and $(Fe^{2+}+ Ti^{4+})$ on the deviation from the octahedral control line exhibited by Al^{3+} in the Dokolwayo concentrate spinels is clearly demonstrated in Figure 8.2 where $[2*Ti^{4+} + Fe^{3+} + Al^{3+}]$ is plotted against Cr^{3+}.

8.2.2 Cr^{3+} - Ti^{4+}

The correlation between Cr^{3+} and Ti^{4+} in the Dokolwayo spinels is defined by a broad, negatively sloped field (Figure 8.3). A noteworthy feature of the trend is the extension of this field well into the region where chromium concentrations are in excess of the ideal stoichiometric limit ($Cr^{3+} > 1.77$ cations/4 oxygens). The relatively high concentrations of the minor element oxide TiO_2 (i.e. >0.7 wt%) in the Dokolwayo concentrate spinels are in contrast to the concentration levels of TiO_2 observed in diamond inclusion spinels from Dokolwayo as well as from other southern African kimberlites (Gurney et al., 1979, 1984a, 1984b; Rickard et al., 1989; Hill 1989; Gurney, unpubl. data; this study, Chapter 5). A histogram of TiO_2 concentrations in the concentrate spinels (Figure 8.4a) indicates that TiO_2 in these spinels is bimodally distributed. The two populations, although some overlap does occur, can be broadly defined as a TiO_2-poor population ($TiO_2 < 0.7$ wt%) and a TiO_2-rich ($TiO_2 > 0.7$ wt%) population. The cutoff of 0.7 wt% TiO_2 between the two concentrate spinel populations is convenient as this corresponds to the maximum

concentration of TiO_2 in diamond inclusion spinels world wide (Daniels, 1991). The Dokolwayo concentrate TiO_2-poor population correlates well with TiO_2 concentration levels observed in diamond inclusion spinels from southern African kimberlites (Figure 8.4b).

8.2.3 Al_2O_3 and TiO_2

The relationship between Al_2O_3 and TiO_2 in the Dokolwayo concentrate spinels defines two major populations and several minor sub-populations (Figure 8.5). The two major populations broadly coincide with the TiO_2-poor and TiO_2-rich populations defined above. There is some overlap towards the low Al_2O_3 (<3.5 wt%) end of the respective populations. The value $TiO_2/Al_2O_3 = 0.2$ is used as a convenient factor to define the two major populations (Figure 8.5).

8.2.4 Fe_2O_3 and Cr^{2+}

The majority (90%) of the Dokolwayo concentrate spinels are characterised by the presence of Fe_2O_3 whereas approximately 10 percent of the spinels are stoichiometrically calculated to be Fe_2O_3-free. Most of these spinels exhibit a deficiency in cations (i.e. <3.000 cations/4 oxygens.), have Cr_2O_3 in excess of the stoichiometric limit and may contain TiO_2. The excess chromium contents are due to a deficiency of divalent cations in tetrahedral coordination (cf meteoritic spinels; Bunch and Olsen, 1975) and a significant proportion of the chromium may be in the 2^+ oxidation state. Based on the assumption that some of the chromium in these spinels is in tetrahedral sites, the weight percent oxides for three of the spinels have been recalculated on the basis of 3 cations per 4 oxygens. The results are presented in Table 8.2.

It should be noted that these spinels with excess chromium are represented in both the TiO_2-poor and the TiO_2-rich populations and are also present on both sides of the

TiO_2/Al_2O_3 = 0.2 line (Tial-factor). Perhaps the most convincing case for the presence of Cr^{2+} in these spinels is sample CHR-76 (Table 8.2). No TiO_2 was detected in this spinel and Fe_2O_3 was calculated to be absent or below detection. However, there is a significant deficiency (0.9564) of divalent, tetrahedrally coordinated cations and an excess (2.0291) of trivalent, octahedrally coordinated cations in this spinel. Several possibilities may be inferred to explain these observations. It is possible that the spinel contains elements which have not been determined. In view of the total obtained for the analysis of this spinel (Table 8.2), it is unlikely that the addition of any elements which have not been accounted for will effectively alter the observations. A second possibility is that some of the trivalent cations are in tetrahedral coordination. The high preference for octahedral coordination within the spinel structure exhibited by both Cr^{3+} and Al^{3+} suggests that they are unlikely to be in tetrahedral coordination. The third possibility, and the one which is preferred, is that chromium occurs in both the divalent and trivalent oxidation states within the spinel. Based on crystal field site energy considerations (Burns, 1970a), divalent chromium will be tetrahedrally coordinated. The size of the Cr^{2+} cation will distort the crystal lattice of the spinel and it is likely that the spinel will be non-stoichiometric, which is consistent with the observed calculated deficiency of cations in these spinels. Reduction potentials for various oxidation states of Fe and Cr (Table 8.3) indicate that Cr^{+3} will reduce to Cr^{2+} before Fe^{2+} will reduce to iron metal. It is thus unlikely that the non-stoichiometry of these spinels may be attributed to the presence of native iron.

Unfortunately, in the absence of IR or Mössbauer spectra it is impossible to conclusively rule in favour of the presence of Cr^{2+} at present. Nevertheless, divalent tetrahedrally coordinated chromium is considered to be a strong candidate to account for some of the excess chromium in the concentrate spinels which have Cr_2O_3 above the stoichiometric limit.

8.2.5 Inverse Spinels

The ulvöspinel component (Fe_2TiO_4) of a spinel constitutes an inverse spinel and is expressed by the general formula $R^{2+}[R^{2+}Ti^{4+}]O_4$. Normal spinels are represented by the general formula $R^{2+}[R^{3+}]_2O_4$. The high concentrations of TiO_2 in the majority of the Dokolwayo concentrate spinels suggest that these spinels have a significant inverse spinel component.

8.2.6 Mg^{2+} vs Fe^{2+} - $(2*Ti^{4+})$

The increase in total Fe^{2+} in the spinels which is required to compensate for the degree of inverse component present in the spinels distorts any evaluation of the relationship between FeO and MgO without compensating for the inverse spinel component. In order to compensate for the inverse component it is necessary to remove the Fe^{2+} component associated with Ti^{4+} and hence it is best to evaluate the relationship between iron and magnesium on the basis of cations present per 4 oxygens. Two distinct populations may be observed in Figure 8.6. Although there is overlap between the two populations, the $TiO_2/Al_2O_3 > 0.2$ population exhibits a shift towards lower corrected Fe^{2+} values than the TiO_2-poor population. The range of corrected Fe^{2+} in the TiO_2-rich population is also significantly narrower than the observed range in the TiO_2-poor population.

8.2.7 Zoning

The concentrate spinels were investigated for major element zonation. The spinels characterised by $TiO_2/Al_2O_3 > 0.20$ showed no marked zonation features, and in particular the TiO_2 contents of these spinels were relatively constant in any individual spinel. The largest spinel analysed in this study was approximately 9 mm in diameter. Ten equidistant points were analyzed across this spinel. The data are presented in Figure 8.7. No significant zonation in TiO_2 and Al_2O_3 occurs across this spinel, which forms part of

the TiO_2-rich and TiO_2/Al_2O_3 > 0.2 populations. This spinel has an average Cr_2O_3 content of 58.03 wt% with a standard deviation of 0.34 wt%.

In contrast, some of the TiO_2-poor spinels show significant zonation patterns in Cr_2O_3 and Al_2O_3 contents. The most significant feature is a strong increase in Cr_2O_3 from centre to edge whereas there is a corresponding decrease in Al_2O_3 from centre to edge (Table 8.4). The range in Cr_2O_3 content from centre to edge in these zoned concentrate spinels is similar to the range observed in spinel inclusions from single diamonds (Chapter 5). It should also be noted that the TiO_2 content of the spinels that are characterised by reversed Cr_2O_3 zonation is similar to the TiO_2 concentration levels observed in diamond inclusion spinels.

8.2.8 Trace Elements

Three populations of concentrate spinels were analysed by J.J. Gurney for trace concentrations of Ga, Zn and Ni.

The three populations were identified on the basis of external shapes of the spinels. The shapes of the spinels were defined as follows:

a) Euhedral: 80 - 100% of the original crystal faces can be identified.

b) Subhedral: 20 - 80% of the original crystal faces can be identified.

c) Anhedral: Less than 20% of the original crystal faces can be identified.

Two chemical populations can be identified when plotting Zn and Ga (Figure 8.8a). The majority of the euhedral spinels plot in a field which is separated from the diamond inclusion spinels. This suggests that the euhedral spinels are generally not related to the diamond inclusion spinels. In contrast, the majority of the anhedral spinels plot in the same field as the diamond inclusion spinels. The same relationship can be observed when plotting Ni and Ga (Figure 8.8b).

Nickel generally has a positive relationship with Zn for the spinel population as a whole. However, the anhedral spinels and the diamond inclusion spinels are for the most part characterised by lower concentrations of both Zn and Ni as opposed to the euhedral spinels (Figure 8.8c).

The relationship between Al_2O_3 and Zn defines two major populations and a few scattered points. One population is defined by the majority of the diamond inclusion spinels and five of the anhedral spinels. None of the other concentrate spinels plot in this field (Figure 8.9a). A similar relationship is exhibited by Ni and Al_2O_3 (Figure 8.9b). The concentrate spinels generally define a positive trend between Ni and Al_2O_3 and correspondingly a negative trend between Cr^{3+} and Ni (Figure 8.10). In contrast the diamond inclusions plot into a tight cluster. The clearest distinction between the different spinel groups are observed when plotting the trace elements against TiO_2. The majority of the concentrate spinels analysed for trace elements have $TiO_2 > 0.7$ wt%. All the spinels with $TiO_2 < 0.7$ wt%, including the diamond inclusion spinels, plot into a tight cluster when plotting TiO_2 against Zn, Ga or Ni (Figures 8.11a, 8.11b, 8.11c). The spinels with $TiO_2 > 0.7$ wt% define a diffuse field when plotted against Zn (Figure 8.11a) and Ga (Figure 8.11b), whereas they define a distinct positive trend with Ni (Figure 8.11c).

8.3 DISCUSSION

High concentrations of chromium in concentrate spinels at Dokolwayo are not unique for kimberlite concentrate spinels (e.g. Hunt 1987). However, the average Cr_2O_3 content of the spinels (Table 8.1) is exceptional. Based on several major and trace element relationships, there are at least two major populations of spinels present in the concentrate. In particular, it would appear that the concentration of titanium, the relationship between TiO_2 and Al_2O_3 and the relationship between Mg^{2+} and $[Fe^{2+}-2*Ti^{4+}]$ may be used to define between the two populations. Comparing the major and trace element compositions of the TiO_2-poor population of the concentrate spinels with the compositions of the diamond inclusions from Dokolwayo (Chapter 5) suggests that the majority of the TiO_2-poor population is closely related to the diamond inclusion spinels and may have a similar paragenesis. However, the TiO_2-rich population is clearly not related to the diamond inclusion spinels and therefore probably had a different genesis.

Perhaps the simplest explanation is that the TiO_2-rich population represents a portion of the TiO_2-poor population that was metasomatised by a TiO_2-rich fluid. However, the mechanics of this process should be considered. Diamond inclusion-type spinels (Daniels, 1991) and subcalcic chromium-rich garnets (G10 garnets) have been found to coexist in a number of instances (Meyer and Boyd, 1968; Danchin and Boyd, 1976; Dawson et al., 1978; Pokhilenko et al., 1977; Gurney et al., 1984a; Sobolev et al., 1984; Nixon et al., 1987; Hill, 1989) and therefore have the same paragenesis. It would therefore be reasonable to assume that if the majority of the spinels have been metasomatised by a TiO_2-rich fluid, then the effect of this metasomatic event should, to some extent, be manifested in the G10 garnet population at Dokolwayo as well (Chapter 7).

Partition coefficients for TiO_2 between spinel and ultrabasic liquids (Akella et al., 1976; Murck and Cambell, 1986; Barnes, 1986) are in the order of D_{Ti}spinel/liquid $=>$ 0.75. Considering the average and the maximum concentrations of TiO_2 in the Dokolwayo

concentrate spinels (Table 8.1), this partition coefficient suggests that the Dokolwayo spinels equilibrated against a fluid which must have had TiO_2 concentrations averaging 1.57 wt% and possibly as high as 5.2 wt% TiO_2.

Although there is no reliable partition coefficient for titanium between garnet and liquid, it is possible to infer a partition coefficient of D_{Ti}garnet/liquid = 0.35. This partition coefficient is based on the partitioning of Ti^{4+} between orthopyroxene and liquid (Barnes, 1986) and the concentration of TiO_2 in garnets coexisting with orthopyroxenes in mantle derived garnet lherzolites (Bishop et al., 1978). Therefore, assuming that the G10 garnets and the majority of the spinels coexisted, the average TiO_2 concentration of the concentrate G10 garnets should be in the order of 0.55 wt%. However, although the Dokolwayo concentrate G10 garnets attain a maximum TiO_2 content of 0.17 wt%, which is similar to the TiO_2 contents of Finsch G10 garnets (Gurney and Switzer, 1973), they do not support a suggestion of re-equilibration against a TiO_2-rich metasomatic fluid that would account for the high concentrations of TiO_2 in a significant sector of the concentrate spinels. It seems unlikely that it would only be the spinels that are selectively metasomatised.

An alternative explanation is that it may be possible for the TiO_2-rich spinels to be derived from a different zone in the mantle to the TiO_2-poor garnets and spinels and that the TiO_2-rich spinels do indeed represent metasomatised spinels. However, the trends defined by Ni and TiO_2 in Figure 8.11c and by Mg^{2+} and $[Fe^{2+}-(2*Ti^{4+})]$ (Figure 8.6) suggest that the TiO_2-rich spinels are magmatic in origin. The lack of distinctive TiO_2 zonation in these spinels argue against a metasomatic origin. Furthermore, the occurrence of highly magnesian (Fo 95) euhedral olivine inclusions in the TiO_2-rich concentrate spinels (Daniels and Gurney, 1991) suggests that these spinels are derived from a depleted ultramafic silicate assemblage. The high forsterite content of the olivine inclusions are also inconsistent with a metasomatic origin.

It has been shown in APPENDIX 8.b that the most likely behaviour of trivalent chromium in a silicate melt is one of an octahedrally coordinated network-modifier. Similarly, the structural role of Mg^{2+} is that of a network-modifier and in a highly magnesian melt, e.g. a komatiite, chromium would have to compete with the magnesium for the same limited number of octahedrally coordinated sites within the melt. Therefore, high concentrations of Mg^{2+} in a liquid would limit the solubility of chromium in the melt. A contributing limiting factor would be the smaller field strength of Mg^{2+} relative to Cr^{3+} which would favour the incorporation of Mg^{2+} into the melt structure. It would therefore seem that observed chromium concentrations in ultramafic melts are saturation levels and not depletion levels. This observation is consistent with the experimental results of Murck and Cambell (1986) in which the presence of spinels in komatiite-type liquids was ascribed to chromium saturation of the melts. The corollary of this is that chromium is increasingly favoured towards the residue relative to the MgO-rich melt with increasing degrees of partial melting.

The partitioning of chromium between olivine and liquid has been determined in several experimental studies (Ringwood, 1970; Green et al., 1975; Schreiber and Haskin, 1976). Although a wide range of values was recorded by these investigators, Huebner et al. (1978) suggested that a single value of D_{Cr} olivine/liquid $= 0.85 \pm 0.15$ is consistent with the majority of published experimental D_{Cr} values within statistical uncertainties.

Akella et al.(1976) suggested that the weak increase in D_{Cr} olivine/liquid with decreasing oxygen fugacity may have been due to a change in the Cr^{3+}/Cr^{2+} ratio of their experimental melt. In an extensive study of chromium behaviour in ultrabasic liquids, Murck and Cambell (1986) reported that the partitioning of chromium into olivine in equilibrium with komatiite melt decreases from $D_{Cr,FMQ}$ olivine/liquid $= 0.95$ at 1300°C to 0.53 at 1500°C at constant oxygen fugacity. Although the olivine/liquid partition ratio of chromium decreases with an increasing temperature, the absolute concentrations of chromium in the olivines increases with increasing temperature, indicating increasing

concentrations of chromium in the liquid. Barnes (1986) made similar observations regarding the partitioning of chromium between orthopyroxene and ultrabasic liquid. It was reported by Barnes (1986) that $D_{Cr,FMQ}$orthopyroxene/liquid = 10.4 at 1150°C and decreases to 2.67 at 1330°C. The absolute concentrations of chromium in both orthopyroxene and liquid increases with increasing temperature. D_{Cr} spinel/liquid trends are similar to those observed on orthopyroxene and olivine, but the partitioning of chromium is strongly biased towards the spinel. Experimentally obtained spinel/liquid partition coefficients for chromium vary from 50 to 700 (Schreiber and Haskin, 1976; Akella et al., 1976; Murck and Cambell, 1986; Barnes, 1986). Chromium is more strongly partitioned towards Mg-Al spinels than towards Fe-Ti spinels under the same conditions (Akella et al., 1976).

Discounting any liquid structure-composition effects on the solubility of chromium in ultrabasic melts, an average D_{Cr} residual spinel\melt = 150 can account for the high chromium contents of the Dokolwayo concentrate spinels as an early komatiite residual phase if the chromium contents of Barberton komatiite original melt compositions (Smith and Erlank, 1982) are considered. It hs been argued in Chapter 3 that the Barberton komatiites represent the most significant mantle melting event prior to the extrusion of the Dokolwayo kimberlite and that the Dokolwayo kimberlite probably sampled the residue of this melting event.

Normal melt - residue relationships between komatiitic melts and the resultant residues can account for the chromium compositions observed in the Dokolwayo concentrate spinels. However, known komatiite compositions and partition coefficients for spinel/liquid cannot account for the TiO_2 contents of the spinels without considering the behaviour of Ti^{4+} in silicate melts, which is discussed in APPENDIX 8b. Briefly, spectroscopic data have indicated that Ti^{4+} can be present in a silicate liquid as titanate complexes and exist in clusters where Ti-O-Ti bonds prevail (Mysen et al., 1980a,b, 1981b). These titanate complexes tend to unmix with the silicate melt as depolymerisation of the melt increases.

The increased depolymerisation of komatiite-type liquids with increasing temperature and MgO concentrations would produce strong deviations from ideality, resulting in the formation of titanate complexes. These titanate clusters are structurally similar to submicroscopic, octahedrally coordinated spinelloid aggregates observed in silicate melts (O'Reilly and MacIver, 1962; Fournier et al., 1971; Mysen et al., 1980a,b, 1981b). The unmixing of these titanate clusters may increasingly favour the partitioning of titanium into the residue. In the absence of a TiO_2-rich phase in the residue, it is suggested that these unmixed titanate clusters will preferentially complex with the residual spinel rather than with the orthopyroxene or olivine in the residue. The titaniferous spinels produced under these conditions may be expected to deviate from ideality and be non-stoichiometric.

The Dokolwayo spinel concentrate population characterised by TiO_2-rich compositions and major inverse spinel components are consistent with the model for the formation of residual TiO_2-rich spinels presented above. It is of interest to note that Hatton (1978) reported a harzburgite from the Roberts Victor kimberlite that contains spinels with the same compositional characteristics as the Dokolwayo TiO_2-rich concentrate population (i.e. $TiO_2/Al_2O_3 > 0.2$; $TiO_2 > 0.7$ wt%; $Cr_2O_3 > 60$ wt%) and which shows no evidence of any metasomatism by a TiO_2-rich fluid. It should be noted that this model does not exclude the possibility that these TiO_2-rich spinels were subjected to the same TiO_2-poor and REE-enriched metasomatic event that affected G10 garnets (Richardson et al., 1984). However, due to the refractory nature of the spinels it is unlikely that they will bear any witness to this latter metasomatic event.

'What do you think of my theory?'
'It is all surmise.'
'But at least it covers the facts. When new facts come to our knowledge which cannot be covered by it, it will be time enough to reconsider it.'

Sir Arthur Conan Doyle in 'The Musgrave Ritual' (1892)

Dedicated to John J. Gurney

TABLE 8.1

SUMMARY STATISTICS OF THE DOKOLWAYO CONCENTRATE SPINELS

OXIDE	TiO_2	Al_2O_3	Cr_2O_3	Fe_2O_3	FeO	MnO	MgO
N	288	288	288	288	288	288	288
AVERAGE	1.22	5.04	63.8	2.79	13.9	0.25	12.8
MEDIAN	1.09	3.94	63.8	2.96	13.4	0.25	13.0
STD.DEV.	1.00	3.29	4.61	1.94	2.22	0.05	1.46
STD ERR.	0.06	0.19	0.27	0.11	0.13	<.01	0.09
MINIMUM	N.D.	0.70	39.4	N.C.	6.70	N.D.	8.50
MAXIMUM	3.89	29.4	73.9	9.64	20.8	0.38	19.4
SKEWNESS	0.41	2.92	-1.02	0.40	0.64	-0.63	0.06

TABLE 8.1 Summary statistics of the Dokolwayo concentrate spinel compositions.

TABLE 8.2

	SAMPLE NUMBER					
	CHR-35	CHR-35*	CHR-54	CHR-54*	CHR-76	CHR-76*
OXIDE	(Weight Percent)					
TiO_2	1.06	1.06	0.13	0.13	N.D.	N.D.
Al_2O_3	3.46	3.46	2.64	2.64	1.01	1.01
Cr_2O_3	68.19	67.72	71.47	69.89	73.87	72.58
FeO	14.05	14.05	13.07	13.07	12.69	12.69
MnO	0.24	0.24	0.24	0.24	0.27	0.27
MgO	12.03	12.03	11.28	11.28	11.58	11.58
NiO	0.14	0.14	N.D.	N.D.	N.D.	N.D.
CrO	-	0.46	-	1.62	-	1.34
TOTAL	**99.17**	**99.16**	**98.83**	**98.87**	**99.42**	**99.47**

* Recalculated analyses.

N.D. Not Detected

TABLE 8.2 Representative Dokolwayo concentrate spinels with Cr_2O_3 in excess of the stoichiometric limit and calculated to contain divalent CrO.

TABLE 8.3	
STANDARD REDUCTION POTENTIALS	
REACTION	**POTENTIAL volts**
$Ag^{+} + e^{-} <-> Ag$	0.7996
$Cr^{2+} + 2e^{-} <-> Cr$	-0.557
$Cr^{3+} + e^{-} <-> Cr^{2+}$	-0.41
$Fe^{2+} + 2e^{-} <-> Fe$	-0.409
$Fe^{3+} + e^{-} <-> Fe^{2+}$	0.770
$Mg^{2+} + 2e^{-} <-> Mg$	-2.375
$Mn^{2+} + 2e^{-} <-> Mn$	-1.029
$Ni^{2+} + 2e^{-} <-> Ni$	-0.23
$Zn^{2+} + 2e^{-} <-> Zn$	-0.7628

TABLE 8.3 Standard reduction potentials for selected reactions.

TABLE 8.4

SAMPLE NUMBER	OXIDE	EDGE 1 wt%	CENTRE wt%	EDGE 2 wt%
SP-3	Cr_2O_3	63.1	61.5	63.4
TiO_2	Al_2O_3	6.44	7.67	6.74
POOR	TiO_2	0.39	0.45	0.47
SP-8	Cr_2O_3	65.8	62.7	67.6
TiO_2	Al_2O_3	4.60	6.42	3.97
POOR	TiO_2	0.33	0.26	0.27
SP-5	Cr_2O_3	57.5	57.3	57.2
TiO_2	Al_2O_3	3.65	3.60	3.65
RICH	TiO_2	2.49	2.47	2.49
SP-15	Cr_2O_3	54.1	54.6	54.2
TiO_2	Al_2O_3	6.13	6.21	6.35
RICH	TiO_2	2.26	2.29	2.33

TABLE 8.4 Table of selected TiO_2-poor and TiO_2-rich concentrate spinels from Dokolwayo to illustrate the zonation characteristics of the spinels.

CHAPTER 8 - FIGURE CAPTIONS

FIGURE 8.1

Plot of Cr^{3+} vs Al^{3+} cations/4 oxygens for the Dokolwayo concentrate spinels.

FIGURE 8.2

Plot of Cr^{3+} vs $[(2*Ti^{4+})+Fe^{3+}+Al^{3+}]$ cations/4 oxygens for the Dokolwayo concentrate spinels.

FIGURE 8.3

Plot of Cr^{3+} vs $Ti4+$ cations/4 oxygens for the Dokolwayo concentrate spinels.

FIGURE 8.4

Histogram of the TiO_2 (wt%) contents of (a) the concentrate spinels from Dokolwayo and (b) the diamond inclusion spinels from southern Africa.

FIGURE 8.5

Plot of Al_2O_3 versus TiO_2 (wt%) for the spinels from the Dokolwayo heavy mineral concentrate.

FIGURE 8.6

Plot of Mg^{2+} vs $[Fe^{2+}-(2*Ti^{4+})]$ cations/4 oxygens for the concentrate spinels from Dokolwayo.

FIGURE 8.7

Plot illustrating variations in concentration of TiO_2, Cr_2O_3, Al_2O_3, FeO and MgO (wt%) across a 9mm diameter concentrate spinel from Dokolwayo. The spinel was characterised by $TiO_2/Al_2O_3 > 0.2$. Analyses were done along ten equidistant points across the spinel.

FIGURE 8.8

Plot of (a) Zn versus Ga; (b) Ni versus Ga; and (c) Ni versus Zn ppm concentrations in Dokolwayo euhedral, subhedral and anhedral concentrate spinels and Dokolwayo diamond inclusion spinels.

FIGURE 8.9

Plot of (a) Al_2O_3 (wt%) versus Zn (ppm) ; (b) Al_2O_3 (wt%) versus Ni (ppm) for Dokolwayo euhedral, subhedral and anhedral concentrate spinels and Dokolwayo diamond inclusion spinels.

FIGURE 8.10

Plot of Cr_2O_3 (wt%) versus Ni (ppm) for Dokolwayo euhedral, subhedral and anhedral concentrate spinels and Dokolwayo diamond inclusion spinels.

FIGURE 8.11

Plot of (a) TiO_2 (wt%) versus Zn (ppm); (b) TiO_2 (wt%) versus Ga (ppm); and (c) TiO_2 (wt%) versus Zn (ppm) concentrations in Dokolwayo euhedral, subhedral and anhedral concentrate spinels and Dokolwayo diamond inclusion spinels.

DOKOLWAYO - SWAZILAND
CONCENTRATE SPINELS

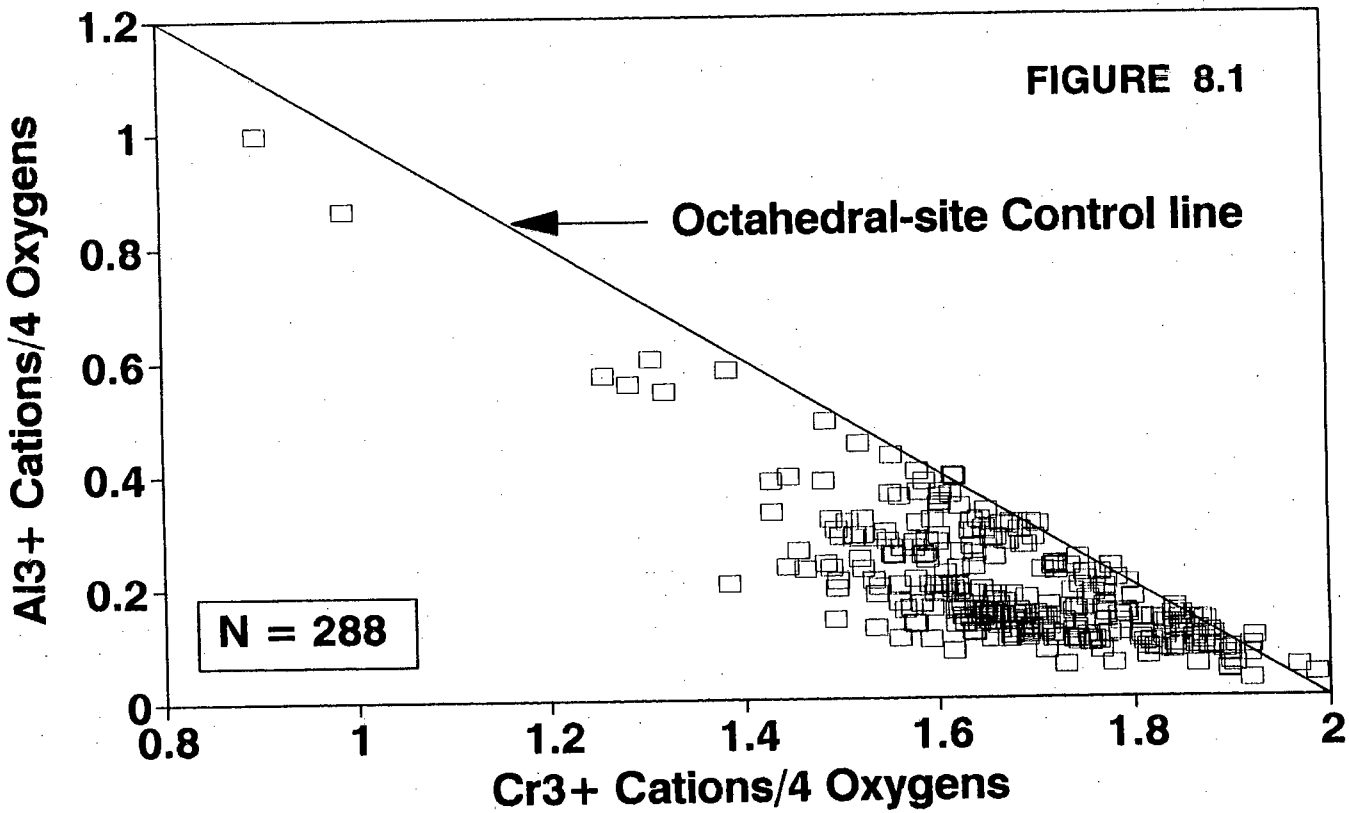

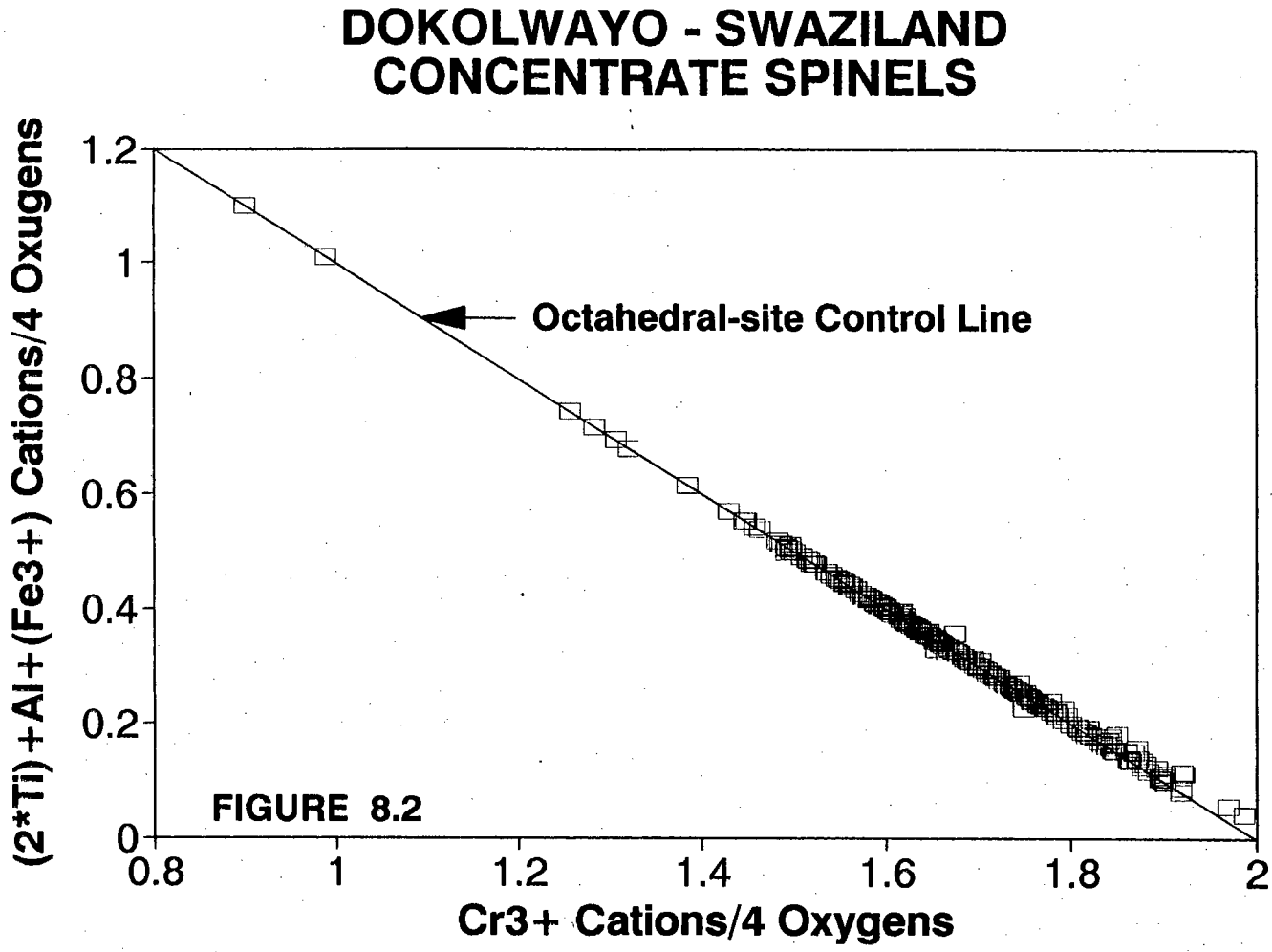
DOKOLWAYO - SWAZILAND
CONCENTRATE SPINELS
(2*Ti)+Al+(Fe3+) Cations/4 Oxugens
1.2
1
0.8
0.6
0.4
0.2
0
Octahedral-site Control Line
FIGURE 8.2
0.8
1
1.2
1.4
1.6
1.8
2
Cr3+ Cations/4 Oxygens

DOKOLWAYO - SWAZILAND
CONCENTRATE SPINELS

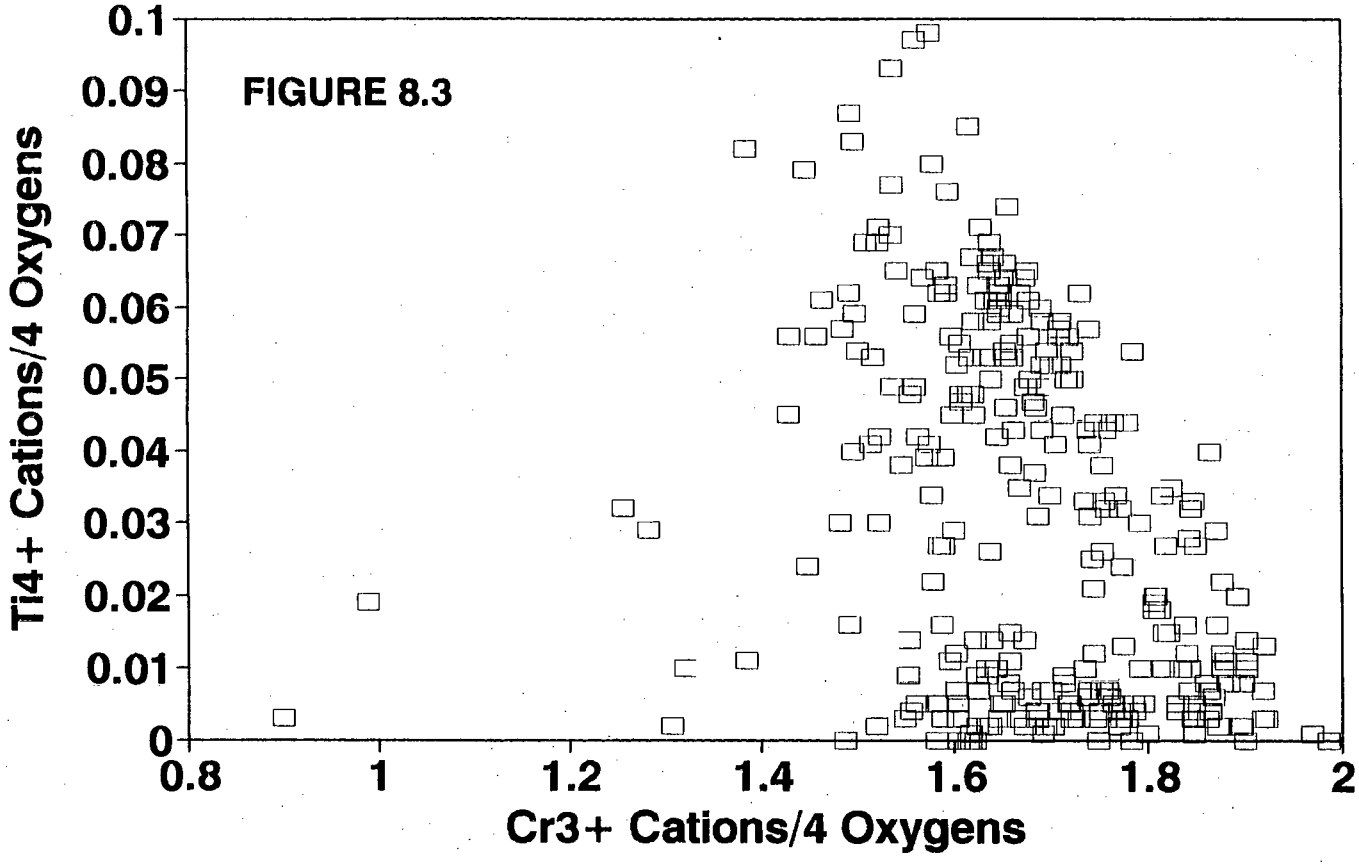

FIGURE 8.4a

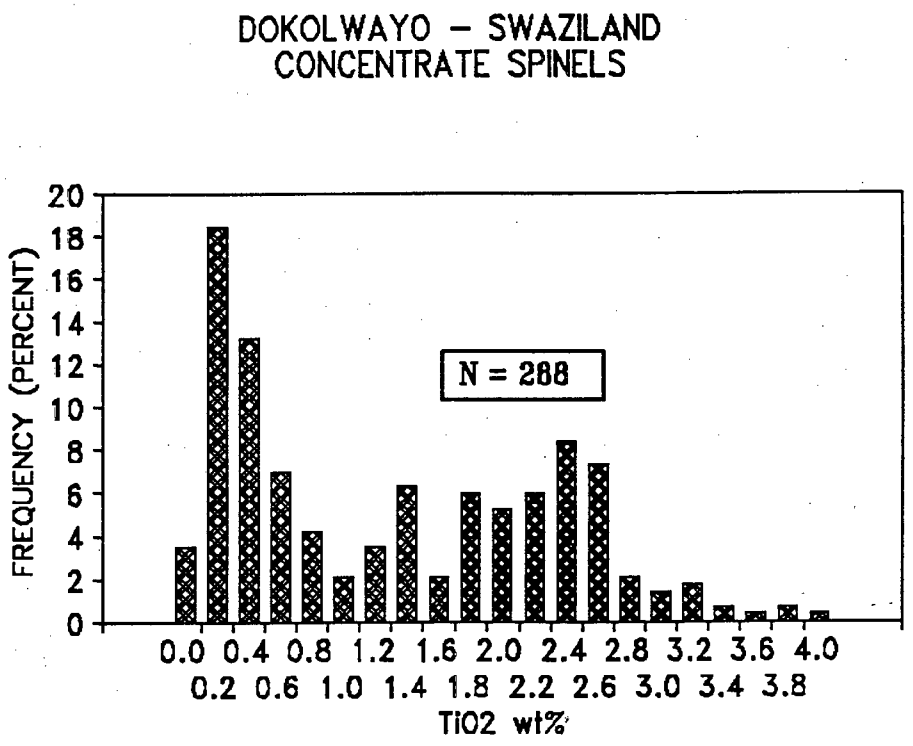

FIGURE 8.4b

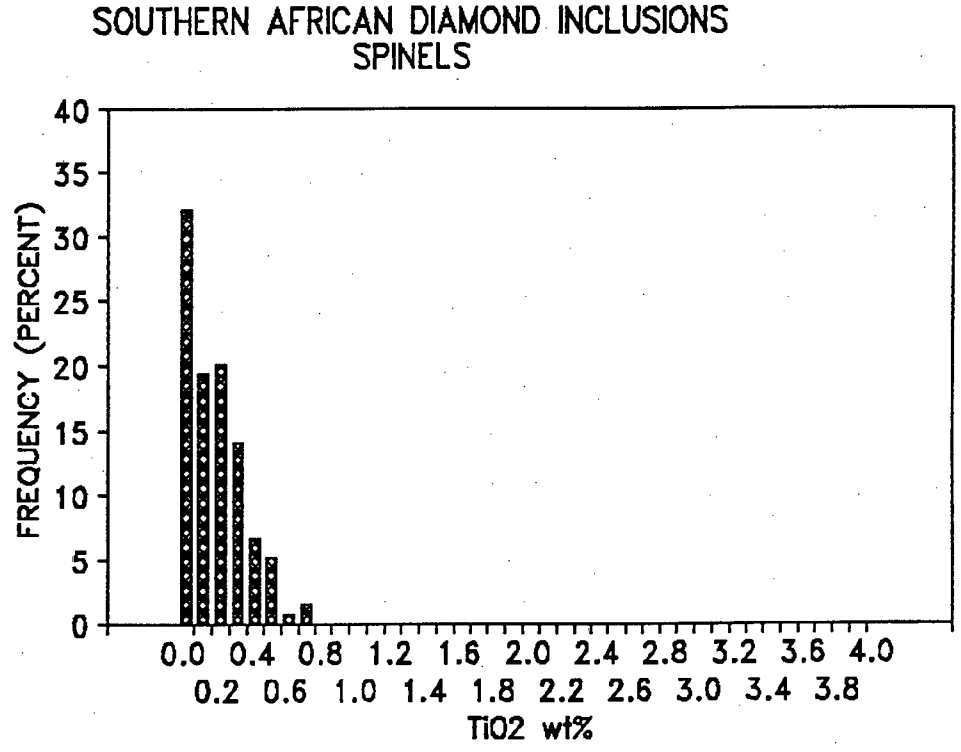

DOKOLWAYO - SWAZILAND
CONCENTRATE SPINELS

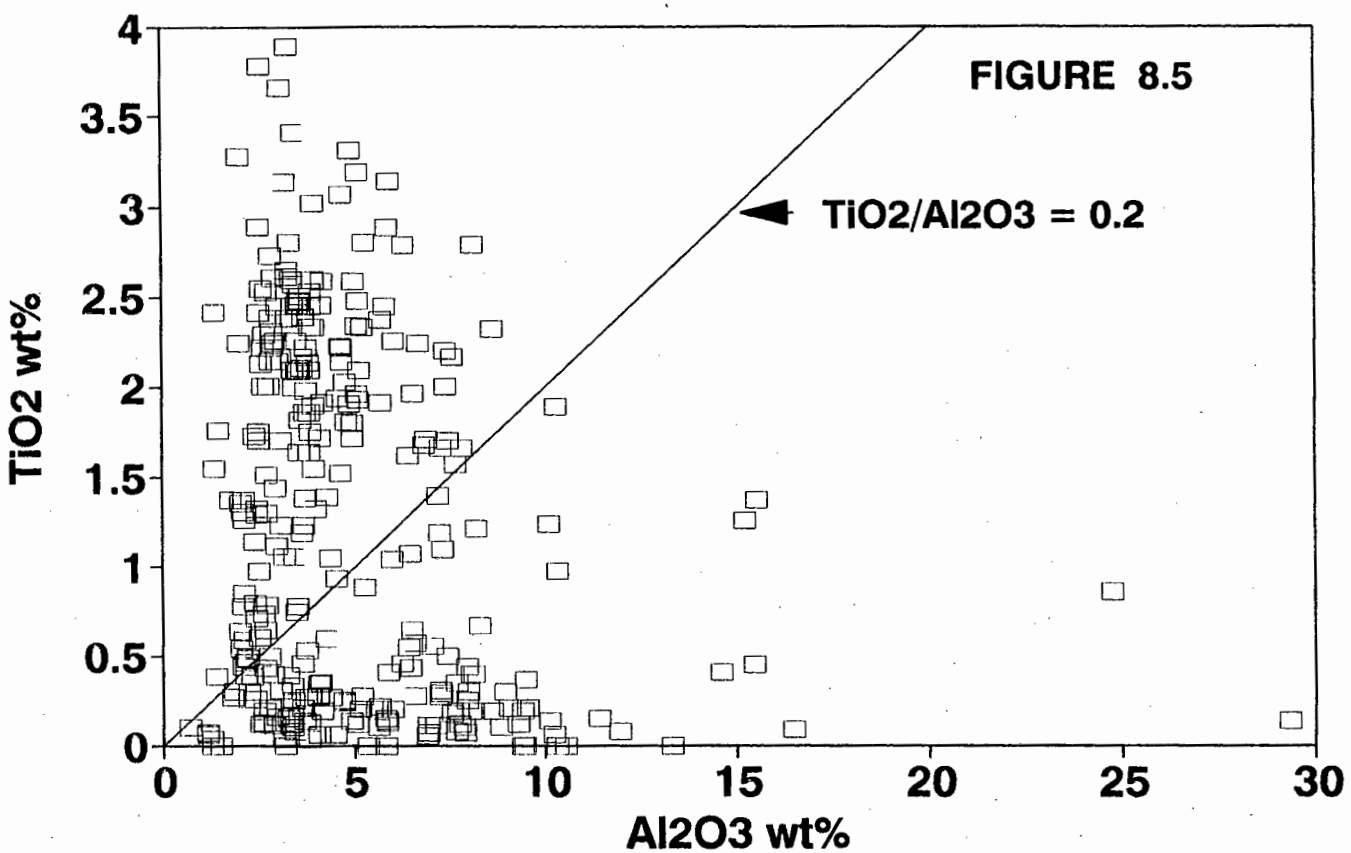

DOKOLWAYO - SWAZILAND
CONCENTRATE SPINELS

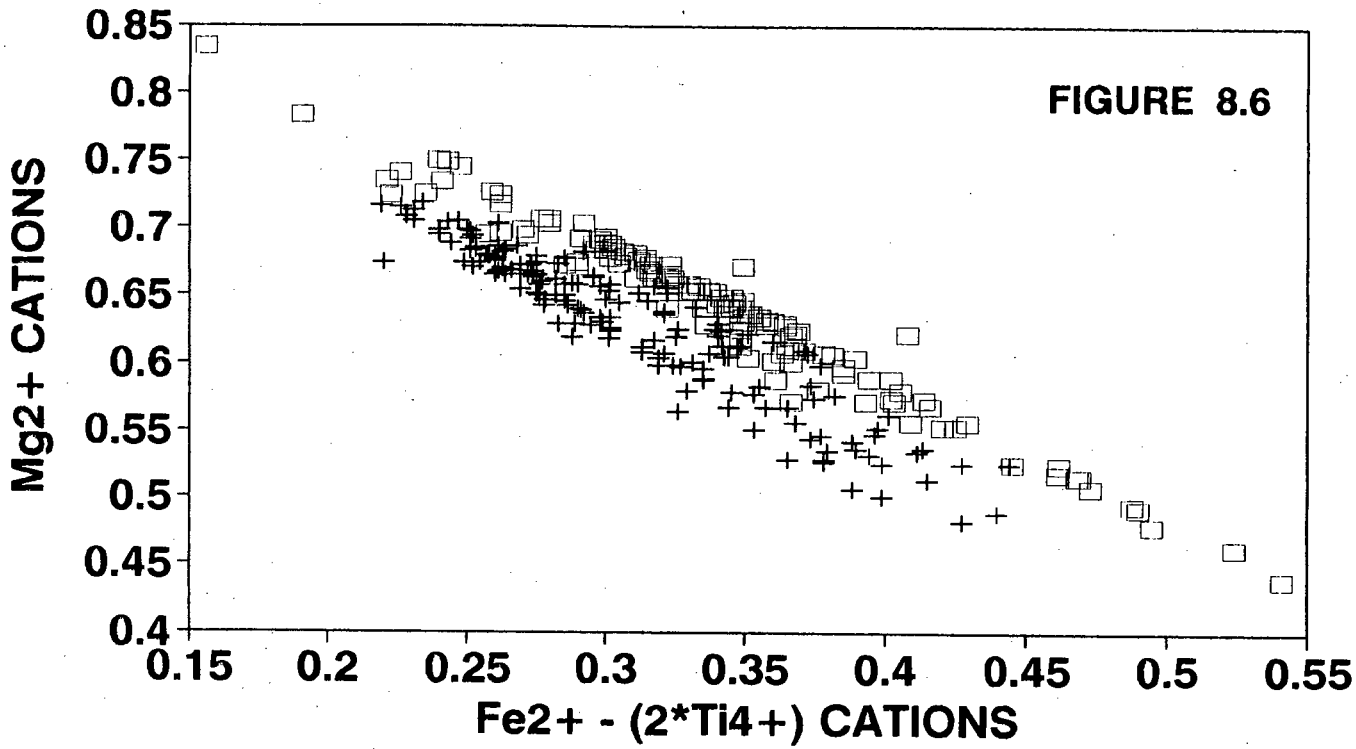

□ TiO2/Al2O3 < 0.2 + TiO2/Al2O3 > 0.2

FIGURE 8.7

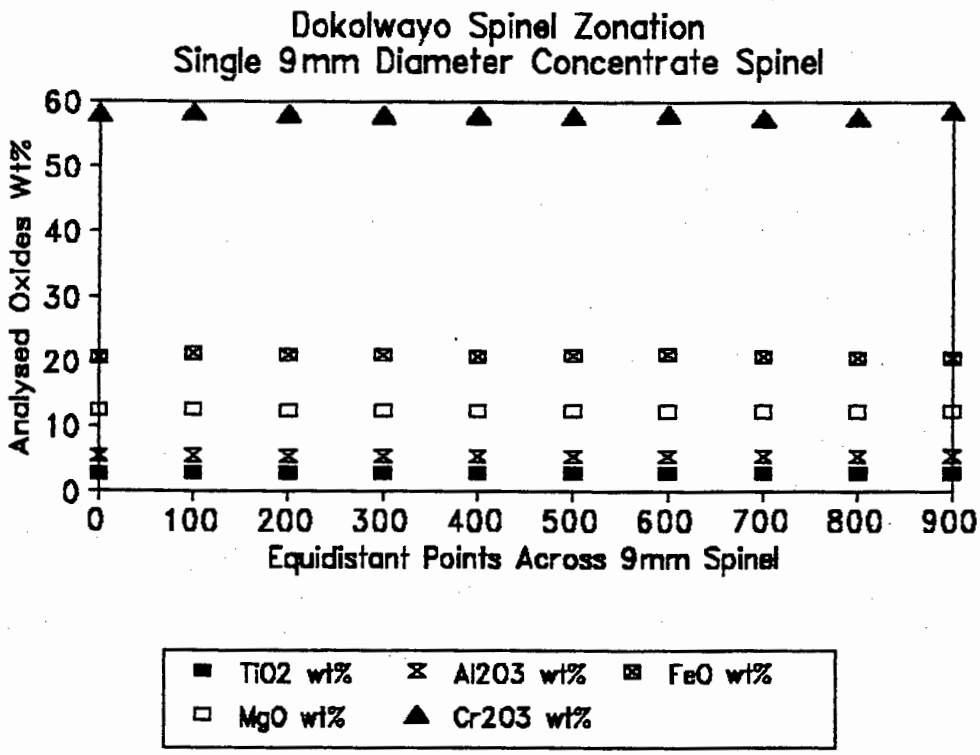

FIGURE 8.8a

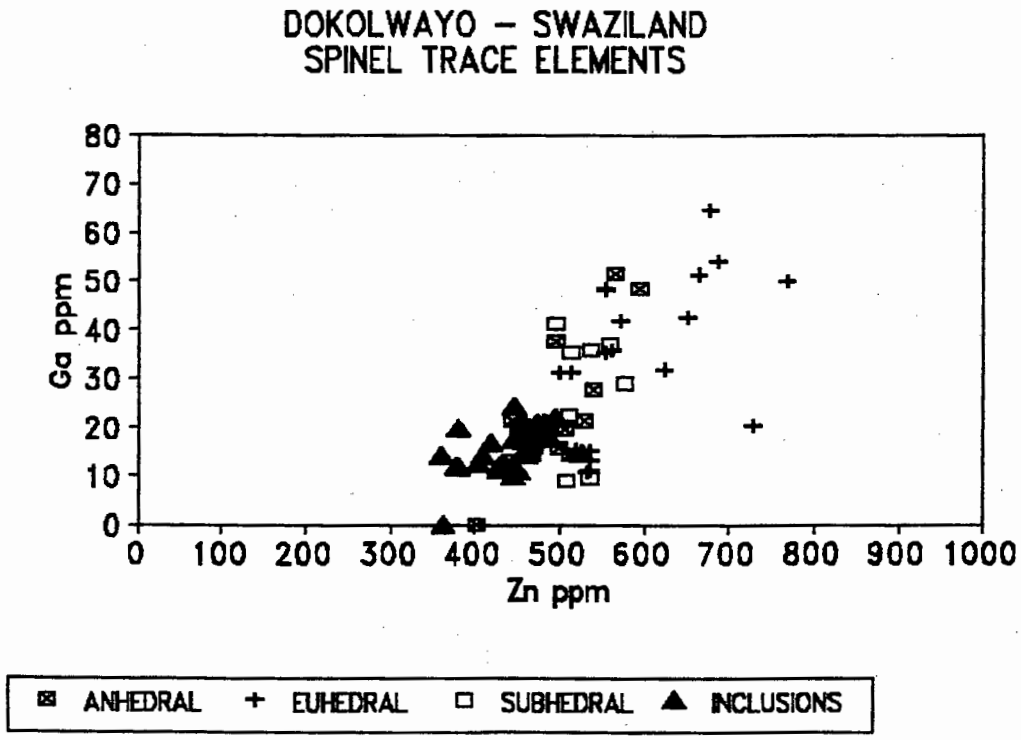

FIGURE 8.8b

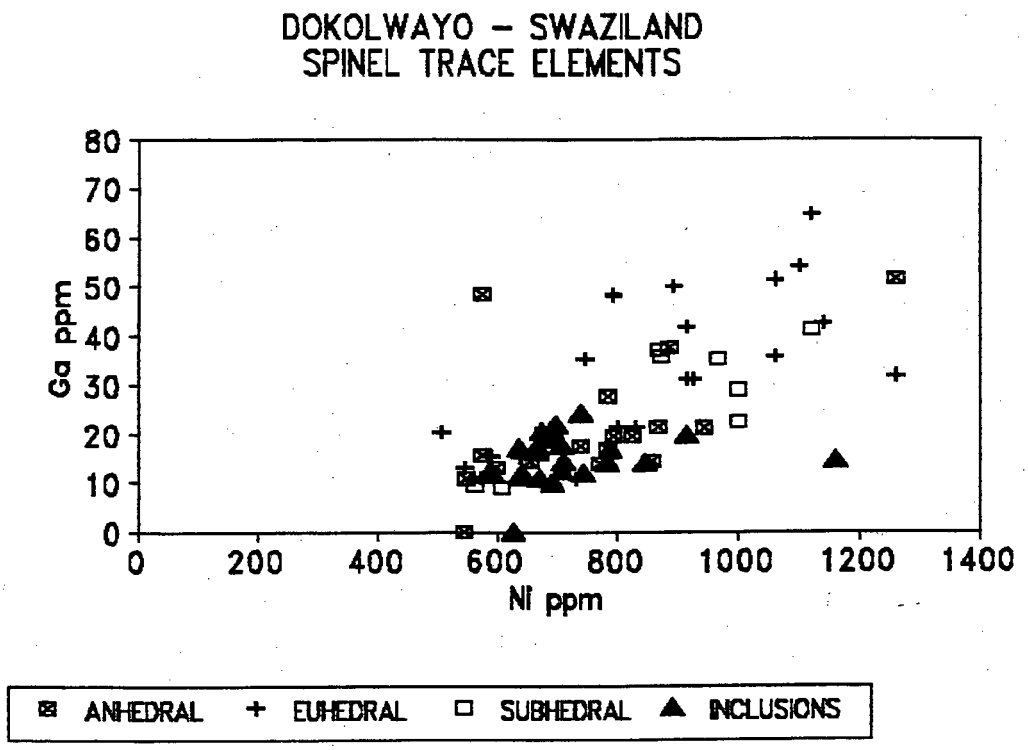

FIGURE 8.8c

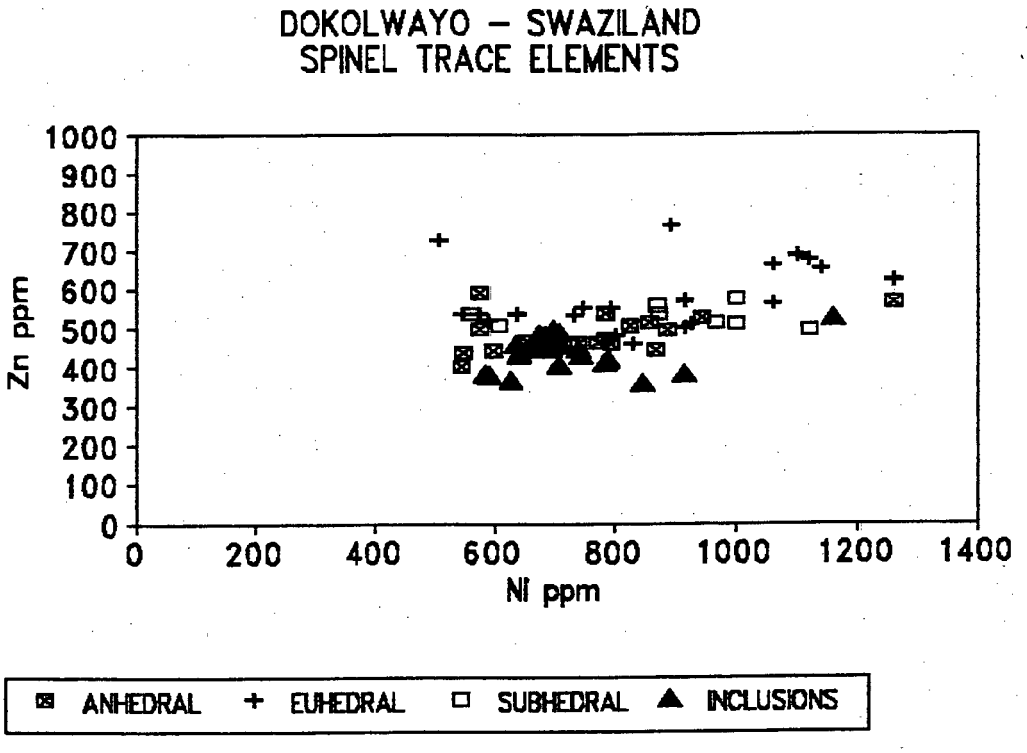

FIGURE 8.9a

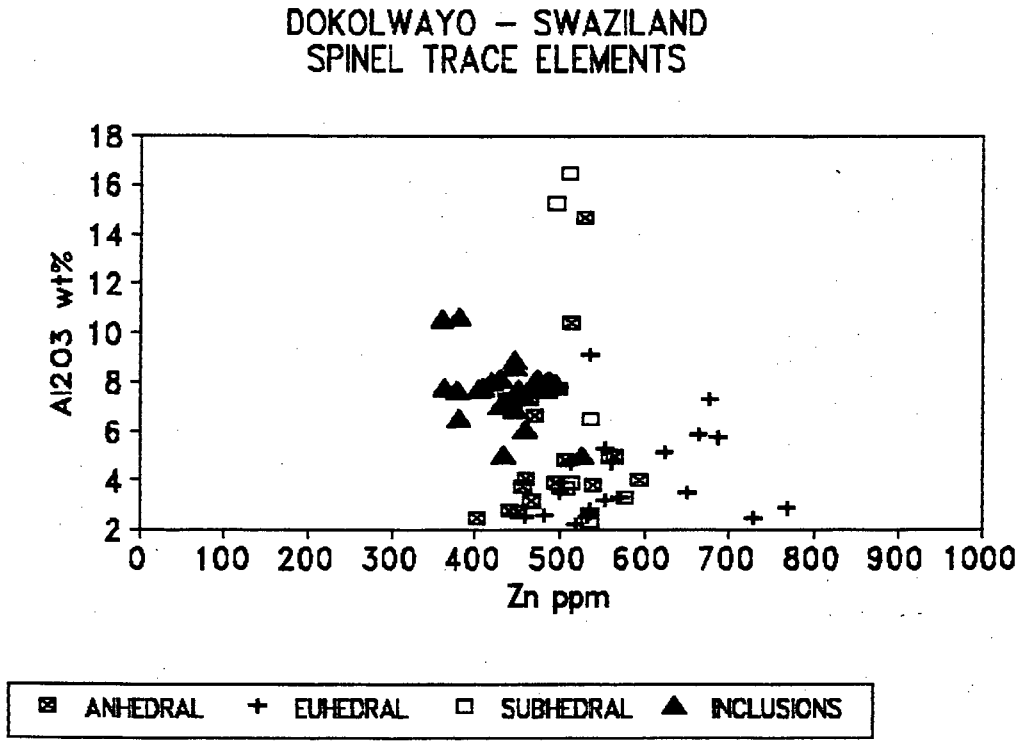

FIGURE 8.9b

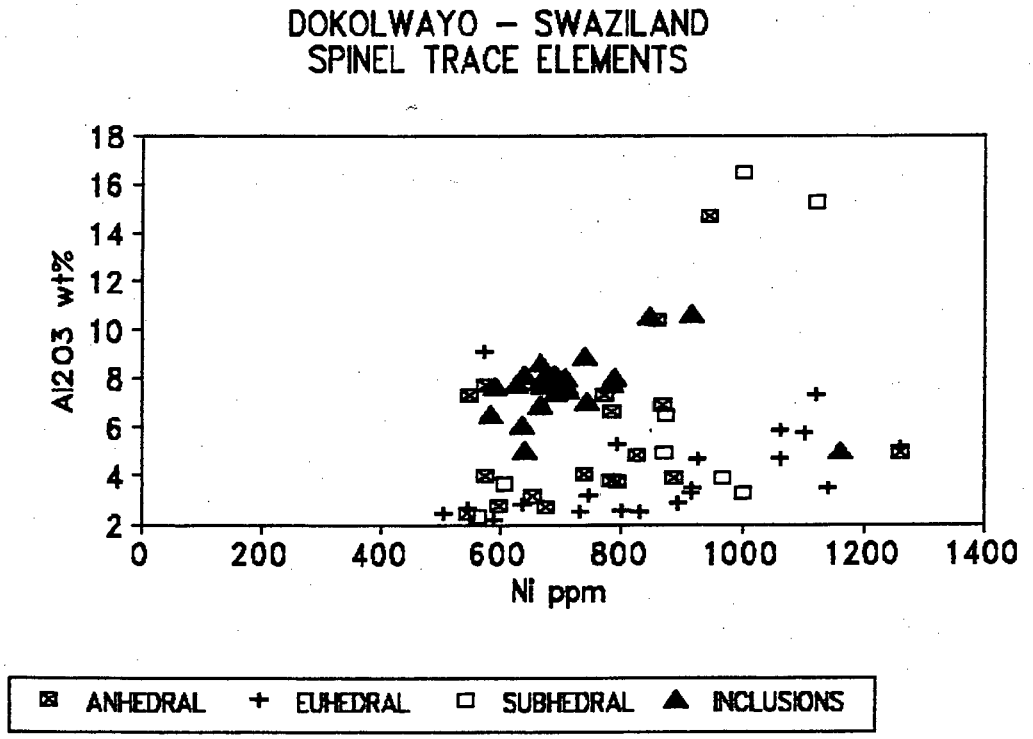

FIGURE 8.10

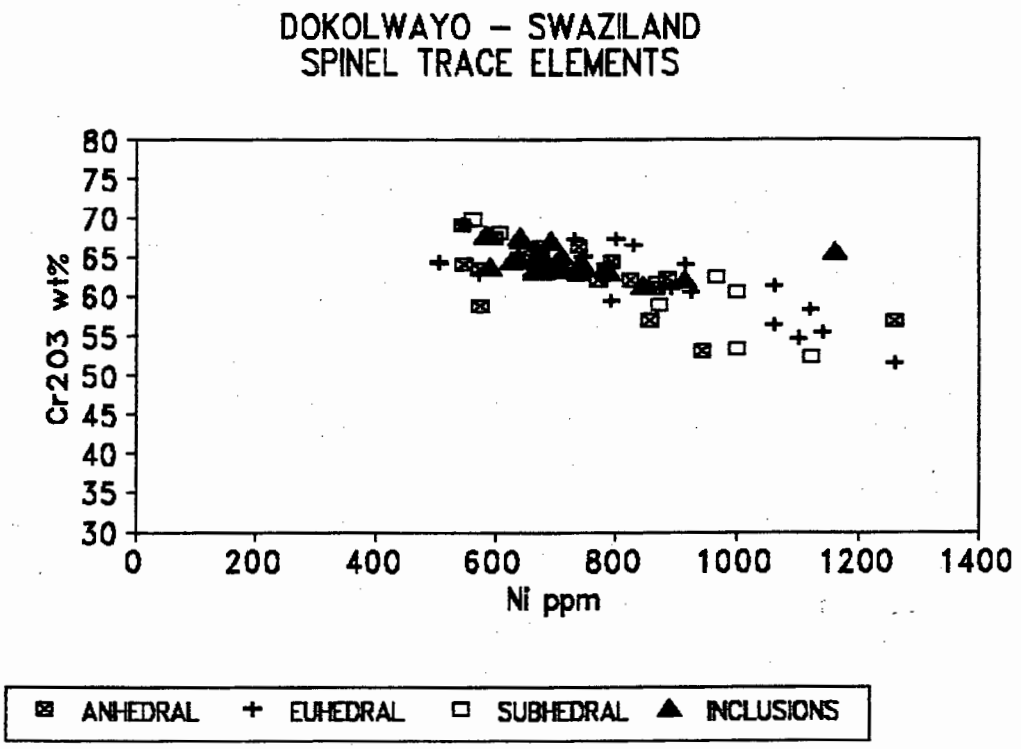

FIGURE 8.11a

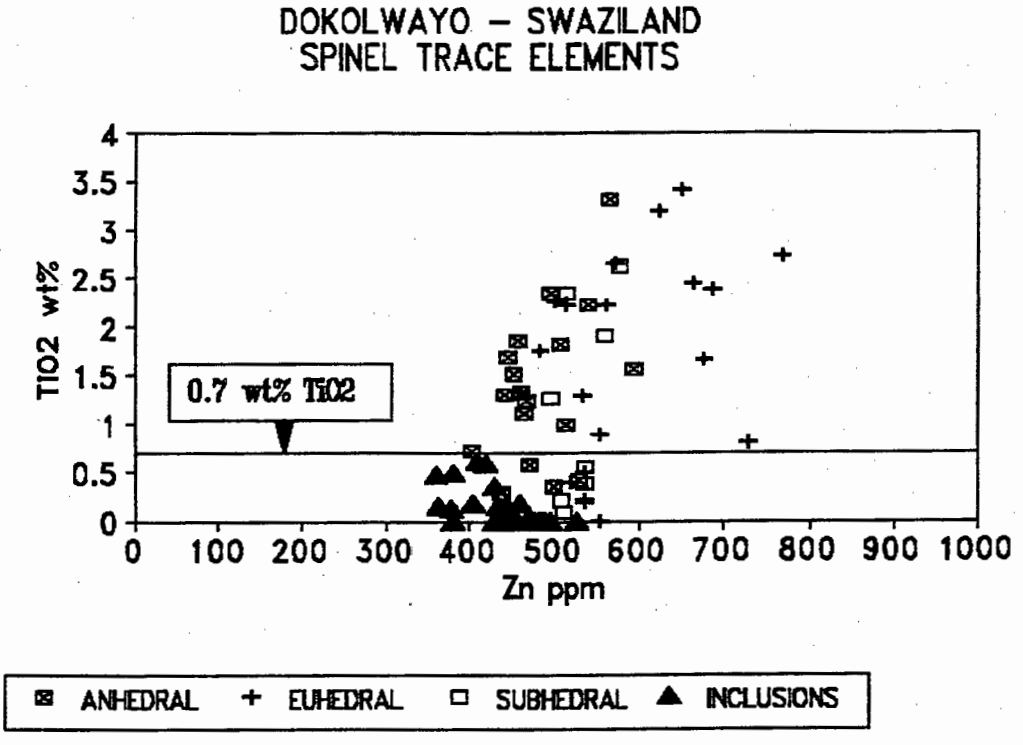

FIGURE 8.11b

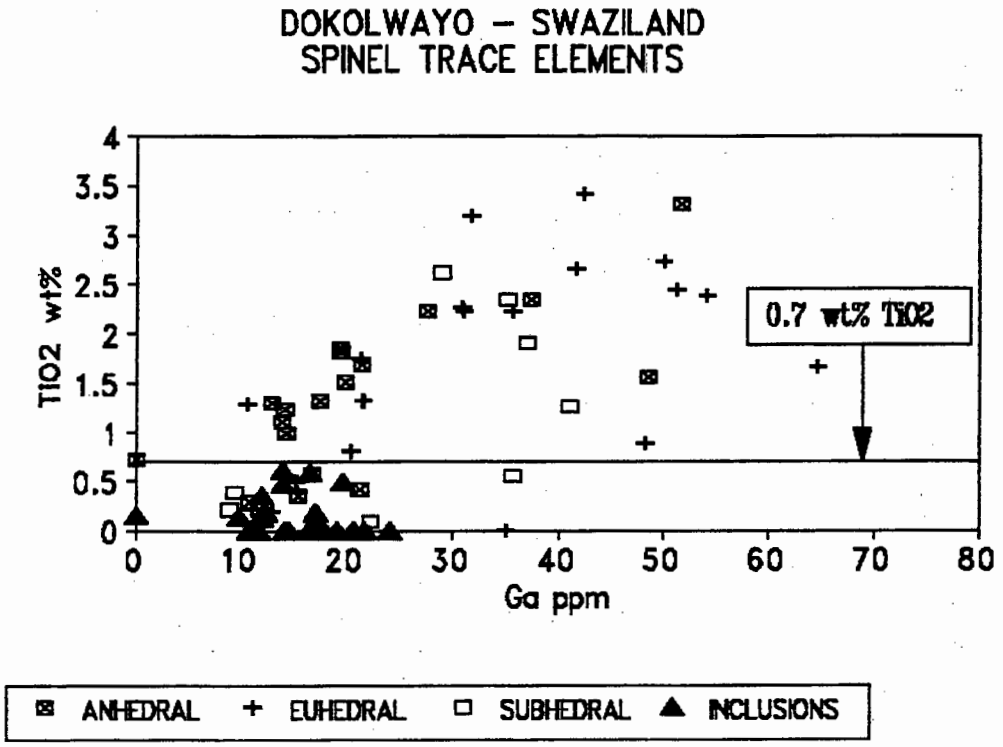

FIGURE 8.11c

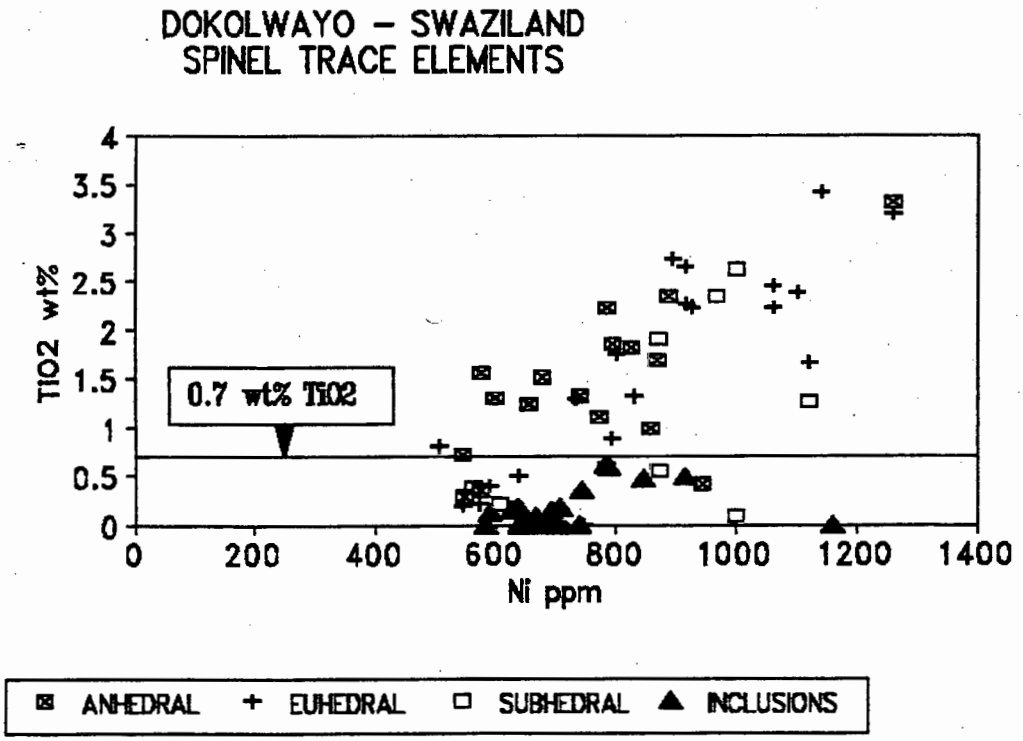

APPENDIX 8.a (1) - DOKOLWAYO CONCENTRATE SPINELS

	OXIDES (wt%)				Fe2O3 CALCULATED STOICHIOMETRICALLY					
SAMPLE NUMBER	SIO2	TIO2	AL2O3	CR2O3	FE2O3	FEO	MNO	MGO	NIO	TOTAL
CHR-9	N.D.	0.00	13.34	60.26	0.96	9.51	0.15	16.04	0.11	100.37
CHR-139	N.D.	0.00	5.84	61.66	5.98	10.86	0.23	13.89	0.13	98.59
CHR-47	N.D.	0.00	10.57	62.07	0.71	12.00	0.18	14.00	0.00	99.53
DCO-34	N.D.	0.00	9.48	62.10	1.19	12.63	0.21	13.32	0.07	99.00
CHR-141	N.D.	0.00	9.45	63.34	1.14	10.83	0.18	14.66	0.00	99.60
CHR-80	N.D.	0.00	10.33	63.67	0.00	11.36	0.25	14.09	0.00	99.70
CEU-03	N.D.	0.00	3.19	65.10	3.82	14.38	0.26	12.30	0.00	99.05
CHR-44	N.D.	0.00	5.38	67.81	0.26	13.99	0.25	12.20	0.00	99.89
CHR-104	N.D.	0.00	1.54	71.57	1.50	12.42	0.18	12.91	0.00	100.12
CHR-76	N.D.	0.00	1.28	72.88	0.00	12.40	0.00	12.40	0.27	99.23
CSH-12	N.D.	0.04	3.82	67.56	2.20	13.11	0.31	12.51	0.00	99.55
CSH-10	N.D.	0.04	3.16	70.16	1.00	13.12	0.23	12.67	0.00	100.38
CHR-117	N.D.	0.04	1.30	73.51	0.00	12.47	0.25	11.96	0.00	99.53
CHR-93	N.D.	0.05	6.90	64.58	1.53	13.40	0.22	12.65	0.00	99.33
FEC-15	N.D.	0.06	10.27	63.06	0.00	11.56	0.22	13.73	0.00	98.90
CSH-09	N.D.	0.06	4.08	67.33	2.66	12.34	0.19	13.18	0.00	99.84
CHR-115	N.D.	0.06	4.53	68.78	0.84	10.92	0.18	14.08	0.00	99.39
CHR-150	N.D.	0.06	1.19	71.59	2.11	12.43	0.32	12.82	0.15	100.67
CHR-130	N.D.	0.07	6.96	63.38	3.85	11.83	0.18	13.80	0.13	100.20
CHR-20	N.D.	0.07	7.93	64.76	0.78	11.79	0.22	13.84	0.00	99.39
FEC-24	N.D.	0.07	7.93	64.91	0.00	13.48	0.20	12.47	0.00	99.06
DCO-61	N.D.	0.07	1.17	71.47	2.25	11.37	0.24	13.37	0.00	99.94
CHR-34	N.D.	0.08	11.99	60.12	1.06	11.89	0.20	14.25	0.00	99.59
CHR-148	N.D.	0.08	7.69	63.82	2.65	11.21	0.18	14.26	0.14	100.03
CHR-110	N.D.	0.08	3.45	71.25	0.00	11.54	0.00	13.38	0.00	99.70
CSH-20	N.D.	0.09	16.49	53.34	3.78	9.53	0.23	16.24	0.00	99.70
FEC-09	N.D.	0.10	8.84	62.99	1.34	12.69	0.23	13.34	0.11	99.64
CHR-125	N.D.	0.10	5.65	64.94	2.03	15.06	0.30	11.40	0.11	99.59
CHR-12	N.D.	0.10	7.90	65.59	0.00	13.37	0.23	12.42	0.11	99.72
CHR-1	N.D.	0.10	3.41	69.13	0.51	14.45	0.21	11.69	0.00	99.50
FEC-22	N.D.	0.10	0.70	69.51	1.76	18.14	0.32	8.90	0.00	99.43
CHR-124	N.D.	0.11	7.16	59.35	6.73	15.21	0.22	11.65	0.15	100.58
CHR-66	N.D.	0.11	6.96	64.65	1.54	12.31	0.20	13.38	0.00	99.15
FEC-25	N.D.	0.11	2.94	70.04	1.22	12.62	0.19	12.97	0.00	100.09
FEC-29	N.D.	0.12	9.31	62.45	1.43	12.62	0.24	13.51	0.00	99.68
CHR-112	N.D.	0.12	3.37	64.48	5.13	16.76	0.32	10.21	0.12	100.51
DCO-70	N.D.	0.12	7.77	65.04	2.55	10.00	0.20	15.06	0.00	100.74
CHR-144	N.D.	0.12	5.10	67.27	2.08	11.75	0.19	13.75	0.11	100.37
CHR-152	N.D.	0.12	2.58	69.87	1.13	13.28	0.23	12.38	0.00	99.59
CHR-73	N.D.	0.13	5.89	67.34	0.00	13.33	0.20	12.09	0.00	98.98
CHR-128	N.D.	0.13	3.81	67.82	2.89	11.94	0.24	13.46	0.13	100.42
CHR-54	N.D.	0.13	2.64	71.47	0.00	13.07	0.24	11.28	0.00	98.83
FEC-39	N.D.	0.14	29.35	39.44	4.40	6.70	0.10	19.40	0.20	99.73
CHR-105	N.D.	0.14	10.12	62.52	0.96	11.93	0.20	14.11	0.11	100.09
CHR-31	N.D.	0.14	5.87	64.72	1.59	14.69	0.25	11.59	0.11	98.96
CHR-114	N.D.	0.14	4.95	66.94	1.14	13.11	0.17	12.69	0.00	99.14
CHR-103	N.D.	0.14	3.70	70.10	0.00	13.19	0.17	12.70	0.00	100.00
CHR-17	N.D.	0.15	11.46	61.73	0.34	10.15	0.19	15.28	0.12	99.42
CHR-122	N.D.	0.15	5.85	65.78	2.37	11.65	0.19	13.81	0.12	99.92
CHR-131	N.D.	0.15	3.27	68.97	1.25	12.42	0.24	12.95	0.00	99.25
CHR-101	N.D.	0.16	3.00	69.94	0.28	13.18	0.19	12.47	0.00	99.22
CHR-135	N.D.	0.17	3.40	67.97	2.87	11.89	0.22	13.41	0.13	100.06
CHR-14	N.D.	0.18	7.59	64.34	0.42	13.96	0.25	12.31	0.14	99.19
CHR-153	N.D.	0.19	9.44	61.60	2.98	10.81	0.16	14.80	0.13	100.11
CHR-136	N.D.	0.19	8.12	61.68	4.08	11.45	0.20	14.17	0.17	100.06
CHR-90	N.D.	0.19	7.73	63.39	1.75	13.16	0.25	12.98	0.00	99.45
CHR-38	N.D.	0.19	8.61	64.27	0.44	11.69	0.20	14.03	0.11	99.54
CHR-113	N.D.	0.19	4.18	67.98	2.18	12.02	0.25	13.54	0.00	100.34
CEU-20	N.D.	0.19	2.66	69.36	2.17	12.18	0.23	13.22	0.00	100.01
FEC-34	N.D.	0.20	6.01	65.58	1.45	12.90	0.25	12.96	0.00	99.35

Sample Number	SiO_2	TiO_2	Al_2O_3	Cr_2O_3	Fe_2O_3	FeO	MnO	MgO	NiO	Total
CHR-126	N.D.	0.20	5.61	66.40	0.98	13.38	0.18	12.30	0.14	99.19
CHR-106	N.D.	0.20	6.04	66.56	1.65	11.49	0.20	14.10	0.00	100.24
CHR-92	N.D.	0.20	5.18	68.09	0.00	12.36	0.27	12.88	0.00	98.98
CHR-95	N.D.	0.21	9.54	61.65	1.76	12.26	0.22	13.78	0.00	99.42
CEU-04	N.D.	0.21	9.10	62.93	1.66	9.29	0.20	15.61	0.00	99.00
CSH-19	N.D.	0.21	3.67	68.13	2.47	12.52	0.18	13.25	0.00	100.43
FEC-58	N.D.	0.21	2.81	69.79	1.24	12.81	0.23	12.83	0.00	99.92
CHR-94	N.D.	0.22	5.66	67.37	0.12	13.17	0.23	12.84	0.00	99.61
FEC-40	N.D.	0.24	4.76	65.91	2.51	14.09	0.24	12.20	0.00	99.95
CHR-26	N.D.	0.25	7.95	64.56	0.15	13.21	0.19	12.99	0.10	99.40
DCO-37	N.D.	0.25	4.74	68.06	1.84	9.92	0.20	14.92	0.11	100.04
FEC-04	N.D.	0.25	3.44	69.67	0.00	13.68	0.27	11.51	0.13	98.95
CHR-60	N.D.	0.26	2.44	64.17	4.92	19.14	0.34	8.50	0.12	99.89
FEC-51	N.D.	0.26	2.25	69.47	1.30	13.13	0.21	12.42	0.00	99.04
CHR-96	N.D.	0.27	4.38	62.95	4.70	17.75	0.35	9.73	0.00	100.13
CHR-138	N.D.	0.27	3.84	66.37	3.91	12.46	0.16	13.24	0.12	100.37
CHR-65	N.D.	0.27	3.75	68.59	0.00	14.66	0.22	11.33	0.00	98.82
CHR-70	N.D.	0.27	1.86	70.79	0.00	14.54	0.22	11.19	0.00	98.87
FEC-28	N.D.	0.28	6.60	62.11	4.17	16.01	0.29	11.27	0.00	100.73
FEC-03	N.D.	0.28	7.28	65.29	0.21	13.82	0.19	12.67	0.00	99.74
CHR-45	N.D.	0.28	5.22	65.61	1.05	16.88	0.24	10.41	0.00	99.69
FEC-18	N.D.	0.28	4.04	69.02	0.00	12.50	0.17	12.59	0.00	98.60
CAN-12	N.D.	0.29	7.32	64.10	1.77	11.40	0.16	14.16	0.00	99.20
CHR-147	N.D.	0.30	8.96	62.65	1.77	11.86	0.17	14.16	0.00	99.87
CHR-13	N.D.	0.30	7.99	64.92	0.58	11.70	0.21	14.09	0.11	99.90
CHR-16	N.D.	0.30	2.26	70.50	0.44	14.20	0.32	11.86	0.00	99.88
FEC-27	N.D.	0.30	1.88	70.82	0.44	12.74	0.15	12.71	0.00	99.04
CHR-85	N.D.	0.31	7.27	63.76	1.91	12.97	0.26	13.16	0.00	99.64
CHR-134	N.D.	0.31	3.08	63.85	5.81	17.23	0.27	10.05	0.13	100.73
CHR-61	N.D.	0.33	3.39	69.14	0.00	14.96	0.28	10.98	0.00	99.08
CHR-23	N.D.	0.34	4.08	63.74	4.19	16.86	0.29	10.23	0.13	99.86
CHR-121	N.D.	0.35	4.13	60.60	7.59	17.16	0.23	10.22	0.00	100.28
CAN-08	N.D.	0.35	7.68	63.50	2.27	12.27	0.26	13.77	0.00	100.10
FEC-44	N.D.	0.37	9.52	61.05	2.88	11.48	0.19	14.44	0.14	100.07
CSH-15	N.D.	0.38	2.33	69.80	1.86	12.37	0.24	13.22	0.00	100.20
FEC-59	N.D.	0.38	1.43	71.49	0.83	13.90	0.27	12.17	0.00	100.47
CEU-06	N.D.	0.39	2.20	67.99	3.09	12.42	0.24	12.98	0.00	99.31
CHR-77	N.D.	0.39	3.27	68.50	0.64	14.64	0.22	11.68	0.00	99.34
CHR-32	N.D.	0.40	8.09	63.13	0.99	13.42	0.24	12.86	0.14	99.27
CSH-06	N.D.	0.40	8.17	63.79	1.39	11.09	0.24	14.56	0.00	99.64
CHR-137	N.D.	0.40	2.87	70.15	0.00	13.42	0.19	11.94	0.11	99.08
CAN-03	N.D.	0.41	14.65	53.09	4.92	11.30	0.20	15.09	0.00	99.66
CHR-29	N.D.	0.41	5.90	66.12	0.56	13.25	0.22	12.87	0.00	99.33
CSH-03	N.D.	0.43	6.50	64.43	2.94	11.71	0.27	14.13	0.00	100.41
CHR-63	N.D.	0.43	2.71	69.83	0.00	14.59	0.22	11.28	0.00	99.06
CHR-55	N.D.	0.44	7.97	60.29	2.77	18.25	0.24	9.91	0.00	99.87
CHR-74	N.D.	0.44	2.13	71.12	0.00	12.82	0.20	12.49	0.00	99.20
CHR-88	N.D.	0.45	15.50	55.10	0.54	14.77	0.28	12.89	0.00	99.53
CHR-108	N.D.	0.46	6.26	66.23	0.00	13.38	0.18	12.36	0.11	98.98
FEC-11	N.D.	0.46	3.67	69.46	0.00	13.16	0.26	12.40	0.10	99.51
CHR-111	N.D.	0.47	2.20	70.18	0.47	13.99	0.22	12.05	0.11	99.69
CHR-46	N.D.	0.49	2.24	70.99	0.00	14.50	0.22	10.53	0.00	98.97
CHR-151	N.D.	0.50	7.45	62.35	3.65	11.79	0.15	14.21	0.00	100.10
CEU-02	N.D.	0.50	2.80	66.41	3.46	12.81	0.28	12.75	0.00	99.01
CHR-123	N.D.	0.53	3.79	60.16	7.74	18.33	0.28	9.43	0.14	100.40
CHR-21	N.D.	0.54	2.09	70.35	0.00	14.34	0.27	11.31	0.00	98.90
CSH-18	N.D.	0.55	6.46	58.96	6.58	16.24	0.30	11.13	0.00	100.22
FEC-54	N.D.	0.56	7.07	63.90	0.93	13.58	0.20	12.73	0.16	99.13
CAN-07	N.D.	0.57	6.61	63.45	3.21	12.09	0.22	13.94	0.00	100.09
CHR-37	N.D.	0.59	2.16	68.96	2.54	12.95	0.30	12.90	0.10	100.50
CHR-142	N.D.	0.60	4.29	62.37	5.67	16.03	0.27	11.06	0.14	100.43
FEC-49	N.D.	0.61	2.52	68.91	2.09	12.64	0.23	13.20	0.00	100.20
FEC-53	N.D.	0.64	2.03	68.92	1.91	13.91	0.26	12.26	0.00	99.93
FEC-37	N.D.	0.65	6.55	61.09	5.11	15.18	0.22	12.10	0.00	100.90
CHR-51	N.D.	0.65	2.69	70.29	0.00	13.45	0.25	12.20	0.12	99.65
DCO-07	N.D.	0.67	8.32	58.33	6.58	10.09	0.20	15.27	0.11	99.57
CAN-04	N.D.	0.71	2.46	69.06	2.26	11.83	0.24	13.81	0.00	100.37
CHR-81	N.D.	0.74	2.65	68.75	2.12	12.71	0.27	13.28	0.00	100.52

Sample Number	SiO_2	TiO_2	Al_2O_3	Cr_2O_3	Fe_2O_3	FeO	MnO	MgO	NiO	Total
FEC-57	N.D.	0.75	3.51	67.56	0.61	14.66	0.20	11.88	0.00	99.17
FEC-07	N.D.	0.78	3.53	68.00	0.49	13.91	0.21	12.42	0.00	99.34
CHR-4	N.D.	0.78	2.11	71.46	0.00	13.71	0.24	12.13	0.00	100.43
CAN-20	N.D.	0.79	2.74	68.47	1.78	12.96	0.21	13.11	0.00	100.06
CEU-05	N.D.	0.80	2.44	64.31	4.47	16.94	0.29	10.30	0.00	99.55
CHR-86	N.D.	0.85	2.16	70.36	0.00	12.94	0.21	12.69	0.11	99.32
CHR-48	N.D.	0.86	24.79	42.27	4.83	9.24	0.15	17.75	0.16	100.05
CEU-11	N.D.	0.89	5.28	59.39	6.67	17.40	0.31	10.49	0.00	100.43
FEC-30	N.D.	0.94	4.57	66.96	0.00	13.83	0.21	12.52	0.11	99.14
CAN-11	N.D.	0.98	10.36	56.95	4.61	11.82	0.24	14.59	0.00	99.55
CHR-118	N.D.	0.98	2.55	65.04	4.12	15.90	0.29	11.13	0.15	100.16
CHR-100	N.D.	1.04	6.04	63.42	3.26	12.54	0.17	13.89	0.12	100.48
FEC-14	N.D.	1.05	4.39	66.44	0.87	14.08	0.20	12.55	0.15	99.73
CHR-35	N.D.	1.06	3.46	68.19	0.00	14.05	0.24	12.03	0.14	99.17
CHR-53	N.D.	1.06	3.20	68.62	0.00	15.21	0.24	10.53	0.15	99.01
CHR-143	N.D.	1.08	6.50	60.82	4.43	13.65	0.22	13.04	0.17	99.91
CAN-15	N.D.	1.10	7.33	62.12	3.20	12.05	0.20	14.43	0.00	100.43
CHR-69	N.D.	1.12	3.01	69.15	0.00	13.75	0.28	11.97	0.12	99.40
CHR-10	N.D.	1.14	2.44	69.30	0.00	15.09	0.25	10.69	0.16	99.07
CHR-41	N.D.	1.19	7.28	63.02	2.81	10.93	0.22	15.18	0.13	100.76
CHR-50	N.D.	1.19	3.68	67.24	0.00	14.46	0.26	12.20	0.00	99.03
DCO-31	N.D.	1.22	8.24	59.20	4.19	12.69	0.28	13.90	0.12	99.84
FEC-60	N.D.	1.23	3.69	63.80	4.21	15.54	0.26	11.72	0.19	100.64
CAN-17	N.D.	1.23	3.12	66.10	3.01	13.43	0.20	13.13	0.00	100.22
CHR-82	N.D.	1.24	10.12	58.27	3.05	13.00	0.23	13.99	0.13	100.03
CSH-01	N.D.	1.26	15.26	52.37	4.27	10.96	0.15	16.05	0.00	100.32
FEC-48	N.D.	1.27	2.15	69.28	0.20	13.46	0.23	12.88	0.00	99.47
CEU-14	N.D.	1.29	2.50	67.24	3.18	13.02	0.24	13.50	0.00	100.97
CAN-18	N.D.	1.30	2.74	67.43	2.20	12.56	0.22	13.68	0.00	100.13
FEC-10	N.D.	1.31	2.11	69.02	0.03	14.33	0.23	12.30	0.00	99.33
CAN-13	N.D.	1.32	4.03	66.36	1.66	13.29	0.25	13.36	0.00	100.27
CEU-15	N.D.	1.32	2.49	66.45	3.21	12.96	0.26	13.34	0.00	100.03
DCO-38	N.D.	1.36	2.08	66.45	3.19	12.48	0.21	13.45	0.10	99.32
FEC-06	N.D.	1.37	15.57	50.93	4.49	10.93	0.22	15.82	0.21	99.54
CHR-97	N.D.	1.37	2.15	68.24	0.77	13.82	0.25	12.63	0.00	99.23
CHR-57	N.D.	1.37	1.80	68.61	1.79	13.07	0.28	13.18	0.15	100.25
CHR-133	N.D.	1.38	3.75	64.73	3.37	14.78	0.22	12.38	0.19	100.80
CHR-127	N.D.	1.39	4.32	63.37	3.71	13.33	0.22	13.19	0.12	99.65
CHR-7	N.D.	1.40	7.22	61.41	3.23	12.14	0.28	14.40	0.00	100.08
FEC-12	N.D.	1.44	2.98	62.72	4.84	17.02	0.34	10.59	0.14	100.07
CAN-05	N.D.	1.51	2.72	66.34	2.54	12.31	0.26	13.79	0.00	99.47
CHR-36	N.D.	1.52	4.66	63.62	3.40	12.32	0.28	13.95	0.18	99.93
CAN-14	N.D.	1.55	3.99	58.89	7.47	17.88	0.29	10.46	0.00	100.53
CHR-28	N.D.	1.55	1.39	68.55	0.00	16.56	0.25	10.77	0.00	99.07
CHR-102	N.D.	1.57	7.68	60.44	3.44	12.33	0.22	14.45	0.17	100.30
CHR-99	N.D.	1.62	6.44	62.35	3.57	11.56	0.18	14.97	0.13	100.82
DCO-26	N.D.	1.64	3.87	65.09	0.87	14.43	0.20	12.40	0.09	98.59
CSH-08	N.D.	1.64	3.60	65.21	2.97	12.91	0.20	13.78	0.00	100.31
CEU-16	N.D.	1.66	7.32	58.26	4.82	14.09	0.32	13.16	0.00	99.63
CHR-129	N.D.	1.66	7.84	58.35	5.44	11.95	0.22	14.27	0.14	99.87
CAN-16	N.D.	1.68	6.89	61.01	3.09	12.03	0.27	14.50	0.00	99.47
CSH-05	N.D.	1.70	7.50	58.83	4.19	13.11	0.28	13.84	0.00	99.45
FEC-16	N.D.	1.70	3.12	64.13	4.03	14.75	0.30	12.46	0.14	100.63
FEC-13	N.D.	1.70	2.54	65.12	2.85	16.29	0.30	11.40	0.00	100.20
FEC-31	N.D.	1.71	6.91	60.81	3.66	12.30	0.22	14.43	0.12	100.16
CHR-107	N.D.	1.72	4.14	63.30	3.62	13.90	0.24	13.07	0.14	100.13
CHR-42	N.D.	1.72	4.98	63.53	3.20	12.59	0.25	14.08	0.13	100.48
FEC-20	N.D.	1.73	2.43	66.99	2.51	12.15	0.30	14.12	0.00	100.23
CHR-68	N.D.	1.75	3.91	66.05	0.45	13.44	0.22	13.22	0.12	99.16
CEU-18	N.D.	1.75	2.53	67.26	2.00	11.93	0.26	14.27	0.00	100.00
DCO-25	N.D.	1.76	1.49	67.10	2.93	11.19	0.37	14.33	0.10	99.27
FEC-21	N.D.	1.80	4.99	60.59	4.62	15.32	0.28	12.22	0.11	99.93
CAN-10	N.D.	1.81	4.81	62.04	4.06	13.74	0.28	13.36	0.00	100.10
CHR-79	N.D.	1.82	3.62	65.59	2.25	12.40	0.18	14.12	0.11	100.09
DCO-28	N.D.	1.86	3.84	63.50	3.65	12.81	0.25	14.35	0.10	100.36
CAN-06	N.D.	1.86	3.73	64.43	3.10	12.85	0.27	13.87	0.00	100.11
CHR-27	N.D.	1.89	10.33	57.06	3.96	11.81	0.17	15.34	0.13	100.69
FEC-42	N.D.	1.90	3.98	64.98	2.91	11.89	0.25	14.65	0.00	100.56

Sample Number	SiO_2	TiO_2	Al_2O_3	Cr_2O_3	Fe_2O_3	FeO	MnO	MgO	NiO	Total
CSH-17	N.D.	1.91	4.90	61.65	3.99	13.65	0.26	13.43	0.00	99.79
CSH-11	N.D.	1.92	4.22	58.51	6.92	17.54	0.23	10.91	0.00	100.25
CHR-52	N.D.	1.92	5.72	61.91	3.10	12.57	0.22	14.15	0.15	99.74
CHR-132	N.D.	1.93	5.14	61.95	4.00	13.52	0.26	13.62	0.14	100.56
CHR-67	N.D.	1.94	4.59	63.20	3.10	11.36	0.13	13.52	0.12	97.96
CHR-83	N.D.	1.97	6.58	60.28	3.84	13.96	0.20	13.52	0.16	100.51
FEC-46	N.D.	1.97	5.10	62.76	3.55	13.53	0.24	13.82	0.00	100.97
FEC-35	N.D.	1.98	3.78	64.52	2.61	13.25	0.24	13.64	0.11	100.13
FEC-02	N.D.	2.00	3.45	64.30	3.55	13.38	0.36	13.54	0.16	100.74
FEC-23	N.D.	2.01	7.43	60.37	3.51	12.11	0.32	14.79	0.20	100.74
FEC-19	N.D.	2.01	2.82	65.55	2.95	12.29	0.28	14.12	0.12	100.14
FEC-47	N.D.	2.01	2.65	66.05	3.00	13.57	0.24	13.60	0.00	101.12
CHR-19	N.D.	2.03	4.77	62.92	3.06	13.50	0.26	13.58	0.19	100.31
DCO-62	N.D.	2.09	3.59	65.40	2.36	12.51	0.26	14.21	0.10	100.52
CHR-40	N.D.	2.10	3.87	61.17	4.95	16.49	0.30	11.70	0.00	100.58
FEC-43	N.D.	2.10	5.16	62.05	3.85	11.83	0.27	14.73	0.14	100.13
FEC-38	N.D.	2.10	3.43	64.78	2.90	13.80	0.28	13.43	0.12	100.84
FEC-55	N.D.	2.10	3.56	65.16	1.85	12.88	0.25	13.86	0.10	99.76
DCO-33	N.D.	2.11	3.65	62.71	3.56	12.96	0.27	13.64	0.07	98.97
CHR-33	N.D.	2.13	2.60	64.98	2.72	13.91	0.30	13.02	0.21	99.87
CHR-43	N.D.	2.14	3.80	63.77	3.80	13.03	0.28	14.00	0.14	100.96
CHR-116	N.D.	2.15	4.72	62.42	3.18	14.78	0.24	12.89	0.15	100.53
CHR-64	N.D.	2.15	3.06	63.83	2.96	15.12	0.25	12.33	0.17	99.87
CHR-8	N.D.	2.15	2.84	67.04	0.00	15.24	0.31	12.09	0.00	99.67
FEC-32	N.D.	2.17	7.63	59.57	3.70	12.08	0.25	14.96	0.12	100.48
DCO-22	N.D.	2.17	3.68	62.95	3.78	12.22	0.22	14.28	0.10	99.40
CHR-87	N.D.	2.21	7.43	58.27	4.33	13.26	0.26	14.13	0.00	99.89
CEU-08	N.D.	2.22	4.69	61.44	4.04	13.37	0.27	13.77	0.00	99.80
CAN-01	N.D.	2.22	3.78	63.41	3.31	13.86	0.28	13.46	0.00	100.32
CHR-71	N.D.	2.22	2.87	64.75	2.70	14.41	0.27	12.90	0.18	100.30
FEC-08	N.D.	2.22	2.64	65.20	2.71	14.25	0.31	13.09	0.00	100.42
CEU-07	N.D.	2.23	4.66	60.64	4.35	13.30	0.26	13.68	0.00	99.12
CHR-109	N.D.	2.25	6.74	55.81	6.76	16.84	0.27	11.73	0.22	100.62
CHR-91	N.D.	2.25	2.02	63.30	3.58	17.64	0.38	10.65	0.00	99.82
CHR-58	N.D.	2.25	2.91	65.11	1.20	15.91	0.26	11.84	0.16	99.64
CHR-140	N.D.	2.26	6.07	56.15	6.41	18.91	0.31	10.30	0.21	100.62
CEU-09	N.D.	2.26	3.50	64.08	2.99	13.43	0.31	13.71	0.00	100.28
CHR-98	N.D.	2.26	3.02	64.81	2.42	14.00	0.30	13.25	0.00	100.06
CHR-39	N.D.	2.30	2.68	63.98	3.50	14.60	0.30	12.79	0.16	100.31
FEC-17	N.D.	2.31	2.90	63.90	3.09	14.54	0.29	12.81	0.15	99.99
CHR-119	N.D.	2.33	8.66	56.12	5.32	14.02	0.20	13.95	0.15	100.75
CHR-5	N.D.	2.34	5.26	56.60	7.02	18.31	0.32	10.66	0.22	100.73
CHR-145	N.D.	2.34	3.96	61.66	4.66	14.37	0.25	12.69	0.15	100.08
CAN-02	N.D.	2.34	3.89	62.33	3.74	13.85	0.28	13.46	0.00	99.89
CSH-16	N.D.	2.34	3.89	62.43	3.32	14.93	0.30	12.76	0.00	99.97
CHR-3	N.D.	2.35	5.11	59.28	4.88	17.35	0.29	11.45	0.00	100.71
CEU-12	N.D.	2.38	5.73	54.71	7.40	19.89	0.27	9.70	0.00	100.08
FEC-45	N.D.	2.39	3.26	63.71	3.79	13.75	0.30	13.60	0.14	100.94
FEC-01	N.D.	2.39	2.85	64.52	3.20	14.65	0.27	13.02	0.13	101.03
CAN-19	N.D.	2.40	3.69	62.78	3.57	13.81	0.26	13.55	0.00	100.06
CHR-149	N.D.	2.42	2.53	58.45	6.96	18.23	0.25	10.23	0.20	99.27
CHR-11	N.D.	2.42	1.36	64.31	3.53	17.61	0.37	10.76	0.16	100.52
CEU-01	N.D.	2.45	5.84	56.38	5.71	19.12	0.33	10.72	0.00	100.55
DCO-67	N.D.	2.45	3.56	62.20	4.18	13.56	0.27	13.69	0.10	100.01
FEC-33	N.D.	2.45	3.44	62.37	3.72	15.24	0.32	12.58	0.00	100.12
CHR-2	N.D.	2.45	3.90	63.41	3.20	14.05	0.30	13.59	0.00	100.90
CHR-15	N.D.	2.45	3.04	63.58	3.25	15.20	0.32	12.56	0.18	100.58
FEC-50	N.D.	2.46	4.17	59.76	5.07	15.59	0.31	12.26	0.16	99.78
FEC-41	N.D.	2.46	3.55	62.72	3.82	14.34	0.30	13.21	0.12	100.52
CHR-56	N.D.	2.48	3.64	63.35	2.61	14.37	0.26	13.11	0.17	99.99
CSH-02	N.D.	2.49	5.15	60.92	3.37	14.82	0.27	13.12	0.00	100.14
DCO-21	N.D.	2.49	3.59	61.37	4.20	14.40	0.36	12.95	0.08	99.44
CSH-04	N.D.	2.51	3.62	62.22	3.41	15.21	0.28	12.64	0.00	99.89
CHR-120	N.D.	2.54	3.91	59.15	6.00	17.33	0.31	11.36	0.11	100.71
CHR-146	N.D.	2.54	2.73	62.69	3.41	16.07	0.27	11.88	0.16	99.75
CHR-18	N.D.	2.55	2.62	63.34	3.84	16.02	0.32	12.15	0.12	100.96
CHR-84	N.D.	2.58	3.47	63.14	3.29	15.26	0.29	12.73	0.19	100.95
CHR-24	N.D.	2.59	5.02	58.39	5.24	17.46	0.23	11.40	0.16	100.49

Sample Number	SiO_2	TiO_2	Al_2O_3	Cr_2O_3	Fe_2O_3	FeO	MnO	MgO	NiO	Total
FEC-05	N.D.	2.59	4.20	60.00	4.86	16.68	0.31	11.81	0.14	100.59
CSH-13	N.D.	2.60	3.41	62.22	3.23	16.35	0.31	11.94	0.00	100.06
CHR-62	N.D.	2.60	3.96	62.40	3.11	14.70	0.28	13.01	0.21	100.27
FEC-26	N.D.	2.61	2.83	61.52	4.60	16.98	0.21	11.55	0.15	100.55
CSH-14	N.D.	2.62	3.27	60.52	4.64	17.75	0.31	11.03	0.00	100.14
CEU-10	N.D.	2.65	3.26	61.91	3.83	14.38	0.30	13.12	0.00	99.45
CEU-17	N.D.	2.73	2.86	61.17	4.34	16.73	0.27	11.68	0.00	99.78
CHR-89	N.D.	2.79	6.34	58.36	3.82	14.17	0.28	13.66	0.00	99.42
CSH-07	N.D.	2.79	8.14	58.41	1.67	14.19	0.24	13.87	0.00	99.31
CHR-75	N.D.	2.81	5.28	58.44	4.72	15.88	0.27	12.49	0.13	100.02
CHR-6	N.D.	2.81	3.36	61.36	3.87	16.21	0.29	12.16	0.00	100.06
CHR-72	N.D.	2.89	5.91	58.60	4.29	15.68	0.29	12.85	0.14	100.65
CHR-25	N.D.	2.89	2.55	61.71	3.70	17.35	0.35	11.21	0.17	99.93
FEC-52	N.D.	3.02	3.96	59.93	3.84	16.75	0.27	11.93	0.00	99.70
CHR-30	N.D.	3.07	4.72	58.36	4.99	15.87	0.35	12.51	0.18	100.05
FEC-36	N.D.	3.14	3.24	59.14	5.28	18.19	0.30	10.97	0.24	100.50
CHR-59	N.D.	3.15	5.94	54.63	6.41	19.12	0.26	10.61	0.26	100.38
CEU-19	N.D.	3.20	5.13	51.58	9.64	20.83	0.32	9.52	0.00	100.22
CHR-78	N.D.	3.28	2.05	59.44	5.13	19.82	0.29	9.79	0.21	100.01
CAN-09	N.D.	3.31	4.95	56.76	5.75	17.78	0.28	11.68	0.00	100.51
CEU-13	N.D.	3.41	3.48	55.52	7.52	19.40	0.29	10.40	0.00	100.02
CHR-22	N.D.	3.66	3.13	57.33	6.01	19.45	0.29	10.49	0.17	100.53
FEC-56	N.D.	3.78	2.63	57.79	5.46	20.39	0.27	9.97	0.00	100.29
CHR-49	N.D.	3.89	3.31	59.49	3.71	18.61	0.26	11.27	0.18	100.72

APPENDIX 8a (2) - DOKOLWAYO CONCENTRATE AND DIAMOND INCLUSION TRACE ELEMETS

	OXIDE wt%									ppm		
SAMPLE NUMBER	SIO2	TIO2	AL2O3	CR2O3	FE2O3	FEO	MNO	MGO	TOTAL	NI	Zn	Ga
CAN-01	0.00	2.22	3.78	63.41	3.31	13.86	0.28	13.46	100.32	785	539	27.6
CAN-02	0.00	2.34	3.89	62.33	3.74	13.85	0.28	13.46	99.89	886	496	37.5
CAN-03	0.00	0.41	14.65	53.09	4.92	11.30	0.20	15.09	99.66	944	529	21.2
CAN-04	0.00	0.71	2.46	69.06	2.26	11.83	0.24	13.81	100.37	543	403	0
CAN-05	0.00	1.51	2.72	66.34	2.54	12.31	0.26	13.79	99.47	675	452	19.9
CAN-06	0.00	1.86	3.73	64.43	3.10	12.85	0.27	13.87	100.11	794	457	19.4
CAN-07	0.00	0.57	6.61	63.45	3.21	12.09	0.22	13.94	100.09	785	471	16.8
CAN-09	0.00	3.31	4.95	56.76	5.75	17.78	0.28	11.68	100.51	1260	565	51.6
CAN-10	0.00	1.81	4.81	62.04	4.06	13.74	0.28	13.36	100.10	824	507	19.5
CAN-11	0.00	0.98	10.36	56.95	4.61	11.82	0.24	14.59	99.55	857	514	14.3
CAN-12	0.00	0.29	7.32	64.10	1.77	11.40	0.16	14.16	99.20	548	437	10.8
CAN-13	0.00	1.32	4.03	66.36	1.66	13.29	0.25	13.36	100.27	739	461	17.5
CAN-14	0.00	1.55	3.99	58.89	7.47	17.88	0.29	10.46	100.53	574	594	48.5
CAN-15	0.00	1.10	7.33	62.12	3.20	12.05	0.20	14.43	100.43	771	465	13.9
CAN-16	0.00	1.68	6.89	61.01	3.09	12.03	0.27	14.50	99.47	867	445	21.4
CAN-17	0.00	1.23	3.12	66.10	3.01	13.43	0.20	13.13	100.22	653	467	14.2
CAN-18	0.00	1.30	2.74	67.43	2.20	12.56	0.22	13.68	100.13	597	441	13
CAN-O8	0.00	0.35	7.68	63.50	2.27	12.27	0.26	13.77	100.10	575	499	15.5
CEU-01	0.00	2.45	5.84	56.38	5.71	19.12	0.33	10.72	100.55	1060	663	51.2
CEU-02	0.00	0.50	2.80	66.41	3.46	12.81	0.28	12.75	99.01	637	536	15.2
CEU-03	0.00	0.00	3.19	65.10	3.82	14.38	0.26	12.30	99.05	746	553	35.1
CEU-04	0.00	0.21	9.10	62.93	1.66	9.29	0.20	15.61	99.00	573	536	11.1
CEU-05	0.00	0.80	2.44	64.31	4.47	16.94	0.29	10.30	99.55	505	728	20.4
CEU-06	0.00	0.39	2.20	67.99	3.09	12.42	0.24	12.98	99.31	588	519	15.4
CEU-07	0.00	2.23	4.66	60.64	4.35	13.30	0.26	13.68	99.12	926	513	31.1
CEU-08	0.00	2.22	4.69	61.44	4.04	13.37	0.27	13.77	99.80	1060	562	35.7
CEU-09	0.00	2.26	3.50	64.08	2.99	13.43	0.31	13.71	100.28	917	501	31
CEU-10	0.00	2.65	3.26	61.91	3.83	14.38	0.30	13.12	99.45	914	572	41.7
CEU-11	0.00	0.89	5.28	59.39	6.67	17.40	0.31	10.49	100.43	793	553	48.2
CEU-12	0.00	2.38	5.73	54.71	7.40	19.89	0.27	9.70	100.08	1100	687	54.1
CEU-13	0.00	3.41	3.48	55.52	7.52	19.40	0.29	10.40	100.02	1140	651	42.4
CEU-14	0.00	1.29	2.50	67.24	3.18	13.02	0.24	13.50	100.97	731	533	10.6
CEU-15	0.00	1.32	2.49	66.45	3.21	12.96	0.26	13.34	100.03	829	459	21.5
CEU-16	0.00	1.66	7.32	58.26	4.82	14.09	0.32	13.16	99.63	1120	677	64.6
CEU-17	0.00	2.73	2.86	61.17	4.34	16.73	0.27	11.68	99.78	892	768	50
CEU-18	0.00	1.75	2.53	67.26	2.00	11.93	0.26	14.27	100.00	800	483	21.3
CEU-19	0.00	3.20	5.13	51.58	9.64	20.83	0.32	9.52	100.22	1260	623	31.8
CEU-20	0.00	0.19	2.66	69.36	2.17	12.18	0.23	13.22	100.01	545	536	13
CSH-01	0.00	1.26	15.26	52.37	4.27	10.96	0.15	16.05	100.32	1120	495	41.1
CSH-14	0.00	2.62	3.27	60.52	4.64	17.75	0.31	11.03	100.14	1000	577	29
CSH-15	0.00	0.38	2.33	69.80	1.86	12.37	0.24	13.22	100.20	562	535	9.48
CSH-16	0.00	2.34	3.89	62.43	3.32	14.93	0.30	12.76	99.97	966	514	35.2
CSH-17	0.00	1.91	4.90	61.65	3.99	13.65	0.26	13.43	99.79	870	559	37.1
CSH-18	0.00	0.55	6.46	58.96	6.58	16.24	0.30	11.13	100.22	873	537	35.7
CSH-19	0.00	0.21	3.67	68.13	2.47	12.52	0.18	13.25	100.43	607	509	8.92
CSH-20	0.00	0.09	16.49	53.34	3.78	9.53	0.23	16.24	99.70	1000	511	22.3
DDI14A	0.00	0.00	7.71	64.47	1.80	11.17	0.17	13.93	99.25	684	482	19.10
DDI42A	0.00	0.00	7.71	64.91	1.43	11.43	0.25	13.79	99.52	671	451	10.80
DDI52A	0.00	0.00	6.90	64.82	1.64	12.27	0.30	13.23	99.16	666	447	17.30
DI302B	0.00	0.00	7.96	63.28	2.35	11.35	0.24	13.79	99.10	678	476	19.20
DI302C	0.00	0.00	7.82	63.25	2.66	11.23	0.25	13.72	99.01	666	467	16.50
DI302D	0.00	0.00	7.90	63.42	2.49	11.54	0.21	13.82	99.46	698	496	21.80
DI303A	0.00	0.35	7.02	64.19	2.41	10.35	0.24	14.62	99.26	742	430	12.00
DI305A	0.00	0.00	8.86	63.11	2.80	9.54	0.19	15.25	99.83	739	446	24.10
DI310A	0.00	0.00	7.49	65.13	2.44	10.26	0.23	14.61	100.16	710	455	14.20
DI311C	0.00	0.12	7.67	63.68	3.77	9.56	0.00	14.58	99.47	590	378	12.00
DI315A	0.00	0.14	5.03	67.61	2.01	10.35	0.28	14.35	99.85	642	434	12.00
DI317A	0.00	0.08	8.62	63.67	2.15	9.76	0.27	15.09	99.71	666	447	17.30
DI319A	0.00	0.13	7.40	67.00	0.00	10.98	0.27	13.19	99.08	692	445	9.92

Sample Number	SiO_2	TiO_2	Al_2O_3	Cr_2O_3	Fe_2O_3	FeO	MnO	MgO	Total	Ni	Zn	Ga
DI319B	0.00	0.14	7.76	64.42	1.83	9.69	0.18	15.11	99.20	626	363	0.00
DI319D	0.00	0.18	7.71	64.40	2.29	9.70	0.24	15.16	99.79	707	404	12.40
DI320A	0.00	0.00	8.11	63.38	2.47	10.76	0.20	14.28	99.34	690	473	20.70
DI320B	0.00	0.00	7.98	63.51	2.91	10.97	0.20	14.22	99.92	706	489	17.60
DI320C	0.00	0.00	8.01	63.49	3.05	10.26	0.23	14.66	99.79	673	485	20.60
DI324A	0.00	0.00	5.00	65.75	3.21	13.18	0.36	12.14	99.64	1160	526	14.60
DI328A	0.00	0.47	10.55	61.45	1.30	9.48	0.21	15.68	99.25	846	360	14.00
DI328C	0.00	0.49	10.61	62.11	0.00	11.04	0.17	14.60	99.19	915	381	18.70
DI330A	0.00	0.18	6.07	64.83	3.01	11.57	0.16	13.81	99.70	636	459	17.10
DI331A	0.00	0.00	6.50	67.88	0.72	9.01	0.16	15.23	99.50	584	380	11.70
DI332A	0.00	0.59	8.00	63.10	2.72	9.96	0.28	15.32	100.06	788	419	16.60
DI332B	0.00	0.61	7.76	63.58	2.03	10.55	0.25	14.85	99.73	782	409	14.00
DK038B	0.00	0.00	8.13	64.78	1.74	10.03	0.24	14.76	99.68	639	429	11.00

APPENDIX 8.b

OXIDATION STATES OF CHROMIUM IN MINERALS

Chromium occurs as a minor element of terrestrial gabbroic, basaltic and ultrabasic rocks averaging 0.2 wt% Cr_2O_3 (Turekian, 1963; Prinz, 1967) and as a more abundant element of the lunar basalts (0.5 wt%; Hubbard et al., 1972) and stone meteorites (0.5 wt%; Bunch and Olsen, 1975). It is a transitional metal ion with unfilled d-shells exhibiting a wide range of oxidation states. In addition to the familiar +2, +3 and +6 oxidation states, chromium also occurs in the -2, -1, 0, +4 and +5 oxidation states in natural and synthetic compounds and ions (Dellien et al., 1976). However, the mineralogy of chromium in nature is dominated by the Cr^{3+} and $(CrO_4)^{2-}$ ions (Burns and Burns, 1975).

Apart from rare meteoric minerals most chromium-bearing minerals contain Cr^{3+} ions in octahedral coordination with oxygen (Burns and Burns, 1975). Crystal field studies have shown that trivalent chromium has the largest octahedral site preference energy (relative to regular tetrahedral site) of any ion of the first transition group elements (Burns, 1975). Cr^{3+} has an octahedral radius of 0.615Å (Shannon and Prewitt, 1969) which lies between the values of Al^{3+} (0.53Å), Fe^{3+} (0.645Å), Ti^{4+} (0.68Å), and Mg^{2+} (0.72Å) allowing the substitution of Cr^{3+} ions for Al, Fe^{3+}, Ti and Mg in regular octahedral sites of pyroxene, olivine, and spinel, rather than in the tetrahedral sites. The presence of divalent chromium in both terrestrial and lunar rocks is considerably more ambiguous. Crystal field theory predicts that divalent chromium should be greatly stabilized by the Jahn-Teller effect in distorted octahedral sites such as the M^1 site in olivine and should have geochemical properties intermediate to those of Ni^{2+} and Co^{2+} (Burns, 1970, 1970a, 1975, 1975b).

There is some evidence that in reducing environments Cr^{2+} enters into both pyroxene and olivine structures. The concentration of chromium in lunar olivines is an order of magnitude more than in terrestrial olivines (e.g. Bell, 1970; Keil et al., 1971; Steele and Smith, 1975). Haggerty et al. (1970) described lunar olivines that contain chromium and titanium in excess of the amounts that could be compensated by the small amount of Al^{3+} present and interpreted the IR absorption spectrum of an olivine as that of substituted Cr^{2+} in the absence of Cr^{3+}. Negative values of both [Al-(2Ti+Cr)] and [Al-2Ti], indicating insufficient Al present to compensate for all the chromium as Cr^{3+} and Ti as Ti^{4+}, led Boyd and Smith (1971) to propose the presence of both Cr^{2+} and Ti^{3+} in lunar basaltic pyroxenes. Spectroscopic studies failed to detect Cr^{2+} in lunar pyroxenes (Burns et al., 1972; Mao and Bell, 1971), but confirmed the presence of Cr^{3+} (Burns et al., 1975). Small amounts of Cr^{2+} have been experimentally observed to substitute into spinels under reducing conditions analogous to those of lunar basalt evolution (Stubican and Greskovich, 1966, 1975), but only Cr^{3+} has been found in lunar spinels (Haggerty, 1972; Bell and Mao, 1974a; 1974b). The high abundance of chromium in olivine inclusions in terrestrial diamonds has been attributed to the presence of divalent chromium (Meyer and Boyd, 1972). The high chromium concentrations in those olivines cannot result from high concentrations of chromium in the parent liquidus since the concentration of chromium in olivines of terrestrial chromitites is not correspondingly high (Meyer, 1985).

The evidence for the presence of significant Cr^{2+} in lunar minerals and terrestrial olivine inclusions in diamonds is circumstantial, indirect and contradictory. However, it is widely assumed that Cr^{2+} exists in these minerals (Schreiber and Haskin, 1976).

OXIDATION STATES OF CHROMIUM IN SILICATE MELTS

The oxidation states of chromium in melts were investigated by Schreiber and Haskin(1976) in a series of experiments on silicate compositions in the forsterite-anorthite-silica and forsterite-anorthite-diopside systems over a wide range of oxygen fugacities from 10^{-10} to 1 atm at 1500°C and 1550°C. This experimental study showed that the relative amounts of Cr^{2+} and Cr^{3+} present in a silicate are sensitive to melt composition, temperature and oxygen fugacity. The proportion of the total chromium present as Cr^{2+} in basaltic magmas formed under terrestrial conditions, i.e. in the vicinity of the FMQ buffer (Haggerty, 1978), were estimated to be between 2 - 55%. However, the melts used in the study of Schreiber and Haskin (1976) were iron-free. It was argued by Schreiber and Haskin (1976) and Schreiber (1977) that the presence of Fe^{3+} in terrestrial magmas precludes the stabilization of Cr^{2+}. The higher reduction potential of the Fe^{3+} - Fe^{2+} couple in silica melts in comparison to the reduction potential of Cr^{3+} - Cr^{2+} (Table 8.3) would have spontaneously oxidized Cr^{2+} according to the reaction:

$$Fe^{3+} + Cr^{2+} = Fe^{2+} + Cr^{3+}$$

In the vicinity of the FMQ buffer the concentration of Fe^{3+} in silicate melts can be expected to be greatly in excess over the minor amounts of total chromium which would make this oxidation reaction near complete. Chromium is thus expected to be present almost entirely in the trivalent state in silicate melts at or near FMQ buffer conditions (Schreiber and Haskin, 1976).

Murck and Cambell (1986) investigated the influence of temperature, oxygen fugacity and melt composition on the solubility of chromium in basic and ultrabasic melts in an experimental study using natural materials. The variations in chromium content as a function of oxygen fugacity for both melt and mineral phases (olivine

in particular) in these experiments were attributed to the presence of some divalent chromium. Similarly, Barnes (1986) found that the chromium solubility in a synthetic analogue of a proposed parental magma to the bronzite-chromite rich rocks of the Critical Zone of the Bushveld Complex increased systematically with decreasing oxygen fugacity from the NNO buffer to the IW buffer at constant temperature. This increase in solubility was considered to be due to the reduction of Cr^{3+} to Cr^{2+}. The redox ratio of the Cr^{3+}/Cr^{2+} was also found to decrease with increasing temperature at constant oxygen fugacity. furthermore, Barnes (1986) found that there was good correlation between the data from Fe-present melts and the data from the iron-free forsterite - anorthite - diopside system of Schreiber and Haskin (1976). It would thus appear that Fe^{3+} and Cr^{2+} may coexist in silicate melts. This apparent anomaly may possibly be explained by evaluating the behaviour of iron and chromium in silicate melts.

THE BEHAVIOUR OF IRON AND CHROMIUM IN SILICATE MELTS

The structural state of iron and variations in Fe^{2+}/Fe^{3+} in simple metal oxide - SiO_2 joins at fixed temperature, pressure and oxygen fugacity were investigated by Mysen et al. (1981) to determine the effects of bulk composition on iron redox equilibria. It was concluded that alkali metals (M^+) are required to stabilize Fe^{3+} in network-forming tetrahedral coordination within the silicate melts structure. If M^+/M^{2+} is less than that required to form $(MFe)^{4+}$, mixed coordination of Fe^{3+} is found. Furthermore, if there are only M^+ cations in the system and $M^+ = Fe^{3+} = Al^{3+}$, then $(MAl)^{4+}$ complexes are formed and Fe^{3+} is an octahedrally coordinated network-modifier. However, if there is only sufficient M^+ to stabilize Fe^{3+} or Al^{3+}, but additional M^{2+} is present so that $(M^{2+}_{0.5}T)^{4+}$ may also occur, then $(MFe)^{4+}$ and $(M^{2+}_{0.5}Al)^{4+}$ complexing will take place. Under the circumstances, therefore, $(MFe)^{4+}$ complexes are more stable than $(MAl)^{4+}$ in a silicate melt (Mysen et al., 1981).

With ferric iron in tetrahedral coordination in a melt Fe^{3+}/Fe^{*} ($Fe^{*} = Fe^{3+}+Fe^{2+}$) decreases with increasing temperature at constant oxygen fugacity and also decreases with decreasing oxygen fugacity constant temperature (Mysen et al., 1985). However, Fe^{3+}/Fe^{*} increases with decreasing degree of polymerization [increasing non-bridging oxygens per tetrahedral cation, NBO/T] of the melt (Mysen et al., 1984). Because the bulk melt NBO/T increases with decreasing Fe^{3+}/Fe^{*} as long as the Fe^{3+} is in tetrahedral coordination and Fe^{2+} is in octahedral coordination, the NBO/T will increase with increasing temperature and with decreasing oxygen fugacity. Ferric iron will undergo a coordination transformation from IV-fold to VI-fold coordination at some oxygen fugacity less than that of air for the three systems $MgO-Al_2O_3-SiO_2-FeO$, $CaO-Al_2O_3-SiO_2-FeO$ and $Na_2O-Al_2O_3-SiO_2-FeO$ at 1550°C. This transformation in coordination of the Fe^{3+} will give rise to a decrease in NBO/T with decreasing oxygen fugacity. This apparent contrast in the functional relationship between NBO/T and Fe^{3+}/Fe^{*} for $Fe^{[3+IV]}$ and $Fe^{[3+VI]}$ results from the oxidation of the Fe^{3+} in the VI-fold coordination to Fe^{2+} in the VI-fold coordination:

$$Fe^{[3+VI]} + O^{-} = Fe^{[2+VI]} + 0.5\ O^{2}$$

where O- is a non-bridging oxygen in the silicate network (Mysen et al., 1985). The driving force for the reduction of the $Fe^{[3+VI]}$ to $Fe^{[2+VI]}$ is the lower field strength of Fe^{2+} relative to Fe^{3+} in network-modifying positions (Dickensen and Hess, 1981). Field strength is defined as the charge of the cation divided by the square of the cation-oxygen interatomic distance (Wood and Hess, 1980). The reduction of $Fe^{[3+VI]}$ to $Fe^{[2+VI]}$ is more rapid in the system MAS-FeO-O than CAS-Fe-O and more rapid in the latter than in NAS-FeO-O (Mysen et al., 1985).

The behaviour of chromium in silicate melts has not received much attention in the literature. The partitioning coefficient of $D_{(B/A)}$ of 3.3 (Watson, 1976) between two-liquid basic/acidic melt systems for chromium implies that the substitution of Cr^{3+} <-> Al^{3+}, which is known to occur in crystalline silicates, probably does not occur in liquids, because chromium is strongly depleted in the Al-Si-rich melts. Furthermore, due to its extremely high octahedral site preference energy (Burns, 1970a), Cr^{3+} is not known to exist in tetrahedral coordination in any magmatic mineral (Burns and Burns, 1975) whereas both Al^{3+} and Fe^{3+} are found in tetrahedral and octahedral coordination in magmatic minerals. Since Cr^{3+} is confined to octahedral coordination in magmatic derived minerals it is suggested that it is unlikely that it would deviate from its behaviour in minerals and would not occur in tetrahedral coordination in melts.

Considering the diverse behaviour af Al^{3+} and Fe^{3+} in the structure of silicate melts, it is instructive to evaluate the possibility of Cr^{3+} behaving in a similar fashion. Coupled substitutions with monovalent alkalis and Cr^{3+} do occur in the mineral ureyite (Frondel and Klein, 1965) and in pyroxene solid solutions with ureyite (Ikeda and Yagi, 1972). The Cr^{3+} in these pyroxenes, however, occurs in octahedral coordination. Murck and Cambell (1986) evaluated a model in which the mechanism of solution of Cr^{3+} in a silicate melt depends on charge-balancing by monovalent alkali cations such as K^{+} and Na^{+} in tetrahedral coordination. Several reasons were forwarded to show that such a model was not consistent with their data; in particular the fact that chromium was not concentrated in two immiscible K-rich melts where there was excess K^{+} available for charge balancing.

A second alternative for Cr^{3+} to be tetrahedrally coordinated in a silicate melt is one where Cr^{3+} is charge balanced be Ca^{2+} in an anorthite-type structure as has been observed for Al^{3+} by Seifert et al. (1981). However, the absence of

chromium in naturally crystalline feldspars and the lack of tetrahedrally coordinated Cr^{3+} in nature makes this unlikely.

The thermodynamic effects of both network-forming and network-modifying cations in ternary melts could be qualitatively predicted from their behaviour in binary systems and has been shown to be correlated with field strength. The behaviour of highly charged cations, e.g. Ti^{4+}, Zr^{4+}, P^{5+} and Cr^{3+}, does not follow the trends based on field strength, but deviates from ideality in liquids (Ryerson, 1978). The addition of TiO_2 to silicate melts produces a positive deviation from ideality. However, the deviation produced is not nearly as great as would be predicted for the field strength of the Ti^{4+} cation as a network-modifier. Raman spectra of TiO_2-SiO_2 melts indicate that Ti^{4+} is present in tetrahedral coordination randomly distributed within the SiO_2-network (Mysen et al., 1980). The ease with which Ti^{4+} cations enter tetrahedrally coordinated sites within the silicate melt structure is probably not related to field strength, but to the identical charge between Ti^{4+} and Si^{4+}. Dickensen and Hess (1983) found that Ti^{4+} occurs in octahedral coordination in peraluminous and peralkaline melts suggesting that $(M^{+}Al)^{4+}$ and $(M^{2+}_{0.5}Al)^{4+}$ charge balanced complexes polymerise with Si^{4+} in silicate melts in preference to the high field strength of Ti^{4+} cations. Spectroscopic data have indicated that Ti^{4+} can be present in a silicate liquid as titanate complexes and exist in clusters where Ti-O-Ti bonds prevail (Mysen et al., 1980a, 1980b; 1981b). Such clustering is a precursor to unmixing with the silicate melt and would tend to produce strong deviations from ideality. The increasing deviations from ideality is directly related to an increase in TiO_2 contents in the liquid (Ryerson, 1978).

It has been shown that Cr^{3+} is unlikely to be in tetrahedral coordination in a silicate melt. It would thus seem that the most likely behaviour for trivalent chromium in a silicate liquid is one of an octahedral network-modifier. Octahedrally coordinated Cr^{3+} in silicate melts have been inferred by Landry et al.

(1967) and Kobayashi (1976) with the use of electron paramagnetic spectra. It was observed by Mysen et al. (1985) that the NBO/T of a silicate melt increases with increasing temperature and decreasing oxygen fugacity which implies an increase in the availability of octahedrally coordinated sites within the melt with an increase in temperature and/or decrease in oxygen fugacity. The increase in chromium solubility in ultrabasic liquids with an increase in temperature and/or decrease in oxygen fugacity is consistent with the behaviour of Cr^{3+} in silicate melts being positively correlated to the increased availability of octahedrally coordinated sites within the melt (Murck and Cambell, 1986). Coupled octahedrally coordinated Cr^{3+} ion pairs have been documented in melts with high Cr^{3+} contents (O'Reilly and McIver, 1962; Fournier et al., 1971) suggesting the presence of submicroscopic spinel-like aggregates in melts similar to Ti^{4+} titanate clusters described by Mysen et al. (1980a,b, 1981b).

These observations are consistent with the model Burnham (1975, 1979) proposed for silicate melts in which, at temperatures near its liquidus, the melt is considered to contain clusters of components or units which mix ideally with one another, and are similar in structure and stoichiometry to the crystalline phases which appear on the liquidus.

The concentration of divalent chromium relative to total chromium concentration (i.e. Cr^{2+}/Cr^{*}) in both iron-bearing and iron-free experimental melts have been reported to increase with increasing temperature and decreasing oxygen fugacity at constant fO_2 and temperature respectively (Schreiber and Haskin, 1976; Barnes, 1986). These observations are analogous to the behaviour of Fe^{2+}/Fe^{*} in silicate melts which have been attributed to the reduction of Fe^{3+} to Fe^{2+} in octahedrally coordinated sites within the melt by Mysen et al. (1985). Since the difference in field strength between the Cr^{2+} and Cr^{3+} is significantly greater than the

difference in field strength between Fe^{2+} and Fe^{3+}. it is suggested that the octahedrally coordinated Cr^{3+} will reduce more readily to Cr^{2+} within the silicate melt compared to the Fe^{3+}-Fe^{2+} reduction pair in octahedral coordination. This implies that Cr^{2+} will be octahedrally coordinated within the melt. The octahedral coordination of Cr^{2+} is further supported by that fact that its crystal field site energy for octahedral coordination (22.7 Kcal/mole; Burns, 1975b) which is between the CFSE of divalent octahedrally coordinated Ni^{2+} (29 Kcal/mole) and Fe^{2+} (11.9 Kcal/mole; Cambell et al., 1979). The observed increasing Cr^{2+}/Cr^{*} with increasing temperature and/or decreasing oxygen fugacity (Schreiber and Haskin, 1976; Barnes, 1986) is consistent with both the CFSE data and increased number of octahedrally coordinated sites available in the silicate melt under these conditions. The CFSE in octahedral coordination of Cr^{2+} suggests that its solubility is more strongly dependent than Fe^{2+}, but less dependent than Ni^{2+} and considerably less dependent than Cr^{3+} (53.7 Kcal/mole).

THE COEXISTENCE OF Cr^{2+} AND Fe^{3+} IN SILICATE MELTS

The presence of Cr^{2+} in iron-bearing melts (Murck and Cambell, 1986; Barnes, 1986) necessitates the consideration of several possibilities in order to evaluate the apparent coexistence of Cr^{2+} and Fe^{3+}, in a silicate melt. The behaviour of Fe^{3+} and Cr^{2+} in silicate melts has been presented above. Several salient points have arisen and will be briefly summarized:

a) In the presence of alkalis Fe^{3+} is charge-balanced and tetrahedrally coordinated within the structure of the melt and is thus unlikely to affect the oxidation state of any octahedrally coordinated cations.

b) If $[Fe^{3+}]$ is in excess of $[M^{+}]$ in the melt, then the excess Fe^{3+} is octahedrally coordinated where it might reduce to Fe^{2+}.

c) Increasing temperature and/or decreasing oxygen fugacity of the melt enhances the rate of reduction of $Fe^{[3+VI]}$ to $Fe^{[2+VI]}$.

d) Increasing temperature and/or decreasing oxygen fugacity of the melt favours the reduction of Cr^{3+} to Cr^{2+}.

Considering the above, three possibilities arise to account for the coexistence of Fe^{3+} and Cr^{2+} in a silicate melt

1) The combined reduction potentials of

$$Cr^{[3+VI]} + O^{-} = Cr^{[2+VI]} + 0.5\ O^{2}$$

and

$$Fe^{[3+VI]} + O^{-} = Fe^{[2+VI]} + 0.5\ O^{2}$$

is greater than the reduction potential of the electron transfer reaction

$$Fe^{3+} + Cr^{2+} = Fe^{2+} + Cr^{3+}$$

at mantle temperatures and pressures. Unfortunately, in the absence of available literature on reaction kinetic data for these reactions under the envisaged conditions, it is not possible to predict the effect reaction kinetics may have on the above reactions.

2) With increasing temperature and decreasing oxygen fugacity the concentration of Fe^{3+} in the melt decreases to such low levels that the concentration of Cr^{2+} is not affected by any remaining Fe^{3+} in octahedral coordination.

3) All the $Fe^{[3+VI]}$ has been reduced to $Fe^{[2+VI]}$ and the remaining Fe^{3+} in the melt is in tetrahedral coordination and thus cannot affect the concentration of Cr^{2+} in the melt.

The reduction of octahedrally coordinated ferric iron in a silicate melt to levels where $Fe^{[3+VI]}/Fe^{*} = 0.1$ would result in the appearance of a metasilicate phase (pyroxene) and complete reduction in the stabilization of an orthosilicate (olivine) liquidus phase (Mysen et al., 1985). Concomitantly, the concentration ratio of Cr^{2+}/Cr^{*} is greatly increased and it is suggested that Cr^{2+} may be present in olivines and pyroxenes. It should be noted that, hitherto, only silicate minerals have been suggested to contain divalent chromium under natural terrestrial conditions (Meyer and Boyd, 1972; Ikeda, 1972).

The model presented above for the stability of chromium in mantle melts suggests that Cr^{2+} may well be stabilized and survive in the (M^{1}) site of pyroxenes and olivines, both minerals of which, significantly, do not allow for Fe^{3+} to be incorporated in their structures. It is possible to extend this model to oxide phases that are stoichiometrically Fe^{3+}-free and have an apparent excess of trivalent cations, e.g spinels. The Dokolwayo concentrate spinel population is characterised by a sub-population (approximately 10 per cent) of spinels that are stoichiometrically calculated to be free of Fe^{3+}, contain chromium concentrations in excess of stoichiometric limits and have an apparent deficiency in divalent cations. These spinels probably contains significant proportions of Cr^{2+} (Table 8. 2) and presumably are indicative of low oxygen fugacities.

Since Cr^{2+} and Fe^{3+} are unlikely to coexist in octahedral coordination the upper limit in oxygen fugacity for the existence of Cr^{2+} in silicate melts must be the wustite-magnetite (WM) buffer. Reduction potentials (Table 8. 3) suggest that Cr^{3+} will reduce to Cr^{2+} more readily than Fe^{2+} reduces to native iron. It

would therefore seem that the elimination of Cr^{3+} from mantle derived minerals will be determined by the position of the IW (iron-wustite) oxygen buffer. However, stoichiometric constraints and pressure induced crystallographic phase transitions in the mantle suggest that oxygen fugacity may not be the determining factor for the preservation of Cr^{3+} in mantle derived minerals below IW.

CHAPTER 9 - Cr-SPINEL COMPOSITION - PRESSURE RELATIONSHIPS IN THE MANTLE.

ABSTRACT

The behaviour of the Cr/(Cr+Al) ratio of chromium spinels with respect to mantle pressures and temperatures has been investigated. The spinels are from spinel-garnet peridotites derived from the southern African lithosphere.

Chromium spinels and garnets coexist in the mantle to at least 50 kbars pressure, which is significantly in excess of the CMAS predicted limit of 18 kbar. The Cr/(Cr+Al) ratio of chromium spinels increases with increasing pressure in the mantle. At pressures in excess of 40 kbars the Cr/(Cr+Al) ratio of the spinels is restricted by stoichiometric constraints. A limited study of the concentrate spinels from kimberlites indicate that economically diamondiferous kimberlites are characterised by spinel compositions in which the average Cr/(Cr+Al) is >0.8. Concentrate spinels from kimberlites characterised by a paucity in diamonds have an average Cr/(Cr+Al) < 0.8.

INTRODUCTION

Spinels are common accessory mineral phases in a variety of mantle derived ultramafic xenoliths. Spinel-peridotites have been reported in basalts (e.g. Ross et al., 1954; Basu and MacGregor, 1975), basanites, nephelinites (Mitchell, 1987), camptonites and lamproites (Eggler et al., 1987) and kimberlites (e.g. Boyd, 1971; Daniels, 1980).

Upper mantle spinel-peridotites sampled by kimberlites exhibit three textural varieties. Discrete spinels may occur in lherzolites, harzburgites and dunites (Nixon and Boyd, 1973; Pokhilenko et al., 1977; Kirkley et al., 1984). More commonly, spinels occur as

intergrowths with silicates in these xenoliths (Boyd, 1971; Smith and Dawson, 1975; Daniels, 1980) and as small crystals within kelyphytic rims surrounding garnets (Nixon and Boyd, 1973; Carswell et al., 1979).

The Cr/(Cr+Al) variations of spinels in peridotitic suites have been suggested to conform to systematic patterns which are dependent on pressure and temperature (Irvine, 1965, 1967; Haggerty, 1979; Dick and Bullen, 1984). In low pressure plagioclase-spinel peridotites the Al is predominantly partitioned into the plagioclase resulting in spinels with high Cr/(Cr+Al) ratios (Haggerty, 1976; Dick and Bullen, 1984). It was observed by Haggerty (1979) that at intermediate pressures the spinels in spinel-peridotites have variable Cr/(Cr+Al) ratios whereas in high pressure garnet lherzolites both Cr and Al are preferentially partitioned into garnet and diopside resulting in a spinel-free assemblage. It would thus appear that the Cr/(Cr+Al) ratio of spinels is systematically and inversely related to pressure within the spinel-bearing lherzolite field at constant bulk composition (Haggerty, 1979).

In an extensive study of spinels from ultramafic xenoliths, Basu and MacGregor (1975) concluded that there is an apparent relationship between the Cr/(Cr+Al) ratio of spinels which indicates that spinels formed at higher pressures have higher Cr/(Cr+Al) ratios. This is in marked contrast to the observations of Irvine (1965) and Haggerty (1976, 1979). Furthermore it was observed by Basu and MacGregor (1975) that there was a close correspondence between spinel composition and coexisting orthopyroxene composition with respect to Al_2O_3 contents, suggesting that the bulk composition, and not simply a pressure effect, is the critical variable in the determination of spinel compositions in mantle peridotites.

Quite apart from these observations, it is well established that spinels with high Cr/(Cr+Al) ratios are found as relatively common inclusions in diamonds that are thought to have equilibrated at pressures in excess of 50 kilobars (Gurney et al., 1984; Meyer,

1985; Daniels and Gurney, 1989).

In an attempt to resolve this dichotomy of observations the equilibration temperatures and pressures of mantle derived spinel-garnet peridotites have been determined by means of spinel-independent geothermometers and geobarometers. The calculated temperatures and pressures have then been correlated with the compositions of spinels in the respective xenoliths.

SPINEL-GARNET PERIDOTITE GEOTHERMOMETRY

Natural garnet-peridotites commonly contain secondary spinels in kelyphytic rims surrounding garnets formed during reactions related to either metasomatic fluid infiltration, interacttion with kimberlitic fluids, or retrograde subsolidus alteration. Occurrences of coexisting primary spinel and garnet are by contrast comparatively rare, but have been recorded from a number of kimberlite provinces in southern Africa (Nixon and Boyd, 1973; Danchin and Boyd, 1976; Lawless, 1978; Mitchell, 1984; Moore, 1986; Nixon et al., 1987).

In this study temperatures and pressures have been calculated for xenoliths with the mineral assemblage olivine - orthopyroxene - garnet - spinel $\pm$ clinopyroxene. All the xenoliths used in this study were derived from kimberlites situated on the Kaapvaal Craton in southern Africa (Figure 9.1). The mineral compositions were extracted from Nixon and Boyd (1973), Danchin and Boyd (1976), Dawson et al. (1978); Lawless (1978); Robey (1981); Moore (1986) and Nixon et al. (1987).

There are several reasons for the choice of garnet-spinel peridotites to determine the behaviour of the Cr/(Cr+Al) ratio of spinels in mantle derived xenoliths with respect to temperature and pressure:

i) There is no satisfactory geobarometer for garnet-free spinel-peridotites that adequately takes into account the effect of chromium on mineral phase equilibria as observed in experimental studies (Nickel, 1986). However, Nickel and Green (1985) have thermodynamically modeled an orthopyroxene - garnet geobarometer based on experiments in the CMAS - Cr_2O_3 system which closely approximates natural garnet-bearing peridotites. Their barometer is used in this study.

ii) The general applicability of the olivine - garnet geothermometer of O'Neill and Wood (1979) to calculate the equilibration temperatures of the xenoliths is advantageous. Unlike the two-pyroxene and garnet-clinopyroxene geothermometers (e.g. Lindsley and Dixon, 1976; Powell, 1985) it is applicable to clinopyroxene-free assemblages, such as garnet harzburgites which may contain chromian spinels.

In an assessment of the accuracy of various barometers from the literature Carswell and Gibb (1987) found that the geobarometer of Nickel and Green (1985) yielded the most accurate calculated pressures for garnet-harzburgite and lherzolite assemblages equilibrated under mantle P-T conditions. Carswell and Gibb (1987) also concluded that this barometer is the only formulation currently available which adequately takes into account of the considerable influence of X_{Al}^{M1} in orthopyroxene coexisting with garnet that results from the presence of significant Cr^{3+} and Fe contents.

RESULTS AND DISCUSSION

Chromian spinel-garnet peridotites derived from the upper mantle of southern Africa may be divided into four groups.

Group I xenoliths are characterised by sub-calcic G10 garnets and the absence of clinopyroxene (Dawson et al., 1978; Nixon et al., 1987). The compositions of the garnets from these xenoliths are similar in composition to diamond inclusion G10 garnet

compositions. However, pressure and temperature calculations for these xenoliths (< 20 kbars; <800°C) suggest an origin well outside of the diamond stability field. These calcium-depleted harzburgites are derived from on-craton kimberlites in Lesotho.

The Group II xenoliths also are derived from on-craton kimberlites and are characterised by lherzolitic garnet compositions (Figure 9.2) which suggest that they are derived from CaO-saturated environments (Gurney and Switzer, 1973; Sobolev et al., 1973).

The third group of xenoliths is defined by only two samples, both of which are CaO depleted harzburgites (RVD 183, Danchin and Boyd, 1976; PHN 2818b, Nixon et al., 1987). Mineral compositions from these two xenoliths are similar to the compositions of the sub-calcic chromium-enriched peridotitic diamond inclusion suite. Calculated equilibrium pressures (>50 kbars) and temperatures (>1000°C) from the Group III xenoliths suggest a derivation within the diamond stability field which is consistent with the suggestion of Gurney et al. (1985) that RVD 183 may be representative of the source rock of peridotitic suite diamonds at Premier.

The Group IV xenoliths are all derived from the off-craton Hebron kimberlite (Robey, 1981). The xenoliths are characterised by garnets with lherzolitic garnet compositions (Figure 9.2) suggesting that they are derived from a CaO-saturated environment. These xenoliths are distinguished from the Group II xenoliths by the cratonic positioning of the host kimberlites.

Cr/(Cr+Al) in Spinels

The Cr/(Cr+Al) ratio (Cr^*) of the spinels in the Group I, II and IV xenoliths increase systematically with pressure from Cr^*~0.3 at 10 kbar to Cr^*~0.8 at 40 kbar. At pressures in excess of 40 kbars the $Cr^*_{(sp)}$ - pressure relationship shows no increase in Cr^* with an increase in pressure (Figure 9.3). A first order observation from this study is that spinels

and garnets coexist in mantle-derived peridotites to pressures in excess of the maximum pressures (18 kbar) predicted for their coexistence by experimental observations in the CMAS system (O'Hara et al., 1971; Obata, 1976; Jenkins and Newton, 1979). The results of this study indicates that spinels and garnet may coexist in peridotites to pressures in excess of 50 kbars and well into the diamond stability field. These results are consistent with the experimental results in the SMACCr system (MacGregor, 1970; O'Neill, 1981; Nickel, 1986) and with the coexistence of chrome-rich spinels and garnets in diamonds (Meyer and Boyd, 1972; Gurney et al., 1984). It is apparent that the introduction of chromium into experimental systems stabilizes spinel coexisting with garnet to significantly greater pressures than predicted by the chromium-free experimental systems. Since most natural spinel-garnet peridotites from the Kaapvaal craton are characterised by chromium-rich spinels, it is suggested that observations based on CMAS experimental work be applied to natural chromium-bearing peridotitic assemblages with extreme caution.

The increase in the Cr^* of the spinels in the Groups I, II and IV xenoliths with an increase in pressure to a maximum of 40 kbars (Figure 9.3) is in contrast to the observations of Irvine (1965) and Haggerty (1976, 1979) on Cr^*_{sp}-pressure trends in the upper mantle. However, it is consistent with the observations of Basu and MacGregor (1975) and the fact that chromium-rich spinels are common inclusions in diamond (Meyer, 1985). The narrow range in the Cr^* of the spinels derived from xenoliths with equilibration pressures in excess of 40 kbars may not be due to a levelling off in the Cr/(Cr+Al) ratio in the spinels with increasing pressure (Figure 9.3), but is more likely to be due to stoichiometric constraints on spinel compositions. Alternatively, the apparent narrow range of Cr^* may be due to an insufficient data base for xenoliths with equilibrium pressures in excess of 40 kilobars.

The relationship between the Cr^* of the spinels and the calculated equilibrium temperatures for the host xenoliths defines a general increase in the Cr^* of the spinels with an increase in temperature (Figure 9.4). This relationship defines four groups of xenoliths which can be correlated with the four groups of xenoliths defined above.

It was found that there is a broad negative correlation between the Al_2O_3 content of orthopyroxene and Cr^* of spinels in the xenoliths (Figure 9.5). Basu and MacGregor (1975) interpreted the trend in Figure 9.5 to reflect bulk compositional control on the compositions of coexisting mantle-derived peridotitic orthopyroxenes and spinels. Comparison of the olivines and garnets from the Group I xenoliths with those of the Group II and IV xenoliths (Table 9.1) suggests that the Group I xenoliths are significantly more depleted in basaltic components. During melting events chromium preferentially partitions towards the depleted residue while Al_2O_3 partitions into the melt. Therefore, it may be expected that if bulk composition has a significant control over the compositions of spinel (Basu and MacGregor, 1975), then the Cr^* of spinels in depleted rocks should be higher than the Cr^* of spinels in less depleted rocks. In contrast to the expected trend, the Cr^* of the spinels from the depleted Group I xenoliths are significantly lower than the Cr^* of the spinels from the less depleted Group II and IV xenoliths (Figures 9.3, 9.4 and 9.5). This observed reversal in the expected trend suggests that bulk composition has little influence on the compositions of spinels derived from spinel-garnet peridotites in the upper mantle.

In contrast to bulk composition, it has been demonstrated that there is a very strong correlation between pressure and spinel composition. It is therefore suggested that while bulk composition may have an influence on the compositions of mantle derived spinels, the compositions of chromium spinels are predominantly dependent on pressure. The pressure dependence of chromium spinel compositions suggested above is consistent with the high Cr^* of spinels found as diamond inclusions world wide as well as spinels found in diamondiferous xenoliths (Pokhilenko et al., 1977; Meyer, 1985).

Kimberlite Concentrate Spinels

Chromium spinels are common constituents of kimberlite concentrates. Spinels with Cr_2O_3-rich compositions have been recognised as possibly being indicative of the presence

of diamonds (Mal'kov and Popova, 1972; Gurney, 1984). Assuming that concentrate spinels are derived from the disaggregation of mantle xenoliths, it is expedient to evaluate the relationship between pressure and the Cr^* determined above against the presence of diamonds in the kimberlite from which the concentrate was derived. Spinels comprise approximately forty five percent of the Dokolwayo kimberlite concentrate. The majority (>95%) of these Dokolwayo spinels have Cr/(Cr+Al) >0.8, suggesting that most of these spinels are derived from pressures in excess of 40 kilobars and may be derived from well within the diamond stability field. Such a derivation for these concentrate spinels is consistent with the presence of diamonds and spinels as diamond inclusions at Dokolwayo (Daniels and Gurney, 1989).

The Cr^* of concentrate spinels from several other kimberlites in southern Africa (Figure 9.1; Table 9.2) have been investigated to determine if the observations made on the Dokolwayo spinel concentrate are applicable to other kimberlite concentrates. The average Cr^* for the chromium spinels for the respective kimberlites are presented in Table 9.2.

The Rietfontein and Melton Wold kimberlites are both off-craton kimberlites and are non-diamondiferous. The spinel concentrate from these two kimberlites are characterised by average $Cr^* << 0.8$. None of the spinels from these two kimberlites had $Cr^* > 0.8$, suggesting that spinels from these two kimberlites were derived from levels well above the diamond stability field. This is consistent with the absence of diamonds from these kimberlites. The Kao kimberlite in Lesotho is marginally within the boundary of the Kaapvaal Craton. The kimberlite is diamondiferous, but of low grade. The concentrate spinels from this kimberlite have an average $Cr^* < 0.8$. However, approximately 46% of the concentrate spinels from this kimberlite have $Cr^* > 0.8$, which is consistent with the presence of diamonds in the kimberlite. The concentrate spinels from the Finsch and Koffiefontein kimberlites are characterised by Cr^* values similar to those observed at Dokolwayo, albeit slightly lower values. Both Finsch and Koffiefontein are diamond producing on-craton kimberlites.

The presence of diamonds in kimberlites characterised by concentrates in which the chromium spinels have an average $Cr^* > 0.8$ and the absence or near absence of diamonds from kimberlites characterised by concentrate spinels with an average $Cr^* < 0.8$ supports the relationship between pressure and the Cr^* established from mantle-derived spinel-garnet peridotites in southern Africa.

CONCLUSIONS

1) Spinels and garnets coexist in mantle-derived peridotites to pressures in excess of 50 kbars and well into the diamond stability field. These high pressures are significantly in excess of the maximum pressure (18 kbar) predicted for the coexistence of spinel and garnet by experimental observations in the CMAS system. The results of this study suggest that observations based on CMAS experimental work could only be applied to chromium-bearing assemblages with extreme caution.

2) The Cr^* of mantle-derived chromium spinels coexisting with garnets increase with pressure and temperature. This trend in spinel compositions is in contrast to the observations of Irvine (1965) and Haggerty (1976, 1979). The critical factor influencing the composition of mantle-derived chromium spinels was found to be pressure and not bulk composition as suggested by Basu and MacGregor (1975).

3) There is a close relationship between the Cr^* of concentrate spinels and diamond content of the kimberlites. Concentrate spinels with $Cr^*_{(average)} > 0.8$ appear to be associated with significantly diamondiferous kimberlites whereas values of $Cr^*_{(average)} < 0.8$ indicate only marginally diamondiferous or non-diamondiferous kimberlites.

TABLE 9.1

MINERAL COMPOSITIONS OF SELECTED SPINEL-GARNET PERIDOTITES FROM SOUTHERN AFRICA.

a) OLIVINE

OXIDE	GROUP I	GROUP II	GROUP III	GROUP IV
SiO_2	41.7	41.7	41.5	40.5
TiO_2	<0.03	<0.02	<0.03	<0.01
Al_2O_3	<0.03	<0.01	0.03	<0.01
Cr_2O_3	<0.03	0.02	0.06	<0.01
FeO	4.47	7.53	5.18	8.77
MnO	0.04	0.09	0.08	0.09
MgO	54.7	50.4	52.3	50.93
TOTAL	100.91	99.74	99.15	100.82
Fo	**95.6**	**92.3**	**94.7**	**91.2**

b) ORTHOPYROXENE

OXIDE	GROUP I	GROUP II	GROUP III	GROUP IV
SiO_2	57.3	57.8	57.7	57.3
TiO_2	<0.03	0.02	<0.03	<0.01
Al_2O_3	2.25	0.80	0.85	1.64
Cr_2O_3	0.44	0.29	0.67	0.40
FeO	2.91	4.66	3.13	5.49
MnO	0.06	0.09	0.06	0.12
MgO	37.2	35.2	37.1	34.57
CaO	0.05	0.28	0.45	0.41
TOTAL	100.24	99.14	99.99	99.93

c) GARNET

OXIDE	GROUP I	GROUP II	GROUP III	GROUP IV
SiO_2	42.4	41.8	41.4	41.98
TiO_2	<0.03	0.06	<0.03	<0.01
Al_2O_3	22.1	21.3	16.5	22.51
Cr_2O_3	4.43	4.16	10.2	2.52
FeO	5.25	7.83	4.68	7.97
MnO	0.38	0.39	0.30	0.41
MgO	25.2	19.7	23.1	20.00
CaO	1.36	5.41	3.93	5.25
TOTAL	101.12	100.65	100.11	100.64

d) SPINEL

OXIDE	GROUP I	GROUP II	GROUP III	GROUP IV
SiO2	0.33	<0.02	0.20	<0.01
TiO2	<0.03	0.40	0.05	0.19
Al2O3	38.4	11.2	8.58	19.98
Cr2O3	30.8	52.1	62.2	46.01
Fe2O3*	1.61	10.62	3.60	-
FeO	6.59	13.54	9.41	20.03
MnO	0.15	0.65	0.28	0.65
MgO	20.3	13.3	15.06	13.04
TOTAL	98.18	101.41	100.38	99.90

e) CLINOPYROXENE

OXIDE	GROUP II	GROUP IV
SiO2	55.1	54.3
TiO2	0.07	0.04
Al2O3	2.17	2.73
Cr2O3	1.78	1.29
FeO	2.14	2.26
MnO	0.06	0.09
MgO	16.4	16.25
CaO	20.7	21.6
Na2O	1.87	1.70
TOTAL	100.29	100.26

GROUP I: PHN 2825 (Nixon et al., 1987)
GROUP II: BD 2379 (Lawless, 1978)
GROUP III: RVD 183 (Danchin and Boyd, 1976)
GROUP IV: 07143 (Robey, 1981)

TABLE 9.1 Mineral compositions characteristic of Groups I, II, II and IV spinel-garnet peridotites from southern Africa.

Table 9.2

Kimberlite	Average Cr^*	$\%Cr^*<0.8$
Dokolwayo	0.896	4.9
Koffiefontein	0.862	3.9
Finsch	0.842	6.7
Kao	0.771	53.8
Rietfontein	0.616	100.0
Melton Wold	0.558	100.0

TABLE 9.2 Table of average Cr* calculated from concentrate spinels for kimberlites in southern Africa. Dokolwayo, Koffiefontein and Finsch are productive diamond mines. Kao has a very low grade. Both Rietfontein and Melton Wold are off-craton kimberlites and are non-diamondiferous.

CHAPTER 9 - FIGURE CAPTIONS

FIGURE 9.1

Locality map of selected kimberlites in southern Africa and their distribution with respect to the Kaapvaal Craton.

FIGURE 9.2

Plot of CaO vs Cr_2O_3 (wt%) for garnets from spinel-garnet peridotites from several southern African kimberlites.

FIGURE 9.3

Plot of pressure versus the Cr/(Cr+Al) ratio (i.e. Cr^*) of spinels for spinel-garnet peridotites from several southern African kimberlites. Pressures were calculated with the Nickel and Green (1985) garnet-orthopyroxene barometer.

FIGURE 9.4

Plot of temperature versus Cr^* of spinels for spinel-garnet peridotites from several southern African kimberlites. Temperatures were calculated with the O'Neill and Wood (1979) garnet-olivine geothermometer.

FIGURE 9.5

Plot of $Al_2O_{3[Orthopyroxene]}$ versus $Cr^*_{[Spinel]}$ for several southern African spinel-garnet peridotites.

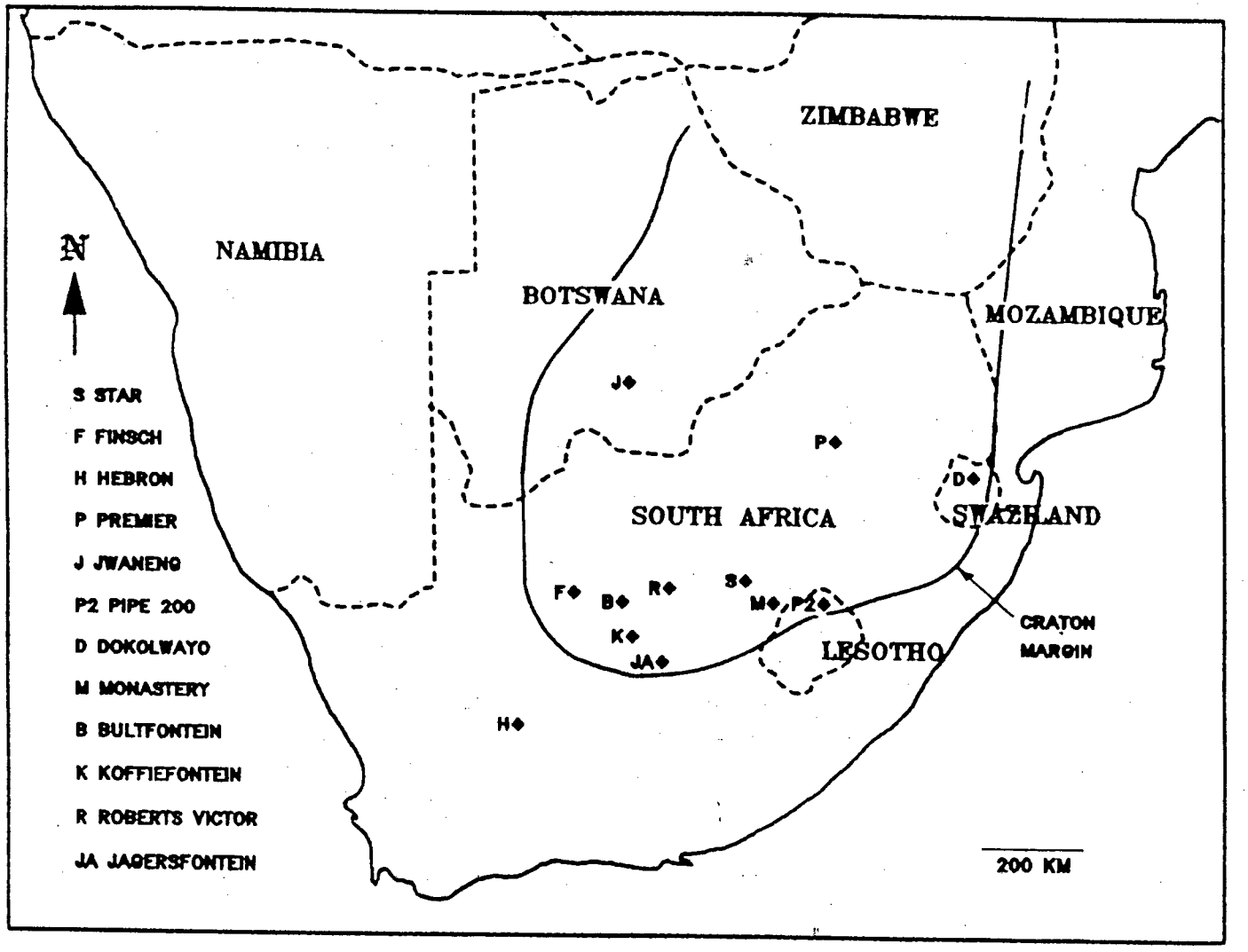
N
NAMIBIA
BOTSWANA
ZIMBABWE
MOZAMBIQUE
SOUTH AFRICA
SWAZILAND
LESOTHO
CRATON MARGIN
200 KM
S STAR
F FINSCH
H HEBRON
P PREMIER
J JWANENG
P2 PIPE 200
D DOKOLWAYO
M MONASTERY
B BULTFONTEIN
K KOFFIEFONTEIN
R ROBERTS VICTOR
JA JAGERSFONTEIN

Fig 9.1

SPINEL-GARNET PERIDOTITES
GARNET COMPOSITIONS

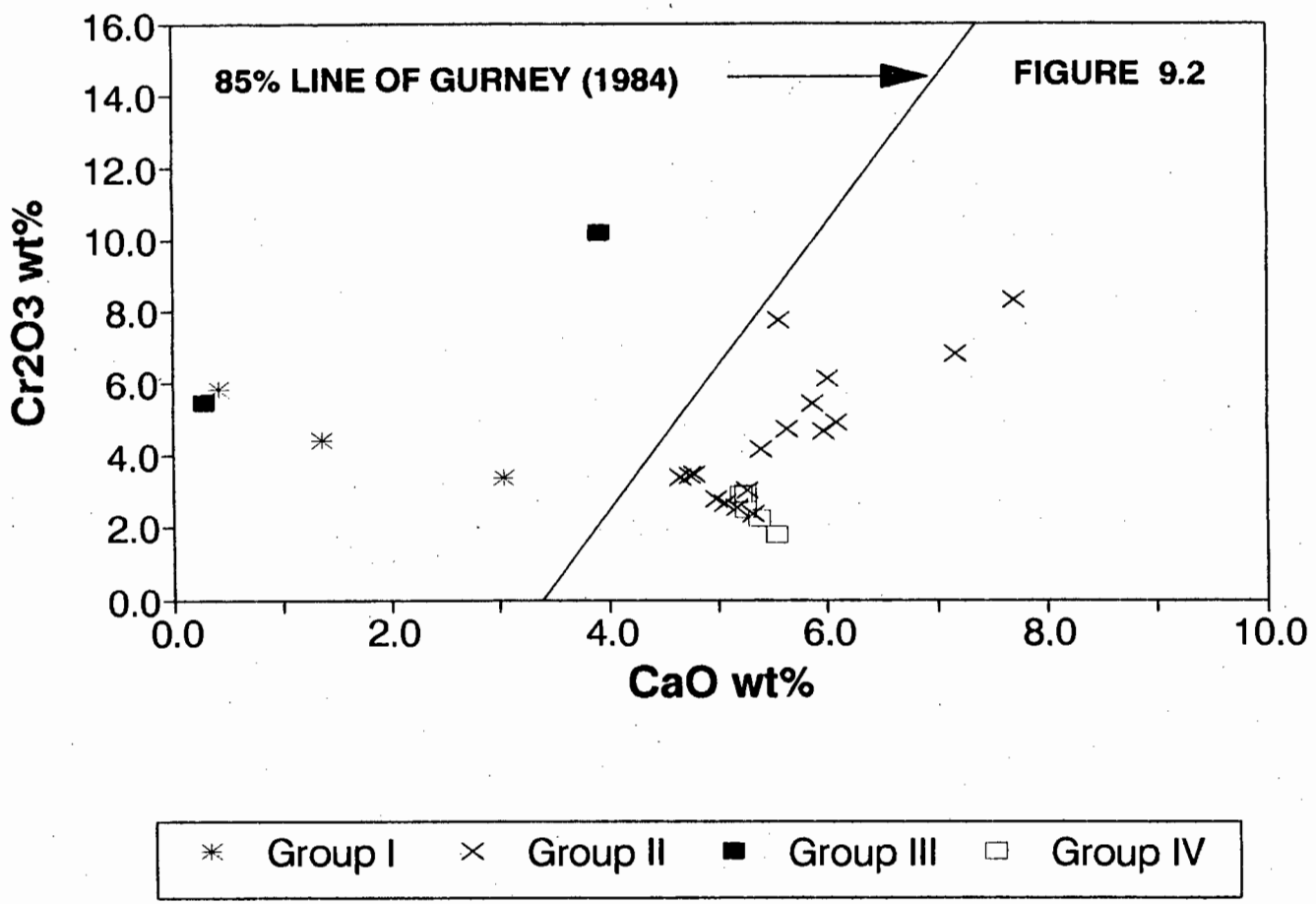

SPINEL-GARNET PERIDOTITES
SOUTHERN AFRICA

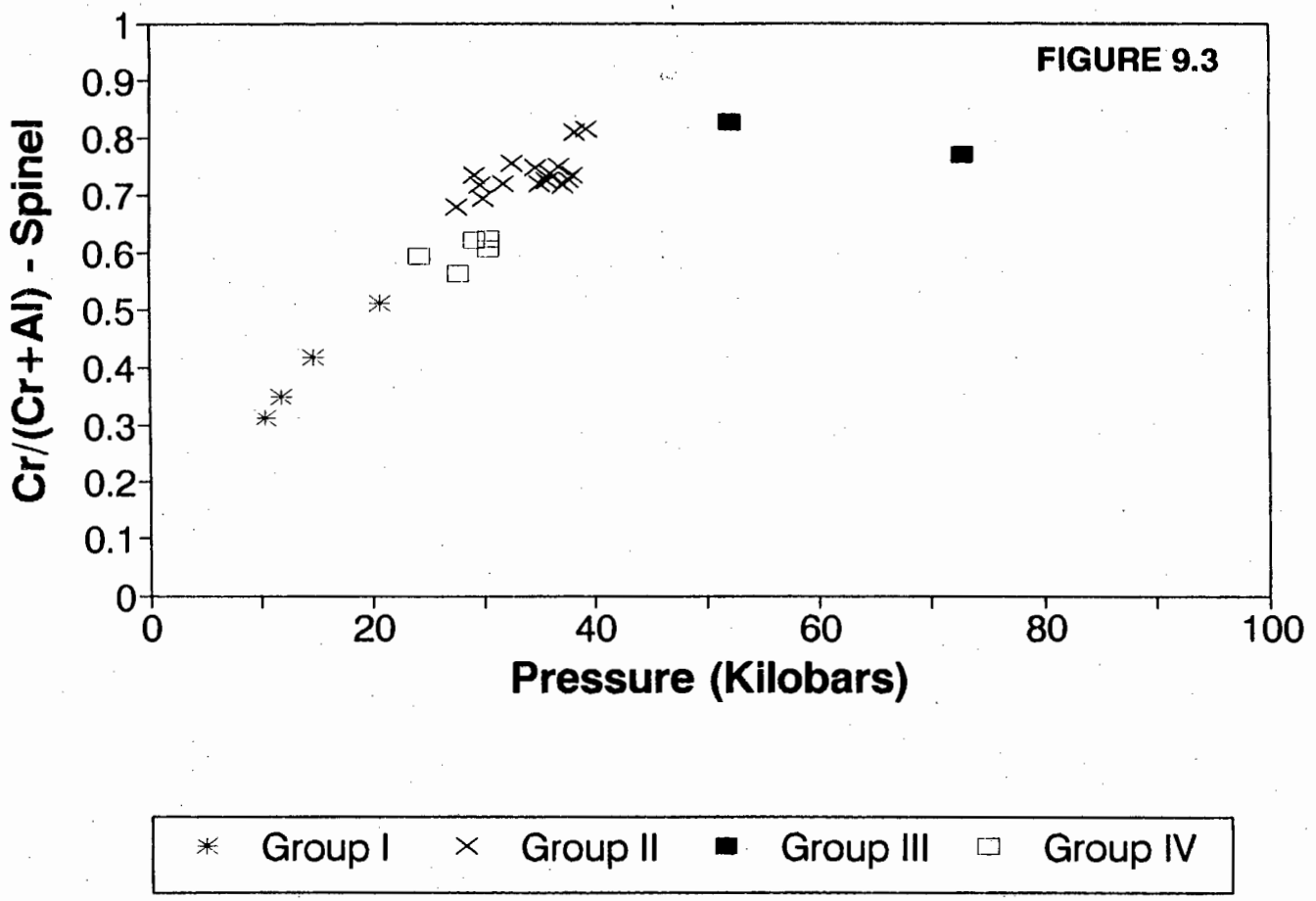

SPINEL-GARNET PERIDOTITES
SOUTHERN AFRICA

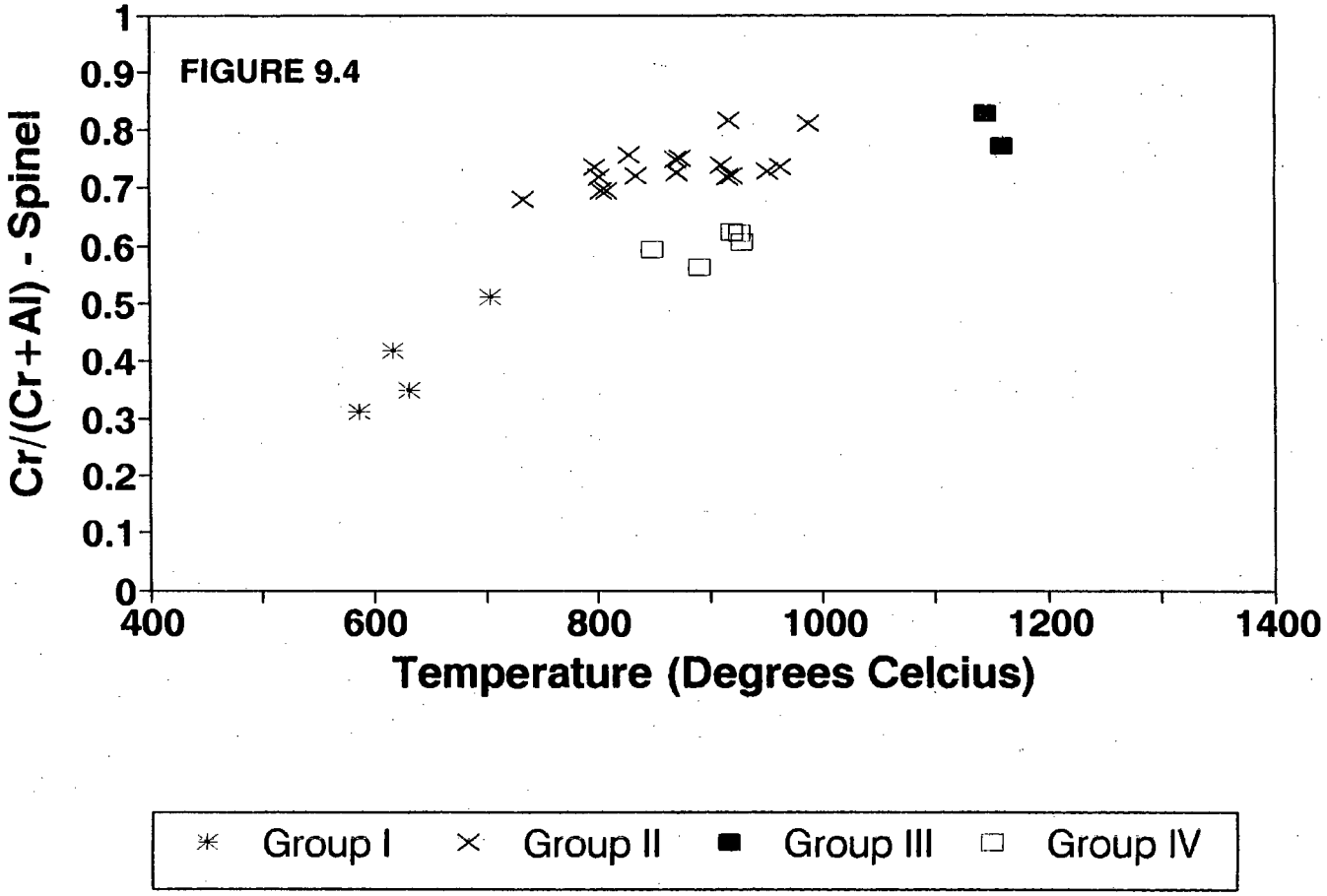

SPINEL-GARNET PERIDOTITES
SOUTHERN AFRICA

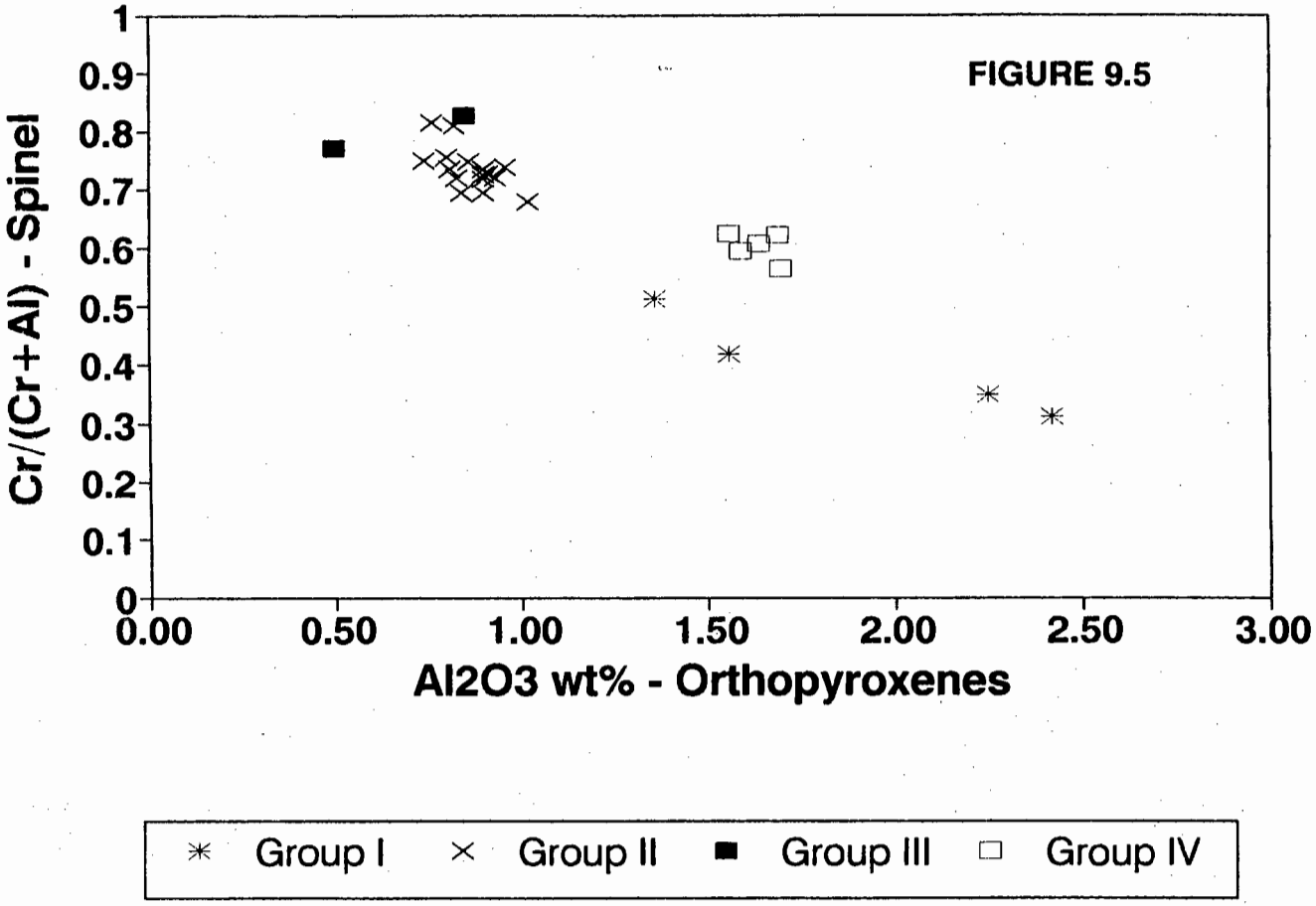

CHAPTER 10 - OXYGEN FUGACITY CONSTRAINTS ON THE SOUTHERN AFRICAN LITHOSPHERE

ASTRACT

Oxygen fugacities are calculated for olivine - spinel ± orthopyroxene assemblages recovered from diamonds and the concentrate of the Dokolwayo kimberlite. In addition, thermobarometric oxygen fugacities are obtained for chrome spinel-garnet peridotites and diamonds from several other southern African kimberlites. The southern African lithosphere appears to be laterally homogeneous with respect to oxygen fugacity. Vertically the oxygen fugacity of the lithospheric upper mantle decreases with an increase in pressure. Locally, oxygen fugacities calculated for Dokolwayo mineral assemblages are indicative of an upper mantle characterised by diverse redox conditions within the range FMQ - IW. Reduced oxygen fugacities calculated for the majority of the Dokolwayo samples suggest that CH_4 may be the dominant carbon volatile species in the lower lithosphere. These reduced conditions also suggest that the Dokolwayo kimberlite is unlikely to be a product of redox melting, but may be the product of a thermal anomaly. Calculated equilibrium temperatures for olivine-spinel pairs from Dokolwayo diamonds and concentrate indicate that the upper mantle in the vicinity of Dokolwayo was characterised by cool subsolidus conditions.

INTRODUCTION

The oxidation state of the mantle is an important parameter, because together with temperature and pressure it strongly affects the nature of melts produced from a given source rock composition (Fisk and Bence 1980; Eggler 1983). In addition, several physical properties of the mantle, e.g. electrical conductivity, diffusivity and mechanical response to deformation, are dependent on the prevailing redox conditions (Duba and Shankland 1982). Furthermore, the oxygen fugacity of the mantle is a relevant parameter in geochemical

models for the accretion of the Earth's crust, core-separation and the evolution of redox conditions following the formation of the core-mantle system. The redox state of the mantle, together with temperature and pressure, also determines to what extent carbon exists as a mantle volatile species (e.g. CO, CO_2, CH_4) or as elemental carbon, i.e. graphite or diamond (Rosenhauer et al. 1977; Deines 1980).

Upper mantle redox conditions have previously been determined either by direct intrinsic measurements or upper mantle-derived spinel peridotites and megacryst assemblages (Ulmer et al. 1976, 1987; Arculus and Delano 1980, 1981; Arculus et al. 1984) or through thermobarometric calculations of upper mantle-derived olivine - orthopyroxene - ilmenite, ilmenite-spinel and olivine-orthopyroxene-spinel assemblages (Eggler 1983; Haggerty and Tompkins 1983; Mattioli and Wood 1986, 1988; O'Neill and Wall 1987). Results obtained from the intrinsic oxygen methods have suggested significant ranges in mantle oxygen fugacities. However, some of the spread obtained from intrinsic methods may be due to autoreduction caused by carbon in mantle xenoliths or individual mineral species (Mathez et al. 1984; Virgo et al. 1988).

The most common method used recently to determine oxygen fugacity conditions in the upper mantle is the thermobarometer developed by O'Neill and Wall (1987) and recently calibrated by Mattioli and Wood (1986, 1988). This method is based on the coexistence of olivine, orthopyroxene and spinel in mantle xenoliths and allows for the calculation of oxygen fugacities and temperatures of the appropriate upper mantle assemblages. The formulations of O'Neill and Wall (1987) were derived from an evaluation of existing data on the thermodynamic properties of each mineral phase defining the equilibrium reaction:

$$3\ Fe_2SiO_4 + O_2 = Fe_3O_4 + 3\ SiO_2$$

and were adopted in this study. The precision of the above method depends on uncertainties in temperature, pressure and the compositions of the constituent phases. For

typical peridotitic compositions and upper mantle temperatures and pressures, an error of ± 100°C in assumed or calculated temperature produces an error of less than ±0.2 log fO_2; ±10 kbar in assumed pressure corresponds to ±0.5 log fO_2 at 1200°K (O'Neill and Wall 1987). The positions of the FMQ, WM and IW buffers in fO_2-T space were calculated at 30 and 50 kilobars pressure using the data of O'Neill (1987, 1988).

The error introduced by uncertainties in the calculated mole fraction Fe_2O_3 from microprobe analyses has received considerable attention (e.g. Dyar et al. 1989; Wood and Virgo 1989). The majority of the mineral compositions used in this study were determined by means of a Cameca Camebax-Microbeam microanalyser with an accelerating voltage of 15kV and a beam current of 40nA. The standards used for the spinel analyses were as follows:

Si	K-P	Kakanui - Pyrope
Ti	RUT	Synthetic Rutile
Al	CHRO	Chromite 52-NL11
Fe	ILMT	Ilmenite, Ilmenite Mountains, USSR
Mn	RHOD	Rhodonite
Ca	K-P	Kakanui - Pyrope
Cr	Cr_2O_3	Pure Cr-oxide

Data reduction was by Cameca ZAF (Henoc et al. 1973). By varying the calculated Fe^{3+} component of the spinels used in this study by 10%, a variation of ±0.2 log fO_2 at 30 kbar was obtained for individual samples. These results are consistent with the results of Mattioli and Wood (1988).

The Dokolwayo kimberlite which is situated in northeastern Swaziland close to the northeastern margin of the Kaapvaal Craton, has the isotopic character of a Group II kimberlite (Smith 1983) and has the preferred emplacement age of 200±5 My (Allsopp and

Roddick 1984). Unlike the majority of kimberlites in southern Africa it predates the Stormsberg volcanism which in the vicinity of Dokolwayo is associated with the Lebombo Monocline. The emplacement age of the Stormsberg volcanics is not well established, but the best estimates are 193±5 My (Manton 1968; Fitch and Miller 1984). The kimberlite is geographically well separated from other established mines in southern Africa (Figure 10.1) and affords the opportunity to investigate pre-Stormsberg upper mantle compositions and conditions on the northeastern margin of the Kaapvaal Craton. The compositions of the concentrate minerals and a number of the diamond inclusions from this locality were briefly described in Daniels and Gurney (1989).

SAMPLES STUDIED

The concentrate spinels (+0.5 - 2 mm) were recovered from heavy mineral concentrates from the mine treatment plant. These spinels occasionally contain silicate inclusions, the majority of which are moderately to severely altered. However, a number of olivine inclusions (N=14) and one orthopyroxene are euhedral in shape and in pristine condition.

The diamond inclusion olivine - spinel ± orthopyroxene assemblages were recovered from diamonds (<2mm) during a general study of Dokolwayo diamond inclusions. Great care was taken to select diamonds which were free of cracks leading to inclusions. The diamonds were cleaned in concentrated HF for 48 hours and the inclusions were extracted from the diamonds by mechanical crushing in an enclosed steel cracker. The analytical procedures are described above (Chapter 2). Representative compositions of the coexisting phases are presented in Table 1.

Both the NiO contents (0.27 - 0.40 wt%) and the range of forsterite compositions (Fo 90.6 - Fo 95.6) of the Dokolwayo olivines from the concentrate spinels and diamonds are within the range reported for olivines from Yakutian diamondiferous harzburgites and dunites (Sobolev et al. 1984) and diamond inclusions worldwide (Meyer 1985).

Most concentrate spinels carrying olivine and orthopyroxene inclusions have compositions within the overall field defined by Dokolwayo concentrate spinels (Figure 10.2), the compositions of the diamond inclusion spinels are typical of Dokolwayo diamonds as well as diamonds worldwide (Figures 10.3a and 10.3b). All the spinels containing olivine as inclusions have $Cr/(Cr+Al) > 0.8$.

Orthopyroxenes recovered from the Dokolwayo diamond (En 94.5) and the concentrate spinel (En 96.2) are similar in composition to diamond inclusion orthopyroxenes recovered from the Finsch, Roberts Victor and Premier kimberlites (Gurney et al. 1979, 1984, 1985).

In addition to the Dokolwayo samples, calculated oxygen fugacities were also obtained for spinel-garnet peridotites from the Premier (Danchin and Boyd 1976), Bultfontein (Lawless 1978), Hebron (Robey 1981), Monastery (Moore 1986) and Jagersfontein (Nixon et al. 1987) kimberlites. The Cretaceous Bultfontein and Proterozoic Premier kimberlites are situated well within the Kaapvaal Craton whereas the Monastery kimberlite is close to the eastern margin of the craton. The Jagersfontein kimberlite is situated on but close to the southwestern margin of the craton and the Hebron kimberlite is off the western margin of the craton (Figure 10.1). The garnets from these xenoliths, excluding those from Premier and Jagersfontein, are characterised by lherzolitic compositions (Figure 10.4). The xenoliths from Premier (RVD 183) and Jagersfontein (PHN 2818b) contain minerals with compositions similar to subcalcic peridotite-suite diamond inclusions on a generalized worldwide basis. Xenolith RVD 183, although not containing any form of elemental carbon, has been suggested to be a potential source rock of diamonds at Premier (Gurney et al. 1985).

Oxygen fugacities were also calculated for olivine - spinel $\pm$ orthopyroxene assemblages recovered from diamonds from the Finsch, Roberts Victor, Koffiefontein, Jwaneng

(Botswana) and Star kimberlites (Gurney et al. 1979, 1984; Rickard et al. 1989; Hill 1989).

RESULTS AND DISCUSSION

Where orthopyroxene was not present in the samples studied, the compositions of an orthopyroxene coexisting with spinel and olivine in a diamond from Dokolwayo (DI 362) and an orthopyroxene found as an inclusion in a concentrate spinel (DCO 70; Table 10.1) have been used in these calculations to determine the activity of SiO_2. If orthopyroxene is indeed absent and these samples represent a dunitic and not a harzburgitic or lherzolitic assemblage, then very low SiO_2 activities can be assumed. Such low SiO_2 activities suggest that any oxygen fugacity estimate from the olivine - spinel pairs is an upper, more oxidized limit (O'Neill, 1988, pers. comm.). The sensitivity of the formulation used to calculate oxygen fugacity has been tested for the Dokolwayo samples during this study. It was found that a change in orthopyroxene composition from En 92 to En 96 resulted in an error of <0.2 log fO_2 for any given olivine - spinel pair.

Equilibrium pressures for the peridotites were calculated using the garnet-orthopyroxene barometer of Nickel and Green (1985). The lherzolitic xenoliths are characterised by equilibrium pressures of 24-38 kbars and the harzburgitic xenoliths have equilibrium pressures in excess of 50 kbars. It is assumed that the diamonds crystallized at a minimum pressure of 50 kilobars. Unfortunately, there are no geobarometers currently available to calculate equilibrium pressures for the Dokolwayo concentrate assemblages. However, the high Cr/(Cr+Al) ratios (>0.8) of these concentrate spinels suggest that they are derived from pressures in excess of 40 kbars (Chapter 9).

The equilibrium temperatures for all the samples are calculated using the olivine-spinel geothermometer of O'Neill and Wall (1987). The lherzolitic xenoliths were characterised by a large range in temperatures (824°C - 1076°C). The difference in equilibrium

temperatures between the two harzburgitic xenoliths is ~150°C. The range in temperatures calculated for the concentrate assemblages extends over approximately 300°C (Table 10.2). The largest range in equilibrium temperatures was calculated for the diamond inclusions. This range of temperatures determined for the diamonds (e.g. K22=855°C; RV29=1363°C) is consistent with equilibrium temperatures calculated from silicate diamond inclusions at the respective localities (Gurney et al. 1979; Rickard et al. 1989).

The lherzolitic xenoliths are all confined to a narrow range of oxygen fugacities between FMQ and WM at 30 kbars (Figure 10.5). Calculating oxygen fugacities for the Dokolwayo concentrate at a constant pressure of 30 kbars produces a significantly wider range in oxygen fugacities (6 log units, Figure 10.5) than obtained from the lherzolitic xenoliths. When calculated at the same pressure of 30kb the concentrate is characterised by fO_2's from FMQ to approaching IW. With the exception of six concentrate spinels from Dokolwayo, all the lherzolitic xenoliths and the concentrate mineral pairs were calculated to have oxygen fugacities more oxidized than WM.

At the more probable pressure of 50kb the Dokolwayo concentrate olivine-spinel pairs also cover a wide range of oxygen fugacities of 5.7 log units from slightly more reduced than FMQ to slightly more oxidized than IW (Figure 10.6). A particular feature of the concentrate spinels is a subgroup characterised by a narrow range in temperature (1024°C - 1087°C) and a wide range of >3 log units in oxygen fugacity. The majority of the concentrate olivine-spinel pairs have oxygen fugacities less than WM at 50 kbar. All the inclusions from diamonds plot below WM at 50 kbar. The harzburgite from Jagersfontein plots at similar fO_2 to the diamonds from Star and Koffiefontein as well as two concentrate spinels from Dokolwayo. The Premier xenolith is characterised by fO_2-T conditions similar to diamonds from Jwaneng and Finsch. Both the Premier and Jagersfontein harzburgites are more reduced than WM. One of the Dokolwayo concentrate spinels and inclusions from two of the Roberts Victor diamonds have very similar log fO_2 values.

Inclusions from Dokolwayo diamonds are amongst the most reduced samples studied and plot close to IW (Figure 10.6).

The oxygen fugacities determined for the lherzolitic spinel-garnet peridotites are confined between FMQ and WM [30 kbar] (Figure 10.5). This observation is in agreement with the results obtained for Lesotho xenoliths by O'Neill and Wall (1987). However, the xenoliths in this study have a much wider geographical distribution with respect to the Kaapvaal Craton. It may be inferred that the lithosphere within the stability field of coexisting lherzolitic garnet and chromium spinel, both on and off the Kaapvaal Craton in southern Africa is characterised by fO_2 conditions between FMQ and WM [30 kbar]. The stability of coexisting lherzolitic garnet and chromium spinel is considered to be unlikely at pressures in excess of 40 kbars (Nickel 1986).

The low oxygen fugacities calculated for the diamond inclusion assemblages, together with the wide geographical distribution across the Kaapvaal Craton of the kimberlites from which the diamonds are derived (Figure 10.1) suggest that reduced mantle conditions (fO_2 < WM [50 kbar]) within the diamond stability field are not a localized phenomenon, but may be the norm in the deeper parts of the craton. It is of interest to note that the two spinel-garnet peridotites that are characterised by mineral compositions and equilibrium pressures and temperatures similar to those found in subcalcic harzburgitic-suite diamonds are distinctly more reduced than their lherzolitic counterparts at the appropriate pressure considerations and plot at similar fO_2-T conditions as the diamonds (Figure 10.6).

The fO_2-T conditions calculated for the Dokolwayo concentrate olivine-spinel pairs cover a wide range of oxygen fugacities and temperatures. This wide range in oxygen fugacities determined for the concentrate suite at both 30 and 50 kbar is approximately 15 times the maximum error calculated at 30 kbar by varying the Fe^{3+} component of the spinels by $\pm 10\%$. The observed fO_2 range is considered to be real and not an artefact of the analytical technique used.

The similarity in the range of fO_2-T conditions between the diamonds and a number of the Dokolwayo concentrate olivine-spinel pairs, together with the high Cr/(Cr+Al) ratios of the concentrate spinels (Chapter 9) suggest that a significant proportion of the concentrate spinels may be derived from within the reduced diamond stability field.

The major species in a C-O-H fluid under upper mantle temperatures and pressures will be almost entirely $CO_2 \pm H_2O$ at all oxygen fugacities at or above WM (Ryabchikov et al. 1981; Woermann and Rosenhauer 1985). However, with increasingly reducing conditions between the WM and IW buffers for fluids carrying abundant H as well as C, the dominant carbon volatile species will change from CO_2 to CH_4 (Taylor and Green 1989). The position of the graphite - CO_2 - CO buffer (GCO) and the maximum mole water fraction (GW) in a peridotite-C-O-H system at upper mantle temperatures and pressures (Taylor and Green 1989) were calculated at 30 and 50 kbar pressure and 800°C and 1400°C and are presented in Figures 10.5 and 10.6. At 30 kbar pressure only one xenolith from Bultfontein (Lawless, 1978) and one concentrate mineral pair from Dokolwayo appears to be derived from an area where CO_2 is the dominant carbon volatile species. The majority of the xenoliths and the concentrate mineral pairs plot at fO_2's below the GCO buffer, but above GW. Five of the Dokolwayo concentrate pairs plot at fO_2's below both GW and WM.

The $fO2$ conditions calculated at 50 kbar pressure for all the diamonds and harzburgites and all but one of the concentrate mineral pairs indicate oxygen fugacities below GW. The oxygen fugacities calculated for the diamond inclusions and for the majority of the Dokolwayo concentrate spinels therefore suggest that they were derived from a reduced area in the upper mantle which was characterised by fluids in which CH_4 and not CO_2 is the dominant carbon volatile species.

A comparison between the oxygen fugacities obtained from the lherzolitic spinel-garnet peridotites and those calculated from diamond inclusions (Figures 10.5 and 10.6) suggests that there is a vertical zonation within the lithosphere with respect to redox conditions. This is indicated by the generally higher oxygen fugacities between FMQ and WM obtained from the shallower spinel-garnet lherzolites and the more reduced oxygen fugacities, WM to IW, obtained from the high pressure diamonds. The results of this study strongly suggest that there is a tendency to a more reduced environment with an increase in depth. Haggerty and Tompkins (1983) and Haggerty and Erlank (1987) have suggested a similar trend for oxygen fugacities in the upper mantle.

In a reduced volatile-saturated peridotite-C-O-H system at pressures above 25 kbar, small additions to the fluid of CH_4 will result in the solidii showing large temperature shifts away from the water-saturated solidus (Taylor and Green 1988). For methane-bearing fluids with $\underline{a}H_2O < 0.9$ the peridotite solidii lie at temperatures above the estimated stable continental geotherm. The equilibrium temperatures determined for the Dokolwayo mineral pairs (Table 10.2) are also indicative of solidus temperatures in a mantle with $\underline{a}H_2O < 0.85$ (Figure 10.7). It may be argued that the temperatures determined from the concentrate olivine-spinel pairs are representative of ambient temperatures in the upper mantle prior to incorporation in the kimberlite, and that these minerals may have equilibrated metamorphically in an open system from much higher original magmatic temperatures. However, diamonds are considered to be chemically inert with respect to diffusion into the diamond by major elements and it is thus assumed that the minerals included by diamonds reflect the prevailing conditions at the time of diamond crystallization. The fO_2-T conditions determined from the Dokolwayo diamond inclusions, therefore, suggest that these diamonds crystallized under reduced subsolidus conditions. Extending this argument to the diamonds with olivine-spinel inclusion pairs from other southern African localities discussed above, it is suggested that this particular suite of diamonds represent subsolidus crystallization in general and that they are xenocrysts in the kimberlite.

The fO_2-T conditions calculated for the Dokolwayo diamonds and the majority of the concentrate spinel-olivine pairs suggest that the deep lithosphere beneath Dokolwayo was characterised by reduced conditions and cool (900°C - 1270°C) subsolidus temperatures prior to incorporation in the kimberlite. The presence of a cool, reduced lithosphere at depth holds implications for the genesis of the Dokolwayo kimberlite. Kimberlite magmatism involving reduced C-O-H fluids is restricted to regions of subcontinental mantle where there is a significant thermal perturbation or, alternatively, where a CH_4-rich fluid undergoes appreciable oxidation, e.g. by interaction with high fO_2 regions in the lithosphere (Taylor and Green 1988). However, if the lower lithosphere is reduced and cool, as indicated by the presence of diamonds and the ambient temperatures determined from the Dokolwayo concentrate olivine-spinel pairs, then it is unlikely that the Dokolwayo kimberlite is the result of oxidation induced melting in the lithosphere. In the absence of conditions that would induce redox melting (Taylor and Green 1988) in the lithosphere to account for the lithospheric isotopic signature of the Dokolwayo kimberlite (Allsopp and Roddick 1984) the most likely cause for kimberlite magmatism would be input of thermal energy. On the basis of isotopic and trace element data, le Roex (1986) has suggested that the Group II kimberlites in southern Africa may be related to asthenospheric hotspots with geochemical characteristics similar to those of the Dupal anomaly in the Southern Atlantic (Hart 1984). These hotspots appear to have a major recycled component in their source regions (le Roex 1986). Such a hotspot could account for the isotopic character of the Dokolwayo kimberlite.

SUMMARY AND CONCLUSIONS

1. The redox conditions of the lithosphere within the stability field of coexisting lherzolitic garnets and chromium spinels in southern Africa are predominantly bound by the FMQ and WM buffers where CO_2 and H_2O are the dominant volatile species.

2. The inclusions of olivine - spinel ± orthopyroxene from Dokolwayo diamonds and other southern African diamonds are more reduced lying between WM and IW.

3. Two garnet-spinel harzburgite xenoliths, from Premier and Jagersfontein mines, lie within the same reduced field.

4. Oxygen fugacities calculated from the concentrate olivine - spinel ± orthopyroxene assemblages from the Dokolwayo kimberlite indicate that they have been derived from an upper mantle characterised by a wide range of redox conditions mainly in the range between WM and IW, but also above WM.

5. The present evidence indicates that the lithosphere of the Kaapvaal Craton may be vertically zoned with respect to oxygen fugacity, the deeper parts being more reduced than the shallower parts, as suggested by Haggerty and Tompkins (1983) and Haggerty and Erlank (1987). However, considering the geographical distribution of the kimberlites from which the lherzolites and the diamonds were recovered, the lithosphere may laterally be relatively homogeneous in oxygen fugacity. This lateral homogeneity is consistent with the observations made by O'Neill and Wall (1987) for the lithosphere beneath Western Europe and Eastern Australia.

6. The observed vertical zonation in oxygen fugacities is closely linked to the distribution of volatile species in the upper mantle. The results of this study suggest that at 30 kilobars pressure H_2O is more dominant than CO_2. At 50 kilobars pressure in the upper mantle it would appear that if any volatiles are present then CH_4 would be the dominant species. Additional evidence to this effect is the presence of Dokolwayo concentrate spinels with possible divalent chromium (Daniels and Gurney 1989), indicative of highly reduced conditions.

7. The subsolidus temperatures calculated from the olivine-spinel diamond inclusions from several southern African kimberlites strongly suggests that diamonds with spinel inclusions are not cogenetic with the kimberlites, but are xenocrystic, which is consistent with the observations of Richardson et al. (1984).

Table 10.1 Dokolwayo concentrate spinel-olivine-orthopyroxene assemblages

	DCO 7 Olv	DCO 7 Spn	DCO 21 Olv	DCO 21 Spn	DCO 26 Olv	DCO 26 Spn
SiO_2	41.59	0.01	39.52	0.01	40.33	0.01
TiO_2	0.01	0.67	0.01	2.49	0.01	1.63
Al_2O_3	0.01	8.32	0.01	3.59	0.01	3.87
Cr_2O_3	0.01	58.33	0.01	61.37	0.06	65.09
Fe_2O_3	-	6.58	-	4.20	-	0.87
FeO	4.95	10.09	9.20	14.40	5.76	14.43
MnO	0.0	10.20	0.15	0.36	0.08	0.20
MgO	53.28	15.27	49.71	12.95	52.65	12.40
CaO	0.01	0.01	0.01	0.01	0.03	0.01
NiO	0.36	0.11	0.35	0.08	0.33	0.09
TOTAL	100.23	99.59	98.97	99.46	99.26	98.60

	DCO 34 Olv	DCO 34 Spn	DCO 38 Olv	DCO 38 Spn	DCO 70 Opx	DCO 70 Spn
SiO_2	40.50	0.01	41.26	0.01	57.91	0.01
TiO_2	0.01	0.01	0.01	1.38	0.01	0.12
Al_2O_3	0.01	9.48	0.01	2.08	0.41	7.77
Cr_2O_3	0.08	62.10	0.04	66.45	0.43	65.04
Fe_2O_3	-	1.19	-	3.19	-	2.55
FeO	5.77	12.63	5.51	12.48	2.65	10.00
MnO	0.07	0.21	0.01	0.21	0.01	0.20
MgO	53.01	13.32	53.02	13.45	37.86	15.06
CaO	0.01	0.01	0.01	0.01	0.27	0.01
Na_2O	-	-	-	-	0.06	0.01
K_2O	-	-	-	-	0.01	-
NiO	0.40	0.07	0.04	0.10	-	0.01
TOTAL	99.86	99.03	99.91	99.36	99.62	100.78

TABLE 10.2 - Equilibration temperatures for Dokolwayo spinel - olivine mineral pairs.

SAMPLE NO	**Temp (°C)** (30 Kbars)	**Temp(°C)** (50 Kbars)
DCO 7	1036	1072
DCO 21	1219	1257
DCO 22	1050	1084
DCO 25	1053	1087
DCO 26	923	954
DCO 28	1011	1044
DCO 31	990	1024
DCO 33	1023	1056
DCO 34	907	938
DCO 37	1009	1043
DCO 38	1029	1061
DCO 61	999	1031
DCO 62	1012	1045
DCO 67	1034	1068
DI 310	1225	1266
DI 362	1043	1081

All temperatures are calculated by the method of O'Neill and Wall (1987).

DCO = Dokolwayo heavy mineral concentrate
DI = Dokolwayo diamond inclusion

CHAPTER 10 - FIGURE CAPTIONS

FIGURE 10.1

Locality map of selected kimberlites in southern Africa and their distribution with respect to the Kaapvaal Craton.

FIGURE 10.2

Plot of MgO versus Cr_2O_3 (wt%) for Dokolwayo concentrate spinels showing the compositional relationship between the concentrate spinels with inclusions (*) and the Dokolwayo concentrate spinel population as a whole.

FIGURE 10.3

Plot of MgO versus Cr_2O_3 (wt%) demonstrating the relationship between (A) the Dokolwayo diamond inclusion spinels used in this study (+) and the Dokolwayo diamond inclusion spinel population and (B) between the Dokolwayo diamond inclusion spinel population and diamond inclusions world wide.

FIGURE 10.4

Plot of CaO versus Cr_2O_3 (wt%) for garnets from spinel-garnet peridotites from several southern African kimberlites. Symbols are carried through to Figure 10.5.

FIGURE 10.5

Southern African lithospheric oxygen fugacities recorded by olivine-spinel $\pm$ orthopyroxene assemblages from kimberlite concentrate (c) and spinel-garnet lherzolites relative to the QFM buffer and plotted against temperature. Oxygen fugacities and temperatures were calculated using the formulations of O'Neill and Wall (1987). Also shown is the position of some common oxygen buffers. A pressure of 30 kilobars was assumed for all mineral assemblages and buffer curves.

FIGURE 10.6

Southern African lithospheric oxygen fugacities recorded by olivine-spinel ± orthopyroxene assemblages from diamonds (*), kimberlite concentrate (c) and spinel-garnet harzburgites (x) relative to the QFM buffer and plotted against temperature. Oxygen fugacities and temperatures were calculated using the formulations of O'Neill and Wall (1987). Also shown is the position of some common oxygen buffers. A pressure of 50 kilobars was assumed for all mineral assemblages and buffer curves. J = Jwaneng; Ja = Jagersfontein; K = Koffiefontein; R = Roberts Victor; S = Star; P = Premier; F = Finsch; D = Dokolwayo.

FIGURE 10.7

Pressure and temperature projection of the P-T-aH_2O solidus surface for the system peridotite-C-O-H (graphite/diamond present). Solidi for H_2O activities of ~0, 0.35, 0.70, 0.85 and the H_2O maximum are shown. CG: Continental Geotherm; G: Graphite; D: Diamond. (After Taylor and Green 1989).

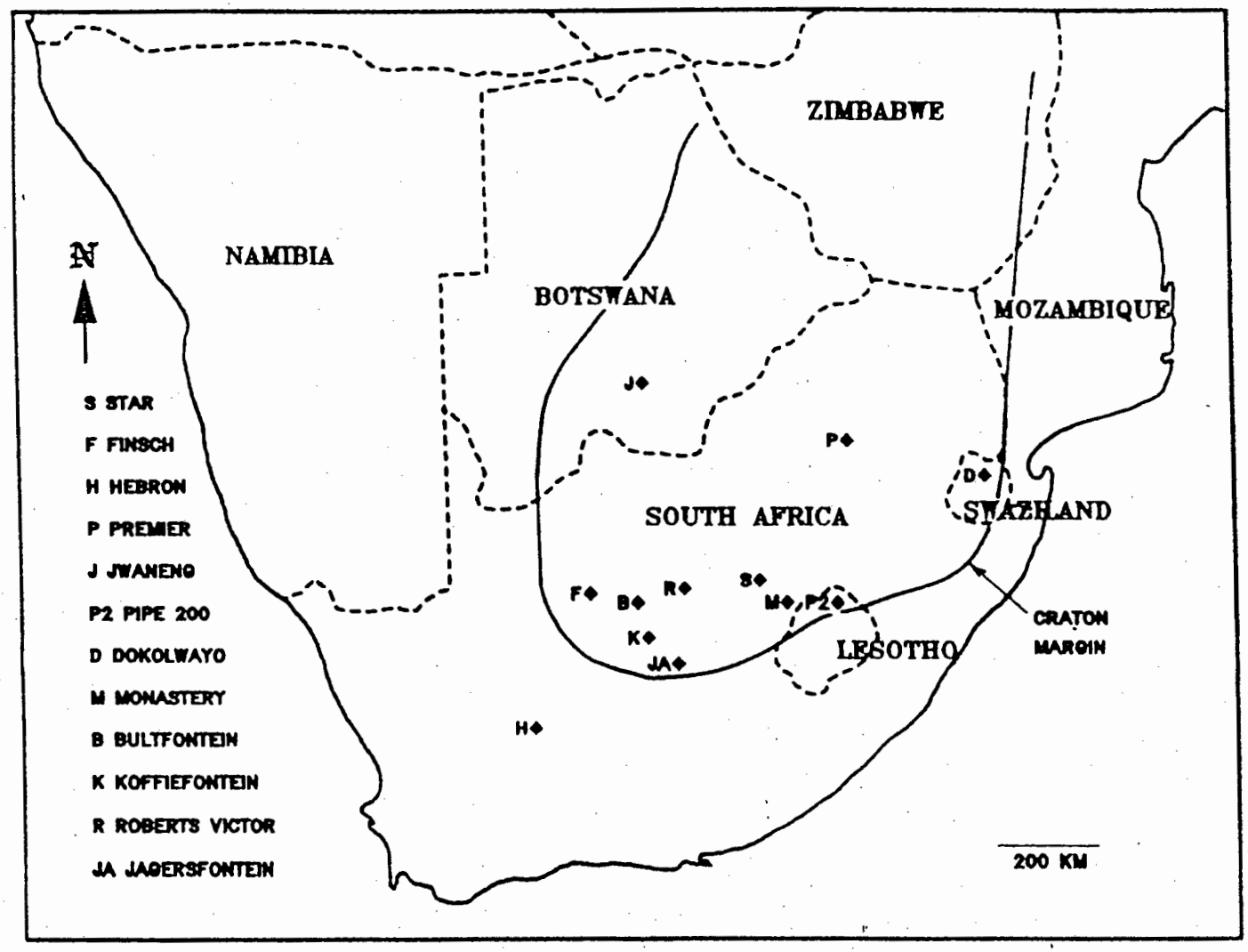
N
NAMIBIA
BOTSWANA
ZIMBABWE
MOZAMBIQUE
SOUTH AFRICA
SWAZILAND
LESOTHO
CRATON MARGIN
S STAR
F FINSCH
H HEBRON
P PREMIER
J JWANENG
P2 PIPE 200
D DOKOLWAYO
M MONASTERY
B BULTFONTEIN
K KOFFIEFONTEIN
R ROBERTS VICTOR
JA JAGERSFONTEIN
200 KM

Fig 10·1

Figure 10.2

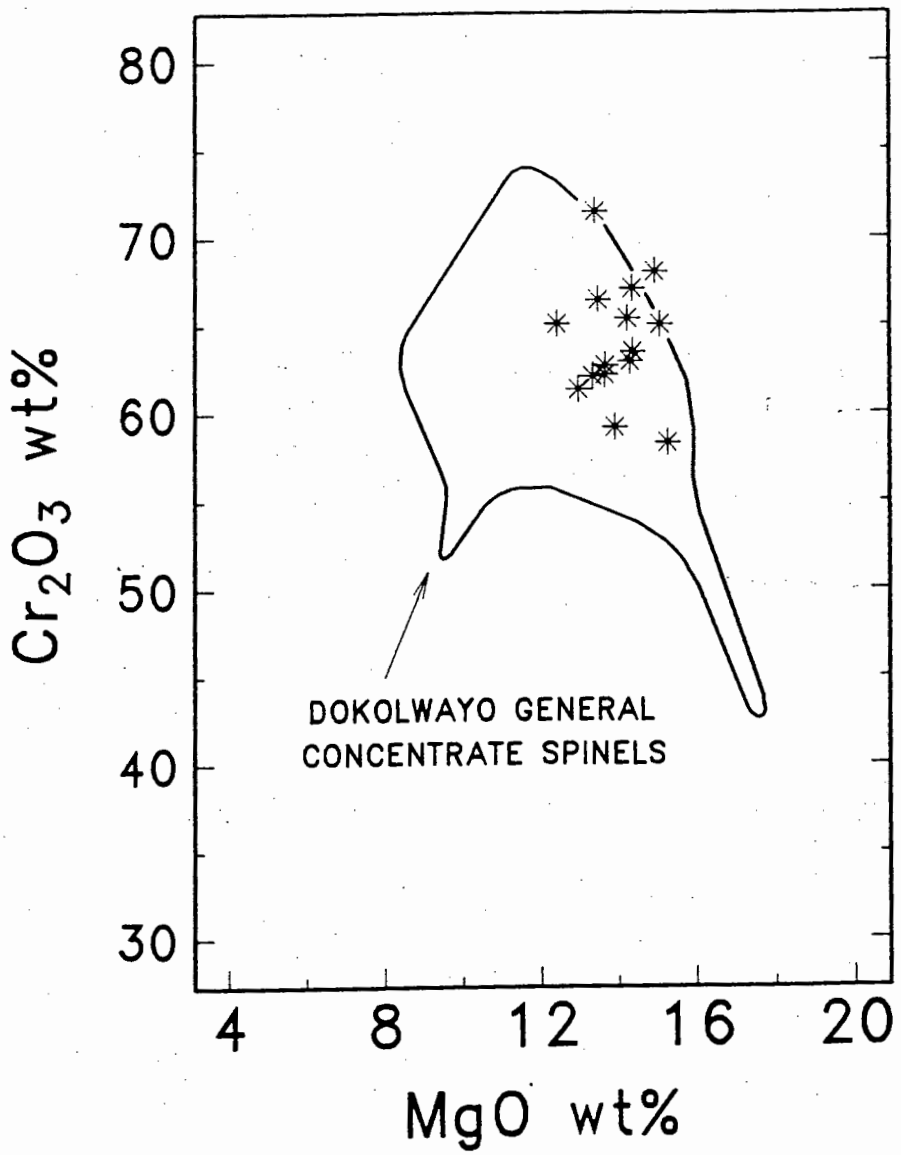
80
70
60
50
40
30
Cr_2O_3 wt%
4
8
12
16
20
MgO wt%
DOKOLWAYO GENERAL
CONCENTRATE SPINELS

Figure 10.3

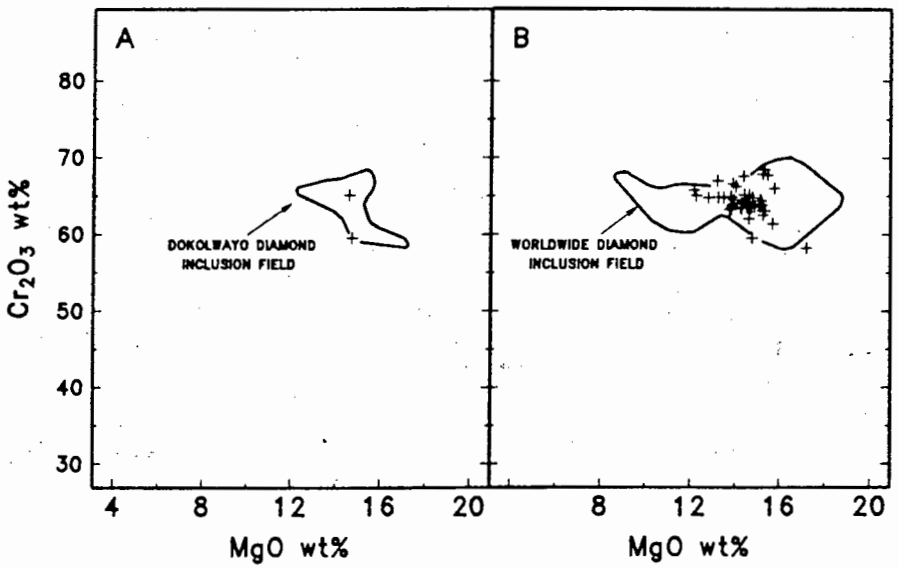
A
B
80
70
60
50
40
30
Cr_2O_3 wt%
DOKOLWAYO DIAMOND
INCLUSION FIELD
WORLDWIDE DIAMOND
INCLUSION FIELD
4
8
12
16
20
MgO wt%
MgO wt%

Figure 10.4

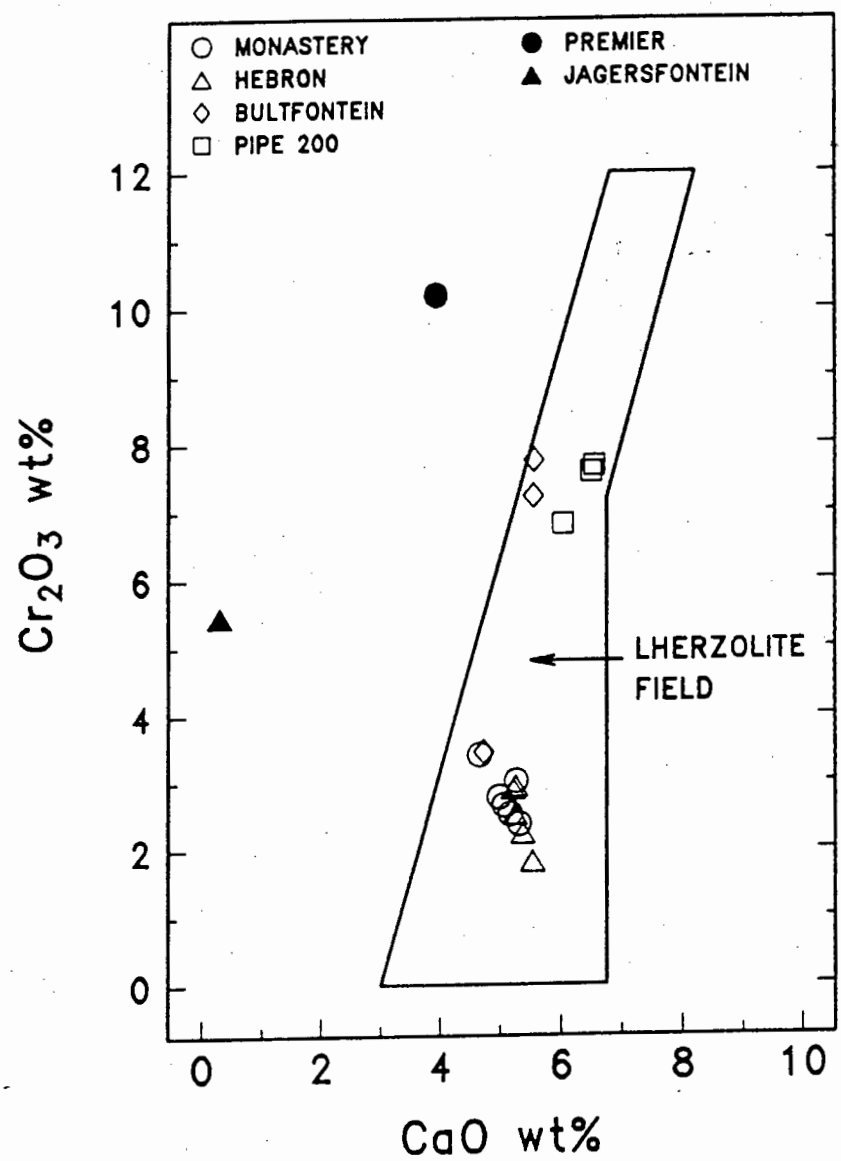
MONASTERY
HEBRON
BULTFONTEIN
PIPE 200
PREMIER
JAGERSFONTEIN
LHERZOLITE FIELD
Cr_2O_3 wt%
CaO wt%
0
2
4
6
8
10
12

Southern African Oxygen Fugacities

30 kilobars

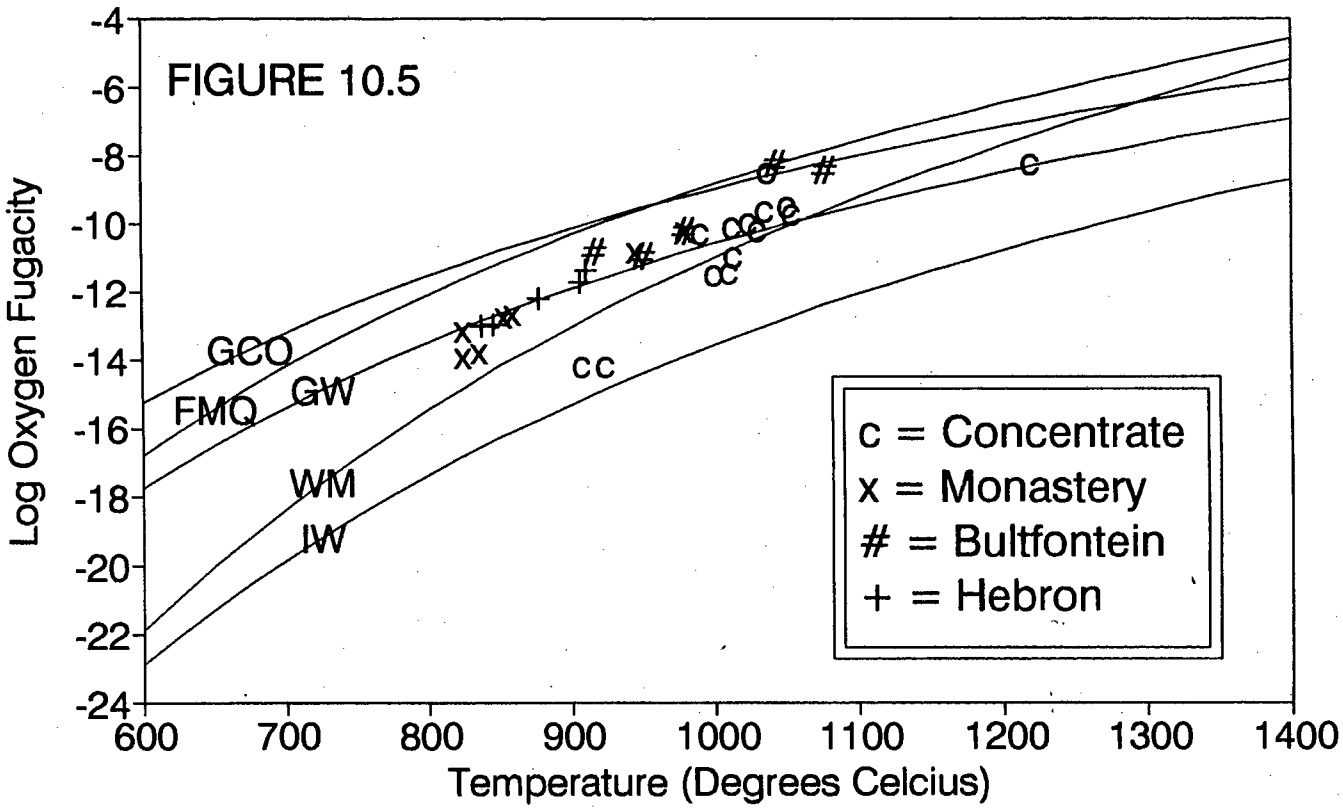

Southern African Oxygen Fugacities

50 Kilobars

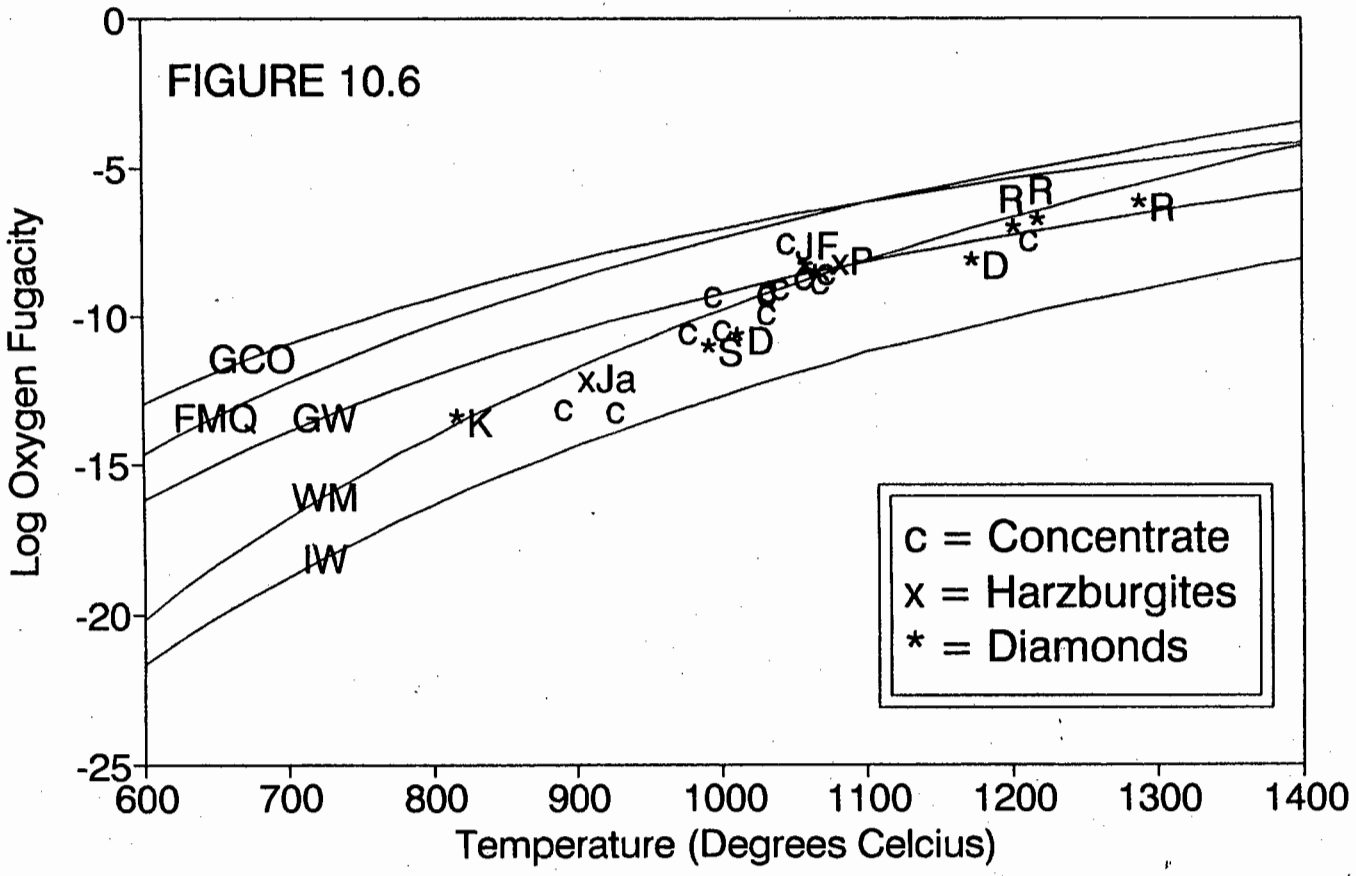

Figure 10.7

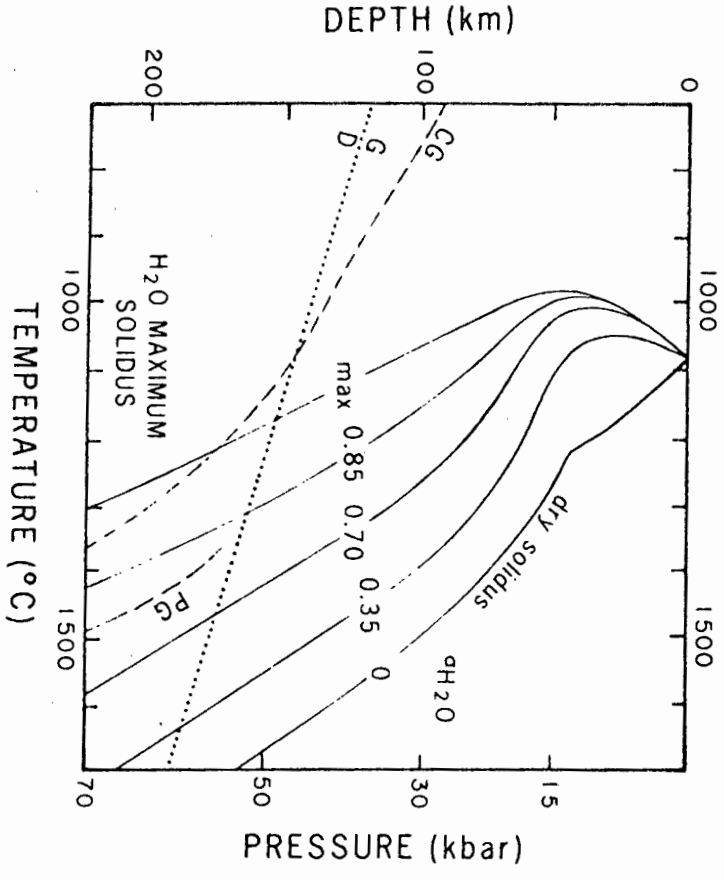
DEPTH (km)
200
100
0
1000
1500
TEMPERATURE (°C)
70
50
30
15
PRESSURE (kbar)
H2O MAXIMUM SOLIDUS
max
0.85
0.70
0.35
0
dry solidus
aH2O
G
D
GG
PG

CHAPTER 10 - ADDENDUM

OXYGEN FUGACITY CONSTRAINTS ON THE SOUTHERN AFRICAN LITHOSPHERE: ADDENDUM

INTRODUCTION

Daniels and Gurney (1991) reported oxygen fugacities for olivine - spinel ± orthopyroxene assemblages in lherzolites, harzburgites, diamonds and concentrate from several southern African kimberlites. The method used by these authors to calculate oxygen fugacities (fO_2's) was the thermodynamically derived oxybarometer of O'Neill and Wall (1987). Recently Ballhaus et al. (1990, 1991) equilibrated synthetic spinel harzburgite and lherzolite assemblages between 1040°C and 1300°C and 3 to 27 kilobars under controlled fO_2. A semi-empirical oxygen barometer in terms of divergence from the fayalite - magnetite - quartz (FMQ) buffer was derived through a linear least squares fit to the experimental data. Ballhaus et al. (1990, 1991) suggested that the O'Neill and Wall (1987) formulations (1) underestimate fO_2 by about two log units at the magnetite-hematite buffer (MH) and (2) the corrections for Cr-Fe^{3+} size mismatch are too small resulting in Cr-spinels calculating up to 1.5 log units lower than Al-spinels at a given observed fO_2. The data of Daniels and Gurney (1991) have been recalculated using the semi-empirical formulations of Ballhaus et al. (1991), both for fO_2 and temperature. The positions of the FMQ, WM and IW buffers in fO_2-T space were calculated at 30 and 50 kilobars pressure using the data of O'Neill (1987, 1988). The positions of the graphite -CO_2 - CO buffer (GCO) and the maximum mole water fraction (GW) in a peridotite-C - O - H system at upper mantle temperatures (Taylor and Green, 1989) are also presented.

SAMPLE DESCRIPTIONS AND LOCALITIES

Oxygen fugacities were obtained for:

1) Garnet-spinel lherzolites from the on-craton Bultfontein, Monastery and Schuller kimberlites (Lawless, 1978; Moore, 1986; De Bruin, 1991).

2) Garnet-spinel lherzolites from the off-craton Hebron kimberlite (Robey, 1981).

3) Subcalcic garnet-spinel harzburgites from the Premier (Danchin and Boyd, 1976) and Jagersfontein (Nixon et al., 1987) kimberlites.

4) Olivine-spinel diamond inclusion pairs from the Finsch, Roberts Victor, Koffiefontein, Jwaneng (Botswana), Star and Dokolwayo (Swaziland) kimberlites (Gurney et al., 1979, 1984; Hill, 1989; Rickard et al., 1989; Daniels and Gurney, 1991).

5) Macrocryst concentrate spinels with olivine inclusions from the Dokolwayo kimberlite (Figure 10A.1; Daniels and Gurney, 1991).

RESULTS

The lherzolitic xenoliths are all confined within a narrow range of oxygen fugacities around FMQ (30 kbar; Figure 10A.2). The majority of these xenoliths have calculated oxygen fugacities immediately above FMQ, but are more reduced than the GCO buffer. The most oxidized xenolith is from Bultfontein with an oxygen fugacity of 1.45 log units above FMQ. Lherzolites from the Monastery and Hebron kimberlites, on and off the Kaapvaal craton respectively, have similar oxygen fugacities. Only one lherzolite from Schuller is more reduced than GW.

The concentrate spinel-olivine pairs from the Dokolwayo kimberlite span both a wide range in temperatures (~300°C) and in oxygen fugacity (5.8 log units). However, the range in oxygen fugacities relative to FMQ is only in the order of 4.3 log units. Two of the concentrate pairs approach the WM buffer and are more reduced than GW. AT 30 kilobars the majority of the Dokolwayo concentrate assemblages are more oxidized than GCO. However, the high Cr\(Cr+Al) ratios (>0.8) of these concentrate spinels suggests that they are derived from pressures well in excess of 40 kilobars (Chapter 9).

At 50 kilobars the Dokolwayo concentrate spinel-olivine pairs cover a wide range of oxygen fugacities of 5. 5 log units from more oxidized than FMQ to WM (Figure 10A.3). Excepting one, all the concentrate pairs are more reduced than the GCO buffer. All the inclusions from diamonds and the subcalcic harzburgites from Jagersfontein and Premier are more reduced than FMQ and GCO. One of the Dokolwayo diamonds (DI 310) is more reduced than WM. The other Dokolwayo diamond (DI 362), the harzburgite from Jagersfontein and two concentrate spinel-olivine pairs from Dokolwayo are more reduced than GW.

DISCUSSION

Calculating oxygen fugacities with the use of the oxygen barometer of Ballhaus et al. (1990, 1991) suggest that the southern African lithosphere is more oxidized than initially estimated by Daniels and Gurney (1991) when using the formulations of O'Neill and Wall (1987). The present results indicate that the Kaapvaal lithosphere within the stability field of coexisting lherzolitic garnet and chromium spinel, both on and off the craton is in general slightly more oxidized than FMQ, but more reduced than GCO. It is unlikely that lherzolitic garnets and chromium spinels coexist at pressures in excess of 40 kilobars (Nickel, 1986).

The oxygen fugacities calculated for the diamond inclusion assemblages are generally more reduced with reference to FMQ than the fO_2's calculated for the lherzolites. The similarity between the fO_2 conditions calculated for the subcalcic harzburgites and diamond inclusions is consistent with the observations of Daniels and Gurney (1991) that reduced conditions may prevail in the deeper parts of the Kaapvaal craton and that the craton may be progressively more reduced with depth. In an oxidized mantle near FMQ, diamond is not a stable phase above 50 kilobars on the continental geotherm and fluids are H_2O-CO_2 mixtures (Taylor and Green, 1989). Significantly, all the diamonds used in this study have estimated fO_2's more reduced than GCO and FMQ at 50 kilobars, suggesting the presence of elemental carbon and CH_4, and not CO_2, as the main carbon-species at these depths over large parts of the Kaapvaal Craton.

The spinel-olivine concentrate pairs from the Dokolwayo kimberlite covers a range of fO_2's in excess of 4 log units relative to FMQ. The presence of concentrate spinels that are deficient in Fe^{3+} and may contain Cr^{2+} (Table 10a.1; Daniels and Gurney, 1989) suggests that the mantle sampled by the Dokolwayo kimberlite may be reduced as low as IW and that the total range in mantle oxygen fugacities at this locality far exceeds four log units fO_2. It should be noted that the presence of Cr^{2+} in spinels does not imply that Fe should be present in its native state. Reduction potentials indicate that Cr^{3+} will reduce to Cr^{2+} before Fe^{2+} reduces to native iron. It is likely that the transition of Cr^{3+} to Cr^{2+} occurs at the IW buffer. An oxygen fugacity range of four log units in the upper mantle cannot be reconciled with a single buffer reaction such as FMQ or GCO (Ballhaus et al., 1990). One alternative to single buffer reactions in the mantle is sliding Fe^{2+}/Fe^{3+} equilibria. However, while Fe^{2+}/Fe^{3+} equilibria do provide effective fO_2 buffering above ~FMQ+1, they are inefficient below FMQ (Ballhaus et al., 1990). The majority of the samples from Dokolwayo and from the Kaapvaal craton as a whole is more reduced than FMQ+1 (Figures 10A.2, 3) which suggests that Fe^{2+}/Fe^{3+} equilibria does not act as an efficient buffer in the Kaapvaal craton, particularly at depth.

One of the Dokolwayo diamonds (DI362) and two of the concentrate spinel-olivine pairs are more reduced than GW at 50 kilobars which implies that CH_4 is the dominant carbon volatile species in parts of the mantle below Dokolwayo. The presence of CH_4 in the mantle is consistent with the estimated fO_2 conditions for the subcalcic harzburgite from Jagersfontein. In contrast, a concentrate spinel-olivine mineral pair from Dokolwayo has an estimated fO_2 > FMQ+1, suggesting the absence of elemental carbon and that CO_2 is the dominant carbon volatile species.

The wide range in oxygen fugacities from Dokolwayo indicates that the mantle is poorly buffered. In the absence of a single operating oxygen buffer or Fe^{2+}/Fe^{3+} equilibria control on oxygen fugacity in the mantle it is suggested that an open-system buffering (Ballhaus et al., 1990) through pervasive C-H-O degassing prevails.

Daniels and Gurney (1991) have argued that the diamonds with spinel inclusions are xenocrysts in the kimberlites. Elsewhere it has been shown that peridotitic diamonds may be Archaean in age (Richardson et al., 1984). A detailed study of the geology of Swaziland suggests that the extrusion of the 3.5 billion year old Onverwacht Volcanics was the last major melting event affecting the mantle prior to the eruption of the Jurassic Dokolwayo kimberlite. It is therefore likely that the Dokolwayo kimberlite sampled the residue of an Archaean melting event. The spinel-olivine inclusions from the Dokolwayo diamonds are essentially derived from chemically "closed" systems since the diamonds are impermeable to major element re-equilibration. In contrast, the concentrate spinel-olivine pairs can be viewed as "open" systems which re-equilibrate to accommodate changes in prevailing conditions in the mantle and may therefore be a record of changing conditions in the mantle from the Archaean to the Jurassic. Both the concentrate spinels and the diamonds from Dokolwayo are derived from pressures in excess of 45 kilobars (Kennedy and Kennedy, 1976; Chapter 9). The similarity in fO_2's and temperatures calculated for the Dokolwayo diamonds and some of the associated concentrate mineral pairs suggests that parts of the mantle may not have changed significantly in fO_2-T conditions from the

Archaean to the Jurassic. This observation is consistent with the preservation of diamonds in the lithosphere until sampled by the Dokolwayo kimberlite.

SUMMARY AND CONCLUSIONS

1. Oxygen fugacities calculated form spinel-olivine mineral pairs using the semi-empirical formulations of Ballhaus et al. (1990, 1991) suggest a significantly more oxidized Kaapvaal lithosphere than fO_2's calculated with the thermodynamically derived method of O'Neill and Wall (1987).

2. Recalculating the data of Daniels and Gurney (1991) using the formulations of Ballhaus et al. (1990; 1991) indicates that within the stability field of garnet-spinel lherzolites redox conditions in the lithosphere are generally slightly more oxidized than FMQ.

3. Oxygen fugacities from spinel-olivine inclusions from southern African diamonds and from subcalcic garnet-spinel harzburgites suggest more reduced conditions from $fO_2 <$ QFM to $fO_2 <$ WM at 50 kilobars. All these assemblages are more reduced than GCO and may have $fO_2 <$ GW. At pressures in excess of 50 kilobars CH_4 and elemental carbon and not CO_2 is the dominant carbon species.

4. The wide geographical distribution of the kimberlites from which these diamonds and xenoliths are derived is consistent with the suggestion of Daniels and Gurney 1991 that laterally the Kaapvaal lithosphere may approach homogeneity with respect to fO_2 while there appears to be a general decrease in fO_2 with an increase in pressure.

5. Locally the fO_2 of the lithosphere may vary by >4 log units, thus eliminating fO_2 control by single buffer reactions. The reduced nature of the Kaapvaal lithosphere at depth ($fO_2 <$ QFM) suggests that Fe^{2+}/Fe^{3+} equilibria do not provide effective fO_2 buffering. It is suggested that an open-system buffering through pervasive C-H-O degassing prevails.

6. A single kimberlite may sample areas of the lithosphere where CH_4 and CO_2 are respectively the dominant carbon volatile species. This is the case for the Dokolwayo kimberlite.

7. The fO_2-T conditions of the Kaapvaal lithosphere may not have changed significantly from the Archaean until it was sampled by the Dokolwayo kimberlite.

TABLE 10A.1

	SAMPLE NUMBER					
	CHR-35	CHR-35*	CHR-54	CHR-54*	CHR-76	CHR-76*
OXIDE	(Weight Percent)					
TiO_2	1.06	1.06	0.13	0.13	N.D	N.D.
Al_2O_3	3.46	3.46	2.64	2.64	1.01	1.01
Cr_2O_3	68.19	67.72	71.47	69.89	73.87	72.58
FeO	14.05	14.05	13.07	13.07	12.69	12.69
MnO	0.24	0.24	0.24	0.24	0.27	0.27
MgO	12.03	12.03	11.28	11.28	11.58	11.58
NiO	0.14	0.14	N.D.	N.D.	N.D.	N.D.
CrO	-	0.46	-	1.62	-	1.34
TOTAL	**99.17**	**99.16**	**98.83**	**98.87**	**99.42**	**99.47**

* Recalculated analyses.

N.D. Not Detected

Table 10A.1: Analyses of selected Dokolwayo concentrate spinels deficient in Fe^{3+} and divalent cations with recalculated analyses reflecting possible CrO concentrations.

CHAPTER 10 ADDENDUM - FIGURE CAPTIONS

FIGURE 10A.1

Locality map of selected kimberlites in southern Africa and their distribution with respect to the Kaapvaal Craton.

FIGURE 10A.2

Southern African lithospheric oxygen fugacities recorded by olivine-spinel ± orthopyroxene assemblages from the Dokolwayo kimberlite concentrate (c) and spinel-garnet peridotites plotted against temperature. Oxygen fugacities and temperatures were calculated using the formulations of Ballhaus et al. (1990, 1991). Also shown is the position of some common oxygen buffers (QFM, WM, IW, GCO and GW). A pressure of 30 kilobars was assumed for all mineral assemblages and buffer curves.

FIGURE 10A.3

Southern African lithospheric oxygen fugacities recorded by olivine-spinel ± orthopyroxene assemblages from diamonds (*), kimberlite concentrate (c) and spinel-garnet harzburgites (x, RVD 183 and PHN 2818b) plotted against temperature. Oxygen fugacities and temperatures were calculated using the formulations of Ballhaus et al. (1990, 1991). Also shown is the position of some common oxygen buffers (QFM, WM, IW, GCO and GW). A pressure of 50 kilobars was assumed for all mineral assemblages and buffer curves. J = Jwaneng; Ja = Jagersfontein; K = Koffiefontein; R = Roberts Victor; S = Star; P = Premier; F = Finsch; D = Dokolwayo.

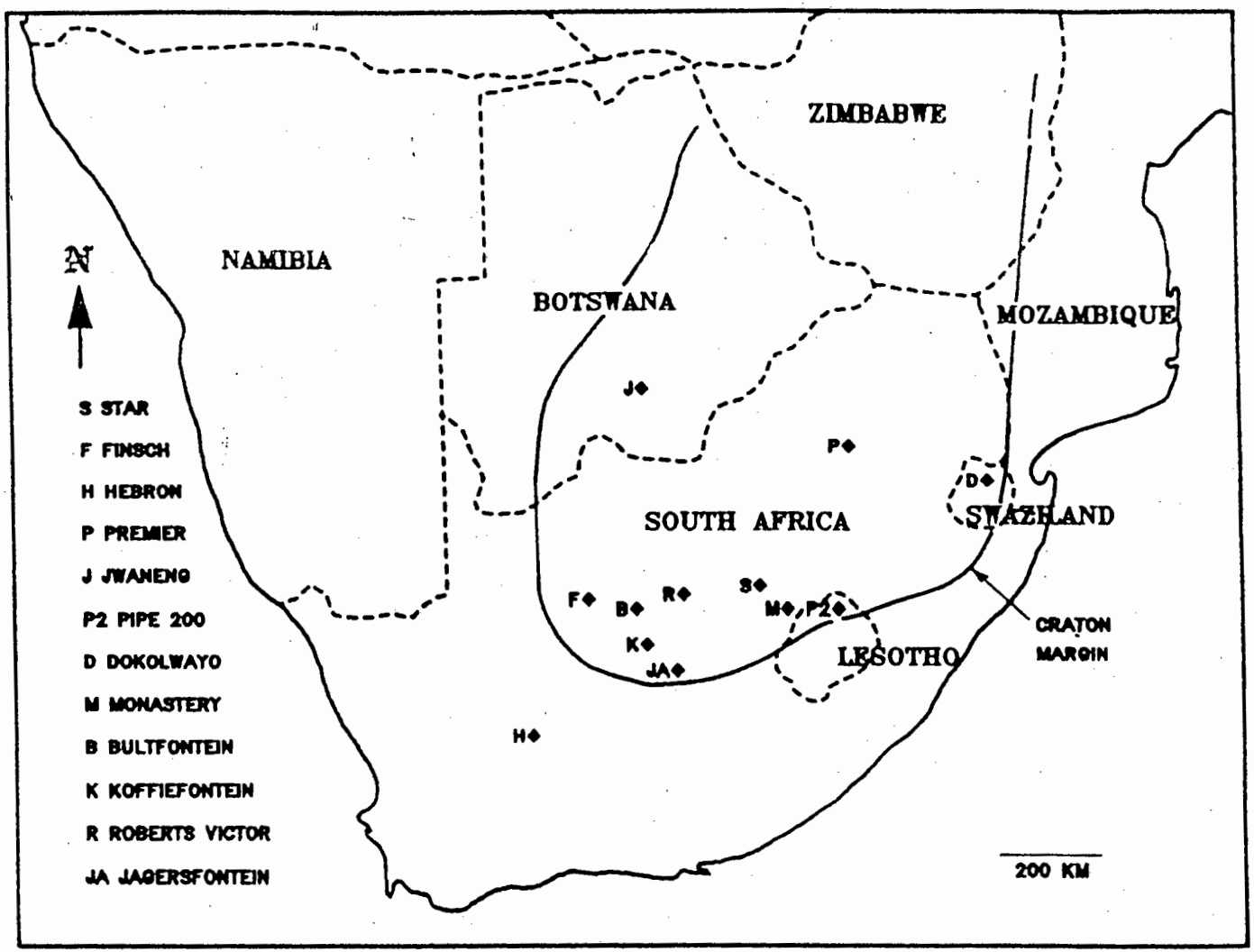
N
NAMIBIA
BOTSWANA
ZIMBABWE
MOZAMBIQUE
SOUTH AFRICA
SWAZILAND
LESOTHO
CRATON MARGIN
S STAR
F FINSCH
H HEBRON
P PREMIER
J JWANENG
P2 PIPE 200
D DOKOLWAYO
M MONASTERY
B BULTFONTEIN
K KOFFIEFONTEIN
R ROBERTS VICTOR
JA JAGERSFONTEIN
200 KM

Fig 10 A-1

Southern African Oxygen Fugacities
30 Kilobars

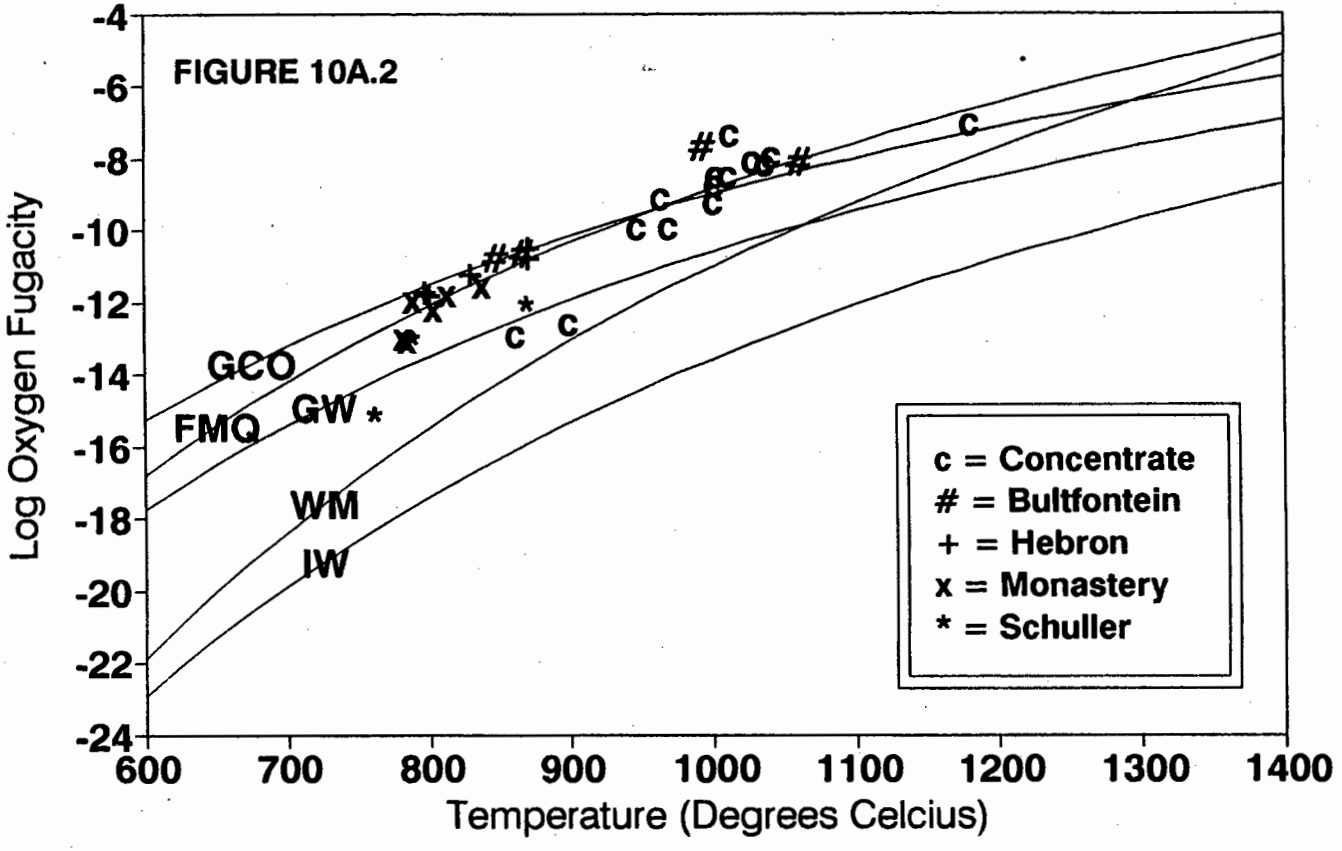

Southern African Oxygen Fugacities
50 Kilobars

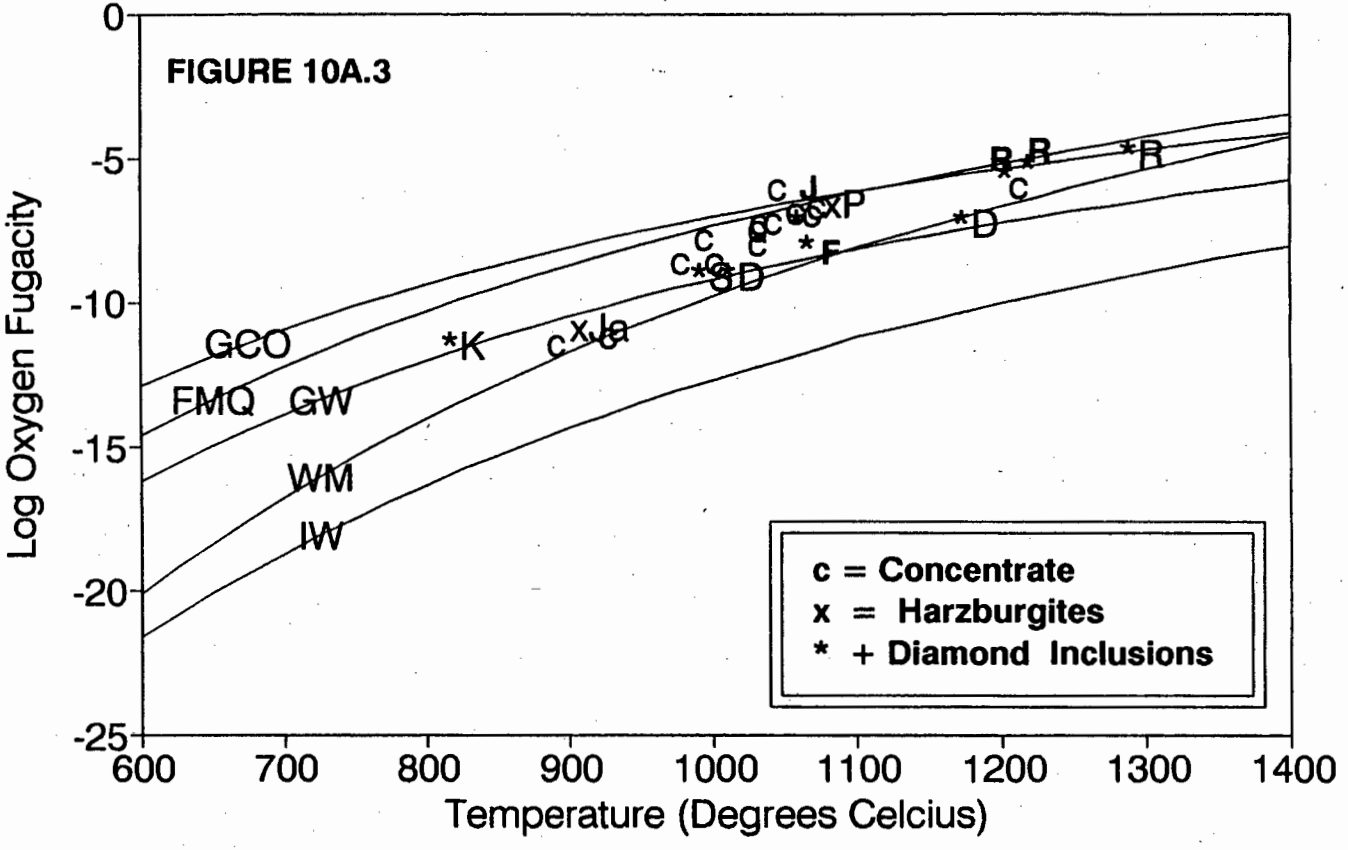

ACKNOWLEDGEMENTS

The opportunity I had to study the diamonds, their inclusions, isotopes and associated concentrate minerals are mainly due to my past association with Dokolwayo Diamond Mines (Pty) Limited, Swaziland and their holding company, Trans Hex Group. The managing director of both companies, Mr F. Hoffman, generously granted time and material for this study. The Minerals Committee of Swaziland granted permission to study the diamonds, sometimes in destructive ways.

I am particularly indebted to the members of staff of Dokolwayo, especially Samson Magagula, Graham and Debbie Crooks, the old folks Ron and Norene Wilsenach, and Philip Shile Dlamini, a man of honour. All pioneers.

At the University of Cape Town I must thank Charlie Basson and Dave Wilson. We all do. Then there are the Kimberlite Kids. Marshall, Rory, Stuart, Scott and especially Jenny, Melissa and the super LT, Thomas. I could not do without them. Thanks Jenny. Stuart Smith and Dave Reid listened, guided and helped on many occasions. Dick Rickard always got the probe going and Dave Hill the computer.

Also with much encouragement, support and help were Tony Erlank, Andy Duncan, James Willis, Steve Haggerty and Hugh O'Neill.

Recently moral support and encouragement came from my colleagues in the field: Jumbo Anderson, Andy Moore, Chris Sharp, Ted Grobicki, Julian Hobbs, Charles Byron, Leni Keough and Chris Jennings. Thanks folks!

All this would not have come about if it was not for the encouragement and enthusiasm of John Gurney. It could take many pages, but lets leave it simple with no walkabouts. Thank You.

Finally, but very definitely not the least, Lucy-Ann, who not only drafted diagrams, but also gave love and encouragement with a great deal of patience. What can I say?

Thank You.

REFERENCES

Akella J, Williams RJ, Mullins O (1976) Solubility of Cr, Ti, and Al in co-existing olivine, spinel, and liquid at 1 atm. Proc Lunar Sci Conf 7th:1179-1194

Allsopp HL, Roddick JC (1984) Rb - Sr and ^{40}Ar - ^{39}Ar age determinations on phlogopite micas from the pre-Lebombo Group Dokolwayo kimberlite pipe. Geol Soc S Afr Spec Publ No 13: 267-271

Allsopp HL, Roberts HR, Schreiner GDL, Hunter DR (1962) Rb-Sr age measurements on various Swaziland granites. J Geophys Res 67:5307-5313

Anhaeusser CR (1980) A geological investigation of the Archaean granite-greenstone terrane south of the Boesmanskop syenite pluton, Barberton Mountain Land. Trans Geol S Afr 83:93-106

Arculus RJ, Delano JW (1980) Implications for the primitive atmosphere of the oxidation state of the Earth's upper mantle. Nature 288:72-74

Arculus RJ, Delano JW (1981) Intrinsic oxygen fugacity measurements: Techniques and results for spinels from upper mantle peridotite and megacryst assemblages. Geochem Cosmochim Acta 45:899-913

Arculus RJ, Dawson JB, Mitchell RH, Gust DA, Holmes RD (1984) Oxidation states of the upper mantle recorded by by megacryst ilmenite in kimberlite and type A and B spinel lherzolites. Contrib Mineral Petrol 85:85-94

Ballevre M, Pinardon JL, Kienast JR, Vuichard JP (1989) Reversal of Fe-Mg partitioning between garnet and staurolite in eclogite-facies metapelites from the Champtoceux Nappe (Brittany, France). J Petrol 30: 1321-1349

Ballhaus C, Berry RF, Green DH (1990) Oxygen fugacity controls in the Earth's upper mantle. Nature 348: 437-440

Ballhaus C, Berry RF, Green DH (1991) High pressure experimental calibration of the olivine-orthopyroxene-spinel oxygen geobarometer: implications for the oxidation state of the upper mantle. Contrib Mineral Petrol 107:27-40

Barnes SJ (1986) The distribution of chromium among orthopyroxene, spinel and silicate liquid at atmospheric pressure. Geochem Cosmochim Acta 50:1889-1909

Barton JM, Hunter DR, Jackson MPA, Wilson AC (1980) Rb-Sr age and source of the Bimodal Suite of the Ancient Gneiss Complex, Swaziland. Nature 283:746-758

Barton JM, Hunter DR, Jackson MPA, Wilson AC (1983) Geochronologic and Sr-isotopic studies of certain units in the Barberton granite-greenstone terrane, Swaziland. Trans Geol Soc S AFr 86:71-80

Barton JM (1983) Isotopic constraints on possible tectonic models for crustal evolution in the Barberton granite-greenstone terrane, southern Africa. Spec Publ Geol Soc S Afr 9:73-79

Barton JM (1983b) Geochronological and Sr-isotope studies of certain units in the Barberton granite-greenstone terrane, Swaziland. Trans Geol Soc S Afr 86:71-80

Basu AR, MacGregor ID (1975) Chromite spinels from ultramafic xenoliths. Geochem Cosmochim Acta 39:937-945

Bell PM (1970) Analysis of olivine crystals in Apollo 12 rocks. Carnegie Inst Wash Yearb 69:228-229

Bell PM, Mao HK (1974a) Crystal field spectra of Fe(II), Fe(III), and Cr(III) in single crystals from rocks 66095, 14063, and deep-drill core 70002: Implications of oxidation/reduction processes in the lunar regolith (abstract). Lunar Science V:50.

Bell MP, Mao HK (1974b) The oxidation states of iron and chromium in lunar rocks and soils from Apollo 14, 16 and 17 landing sites. EOS 55:324

Bishop FC, Smith JV, Dawson JB (1976) Na, P, Ti and coordination of Si in garnet from peridotite and eclogite xenoliths. Nature 260:696-697

Bishop FC, Smith JV, Dawson JB (1978) Na, K, P and Ti in garnet, pyroxene and olivine from peridotite and eclogite xenoliths from African kimberlites. Lithos 11:155-173

Boyd FR (1971) Pargasite-spinel peridotite xenolith from the Wesselton Mine. Carnegie Inst Wash Yearb 70:138-142

Bottinga Y (1969a) Calculated fractionation factors for carbon and hydrogen isotope exchange in the system calcite-carbon dioxide-graphite-methane-hydrogen-water vapour. Geochim Cosmochim Acta 33:49-64

Bottinga Y (1969b) Carbon isotope fractionation between graphite, diamond and carbon dioxide. Eart Planet Sci Lett 5:301-307

Boyd FR, Smith D (1971) Compositional zoning in pyroxenes from lunar rock 12021, Oceanus Procellarum. J Petrol 12:439-464

Boyd FR, Gurney JJ (1982) Low-calcium garnets: keys to craton structure, Carnegie inst Wash Ybook 81:261-267

Bruton E (1970) Diamonds. NAG Press Ltd, London

Bunch TE, Olsen E (1975) Distribution and significance of chromium in meteorites. Geochim Cosmochim Acta 39:911-927

Burnham CW (1975) Water and magmas: a mixing model. Geochem Cosmochim Acta 39:1077-1084

Burnham CW (1979) The importance of volatile constituents. In: Yoder HS (Ed) The Evolution of Igneous Rocks. Princeton University Press, 439-482

Burns RG (1970a) Mineralogical Applications of Crystal Field Theory. In: Harland WB, Agrell SO, Davies D, Hughes HF (Eds), Cambridge Earth Sci Series, London pp 224

Burns RG (1970) Site preferences of trnsition metal ions in silicate crystal structures. Chem Geol 5:275-283

Burns RG (1975) Crystal field effects in chromium and its partitioning in the mantle. Geochem Cosmochim Acta 39:857-864

Burns RG (1975b) On the occurence of the stability of divalent chromiumj in olivines included in diamonds. Contrib Mineral Petrol 51:213-221

Burns RG, Abu-Reid RM, Huggins FE (1972) Crystal field spectra of lunar pyroxenes. Proc Lunar Sci Conf 3rd:533-543

Burns RG, Vaughan DJ, Abu-Eid RM, Witner M (1973) Spectral evidence for Cr_{3+}, Ti_{3+} and Fe_{2+} rather than Cr_{2+} and Fe_{3+} in lunar ferromagnesian silicates. Proc Lunar Sci Conf 4th:983-994

Burns VM, Burns RG (1975) Mineralogy of chromium. Geochem Cosmochim Acta 39:903-910

Cambell IH, Naldrett AJ, Roeder, PC (1979) Nickel activity in silicate melts: Some preliminary results. Can Mineral 17:495-505

Carlson RW, Hunter DR, Barker F (1983) Sm-Nd age and isotopic systematics of the Bimodal Suite, Ancient Gneiss Complex, Swaziland. Nature 305; 701-704

Carswell DA, Gibb FGF (1987) Evaluation of mineral thermometers and barometers applicable to garnet lherzolite assemblages. Contrib Mineral Petrol 95:499-511

Carswell DA, Clarke DB, Mitchell RH (1979) The petrology and geochemistry of ultramafic nodules from Pipe 200, northern Lesotho. In: Boyd FR, Meyer HOA (Eds) The Mantle Sample inclusions in kimberlites and other volcanics. Am Geophys Union, pp 127-144

Clark CD (1965) Optical properties of natural diaomond. In: Berman R (Ed) Physical Properties of Diamond. Clarendon Press, Oxford, 295-324

Clark CD, Ditchburn RW, Dyer HB (1956)Absorption spectra of irradiated diamonds after heat treatment. Proc Roy Soc Lond 237:75-89

Danchin RV, Boyd FR (1976) Ultramafic nodules from the Premier kimberlite pipe, South Africa. Carnegie Inst Wash Ybk 75:531-538

Daniels LRM (1980) Some aspects of the xenolith suite from the Newlands kimberlites, South Africa. Unpbl BSc Hons thesis, Univ Cape Town, South Africa pp 57

Daniels LRM (1991) A crystallization model for peridotitic diamond inclusion spinels. Extended Abstr Fifth Int Kimberlite Conf pp 55-57

Daniels LRM, Gurney JJ (1989) The chemistry of the garnets, chromite and diamond inclusions of the Dokolwayo kimberlite, Kingdom of Swaziland. In Ross J, Jacques AL, Ferguson J, Green DH, O'Reilly SY, Danchin RV, Janse AJA (Eds) Kimberlites and Related Rocks, Volume 2: Their Mantle/Crust Setting, Diamonds and Diamond Exploration. GSA Spec Publ No 14, Blackwell Scientific Publications, pp 1012-1021

Daniels LRM, Gurney JJ (1990) Ilmenite in the Group II Newlands kimberlite. Abs 23 Earth Sci Cong Geol Soc S Afr, 112-113

Daniels LRM, Gurney JJ (1991) Oxygen fugacity constraints on the southern African lithosphere. Contrib Mineral Petrol 108:154-161

Daniels LRM, Gurney JJ, Moore RO (1991) The pressure-composition relationship of mentle-derived chromium spinels. S Afr J Geol (Submitted)

Davies RD (1971) Geochronology and isotopic evolution of early Precambrian crustal rocks in Swaziland. Unpbl PhD thesis, Univ Witwatersrand, South Africa pp 135

Davies RD, Allsopp HL (1976) Strontium isotopic evidence relating to the evolution of the Lower Precambrian crust in Swaziland. Geology 4:553-556

Dawson JB (1980) Kimberlitess and their xenoliths. Springer Verlag, Berlin

Dawson JB, Stephens WE (1975) Statistical classification of garnets from kimberlite and associated xenoliths. J Geol 83:589-605

Dawson JB, Smith JV, Delaney JS (1978) Multiple spinel-garnet peridotite transitions in upper mantle: Evidence from a harzburgite xenolith. Nature 273:741-743

De Bruin D (1991) The megacryst suite from the Schuller kimberlite, South Africa. PhD thesis, Univ Cape Town, South Africa

Deer WA, Howie RA, Zussman J (1966) An introduction to rock forming minerals. Longman Group Limited, London.

Deines P (1980) The carbon isotopic composition of diamonds: relationship to diamond shape, color, occurrence and vapor composition. Geochem Cosmochim Acta 44:943-961

Deines P, Gurney JJ, Harris JW (1984) Associated chemical and carbon isotopic composition variations in diamonds from Finsch and Premier kimberlite, South Africa. Geochem Cosmochim Acta 48:325-342

Deines P, Harris JW, Gurney JJ (1986) On the existence of C-13 depleted carbon in the mantle; evidence from diamond studies. In: Fourth International Kimberlite Conference, Perth: Abstr Geol Soc Aust 16:383-385

Deines P, Harris JW, Gurney JJ (1987) Carbon isotopic composition, nitrogen content and inclusion composition of diamonds from the Roberts Victor kimberlite, South Africa: Evidence for 13C depletion in the mantle. Geochim Cosmochim Acta 51:1227-1243

Deines P, Gurney JJ, Harris JW (1989) Nitrogen and ^{13}C content of Finsch and Premier diamonds and their implications. Geochim Cosmochim Acta 53:1367-1378

Deines P, Wickman FE (1973) The isotopic composition of 'graphitic' carbon from iron meteorites and some remarks on the troilitic sulfur of iron meteorites. Geochim Cosmochim Acta 37: 1295-1319

Dellien I, Hall FM, Hepler LG (1976) Chromium, molybdenum, and tungsten: Thermodynamic properties, chemical equilibria, and standard potentials. Chem Reviews 76:283-310

De Wit MJ, Stern CR (1980) A 3500 Ma ophiolite complex from the Barberton greenstone belt, South Africa: Archean oceanic crust and its geotectonic implications. 2nd Intl Archean Symp Extended Abtracts, Perth, Geol Soc Aust pp 85-87

De Wit MJ, Tredoux M (1987) PGE in the 3.5 Ga Jamestown ophiolite complex, Barberton greenstone belt, with implications for PGE distribution in simatic lithosphere. In: Prichard HM, Potts PJ, Bowles JFW, Cribb SJ (Eds) Geo-Platinum pp 319-341

De Wit MJ, Tredoux M, De Ronde C, Armstrong R, Hart RA, Hart RJ (1990) Formation of the Archaean Kaapvaal Craton: Part I The early Archaean (>3.0 Ga); evidence from the Barberton Mountain Belt. Recent Data in African Earth Sciences. 15th Colloquim of African Geology, Occasional Pub 1990/22 pp 3-5

Dick HJB, Bullen T (1984) Chromian spinel as a petrogenetic indicator in abyssal and alpine-type peridotites and spatially associated lavas. Contrib Mineral Petrol 86:54-76

Dickensen JE, Hess PC (1983) TiO_2 in silicate melts: Results from rutile saturation and TiK x-ray emission spectroscopy. EOS 64:869

Dickenson MP, Hess PC (1981) Redox equilibria and the structural role of iron in alumino-silicate melts. Contrib Mineral Petrol 78:352-357

Dong Z, Zhou J (1980) The typomorphic characteristics of chromites from kimberlites in China and the significance in exploration of diamond deposits. Acta Geologica Sinica 4:284-298

Duba AG, Shankland TJ (1982) Free carbon and electrical conductivity in the earth's mantle. Geophys Res Lett 9:1271-1274

Dyar MD, McGuire AV, Ziegler RD (1989) Redox equilibria and crystal chemistry of coexisting minerals from spinel lherzolite mantle xenoliths. Am Mineral 74:969-980

Eggler DH (1983) Upper mantle oxidation state: evidence from olivine-orthopyroxene-ilmenite assemblages. Geophys Res Lett 10:365-368

Eggler DH, Dudas FO, Hearn BC, McCallum ME, McGee ES, Meyer HOA, Schulze DJ (1987) Lithosphere of the continental United States: Xenoliths in kimberlites and other alkaline magmas. In Nixon PH (Ed) Mantle Xenoliths. John Wiley and Sons, Chichester, 41-58

Fisk MR, Bence AC (1980) Experimental crystallisation of chrome spinel in FAMOUS basalt 527-1-1. Earth Planet Sci Lett 48(1):111-123

Fitch FJ, Miller JA (1984) Dating Karoo igneous rocks by the conventional K-Ar and ^{40}Ar-^{39}Ar age spectrum methods. Spec Publ Geol Soc S Afr No 13:247-266

Fournier JT, Landry RJ, Bartham RH (1971) ESR exchange coupled Cr^{3+} ions in phosphate glass. J Chem Phys 55:2522-2526

Frondel C, Klein CJr (1965) Ureyite, $NaCrSi_2O_6$: A new meteoric pyroxene. Science 149:742-744

Galimov EM (1984) Variations in isotopic composition of diamonds and inferences for diamond genesis conditions. Geokhimyva 8:1091-1118 (In Russian)

Giardini AA, Hurst VJ, Melton CE, Stormer JC (1974) Biotite as a primary inclusion in diamond: its nature and significance. Am Mineral 59:783-789

Green DH, Ringwood AE, Hibberson WO, Ware NG (1975) Experimental petrology of Apollo 17 mare basalts. Proc Lunar Sci Conf 6th:871-893

Gurney JJ (1984) A correlation between garnets and diamonds in kimberlites. In Glover JE, Harris PG (Eds) Kimberlites. Occurence and Origin: A basis for Conceptual Models in Exploration. Univ Western Aust, Extension Services, Perth, Publ No 8:

Gurney JJ, Boyd FR (1982) Mineral intergrowths with polycrystalline diamonds from the Orapa Mine, Botswana. Ann Rep Geophys Lab, Carnegie Inst 81:267-272

Gurney JJ, Harte B (1980) Chemical variations in upper mantle nodules from southern African kimberlites. Phil Trans R Soc Lond A297:273-293

Gurney JJ, Switzer G (1973) The discovery of garnets closely related to diamonds in the insch pipe, South Africa. Contrib Mineral Petrol 39:103-116

Gurney JJ, Harris JW, Rickard RS (1979) Silicate and oxide inclusions in diamonds from the Finsch kimberlite pipe. In: Boyd FR, Meyer HOA (Eds) Kimberlites, Diatremes and Diamonds. American Geophysical Union, Washington D.C., pp 1-15

Gurney JJ, Harris JW, Rickard RS (1984a) Silicate and oxide inclusions in diamonds from the Orapa Mine, Botswana. In: Kornprobst J (Ed) Kimberlites II: The Mantle and Crust-Mantle Relationships. Elsevier, Amsterdam pp 3-10

Gurney JJ, Harris JW, Rickard RS (1984b) Minerals associated with diamonds from the Roberts Victor Mine. In: Kornprobst J (Ed) Kimberlites II: The Mantle and Crust-Mantle Relationships. Elsevier, Amsterdam pp 25-32

Gurney JJ, Harris JW,Rickard RS, Moore RO (1985) Inclusions in Premier Mine diamonds. Trans Geol Soc S Afr 88:301-310

Gurney JJ, Jakob WRO, Dawson JB (1979b) Megacrysts from the Monastery mine. In: Boyd FR, Meyer HOA (Eds) The Mantle Sample: Inclusions in kimberlites and other volcanics. Am Geophys Union, pp 227-243

Haggerty SE (1972) Apollo 14: Subsolidus reduction and compositional variations of spinels. Proc Lunar Sci Conf 3rd:305-332

Haggerty SE (1976) Opaque mineral oxides in terrestrial igneous rocks. In Rumble D (Ed) Oxide Minerals: Short Course Notes. Mineral Soc Am, Washington, pp Hg101-Hg300

Haggerty SE (1978) The redox state of plantary basalts. Geophys Res Lett 5:443-446

Haggerty SE (1979) Spinel in high pressure regimes. In Boyd FR, Meyer HOA (Eds) Kimebrlites, Diatremes, and Daimonds. American Geophyscical Union, Washington, pp183-193

Haggerty (1986) Diamond genesis in a multiply-constrained model. Nature 320:34-38

Haggerty SE, Boyd FR, Bell PM, Finger LW, Bryan WB (1970) Opaque minerals and olivine in lavas and breccias from Mare Tranquillitatis. Proc Apollo 11 Lunar Sci Conf, Geochem Cosmochim Acta Suppl VI,1:513-538

Haggerty SE, Tompkins LA (1983) Redox state of the Earth's upper mantle from kimberlitic ilmenites. Nature 303:295-300

Haggerty SE, Erlank AJ (1987) Lithospheric redox states. Terra Cognita 7:610-611

Haggerty SE, Boyd, FR, Bell PM, Finger LW, Byan WB (1970) Opaque minerals and olivine in lavas and breccias from Mare Tranquillitatis. Proc Apollo 11 Lunar Sci Conf, Geochim Cosmocim Acta Suppl 1:513-538

Hamilton PJ, Evensen NM, O'Nions RK, Smith HS, Erlank AJ (1979) Sm-Nd dating of the Onverwacht Group volcanics, southern Africa. Nature 179:298-300

Harris JJ, Hawthorne JB, Oosterveld MM, Welmeyer E (1975) A classification Scheme for diamond and a comparitive study of South African diamond characteristics. In: Ahrens LH, Dawson JB, Duncan AR, Erlank AJE (Eds) Physics and Chemistry of the Earth, Pergamon Press, Oxford, England, 9:477-506

Harris JJ, Hawthorne JB, OOsterveld MM (1979) Regional and local variations in the characteristics of diamonds from some southern African kimberlites. In: Boyd FR, Meyer HOA (Eds) Kimberlites, Diatremes and Diamonds. American Geophysical Union, Washington D.C., pp 27-41

Hart SR (1984) A large-scale isotopic anomaly in the Southern Hemisphere mantle. Nature 309:753-757

Hatton CJ (1978) The geochemistry and origin of xenoliths from the Roberts Victor Mine. Unpbl PhD thesis, Univ Cape Town, South Africa

Hatton CJ, Gurney JJ (1987) Roberts Victor eclogites and their relationship to the mantle. In: Nixon PH (Ed) Mantle Xenoliths. Wiley and Sons, Chichester, pp 453-463

Hawthorne JB, Carrington AJ, Clement CR, Skinner EMW (1979) Geology of the Dokolwayo kimberlite and associated palaeo-alluvial diamond deposits. In: Boyd FR, Meyer HOA (Eds) Kimberlites, Diatremes and Diamonds. American Geophysical Union, Washington D.C., pp 59-70

Hegner E, Kroner A, Hoffmann AW (1984) Age and isotopic geochemistry of the Archaean Pongolo and Ushushwana suites in Swaziland, southern Africa: a case for crustal conamination of mantle-derived magmas. Earth Planet Sci Lett 70:267-279.

Henoc J, Heinrich KFJ, Myklebust RL (1973) A rigorous correction procedure for quantitative electron probe microanalysis. US Bureau of Standards, Technical Note 769, US Govt. Printing Office, Washington.

Herrman AG, Blanchard DP, Haskin LA, Jacobs JW, Knake D, Korotev RL, Brannon JC (1976) Major, minor and trace element compositions of peridotitic and basaltic komatiites from the Precambrian crust of southern Africa. Contrib Mineral Petrol 59:1-12

Hill SJ (1989) A study of diamonds and xenoliths from the Star kimberlite, Orange Free Stae, South Africa. Unpbl MSc thesis, Univ Cape Town, South Africa, pp 185

Hops JJ (1989) Some aspects of the geochemistry of high-temperature peridotites and megacrysts from the Jagersfontein kimberlite pipe, South Africa. Unpbl PhD thesis, Univ Cape Town, South Africa, pp 207

Hornung G, Nixon PH (1973) Chemical variations in the knorringite-rich garnets. In: Nixon PH (Ed) Lesotho Kimberlites, Lesotho National Development Corporation, Maseru, pp 122-127

Hubbard NJ, Gast PW, Rhodes JM, Bansal BM, Wiesmann H, Church SE (1972) Nonmare Basalts: Part II. Proc Lunar Sci Conf 3rd:1161-1179.

Huebner JS, Lipin BR, Wiggins LB (1976) Partitioning of chromium between silicate crystals and melts. Proc Lunar Sci Conf 7th:1195-1120

Hunt B (1987) Heavy mineral abundance study of the Premier Mine kimberlites. Unpbl BSc Hons thesis, Univ Witwatersrand, South Africa pp 43

Hunter DR, Wilson AH (1988) A continuous record of Archaean evolution from 3,5 Ga to 2,6 Ga in Swaziland and northern Natal. Afr J Geol 91:57-74

Ikeda K (1973) Chrome-rich clinopyroxene from Red Hills, New Zealand with special reference to the exsolution phenomena. J Jap Assoc Min Petrol Econ Geol 68:125-131

Ikeda K, Yagi K (1972) Synthesis of kosmochlor and phase equilibria in the join $CaMgSi_2O_6$-$NaCrSi_2O_6$. Contrib Mineral Petrol 36:63-72

Irvine TN (1965) Chromian spinel as a petrogenetic indicator, Part I. Theory. Can J Earth Sci 2:648-672

Irvine TN (1967) Chromian spinel as a petrogenetic indicator, Part II. Petrogenetic Applications. Can J Earth Sci 4:71-103

Jackson ED (1969) Chemical variation in coexisting chromite and olivine in chromite zones of the Stillwater Complex. Econ Geol Mono 4:41-71

Jakob WRO (1977) Geochemical Aspects of the megacryst suite from the Monastery kimberlite pipe. Unpbl MSc thesis, Univ Cape Town, South Africa pp 33

Jenkins DM, Newton RC (1979) Experimental determination of the spinel peridotite to garnet peridotite inversion at 900°C and 1000°C in the system CaO - MgO - Al_2O_3 - SiO_2 and at 900°C with natural garnet and olivine. Contrib Mineral Petrol 68:407-419

Kaiser W, Bond WL (1959) Nitrogen, a major impurity in common type I diamond. Physics Review 115:857-863

Kasch KW (1987) Metamorphism of pelites in the upper Black Nossob River area of the Damara Orogen. Communs Geol Surv SW Africa\Namibia 3:63-81

Keil K, Brett R (1973) $(Fe,Cr)_{1+x}(Ti,Fe)_2S_4$, a new mineral in the Bustee enstatite achondrite. Meteoritics 8:48-49

Keil K, Prinz M, Bunch TE (1971) Mineralogy, petrology, and chemistry of some Apollo 12 samples. Proc Lunar Sci Conf 2nd:319-341

Kennedy CS, Kennedy GC (1976) The equilibrium boundary between graphite and diamond. J Geophys Res 81:2467-2470

Kimura S, Muan A (1971) Phase relations in the system CaO-iron oxide-titanium oxide under strongly reducing conditions. Am Mineral 56:1347-1358

Kirkley MB, Gurney JJ (1989) Carbon isotope modelling of biogenic origins for carbon in eclogitic diamonds. Workshop on Diamonds: Extended Abstracts, 28th Int Geol Cong, Wash D.C. pp 40-43

Kirkley MB, McCallum ME, Eggler DH (1984) Coexisting garnet and spinel in upper mantle xenoliths from Colorado-Wyoming kimberlites. In Kornprobst J (Ed) Kimberlites II: The Mantle and Crust-Mantle Relationships, Elsevier, Ampsterdam, pp 85-96.

Kirkley MB, Gurney JJ, Otter ML, Hill SJ, Daniels LR (1991) The application of carbon isotopes to the identification of the sources of carbon in diamonds: a review. Applied Geochem (In Press)

Kobayashi K (1976) Optical and EPR studies of redox interactions of polyvalent ions (Cr,Cu) in glass. J Am Ceram Soc 59:9-11

Landry RJ, Fournier JT, Young CG (1967) Electron spin resonance and optical absorbtion studies of Cr^{3+} in phosphate glasses. J Chem Phys 46:1285-1290

Lawless PJ (1974) Some aspects of the geochemistry of kimberlite xenocrysts. Unpbl MsC thesis, Univ Cape Town, South Africa, pp 121

Lawless PJ (1978) Some aspects of the mineral chemistry of the peridotite xenolith suite from the Bultfontein Diamond Mine, Kimberley, South Africa. Unpbl PhD thesis, Univ Cape Town, South Africa, pp 193

Layer PW, Kröner A, McWilliams M, York D (1989) Elements of the Archean thermal history and apparent polar wander of the eastern Kaapvaal Craton, Swaziland, from single grain dating and paleomagnetism. Earth Planet Sci Lett 93:23-34

Le Roex AP (1986) Geochemical correlation between southern African kimberlites and South Atlantic hotspots. Nature 324:243-245

Lindsley D, Dixon SA (1976) Coexisting diopside and enstatite at 20 kbar and 900°-1200°C. Am Mineral 59:110-119

Lindsley D, Dixon SA (1976) Diopside-enstatite equilibria at 850 to 1400°C, 5 to 35 kbars. Am J Sci 276:1285-1301

MacGregor ID (1970) The effect of CaO, Cr_2O_3, Fe_2O_3 and Al_2O_3 on the stability of spinel and garnet peridotites. Phys Earth Planet Int 3:372-377

Mal'kov BA, Popova (1972) Chrome spinllids as indicators of the presence of diamonds in Yakutian kimberlite. Doklady Akad Nauk SSR 211:141-144

Manton WI (1968) The origin of associated basic and acid rocks in the Lebombo Nuanetsi igneous province, southern Africa, as implied by strontium isotopes. J Petrol 9:23-39

Mao HK, Bell (1971) Crystal-field spectra. Carnegie Inst Wash Yearb 70:207-215

Mathez EA, Blacic JD, Beery J, Maggoire C, Hollander M (1984) Carbon abundances in mantle minerals determined by nuclear reaction analysis. Geophys Res Lett 11:947-950

Mattioli GS, Wood BJ (1986) Upper mantle oxygen fugacities recorded by spinel lherzolites. Nature 322:626-628

Mattioli GS, Wood BJ (1988) Magnetite activities across the $MgAl_2O_4$-Fe_2O_3 spinel join, with application to thermobarometric estimates of upper mantle oxygen fugacity. Contrib Mineral Petrol 98:148-162

Mazzone P, Haggerty SE (1989) Peraluminous xenoliths in kimberlite: Metamorphosed restites produced by partial melting of pelites. Geochim Cosmochim Acta 53:1551-1561

McCandless TE, Kirkley MB, Robinson DN, Gurney JJ, Griffin WL, Cousens DR, Boyd FR (1989) Some initial observations on polycrystalline diamonds mainly from Orapa. Workshop on Diamonds: Extended Abstracts, 28th Int Geol Cong, Wash D.C. pp 47-51

Meyer HOA (1985) Genesis of diamond: a mantle saga. Am Mineral 70:344-355

Meyer HOA, Boyd FR (1968) Inclusions in diamonds. Carnegie Inst Wash, Yearb 68:315-324

Meyer HOA, Boyd FR (1972) Composition and crystalline inclusions in natural diamonds. Geochem Cosmochim Acta 36:1255-1273

Meyer HOA, Tsai H-M (1976) Mineral inclusions in natural diamonds: their nature and significance. Minerl Sci Eng 8:242-261

Mitchell RH (1984) Garnet lherzolites from the Hanaus 1 and Louwrensia kimberlites of Namibia. Contrib Mineral Petrol 86:178-188

Mitchell RH (1987) Mantle-derived xenoliths in Canada. In: Nixon PH (Ed) Mantle Xenoliths. Wiley and Sons, Chichester, pp 33-40

Moore M, Lang AR (1974) The origin of the rounded dodecahedral habit of natural diamond. J Cryst Growth 26:133-139

Moore RO (1986) A study of the kimberlites, diamonds and associated rocks and minerals from the Monastery Mine, South Africa. Unpbl PhD thesis, Univ Cape Town, South Africa, pp 251

Moore RO, Gurney JJ (1985) Pyroxene solid solution in garnets included in diamonds. Nature 328:553-555

Moore RO, Gurney JJ (1986) Mineral inclusions in diamonds from the Monastery kimberlite, South Africa. In: Fourth International Kimberlite Conference, Perth: Abstr Geol Soc Aust 16:406-409

Moore RO, Gurney JJ (1989) Mineral inclusions in diamond from the Monastery kimberlite, South Africa. In Ross J, Jacques AL, Ferguson J, Green DH, O'Reilly SY, Danchin RV, Janse AJA (Eds) Kimberlites and Related Rocks, Volume 2: Their Mantle/Crust Setting, Diamonds and Diamond Exploration. GSA Spec Publ No 14, Blackwell Scientific Publications, pp 1027-1041

Moore RO, Daniels LRM, Gurney JJ (1990) Garnet megacrysts in the Group II Dokolwayo kimberlite, Swaziland. Ext Abstract 23rd Eart Sci Cong Geol Soc S Afr pp 427-430

Murck BW, Cambell IH (1986) The effects of temperature, oxygen fugacity and melt composition on the behaviour of chromium in basic and ultrabasic melts. Geochim Cosmoschim Acta 50:1871-1887

Mysen BO, Seifert FA, Virgo D (1980a) Structure and redox equilibria of iron-bearing silicate melts. Am Mineral 65:867-884

Mysen BO, Virgo D, Scarfe CM (1980b) Relations between the anionic structure and viscosity of silicate melts - a Raman spectroscopic study. Am Mineral 65:690-711

Mysen BO, Virgo D, Seifert FA (1981a) Ferric iron as a network former and as a network modifier in melts relevant to petrological processes. Carnegie Inst Wash Yearb 80:311-313

Mysen BO, Virgo D, Kushiro, I (1981b) The structural role of aluminum in silicate melts - a Raman spectroscopic study at 1 atm. Am Mineral 66:678-741

Mysen BO, Virgo, D, Seifert, FA (1984) Redox equilibria of iron in alkaline earth silicate melts: Relations between melt structure, oxygen fugacity, temperature and properties of iron-bearing silicate liquids. Am Mineral 69:834-847

Mysen BO, Virgo D, Neumann E-R, Seifert, FA (1985) Redox equilibria and the structural states of ferric and ferrous iron in melts in the system CaO-MgO-Al_2O_3-SiO_2-FeO: Relationships between redox equilibria, melt structure and liquidus phase equilibria. Am Mineral 70:317-331

Nickel KG (1986) Phase equilibria in the system SiO_2-MgO-Al_2O_3-CaO-Cr_2O_3 (SMACCR) and their bearing on spinel/garnet lherzolite relationships. Neues Jahrbuch Miner Abh 155:259-287

Nickel KG, Green DH (1985) Empirical geothermobarometry for garnet peridotites and implications for the nature of the lithosphere, kimberlites and diamonds. Earth Planet Sci Lett 73:158-170

Nixon PH, Boyd FR (1973) Petrogenesis of the granular and sheared ultrabasic nodule suite in kimberlites. In: Nixon PH (Ed) Lesotho Kimberlites, Lesotho National Development Corporation, Maseru, pp 48-56

Nixon PH, van Carlsteren PWC, Boyd FR, Hawkesworth, CJ (1987) Harzburgites with garnets of diamond facies from southern African kimberlites. In: Nixon PH (Ed) Mantle Xenoliths. Wiley and Sons, Chichester, pp 523-533

Obata M (1976) The solubility of Al2O3 in orthopyroxenes in spinel and plagioclase peridotites and spinel pyroxenites. Am Mineral 61:804-816

O'Hara MJ, Richardson SW, Wilson G (1971) Garnet peridotite stability and occurence in crust and mantle. Contrib Mineral Petrol 32:48-68

O'Neill HStC (1981) The transition between spinel lherzolite and garnet lherzolite, and its use as a barometer. Contrib Mineral Petrol 77:185-194

O'Neill HStC (1987) Quartz-fayalite-iron and quartz-fayalite-magnetite equilibria and the free energy of formation of fayalite (Fe_2SiO_4) and magnetite (Fe_3O_4). Am Mineral 72:67-75

O'Neill HStC (1988) Systems Fe-O and Cu-O: Thermodynamic data for the equilibria Fe-"FeO," Fe-Fe_3O_4, "FeO"-Fe_3O_4, Fe_3O_4-Fe_2O_3, Cu-Cu_2O, and Cu_2O-CuO from emf measurements. Am Mineral 73:470-486

O'Neill HStC, Wall VJ (1987) The olivine-orthopyroxene-spinel oxygen geobarometer, the nickel precipitation curve, and the oxygen fugacity of the Earth's upper mantle. J Petrol 28:1169-1191

O'Neill HStC, Wood BJ (1979) An experimental study of Fe-Mg partitioning between garnet and olivine and its calibration as a geothermometer. Contrib Mineral Petrol 70:59-70

O'Reilly DE, MacIver DS (1962) Electron paramagnetic resonance absorption of chromia-alumina catalysts. J Phys Chem 66:276-281

Otter ML (1990) Diamonds and their mineral inclusions from the Sloan diatremes of the Colorado-Wyoiming State Line kimberlite district, North America. Unpbl PhD thesis, Univ Cape Town, South Africa pp 171

Pokhilenko NP, Sobolev NV, Lavrent'ev YuG (1977) Xenoliths of diamondiferous ultramafic rocks from Yakutian kimberlites. In Second Int Kimb Conf, Santa Fe, Extend Abstr

Powell R (1985) Regression diagnostics and robust regression in geothermometer/geobarometer calibration: the garnet-clinopyroxene geothermometer revisited. J Metamorphic Petrol 3:231-243

Prinz M (1967) Geochemistry of basalts: Trace elements. In: Hess HH, Poldevaart A (Eds) Basalts - The Poldevaart Treatise on Rocks of Basaltic Composition. Interscience, New York, 1:271-323

Richardson SH, Gurney JJ, Erlank AJ, Harris JW (1984) Origin of diamonds in old enriched mantle. Nature 310:198-202

Rickard RS, Gurney JJ, Harris JW, Cardoso P (1989) Mineral inclusions in diamonds from Koffiefontein Mine. In Ross J, Jacques AL, Ferguson J, Green DH, O'Reilly SY, Danchin RV, Janse AJA (Eds) Kimberlites and Related Rocks, Volume 2: Their Mantle/Crust Setting, Diamonds and Diamond Exploration. GSA Spec Publ No 14, Blackwell Scientific Publications, pp 1054-1062

Ringwood AE (1970) Petrogenesis of Apollo 11 basalts, internal constitution and origin of the Moon. Proc Apollo 11 Lunar Sci Conf pp 769-799

Robey JvA (1981) Kimberlites of the Central Cape Province, R.S.A. Unpbl PhD thesis, Univ Cape Town, South Africa, pp 261

Robinson DN (1979) Surface textures and other features of diamonds. Unpbl PhD thesis, Univ Cape Town, South Africa

Rosenhauer M, Woermann E, Knecht B, Ulmer CG (1977) The stability of graphite and diamond as a function of the oxygen fugacity in the mantle. Extended Abstr, 2nd Int Kimb Conf, Santa Fe

Ross CS, Foster MD, Myers AT (1954) Origin of dunites and of olivine-rich inclusions in basaltic rocks. Am Mineral 39:693-737

Ryabchikov ID, Green DH, Wall VJ, Brey B (1981) The oxidation state of carbon in the environment of the low velocity zone. Geokhimiya 2:221-232

Ryerson FJ (1978) Oxide solution mechanisms in silicate melts: Systematic variations in the activity coefficient of SiO_2. Geochem Cosmochim Acta 49:637-649

Schreiber HD (1977) Redox states of Ti, Zr, Hf, Cr, and Eu in basaltic magmas: An experimental study. Proc Lunar Sci Conf 8th:1785-1807

Schreiber HD, Haskin LA (1976) Chromium in basalts: Experimental determination of redox states and partitioning among synthetic silicate phases. Proc Lunar Sci Conf 7th:1221-1259

Schreyer W (1988) Subduction of continental crust to mantle depths: Petrological evidence. Episodes 11:97-104

Seifert FA, Mysen BO, Virgo D (1981) Structure and properties of alumino-silicate melts with three dimensional network structure. Carnegie Inst Wash Yearb 80:305-308

Shannon RD, Prewitt CT (1969) Effective ionic radii in oxides and fluorides. Acta Crystal B25:925-946

Shee SR (1978) The mineral chemistry of xenoliths from the Orapa kimberlite pipe, Botswana. Unpbl MSc thesis, Univ Cape Town, South Africa

Skinner EMW (1986) Contrasting Group I and Group II kimberlite petrology: Towards a genetic model for kimberlites. Fourth Int Kimb Conf, Perth Extend Abstr, Abstr Geol Soc Aust 16:202-203

Skinner EMW, Scott BH (1979) Petrography, mineralogy and geochemistry of kimberlite and associated lamprophyre dykes near Swartruggens, Western Transvaal, RSA. Cambridge Kimberlite Conf II

Smith CB (1983) Pb, Sr and Nd isotopic evidence for sources of southern African Cretaceous kimberlites. Nature 304:51-54

Smith HS, Erlank AJ (1982) Geochemistry and petrogenesis of komatiites from the Barberton greenstone belt South Africa. In Arndt NT, Nisbet EG (Eds) Komatiites. George Allen and Unwin pp347-397

Smith JV, Dawson JB (1975) Chemistry of Ti-poor spinels, ilmenites and rutiles from peridotite and eclogite xenoliths. Phys Chem Earth 9:309-322

Sobolev NV, Lavrent'ev YuG (1971) Isomorphic sodium admixture in garnets formed at high pressures. Contrib Mineral Petrol 31:1-12

Sobolev NV, Shatsky VS (1987) Geologiya Geofizika 7:77-80 (In Russian)

Sobolev NV, Lavrent'ev YuG, Pokhilenko NP, Usova LV (1973) Chrome-rich garnets from the kimberlites of Yakutia and their paragenesis. Contrib Mineral Petrol 40:39-52

Sobolev NV, Pokhilenko NP, Efimova ES (1984) Xenoliths of diamond-bearing peridotites in kimberlites and the problem of diamond origin. Geol Geofiz 25:63-80

Steele IM, Smith JV (1975) Minor elements in lunar olivine as a petrologic indicator. Proc Lunar Sci Conf 6th:451-467

Stubican VS and Greskovich C (1966) Jahn-Teller distortion induced by tetrahedral-site Cr^{2+} ions in spinels. J Amer Ceram Soc 49:518-519

Stubican VS, Greskovich C (1975) Trivalent and divalent chromium ions in spinels. Geochim Cosmochim Acta 39:875-881

Sunagawa I (1984a) Growth of crystals in nature. In: Sunagawa, I (Ed) Materials Science of the Earth's Interior. Terra Scientific, Tokyo pp 66-105

Sunagawa I (1984b) Morphology of natural and synthetic diamond crystals. In: Sunagawa, I (Ed) Materials Science of the Earth's Interior. Terra Scientific, Tokyo pp 303-330

Swart PK, Pillinger CT, Milledge HJ and Seal M (1983) Carbon isotopic variation within individual diamonds. Nature 303:793-795

Tankard AJ, Jackson MPA, Eriksson KA, Hobday DK, Hunter DR, Minter WEL (1982) Crustal Evolution of Southern Africa. Springer Verlag, New York, pp523

Taylor WR, Green DH (1988) Measurement of reduced peridotite-C-O-H solidus and the implications for redox melting of the mantle. Nature 332:349-352

Taylor WR, Green DH (1989) The role of reduced C-O-H fluids in mantle partial melting. In Ross J, Jacques AL, Ferguson J, Green DH, O'Reilly SY, Danchin RV, Janse AJA (Eds) Kimberlites and Related Rocks, Volume 1: Their Composition, Occurrence, Origin and Emplacement. GSA Spec Publ No 14, Blackwell Scientific Publications, pp 1054-1062

Tollo RP (1982) Petrography and mineral chemistry of ultramafic and related inclusions from the Orapa A/K-1 kimberlite pipe, Botswana. Contrib 39 Dept Geol Geog, Univ Mass, Amherst, Mass, U.S.A pp 202

Tugovik GI, Safronov PP, Kirasirova VI (1987) Doklady Akad Nauk SSSR 297:187-191

Turekian KK (1963) The chromium and nickel distribution in basaltic rocks and eclogites. Geochim Cosmochim Acta 27:835-846

Ulmer GC, Rosenhauer M, Woermann E, Ginder J, Drory-Wolff A, Wsilewski P (1976) Applicability of electrochemical oxygen fugacity measurements to geothermometry. Am Mineral 61:653-660

Ulmer GC, Grandstaff DE, Weiss D, Moats MA, Buntin TJ, Gold DP, Hatton CJ, Kadik A, Koseluk RA, Rosenhauer M (1987) The mantle redox state; An unfinished story Geol Soc Am Spec Pap 215:5-23

Viljoen MJ, Viljoen RP (1969) The geology and geochemistry of the lower ultramafic unit of the Onverwacht Group and a proposed new class of igneous rocks. Geol Soc S Afr Spec Publ 2:55-86

Virgo D, Luth RW, Moats MA, Ulmer GC (1988) Constraints on the oxidation state of the mantle: An electrochemical and ^{57}Fe Mossbauer study of mantle-derived ilmenites. Geochem Cosmochim Acta 52:1781-1794

Watson EB (1976) Two liquid partition coefficients: experimental data and geochemical implications. Contrib Mineral Petrol 56:119-134

Winkler HGF (1974) Petrogenesis of Metamorphic Rocks. Springer-Verlag, New York pp 329

Whitelock TK (1973) Morphology of the Kao diamonds. In: Nixon PH (Ed) Lesotho Kimberlites. Lesotho National Development Corporation, Maseru pp 128-140

Williams AF (1932) The Genesis of the Diamond. 2 Vols. Benn Ltd, London

Woermann E, Rosenhauer M (1985) Fluid phases and the redox state of the Earth's mantle. Fortschr Miner 83:263-349

Wood BJ, Virgo D (1989) Upper mantle oxidation state: Ferric iron contents of lherzolite spinels by ^{57}Fe Mossbauer spectroscopy and resultant oxygen fugacities. Geochem Cosmochim Acta 53:1277-1291

Wood MI, Hess PC (1980) The structural role of Al2O3 and TiO2 in immiscible silicate liquids in the system SiO_2-MgO-CaO-FeO-TiO_2-Al_2O_3.

Yefimova ES, Sobolev NV (1977) Abundance of crystalline inclusions in Yakutian diamonds. Dokl Akad Nauk SSSR 6:231-234